Kinematical Conservation Laws and Applications

A Thesis

Submitted for the Degree of

Doctor of Philosophy

in the Faculty of Science

by

S. Baskar

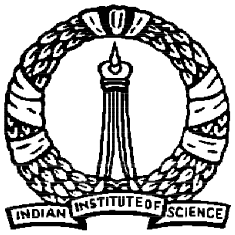

Department of Mathematics

Indian Institute of Science

Bangalore – 560 012 INDIA

February 2003

Declaration

I hereby declare that the matter embodied in this thesis is the result of the investigations carried out by me under the supervision of Professor Phoolan Prasad, Department of Mathematics, Indian Institute of Science, Bangalore 560 012, and has not been submitted for the award of any degree, diploma, associateship, fellowship or membership of any university or institution.

(S. Baskar)

Certified

(Phoolan Prasad)

Name of the Candidate	:	**S. BASKAR**
Degree Registered	:	Ph.D.
Department	:	Department of Mathematics, Indian Institute of Science, Bangalore.
Research Supervisor	:	Prof. Phoolan Prasad
Title of the Thesis	:	Kinematical Conservation Laws and Applications

---

Synopsis

Study of wave motion is important in the field of fluid mechanics. The equations governing the motion of an inviscid compressible fluid form a hyperbolic system of quasi-linear equations and hence give rise to nonlinear waves which are quite difficult to analyse mathematically. Because of the availability of powerful computational facilities, numerical studies are more common in applications. However, in some practical applications, it is very expensive to go for full numerical solutions and hence, in order to minimize the computational difficulties, certain approximations of the actual governing system are needed depending on the nature of the application.

In applications like calculation of the sonic boom signature, extracorporeal shock wave lithotripsy to treat kidney stone disease, tracing the shock front or wavefront is essential. In such applications, it is not necessary to get the full information of the flow between shock and the body producing the shock. Moreover, in the case of the calculation of the sonic boom signature, one need to calculate the far field solution, as the main aim in this problem is to find the pressure disturbance on the ground when a supersonic aircraft flies at a high distance from the ground level. Hence, in such cases, it is expensive and sometimes may not be possible to go for a full numerical solution of gas dynamics equations. To minimize the computational effort, we need to apply certain physically realistic approximations to simplify the system.

Acoustic ray theory or linear ray theory were used to trace the wavefronts or shock fronts, which works well in certain cases like geometrical optics. Since this theory does not take the nonlinear diffraction of the rays into account, a caustic region occurs beyond which the wavefront or the shock front tend to fold and form a cusp type of singularity. Hence, the linear ray theory is not suitable for applications where nonlinear effects play a crucial role. Whitham proposed in 1957 a theory called geometrical shock dynamics (GSD) through which he showed that there are nonlinear waves propagating on the shock fronts that makes the amplitude in the focal region to be finite and instead of folding of the shock front, we get a discontinuity in the slope of the shock front, which is a *kink* (called *shock-shock* by Whitham). This behaviour of a weak shock front in the focal region was experimentally studied by Sturtevant and Kulkarni (1976). Kink is basically a geometrical phenomena (Prasad (1995)) which appears as the image in (x, y)-plane of a shock as a solution of

kinematical conservation laws(KCL)

$$\begin{aligned}(g\sin\theta)_t + (m\cos\theta)_\xi &= 0\\ (g\cos\theta)_t - (m\sin\theta)_\xi &= 0\end{aligned}$$

in an appropriately defined ray coordinate system (ξ, t). Here g is the metric along the wavefront (or shock front) t=constant, θ is the angle between the normal to the wavefront and the x-axis, and m is the wavefront (or shock front) Mach number. KCL was first derived by Morton, Prasad and Ravindran (1993). Prasad and Sangeetha (1999) used KCL to study the formation and propagation of kinks on nonlinear wavefronts. In the weakly nonlinear ray theory (WNLRT), used by Prasad and Sangeetha, KCL is hyperbolic in nature when the wavefront Mach number m is greater than 1 and hence the numerical study of the problem becomes quite easy and efficient.

Since KCL represents evolution of any propagating curve Ω_t, it can be used effectively in many problems in science and engineering which involve propagation of an interface or discontinuity. But KCL, which has two equations in three unknowns, is an under determined system. To make the system closed, we need dynamical conditions depending on the nature of Ω_t ie., in different applications of KCL, we need different additional equation or relation between the unknowns. When Ω_t is a shock front, dynamical consideration leads not only one but infinity of compatibility conditions. Hence, a mathematical analysis of KCL is essential to understand the nature of the solution, limitation of the usage of the theory, etc. This thesis first deals with a mathematical analysis of the KCL with a simple additional closure relation, which appears to be physically realistic for a class of problems and then goes to applications of KCL to some problems including the propagation of a curved shock where more general closure equations are required.

The thesis consists of seven chapters. Chapter 1 starts with a motivation for the work. A brief introduction to the WNLRT and the derivation of the KCL has been presented for the sake of making the material self content. However, a detailed discussion of the subject is available in the book by Prasad (2001). As mentioned above, the KCL is hyperbolic when the wavefront Mach number m is greater than 1. Therefore, we quote some results and definitions regarding hyperbolic systems for the readers to appreciate the work done in this thesis, especially the works discussed in chapter 2 and chapter 3.

Riemann problem and the interaction of elementary waves are the building blocks for the solution of a general initial value problem for any hyperbolic system of conservation laws. So, it is not only interesting but also important to study the solution of the Riemann problem and the interaction of elementary waves of KCL. In chapter 2, we have studied the Riemann problem for the KCL when the metric g, associated with the ray coordinate ξ designating different rays, is an arbitrary function of the velocity of propagation m of the moving curve, subjected to certain assumptions. We have studied the admissible parts of the rarefaction and Hugoniot curves in the (m, θ) plane, the elementary wave solutions in the (ξ, t)-plane and defined the image of an elementary wave solution to the (x, y)-plane as *elementary shapes* of the moving curve Ω_t (or a nonlinear wavefront when interpreted in a physical system) and then we have described their geometrical properties. We have discussed the domain in which the solution of the Riemann problem exists and it has been shown that the solutions of the

Riemann problem with different initial data give the shapes of the nonlinear wavefront with different combinations of elementary shapes.

Interaction of elementary wave solutions of KCL and the geometrical features of the corresponding elementary shapes in the (x, y) plane have been studied in chapter 3. The interaction of elementary waves, when one of the elementary wave is a shock, may or may not be completed in a finite time depending on the strength of the shock. All possible types of interactions of elementary waves and the resulting shapes in the (x, y)-plane has been studied numerically using a finite element scheme called discontinuous Galerkin scheme (see Cockburn et al., 1989).

We have used the KCL to study all possible geometrical shapes of the crest-line (the line joining the highest points) of a curved solitary wave on a shallow water in chapter 4. We assume that the length of the curved solitary wave in the direction transverse to the direction of its propagation is very large compared to a length measuring the breadth of the solitary wave. This allows us to treat a section of the solitary wave by a plane perpendicular to the crest-line to be an one dimensional solitary wave and helps us to find an additional relation between the metric g and m to close the KCL and to solve the problem completely. We have studied the geometrical features of the elementary shapes in the (x, y)-plane using the analysis done in chapter 2.

A shock ray theory (SRT) developed by Monica and Prasad (2001) can be used to study the evolution of a two dimensional shock front in the case when a curved piston moves with a nonconstant velocity. The exact SRT consists of ray equations and an infinite system of compatibility conditions along these rays. However, the system of equations for successive compatibility conditions become too complex to be used. Suitable truncation of these equations in nth compatibility conditions leads to a finite system of equations which was proposed by Prasad and Ravindran (1990) and they called it *new theory of shock dynamics* (NTSD), which simplify considerably for a weak shock. Monica and Prasad (2001) first derived the compatibility conditions for SRT using WNLRT and then their suitable conservation forms to study this system numerically. In chapter 5, we have given a brief introduction to NTSD and method of deriving the governing equation for the SRT. We have modified the conservation form of the two compatibility conditions in SRT used by Monica and Prasad (2001). Our conservation forms appear to be more natural and follow a pattern which are valid for each of the infinite set of compatibility conditions for a curved shock of an arbitrary strength.

In chapter 6, we solve some two-dimensional curved piston problems showing that the SRT with two compatibility conditions gives shock position which is very close to the solution of the same problem obtained by numerical solution of Euler equations (NSEE). The comparison of the results obtained by geometrical shock dynamics (GSD) of Whitham, NSEE, and the numerical solutions obtained from SRT and WNLRT has been carried over in the case of accelerating and decelerating curved pistons. It has been shown that the results obtained by SRT agrees well with NSEE which shows that the SRT takes the acceleration and decelerating of the piston into account more effectively. The aim of this work is not just this comparison but in investigating the role of the nonlinearity in accelerating the process of evolution of a shock, produced by an explosion of a non-circular finite charge, into a circular shock front. We find that the nonlinear waves propagating on the shock front appreciably

accelerate this process. We also study the propagation of shock fronts produced by a wedge shaped piston and also a piston of periodic shape.

Finally, in chapter 7, we use the SRT to study the propagation of the leading shock front produced by a thin two dimensional aerofoil which has a sharp nose and which moves in a supersonic speed. We assume that the aerofoil is moving with a constant speed upto some time say, $t = t_0$, and from this time onwards, it starts accelerating. This problem is complicated as linear rays tend to converge to focus and form a caustic region beyond which the linear solution becomes singular. Plotkin (2002) reviewed some methods used to calculate the sonic boom signature, which consists in finding not only the leading shock but also the flow behind it. We hope that SRT combined with WNLRT, can be effectively used to solve the unsteady sonic boom problem completely and also can be used to solve the sonic boom problem in the case of a maneuvering aircraft. However, we have not calculated the full signature of the sonic boom from the wing, but the results presented in this chapter are the primary results towards this direction.

In this thesis, some basic analysis has been done for the system of kinematical conservation laws which are essential for general mathematical analysis of the system and we have applied the system to a few practical problems. Mathematical questions like existence and uniqueness of the solution of the KCL will be pursued in future and the calculation of sonic boom signature for an accelerating and any maneuvering aerofoil are our ultimate aim in future, whose basic tools are developed and presented in this thesis.

Reference

1. Whitham, G. B. (1957) A new approach to problems of shock dynamics. Part 1. Two-dimensional problems. *J. Fluid Mech.* **2**, 145 - 171.

2. Sturtevant, B. and Kulkarni, V. A. (1976) The focusing of weak shock waves, *J. Fluid Mech.* **73**, 651 - 671.

3. Prasad, P (1993) *Propagation of a curved shock and nonlinear ray theory*, Longman, Pitman Research Notes in Mathematics No. 203.

4. Morton, K. W., Prasad, P. and Ravindran, R., (1992) Conservation forms of nonlinear ray equation, Tech. Rep. 2, Dept. of Mathematics, Indian Institute of Science.

5. Prasad, P and Sangeeta, K. (1999) Numerical simulation of converging nonlinear wavefronts, *J. Fluid Mech.* **385**, 1 - 20.

6. Prasad, P., (2001) *Nonlinear hyperbolic waves in multi-dimensions*, Chapman and Hall/CRC, Monographs and Surveys in Pure and Applied Mathematics - 121.

7. Cockburn, B., San Yih-Lin and Shu, (1989), TVB Runge-Kutta local projection discontinuous Galerkin finite element method for conservation laws III: One dimensional systems, *J. Compu. Phys.* **84** (1), 90 - 113.

9. Monica, A. and Prasad, P., (2001), Propagation of a curved weak shock, *J. Fluid Mech.*, **434**, 119 - 151.

8. Ravindran, R. and Prasad, P. (1990) A new theory of shock dynamics, Part - 1: Analytical consideration, *Appl. Math. Letters* **3**, 107 - 109.

10. Plotkin, K. J., (2002) State of the art of sonic boom modeling, *J. Acoust. Soc. Am.* **111** (1), 530 - 536.

Abstract

Experimental study of Sturtevant and Kulkarni (1976) and theoretical study of Whitham (1957) (Geometrical Shock Dynamics (GSD)) shows that there are nonlinear waves propagating on the shock front that makes the amplitude of the shock in the focal region to be finite and instead of folding of the shock front, which occurs in the linear ray theory, we get a discontinuity in the slope of the shock front, called a *kink* (called *shock-shock* by Whitham). Kink is basically a geometrical phenomena, which appears as the image in (x, y)-plane of a shock in the solution of *kinematical conservation laws* (KCL) (Morton, Prasad and Ravindran, 1993) in an appropriately defined ray coordinate system. KCL is an underdetermined system, which has three unknowns and two equations. Therefore an additional equation or relation is required to make the system closed. The thesis first deals with a mathematical analysis of the KCL with a simple additional closure relation (Weakly nonlinear ray theory (WNLRT)) that appears to be physically realistic for a class of problems and then goes in to the applications of KCL to some problems including the propagation of a curved shock (Shock ray theory (SRT)) where more general closure equations are required.

The thesis consists of seven chapters. Chapter 1 starts with a motivation for the work. A brief introduction to the WNLRT and the derivation of the KCL has been presented. KCL is hyperbolic in nature under certain conditions and so we quote some results and definitions regarding hyperbolic systems.

In chapter 2, we have studied the Riemann problem for the KCL in a general form. We have studied the admissible parts of the rarefaction and Hugoniot curves in the (m, θ) plane, the elementary wave solutions in the (ξ, t)-plane and defined the image of an elementary wave solution to the (x, y)-plane as *elementary shapes* of the moving curve Ω_t (or a nonlinear wavefront when interpreted in a physical system) and then we have described their geometrical properties. We have discussed the domain of right states in which the solution of the Riemann problem exists. Interaction of elementary wave solutions of KCL and the geometrical features of the corresponding elementary shapes in the (x, y) plane have been studied in chapter 3. We have used the KCL to study all possible geometrical shapes of the crest-line (the line joining the highest points) of a curved solitary wave on shallow water in chapter 4.

In chapter 5, we have given a brief introduction to NTSD and method of deriving the governing equation for the SRT. In chapter 6, we solve some two-dimensional curved piston problems showing that the SRT with two compatibility conditions gives shock position, which is very close to the solution of the same problem obtained by numerical solution of Euler equations (NSEE). The comparison of the results obtained by geometrical shock dynamics (GSD) of Whitham, NSEE, and SRT shows that the results from SRT is more accurate when compared to GSD results. This shows that the SRT takes into account of the flow behind the shock more effectively. Finally, in chapter 7, we gave a brief note on the focused sonic boom produced by an accelerating aircraft and we hope that SRT combined with WNLRT, can be effectively used to solve this problem.

Contents

1 Introduction **1**

1.1 Motivation 1

1.2 Hyperbolic Partial Differential Equations 5

1.2.1 Quasi-linear Equations 5

1.2.2 Conservation Laws 6

1.2.3 Admissible Solutions 8

1.2.4 Riemann Invariants and Simple Waves 10

1.2.5 Genuine Nonlinearity and Linear Degeneracy 12

1.3 Kinematical Conservation Laws (KCL) 13

1.4 Weakly Nonlinear Ray Theory (WNLRT) 15

1.5 Author's Contribution 17

2 Riemann Problem for Kinematical Conservation Laws **21**

2.1 Introduction 21

2.2 Basic Equations, Riemann Invariants and Jump Relations 22

2.3 Elementary Wave Solutions 25

2.4 Geometrical Features Arising Out of Elementary Waves: Elementary Shapes 33

2.5 Geometrical Shapes Arising Out of a General Singularity on Ω_t 39

3 Interaction of Elementary Shapes **43**

3.1 Introduction 43

3.2 Interaction of Elementary Shapes 44

3.2.1 Interaction of Elementary Shapes From Different Family 45

3.2.2 Interaction of Elementary Shapes From Same Family 51

4 Kinematical Conservation Laws Applied to Study Geometrical Shapes of a Solitary Wave 63

4.1 Introduction 63

4.2 Multi-Dimensional KdV Equation 65

4.3 Equation for the Average Flux of Energy 67

4.4 Geometrical Shapes of the Crest-Line 70

5 Shock Ray Theory 77

5.1 Introduction 77

5.2 New Theory of Shock Dynamics 78

5.3 Governing Equations of SRT 81

5.4 Conservation Form of the Equations of SRT 83

6 Propagation of Curved Shock Fronts Using Shock Ray Theory and Comparison With Other Theories 87

6.1 Introduction 87

6.2 Initial Conditions for SRT Equations for a Piston Problem 89

6.3 Other Theories 91

6.4 Piston Problem When the Shape of the Piston is a Wedge 94

6.5 Blast Wave From a Square Shaped Container 98

6.6 Shock Produced by a Wavy Piston 113

7 A Note on Application of Shock Ray Theory to Sonic Boom 117

7.1 Introduction 117

7.2 Physical Problem 120

Appendix 1 **121**

0.1 Discontinuous Galerkin Method in One Space Dimension 121

0.2 Multi-Dimensional Case: Dimensional Splitting Method 127

0.3 Inhomogeneous Equations: Source Term Splitting Method 128

0.4 Implementation Details 129

References **131**

Chapter 1

Introduction

§1.1 **Motivation**

Nonlinear wave propagation has been a challenging problem for more than a century. Study of nonlinear wave propagation started in the middle of nineteenth century with the work of Stokes (1848) and Riemann (1860). Soon after the outbreak of second world war, mathematical study of wave propagation in gases became more vigorous. Courant and Friedrichs (1948) reviewed almost all early works in this field. Lax (1954, 1957 and 1973) and Oleinik (1957) gave a complete mathematical theory for hyperbolic conservation laws and shocks, from which this field has grown into one of the most active research area today.

The main complexity in the nonlinear hyperbolic partial differential equations, which governs a class of nonlinear wave propagation is the existence of shocks in the solution. Their nonlinearity generally forbids the existence of global classical solutions. Also, the strong coupling between the different modes of waves, which appears due to nonlinearity present in the case of a system of hyperbolic equations, restrict considerably the tools used for the study of single hyperbolic equation. Hence efforts has been made towards building approximate methods to solve such problems. Numerical method of solving hyperbolic equations is more used in applications. Attempts to solve multi-dimensional nonlinear wave propagation is new and there is almost a complete lack of theory for global solutions. In applications like the prediction of sonic boom signature in the far field, it will be more expensive and almost impossible today to do full numerical computation without a massive parallelization even for mid-field prediction (A. Pilon and A. Lyrintzis, 1995). In certain other applications like extracorporeal shock wave lithotripsy to treat kidney stone disease, we need to study the shape of the leading shock fronts in order to

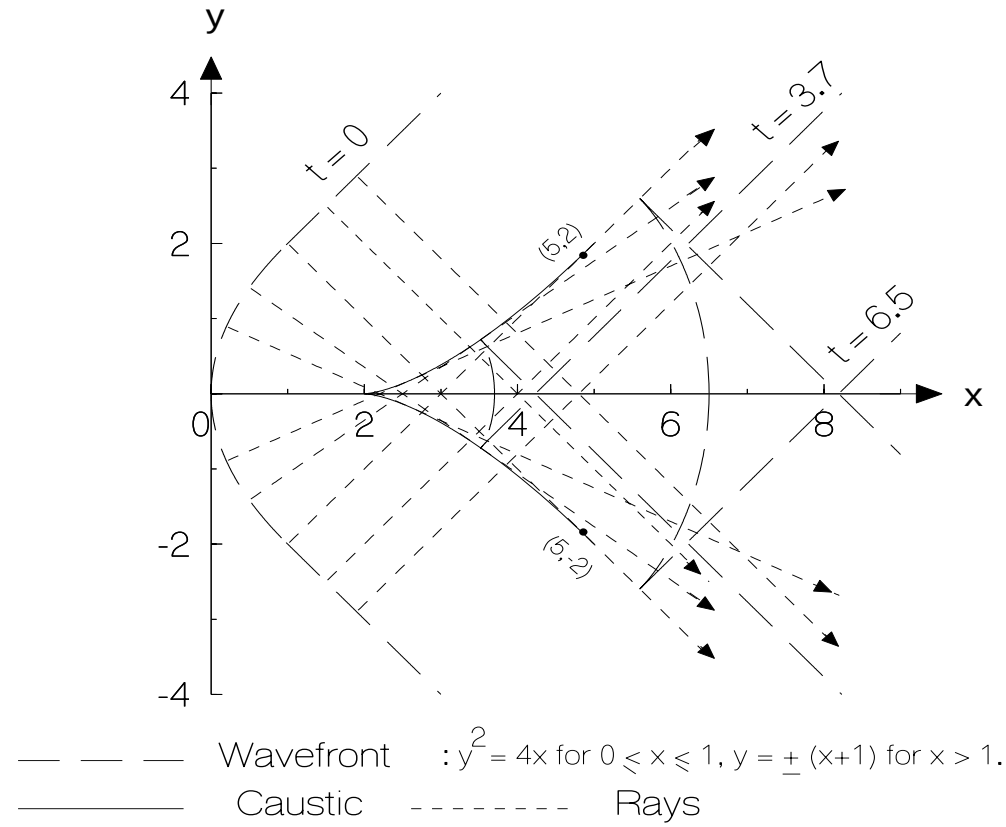

Fig. 1.1.1: *Successive positions of a linear wavefront in an isotropic homogeneous medium.*

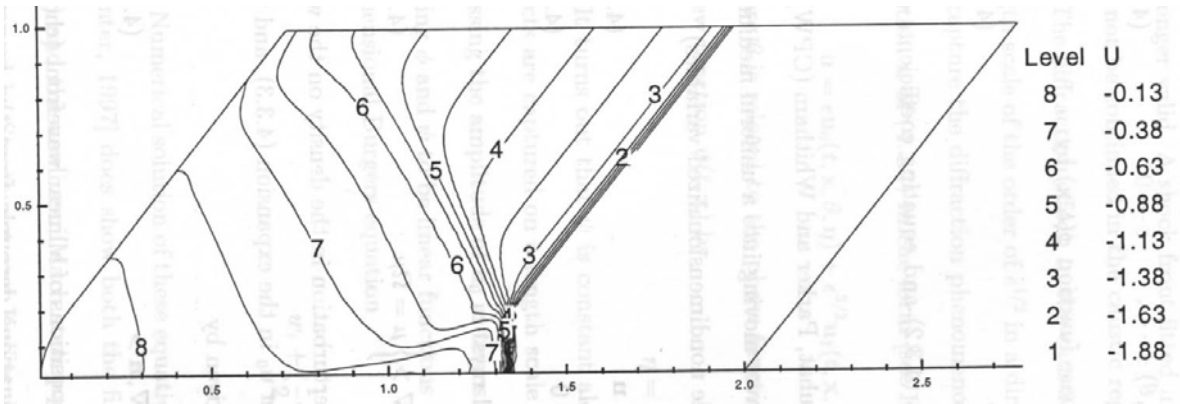

Fig 1.1.2: *Formation of Kink from direct numerical simulation (Monica and Prasad 2000)*

minimize the injuries caused by the shock front to the neighbouring parts of the kidney (Sturtevant, 1989). In this application, since we need only the position and the shape of the shock front, it is not necessary to go for the details of the complete flow field behind the shock by a full numerical simulation of gas dynamics equations. Hence, certain other approximation theories, apart from numerical methods have been developed in order to overcome such difficulties. One such theory is the ray theory which has been used extensively in acoustics.

Early work on ray theory in acoustics starts with Fermat's principle which is called as *acoustic ray theory* or *linear ray theory*. If the wave propagation is assumed to be in a homogeneous isotropic medium, then the linear rays are just straight lines which are orthogonal to the wavefront at a given time. For more details on this topic and the relation between Fermat's principle and another well known result on wavefront construction namely, Huygen's method, we refer to Prasad (2001). The classical ray theory is simple and easy to implement in practical problems. But the main disadvantage with this linear theory is that, we cannot find the solution for a long time because of the converging rays, which form a focal region bounded by an envelop of converging rays called *caustic* (see Prasad, 2001 for more details), beyond which the linear wavefront folds and forms a cusp type of singularity as shown in Fig. 1.1.1. This behaviour is not observed in many experimental datas (Sturtevant and Kulkarni, 1976) and solution from full numerical simulations (see Fig. 1.1.2) where the nonlinear diffraction effects play major role at the caustic in order to reduce the focal intensity, so that the solution remains finite. This shows that the linear ray theory fails in such cases. Thus, a ray theory which can take into account of the nonlinear diffraction effects is necessary to handle such problems.

Whitham (1957, 1959) introduced a theory of shock dynamics in which the geometrical and a part of the nonlinear effects play a dominant role. This theory is derived on the basis of intuitive geometrical arguments and it is also called as *geometrical shock dynamics* (GSD). This theory does not properly take into account the interaction of the shock with the flow behind it, which is also an important nonlinear effect. However, this theory gives good results in certain particular problems and hence this theory is being widely used in applications with suitable modifications (see Henshaw, Smyth and Schwendeman, 1986, Schwendeman and Whitham 1987, Schwendeman, 2002, Betelu and Aronson 2001, N. Apazidis, et. al., 2002).

Prasad (1975, 1993, 2001) derived the nonlinear shock ray equations, one derivation of which uses extended Fermat's principle. It also uses conservation of energy along a ray tube to derive the transport equation for the amplitude along the nonlinear rays. He worked out the theory for small amplitude in an isotropic medium which is valid in high

frequency limit. This leads to a set of coupled equations for rays and the amplitude and is called *weakly nonlinear ray theory* (WNLRT). Similarly, there exists a *shock ray theory* (SRT) for a shock of arbitrary strength, it consists of a system of equations of shock rays derived from a shock manifold partial differential equation (Prasad, 1993) and an infinite system of compatibility conditions along a shock ray (Grinfel'd, 1978 and Maslov 1980). The infinite system of transport equations can be truncated leading to a *new theory of shock dynamics* (NTSD) by Ravindran and Prasad (1990), which turns out to be quite simple looking with two compatibility conditions (Prasad 1993). The conservation form of these two compatibility conditions has been obtained by Monica and Prasad (2000) (see also Prasad, 2001). The governing equations of the SRT for a weak shock can also be obtained from the equations of WNLRT, derived under short wave or high frequency assumption. We present a brief sketch of the NTSD for scalar conservation laws in section 5.2 and the derivation of SRT for a weak shock using WNLRT in section 5.3.

Under the weak shock assumption, a part of the basic governing equations of propagation of the shock front under GSD and SRT, and a wavefront under WNLRT discussed above are the same and a physically realistic conservation form of the equations has been derived by Morton, Prasad and Ravindran (1992) which are called as *kinematical conservation laws* (KCL). KCL actually governs the evolution of any propagating curve in two dimensions. A brief sketch of the derivation of the KCL has been presented in the section 1.3. A detailed derivation of the system is given in the recent book by Prasad (2001). When GSD was proposed and extensively used, the KCL had not been found. However, by GSD, we shall mean a part of its original equations in the form of KCL.

The KCL is a 2×2 system with three unknowns. Hence, we need one more equation or a system of equations or in simplest case a relation between the unknowns in order to make the system determined. The above three theories (WNLRT, GSD and SRT) differ in this additional relation (or equations) and hence the solutions also differ. It is important to have a knowledge of which theory works efficiently in applications and the limitations of their usages. Also, to apply the KCL in practical applications, we need to analyze the solutions mathematically in order to have a better understanding of the numerical results obtained from the theories. In this thesis, we do some necessary mathematical analysis, obtain some comparison results and present a few applications of KCL.

The KCL, with additional relation(s) to form WNLRT, GSD and SRT are hyperbolic when the Mach number of the wavefront or shock front is greater than 1. So, we present in section 1.2 some basic definitions and properties of the general hyperbolic system of conservation laws which are used frequently in this thesis. A brief discussion of the derivation of the KCL and WNLRT has been presented in the sections 1.3 and 1.4, respectively.

§1.2 Hyperbolic Partial Differential Equations

§1.2.1 Quasi-linear Equations

Let Ω be an open subset of $\mathbb{R}^n$. A quasi-linear system of first order partial differential equations takes the form

$$\frac{\partial \boldsymbol{u}}{\partial t} + \sum_{j=1}^{m} A_j \frac{\partial \boldsymbol{u}}{\partial x_j} = \boldsymbol{S}(\boldsymbol{u}, \boldsymbol{x}, t), \tag{1.2.1}$$

where $\boldsymbol{x} \in \mathbb{R}^m$, $t \in \mathbb{R}^+$, $\boldsymbol{u} = (u_1, ..., u_n)^T \in \Omega$, $A_j = A_j(\boldsymbol{u}, \boldsymbol{x}, t)$ $(j = 1, 2, ..., m)$ is an $n \times n$ real matrix and $\boldsymbol{S}$ is a source function.

The condition for hyperbolicity of the system (1.2.1), when A_j $(j = 1, 2, ..., m)$ is independent of $\boldsymbol{u}$ (i.e., in the case of linear systems), can be motivated (for $\boldsymbol{S} = 0$) by the existence of simple wave-like solution of the form

$$\boldsymbol{u} = \boldsymbol{u}_0 e^{i\phi(\boldsymbol{x},t)}, \tag{1.2.2}$$

for a real valued function $\phi(\boldsymbol{x}, t)$ and a constant $\boldsymbol{u}_0 \in \mathbb{R}^n$. A surface $\phi(\boldsymbol{x}, t) =$ constant $= \phi_0$ (say), is called as a *Characteristic Surface*.

Substituting (1.2.2) in (1.2.1) with the assumption that A_j's are independent of $\boldsymbol{u}$ and $\boldsymbol{S} = 0$, we get

$$\left[\phi_t I + \sum_{j=1}^{m} A_j \phi_{x_j}\right] \boldsymbol{u}_0 = 0, \tag{1.2.3}$$

where I is the $n \times n$ identity matrix. Thus, a linear system of the form (1.2.1) with $\boldsymbol{S}$ =0 admits a wave-like solution of the form (1.2.2), if the equation (1.2.3) admits non-trivial solutions for $\boldsymbol{u}_0$. This will be the case when

$$det \left| \phi_t I + \sum_{j=1}^{m} A_j \phi_{x_j} \right| = 0. \tag{1.2.4}$$

Given ϕ_{x_j} $(j = 1, 2, ..., m)$, the equation (1.2.4) admits at most n real solutions $\phi_t^{(\alpha)}$ $(\alpha = 1, 2, ..., n)$ and there are at most n real linearly independent eigenvectors $\boldsymbol{u}_0$. Given a solution ϕ of the equation (1.2.4), $\phi_t^{(\alpha)}$ and the gradient vector $\nabla\phi^{(\alpha)}$ gives the speed and the direction of propagation, respectively, of a wavefront Ω_t generating the characteristic surface $\phi^{(\alpha)}(\boldsymbol{x}, t) =$ constant. Hence, for describing a propagation phenomenon in space and time, if we need maximum freedom for waves then, given $\nabla\phi^{(\alpha)}$ we must have not only n real $\phi_t^{(\alpha)}(\alpha = 1, 2, .., n)$ but also n linearly independent eigenvectors $\boldsymbol{u}_0$. In a 'physical' sense, a system of hyperbolic partial differential equations will be associated

with n independent propagating waves and that the behaviour and properties of the physical system described by these equations will be dominated by wave-like phenomena.

Equation (1.2.4) is called the *Eikonal equation* and the characteristic curves of this first order partial differential equation is called as the *bicharacteristic curve* for (1.2.1). For a quasi-linear system, the equations (1.2.3) and (1.2.4) should be satisfied at each point of Ω.

We now define the hyperbolicity of the system (1.2.1) mathematically.

1.2.1. Definition The system of quasi-linear equations (1.2.1) is called *hyperbolic* if, for any $\boldsymbol{n} = (n_1, n_2, ..., n_m) \in I\!R^m$, $\boldsymbol{n} \neq 0$, and for $\boldsymbol{u} \in \Omega$ and $(\boldsymbol{x}, t) \in I\!R^{m+1}$, the matrix

$$A(\boldsymbol{u}, \boldsymbol{x}, t, \boldsymbol{n}) = \sum_{j=1}^{m} n_j A_j(\boldsymbol{u}, \boldsymbol{x}, t) \tag{1.2.5}$$

has n real eigenvalues $\lambda_1(\boldsymbol{u}, \boldsymbol{x}, t, \boldsymbol{n}) \leq \lambda_2(\boldsymbol{u}, \boldsymbol{x}, t, \boldsymbol{n}) \leq ... \leq \lambda_n(\boldsymbol{u}, \boldsymbol{x}, t, \boldsymbol{n})$ and n linearly independent corresponding eigenvectors $\boldsymbol{r}_1(\boldsymbol{u}, \boldsymbol{x}, t, \boldsymbol{n}), \boldsymbol{r}_2(\boldsymbol{u}, \boldsymbol{x}, t, \boldsymbol{n}), ..., \boldsymbol{r}_n(\boldsymbol{u}, \boldsymbol{x}, t, \boldsymbol{n})$. The system (1.2.1) is said to be *strictly hyperbolic* if all the n eigenvalues are distinct.

§1.2.2 Conservation Laws

Let us consider the equation (1.2.1) together with an initial data

$$\boldsymbol{u}(x, 0) = \boldsymbol{u}_0(x), \tag{1.2.6}$$

where $\boldsymbol{u}_0 : I\!R^m \to \Omega$.

A very well known result of the hyperbolic system of quasi-linear equations (1.2.1) is that, even for a smooth initial data $\boldsymbol{u}_0$, the solution of the initial value problem (1.2.1) and (1.2.6) may develop jump discontinuities after a finite time (see Prasad, 2001). Thus, we need to look for the solutions of such initial value problems in the class of discontinuous functions, interpreting the equations (1.2.1) in distribution sense. For simplicity in the following discussion, we take A's and $\boldsymbol{S}$ in (1.2.1) to be functions of $\boldsymbol{u}$ only.

If $\boldsymbol{u}$ has a jump discontinuity, then since the left hand side of (1.2.1) contains the product of a discontinuous function $A(\boldsymbol{u})$ with the distributional derivative $\partial \boldsymbol{u}/\partial x_j$ ($j = 1, 2, ..., m$), which in this case contains a Dirac mass at the point of discontinuity, it is not well-defined (see Kesavan, 1989). Thus, if we are looking for the solutions of the IVP (1.2.1) and (1.2.6) in the class of discontinuous functions, we can no longer work with the equation of the form (1.2.1) and we have to rewrite it in the *divergence form*

$$\frac{\partial \boldsymbol{u}}{\partial t} + \sum_{j=1}^{m} \frac{\partial}{\partial x_j} \boldsymbol{f}_j(\boldsymbol{u}) = \boldsymbol{S}(\boldsymbol{u}), \tag{1.2.7}$$

where $\boldsymbol{f}_j$, j=1,2, .. ,m, called as *flux*, are m smooth functions from Ω into $I\!R^n$, in such a way that

$$\left(\frac{\partial f_{ij}(\boldsymbol{u})}{\partial u_k}\right)_{1\leq i,k\leq n} = A_j(\boldsymbol{u}),\ j = 1, 2, ..., m. \tag{1.2.8}$$

Not all equations (1.2.1) can be written in the conservation form (1.2.7).

The system (1.2.7) is called as the system of *balance laws* and when $\boldsymbol{S} = 0$, it is called as the system of *conservation laws*. If the corresponding quasi-linear form (1.2.1) of the balance law (1.2.7) is hyperbolic as defined in the definition 1.2.1, then the system (1.2.7) is called as *hyperbolic system of balance laws* (or *conservation laws* if $\boldsymbol{S} = 0$).

1.2.2. Definition[1] A function $\boldsymbol{u} \in (L^\infty_{loc}(I\!R^m \times I\!R^+))^n$ is called as *weak solution* of the initial value problem (1.2.7) and (1.2.6) with $\boldsymbol{u}_0 \in (L^\infty_{loc}(I\!R^m))^n$, if

$$\int_{I\!R^m}\int_{t\geq 0}\left(\boldsymbol{u}\cdot\frac{\partial\boldsymbol{\phi}}{\partial t} + \sum_{j=1}^{m}\boldsymbol{f}_j(\boldsymbol{u})\cdot\frac{\partial\boldsymbol{\phi}}{\partial x_j}\right)d\boldsymbol{x}dt + \int_{t=0}\boldsymbol{u}_0\cdot\boldsymbol{\phi}(\boldsymbol{x},0)d\boldsymbol{x} = \int_{I\!R^m}\int_{t\geq 0}\boldsymbol{S}(\boldsymbol{u})\cdot\boldsymbol{\phi}d\boldsymbol{x}dt, \tag{1.2.9}$$

for all $\phi \in (C^1_0(I\!R^m \times I\!R^+))^n$.

With the notion of weak solution defined by the above definition, we shall consider solutions of (1.2.7) in the sense of distributions that are only piecewise smooth [2]. In other words, we can look for the solutions of (1.2.7) in the class of discontinuous functions. The following theorem (Godlewski and Raviart, 1996) shows that not every discontinuity is admissible.

1.2.1. Theorem Let $\boldsymbol{u} : I\!R^m \times I\!R^+ \to \Omega$ be a piecewise smooth function which has a jump discontinuity across a surface $\Sigma \in I\!R^{m+1}$. Then, $\boldsymbol{u}$ is a weak solution for the IVP (1.2.7) and (1.2.6) if and only if the following two conditions are satisfied:

1. $\boldsymbol{u}$ is a classical solution of the IVP (1.2.1) and (1.2.6) in the domain where $\boldsymbol{u}$ is smooth;
2. $\boldsymbol{u}$ satisfies the jump condition

$$(\boldsymbol{u}_r - \boldsymbol{u}_l)\boldsymbol{\omega}_t + \sum_{j=1}^{m}(\boldsymbol{f}_j(\boldsymbol{u}_r) - \boldsymbol{f}_j(\boldsymbol{u}_l))\boldsymbol{\omega}_{x_j} = 0 \tag{1.2.10}$$

along the surface of discontinuity Σ.

---

[1]For the definition of spaces L^∞_{loc}, C^1_0, C^∞_0 etc., we refer to Kesavan, 1989.

[2]By *piecewise smoothness* of a function $\boldsymbol{u}$, we mean that $\boldsymbol{u}$ is smooth everywhere in $I\!R^m \times I\!R^+$, but for a finite number of smooth orientable surfaces across which $\boldsymbol{u}$ has a jump discontinuity.

Here, for a point $(\boldsymbol{x}, t) \in \Sigma$

$$\boldsymbol{u}_r(\boldsymbol{x}, t) = lim_{\epsilon \to 0,\ \epsilon > 0} \boldsymbol{u}((\boldsymbol{x}, t) + \epsilon \boldsymbol{\omega}), \tag{1.2.11}$$

$$\boldsymbol{u}_l(\boldsymbol{x}, t) = lim_{\epsilon \to 0,\ \epsilon > 0} \boldsymbol{u}((\boldsymbol{x}, t) - \epsilon \boldsymbol{\omega}), \tag{1.2.12}$$

where $\boldsymbol{\omega} = (\omega_t, \omega_{x_1}, ..., \omega_{x_n})(\neq 0)$ is the normal vector to the surface Σ.

1.2.3. Definition The jump relation (1.2.10) is known as *Rankine-Hugoniot (R-H) condition.*

§1.2.3 Admissible Solutions

The class of discontinuous functions is too large that we may have more than one weak solution for an initial value problem (see Smoller, 1983 and Prasad, 2001). Thus, we need an additional condition to single out one physically realistic solution out of the class of weak solutions. This physically realistic solution is commonly known as the *admissible solution* or the *entropy solution* and the condition imposed on this solution is called as the *admissible condition* or the *entropy condition.* A discontinuity, if any, in such a solution is called a *shock.* There are at least three admissible conditions which we will state below. In what follows, we will take $\boldsymbol{S} = 0$ in the equation (1.2.7).

Admissibility Condition 1

This admissibility condition commonly known as *Lax Entropy Condition* is due to Lax (1957) and is useful because it can be verified easily.

1.2.4. Definition A discontinuity in a weak solution of (1.2.7) (with $\boldsymbol{S} = 0$) is said to satisfy *Lax Entropy Condition* if there exist an index $k \in \{2, ..., n-1\}$ such that

$$\lambda_k(\boldsymbol{u}_r) \leq s \leq \lambda_k(\boldsymbol{u}_l), \tag{1.2.13}$$

where s is the speed of propagation of the shock and λ_k $(k = 1, 2, ..., n)$ are the n eigen values of the system (1.2.7). For $k = 1$ and n, it has to be modified. A weak solution having discontinuities, of which satisfy this entropy condition, is called the *admissible solution.* The Lax entropy condition can be easily generalized to the case $m > 1$. A discontinuity, which satisfies (1.2.13) with strict inequality on both sides, is called a *shock.*

Admissibility Condition 2

The next admissibility condition comes from *vanishing viscosity method.*

Given a small parameter $\epsilon > 0$, we associate with the system (1.2.7) (with $\boldsymbol{S} = 0$), the parabolic system

$$\frac{\partial \boldsymbol{u}_\epsilon}{\partial t} + \sum_{j=1}^{m} \frac{\partial}{\partial x_j} \boldsymbol{f}_j(\boldsymbol{u}_\epsilon) = \epsilon \Delta \boldsymbol{u}_\epsilon, \tag{1.2.14}$$

$$\boldsymbol{u}_\epsilon(\boldsymbol{x}, 0) = \boldsymbol{u}_{0_\epsilon}(\boldsymbol{x}). \tag{1.2.15}$$

We assume that $\boldsymbol{u}_{0_\epsilon}(\boldsymbol{x}) \to \boldsymbol{u}_0(\boldsymbol{x})$ as $\epsilon \to 0$ in an appropriately defined sense. We also assume that the system (1.2.14)-(1.2.15) have sufficiently smooth solution $\boldsymbol{u}_\epsilon$ (see Goodman and Xin, 1992 for the existence of $\boldsymbol{u}_\epsilon$). Then the weak solution $\boldsymbol{u}$ of (1.2.7) (with $\boldsymbol{S} = 0$) is admissible if $\boldsymbol{u}_\epsilon \to \boldsymbol{u}$ as $\epsilon \to 0$ (in an appropriately defined sense).

Admissible Condition 3

1.2.5 Definition Assume that Ω is convex. Then, a convex function $q : \Omega \to I\!R$ is called an *entropy* for the system of conservation laws (1.2.7) (with $\boldsymbol{S} = 0$) if there exist n functions $\eta_j : \Omega \to I\!R$, $j = 1, 2, ..., n$, called *entropy flux*, such that the relations

$$\nabla q \left(\frac{\partial f_{ij}}{\partial u_k} \right)_{1 \le i,k \le n} = \nabla \eta_j^T, \quad j = 1, 2, ..., m \tag{1.2.16}$$

holds. We call (q, η) the *entropy pair* for the system (1.2.7) (with $\boldsymbol{S} = 0$).

A weak solution $\boldsymbol{u}$ of (1.2.7) (with $\boldsymbol{S} = 0$) is said to be *admissible* if there exist an entropy q and entropy flux η_j, such that the inequality

$$\frac{\partial}{\partial t} q(\boldsymbol{u}) + \sum_{j=1}^{m} \frac{\partial}{\partial x_j} \eta_j(\boldsymbol{u}) \le 0 \tag{1.2.17}$$

is satisfied in the sense of distributions on $I\!R^m \times I\!R^+$, which means that for any function $\phi \in C_0^\infty(I\!R^m \times I\!R^+)$, $\phi \ge 0$, we have

$$\int_0^\infty \int_{I\!R^m} \left(q(\boldsymbol{u}) \frac{\partial \phi}{\partial t} + \sum_{j=1}^{m} \eta_j(\boldsymbol{u}) \frac{\partial \phi}{\partial x_j} \right) d\boldsymbol{x} dt \ge 0.$$

The inequality (1.2.17) is often called as *entropy condition*.

In the scalar one-dimensional case, when the flux function $\boldsymbol{f}$ is strictly convex, then it can be proved that the Lax entropy condition (1.2.13) is equivalent to the entropy inequality (1.2.17) (Godlewski and Raviart, 1991).

It is conjectured that an entropy solution of (1.2.7) exists and is necessarily unique. In the scalar case, this has been proved by Kruzkov (1970). This conjecture is still widely open in the case of system ($n \ge 2$). However, the question of existence and uniqueness has been answered up to some extent on some special systems with additional properties,

especially in the case of one dimensional 2×2 systems such as p-system. The advantage with such systems are that their properties can be analyzed in view of the existence of Riemann invariants (see section 1.2.4 for the definition) and a family of entropy functions (see Glimm and Lax, 1970, Lax, 1973, Smoller, 1983, DiPerna, 1983(a, b)). The system of $n \geq 2$ chromatographic equations, (James, Peng and Perthame, 1995), is another example for such systems. The difficulty of analyzing general systems of conservation laws is demonstrated by a negative result due to Temple (1985). Stability and large time behaviour of the solution of the system (1.2.7) are yet other challenging problems. In this thesis, we don't deal much with the stability and large time behaviour and so, we don't make any remarks on these topics. For more details, we refer to the recent work by Bressan, Liu and Yang (1999). However, in Chapter 3, we have some simple results on the behaviour of the solution as $t \to \infty$ when two elementary waves interact.

§1.2.4 Riemann Invariants and Simple Waves

In this section, we consider the hyperbolic conservation law

$$\frac{\partial \boldsymbol{u}}{\partial t} + \frac{\partial \boldsymbol{f}(\boldsymbol{u})}{\partial x} = 0 \tag{1.2.18}$$

in two independent variables (x, t) for the sake of simplicity. It is well known that in the case of a one dimensional scalar conservation law, the conserved quantity u can be shown to be constant along the characteristics. Whereas, this result cannot be expected in a general system of conservation laws (1.2.8), but we may find a function w of $\boldsymbol{u}$ associated with a characteristic field such that it is constant along the characteristic curves corresponding to an eigenvalue λ.

Suppose that the gradient $\nabla_u w$ of the function $w(\boldsymbol{u})$ is parallel to the left eigenvector of an eigenvalue λ, then we have

$$\sum_{i=1}^{n} A_{ij} \frac{\partial w}{\partial u_i} = \lambda \frac{\partial w}{\partial u_j}. \tag{1.2.19}$$

In what follows, we take $m = 1$. Let the characteristic curve corresponding to the eigenvalue λ be given by $t = t(s),\ x = x(s)$, with $dt/ds = 1$ and $dx/ds = \lambda$, then from (1.2.19) we have

$$\begin{aligned}
\frac{\partial w}{\partial s} &= \sum_{i=1}^{n} \frac{\partial w}{\partial u_i} \frac{\partial u_i}{\partial s} = \sum_{i=1}^{n} \frac{\partial w}{\partial u_i} \left(\frac{\partial u_i}{\partial t} + \lambda \frac{\partial u_i}{\partial x} \right) \\
&= \sum_{i=1}^{n} \frac{\partial w}{\partial u_i} \left(-\sum_{j=1}^{n} A_{ij} \frac{\partial u_j}{\partial x} + \lambda \frac{\partial u_i}{\partial x} \right) \\
&= -\sum_{j=1}^{n} \lambda \frac{\partial w}{\partial u_j} \frac{\partial u_j}{\partial x} + \sum_{i=1}^{n} \lambda \frac{\partial w}{\partial u_i} \frac{\partial u_i}{\partial x} = 0.
\end{aligned}$$

This shows that if the equation (1.2.19) is satisfied, then the function w is constant along the characteristic curves corresponding to the eigenvalue λ. This function w is called a *characteristic variable.*

For the study of simple waves associated with a specific characteristic family, we need an important concept which we will introduce in the following

1.2.6. Definition A smooth function $\pi : \Omega \to I\!R$ is called an *i-Riemann invariant* $(i = 1, 2, ..., n)$ of the system (1.2.18), if it satisfies

$$\nabla\pi(\boldsymbol{u}) \cdot \boldsymbol{r}_i(\boldsymbol{u}) = 0, \text{ for all } \boldsymbol{u} \in \Omega, \tag{1.2.20}$$

where $\boldsymbol{r}_i$ $(i = 1, 2, ..., n)$ are the right eigen vectors of the system (1.2.18).

We note from the theory of quasi-linear partial differential equations, that there are $(n-1)$ i-Riemann invariants whose gradients are linearly independent. Riemann invariants are particularly useful in systems with the special structure that the n scalar valued functions $(\pi_1, ..., \pi_n)$ on Ω for any i and $j = 1, ..., n$ with $i \neq j$, where each π_j is an i-Riemann invariant and $\pi_i = w$ is the corresponding characteristic variable, forms a *co-ordinate system* for the system (1.2.18). It can be proved (see C. M. Dafermos, 2000) that when the system (1.2.18) possesses a coordinate system $(\pi_1, ..., \pi_n)$ of Riemann invariants, the map that carries $\boldsymbol{u}$ to $(\pi_1, ..., \pi_n)$ is locally a diffeomorphism.

Consider an initial data which has constant states $\boldsymbol{u}_l$ for $\boldsymbol{x} < 0$ and $\boldsymbol{u}_r$ for $\boldsymbol{x} > 0$ with a jump discontinuity at a point $x = 0$. The equation (1.2.18) along with this initial data is invariant under a transformation $x \to \alpha x$, $t \to \alpha t$, $\alpha =$ constant. Hence, the solution of this initial value problem will be in the self-similar form,

$$\boldsymbol{u}(x, t) = \boldsymbol{v}\left(\frac{x}{t}\right). \tag{1.2.21}$$

1.2.7. Definition A self-similar continuous weak solution of the form

$$\boldsymbol{u}(x, t) = \begin{cases} \boldsymbol{u}_l, & \text{if } \frac{x}{t} \leq \lambda_i(\boldsymbol{u}_l), \\ \boldsymbol{v}\left(\frac{x}{t}\right), & \text{if } \lambda_i(\boldsymbol{u}_l) \leq \frac{x}{t} \leq \lambda_i(\boldsymbol{u}_r) \\ \boldsymbol{u}_r, & \text{if } \frac{x}{t} \geq \lambda_i(\boldsymbol{u}_r) \end{cases} \tag{1.2.22}$$

is called a *i-centered simple wave* or a *i-centered rarefaction wave* connecting the states $\boldsymbol{u}_l$ and $\boldsymbol{u}_r$. A centered rarefaction wave is a particular case of more general rarefaction waves.

1.2.2 Theorem In a i-centered rarefaction wave, all i-Riemann invariants are constant.

Proof: Let $\boldsymbol{u}$ be a i-rarefaction wave of the form (1.2.22), and let π be a i-Riemann invariant. Since, $\boldsymbol{u}$ is continuous and π is assumed to be a smooth function, the function

$\pi(\boldsymbol{u}) : (x,t) \to \pi(\boldsymbol{u}(x,t))$ is continuous for $t > 0$. Obviously, $\pi(\boldsymbol{u})$ is constant for $x/t \le \lambda_i(\boldsymbol{u}_l)$ and $x/t \ge \lambda_i(\boldsymbol{u}_r)$.

We now claim that π is constant in $\lambda_i(\boldsymbol{u}_l) \le x/t \le \lambda_i(\boldsymbol{u}_r)$. Let $\xi = x/t$.

$$\frac{d}{d\xi}\pi(\boldsymbol{u}(x,t)) = \nabla_u \pi(\boldsymbol{v}(\xi)) \cdot \boldsymbol{v}'. \tag{1.2.23}$$

Substituting (1.2.21) in the equation (1.2.18), we get

$$(A(\boldsymbol{v}(\xi)) - \xi I)\boldsymbol{v}'(\xi) = 0,$$

where A is defined in (1.2.8) with $j = 1$. The above equation implies that either $\boldsymbol{v}'(\xi) = 0$ or $\boldsymbol{v}'(\xi)$ is parallel to the corresponding right eigenvector. In both the cases, we get the right hand side of (1.2.23) to be zero. This proves the theorem.

The above theorem is true not only for a centered rarefaction wave but also for a general rarefaction wave or for any simple wave.

§1.2.5 Genuine Nonlinearity and Linear Degeneracy

Definition 1.4

A point $\boldsymbol{u} \in \Omega$ is called a point of *genuine nonlinearity* of the ith characteristic field if

$$\nabla\lambda_i(\boldsymbol{u}) \cdot \boldsymbol{r}_i(\boldsymbol{u}) \neq 0 \tag{1.2.24}$$

or a point of *linear degeneracy* of the ith characteristic field if

$$\nabla\lambda_i(\boldsymbol{u}) \cdot \boldsymbol{r}_i(\boldsymbol{u}) = 0. \tag{1.2.25}$$

When (1.2.24) holds for all $\boldsymbol{u} \in \Omega$, i is a *genuinely nonlinear characteristic field* while if (1.2.25) is satisfied for all $\boldsymbol{u} \in \Omega$, then i is a *linearly degenerate characteristic field*.

It is clear that when ith characteristic field is linearly degenerate, then the corresponding eigenvalue λ_i is a Riemann invariant.

We note here that for a scalar equation, $u_t + f(u)_x = 0$, $\lambda = f'(u)$, $r = 1$ and $\nabla\lambda \cdot r = f''(u)$. Thus in this case, the notion of genuine nonlinearity reduces to convexity.

It can be shown (see Smoller, 1983) that when the ith characteristic field is genuinely nonlinear, then there exists two smooth one-parameter family of states $\boldsymbol{u}(\gamma)$ called i-rarefaction curve and i-Hugoniot curve, defined for $|\gamma|$ sufficiently small, which can be

connected to $\boldsymbol{u}_l$ on the right by a i-rarefaction wave for $\gamma < 0$ and i shock wave, respectively, for $\gamma > 0$, whereas if the ith characteristic field is linearly degenerate, then we get a contact discontinuity with speed of propagation as $\lambda_i(\boldsymbol{u}_l) = \lambda_i(\boldsymbol{u}_r) = \bar{\lambda}$(say), i.e.,

$$\boldsymbol{u}(x,t) = \begin{cases} \boldsymbol{u}_l, & \text{if } x < \bar{\lambda}t, \\ \boldsymbol{u}_r, & \text{if } x > \bar{\lambda}t. \end{cases}$$

For the genuinely nonlinear case, the function $\boldsymbol{u}(\gamma)$ is continuous with its first two derivatives at $\gamma = 0$.

§1.3 Kinematical Conservation Laws (KCL)

In this thesis, we deal with properties and applications of KCL. We present here a derivation of KCL in two-dimensions in the most general form following Prasad (1995) (also see Prasad, 2001).

Let Ω_t be any moving curve in the (x,y)-plane. The problem is to study the propagation of the curve Ω_t in the (x,y)-plane as t varies. For example, this curve can be a wavefront or a shock front in applications. For a given point P on the curve Ω_t, we define a curve which passes through the point P and which is the locus of the point P moving with a velocity $\chi = (\chi_1, \chi_2)$. This gives in (x,y)-plane, a one parameter family of curves, called *rays*. The velocity χ depends on the property of the medium in which the curve Ω_t propagates and depends also on the unit normal $\boldsymbol{n} = (n_1, n_2)$ of Ω_t.

Let the equation of the curve Ω_t be given by

$$\Omega_t : x = x(\xi, t),\ y = y(\xi, t), \tag{1.3.1}$$

where ξ is chosen such that t=constant gives the position of the propagating curve Ω_t and ξ=constant gives a ray. Let (C,T) be the normal and the tangential components of the ray velocity $\chi = (\chi_1, \chi_2)$. Then we have

$$\begin{aligned} C &= n_1\chi_1 + n_2\chi_2, \\ T &= -n_2\chi_1 + n_1\chi_2. \end{aligned}$$

Consider the curves Ω_t and Ω_{t+dt}. Let P' and Q' be the positions at time $t + dt$ of P and Q, respectively, on two rays at a distance $gd\xi$ on Ω_t as shown in Fig 1.3.1. Then we have $PN = Cdt$ in the normal displacement of Ω_t in time dt. Here, g is the metric associated with ξ and C is that with t in the ray coordinate system. If the coordinates of Q' are $(x + dx, y + dy)$ then (dx, dy) is the displacement in the (x,y)-plane corresponding to a displacement $(d\xi, dt)$ in the ray coordinate plane, so that

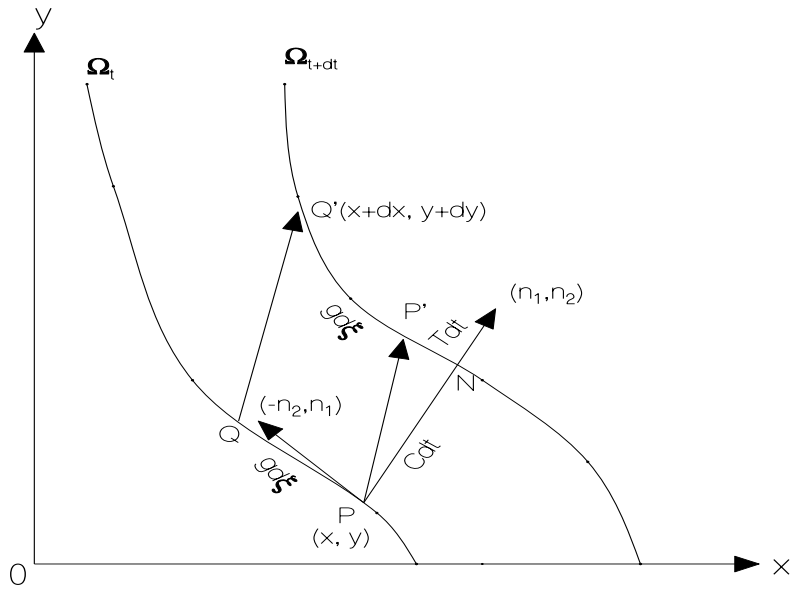

Fig. 1.3.1: *Propagating wavefront and rays*

$$\begin{aligned} dx &= (Cdt)n_1 - (gd\xi + Tdt)n_2, \\ dy &= (Cdt)n_2 - (gd\xi + Tdt)n_1. \end{aligned} \tag{1.3.2}$$

Let θ be the angle between the normal to Ω_t and the x-axis. We note that in two space dimensions, the normal vector $\boldsymbol{n}$ is given by $\boldsymbol{n} = (\cos\theta, \sin\theta)$. Hence, the Jacobian matrix of the transformation from (ξ, t)-plane to (x, y)-plane is given by

$$\begin{pmatrix} x_\xi & x_t \\ y_\xi & y_t \end{pmatrix} = \begin{pmatrix} -g\sin\theta & C\cos\theta - T\sin\theta \\ g\cos\theta & C\sin\theta + T\cos\theta \end{pmatrix}. \tag{1.3.3}$$

Since the determinant of the Jacobian matrix (1.3.3) is $-gC$, the transformation between (ξ, t)-plane to (x, y)-plane is nonsingular when g and C are nonzero and finite.

Following Morton, Prasad and Ravindran (1992), we can derive a pair of kinematical relations in the conservation form by equating $x_{\xi t}$ to $x_{t\xi}$ and $y_{\xi t}$ to $y_{t\xi}$ which takes the form

$$(g\sin\theta)_t + (C\cos\theta - T\sin\theta)_\xi = 0, \tag{1.3.4}$$

$$(g\cos\theta)_t - (C\sin\theta + T\cos\theta)_\xi = 0. \tag{1.3.5}$$

The equations (1.3.4)-(1.3.5) are called the *Kinematical Conservation Laws* (KCL). The differential form of the above system can be obtained as

$$g_t - C\theta_\xi - T_\xi = 0, \tag{1.3.6}$$

$$\theta_t + \frac{1}{g}C_\xi - \frac{1}{g}T\theta_\xi = 0, \tag{1.3.7}$$

which are the kinematical relations for any propagating curve Ω_t. It has been shown by Prasad (2001) that the equations (1.3.6)-(1.3.7) are equivalent to the ray equations (or the bicharacteristic equations) of quasi-linear hyperbolic system (1.2.1) (with $m = 2$), when Ω_t is taken to be the projection on the (x, y)-plane of the section of the characteristic surface $\phi(x, y, t) = 0$ by $t =$ constant plane.

In this thesis, we study the propagation of a wavefront or a shock front in two space dimensions with an assumption that the medium is filled with polytropic gas which is initially at rest with constant density and pressure. Therefore, the flow becomes isotropic and hence, the tangential velocity T becomes identically equal to zero.

The system of KCL (1.3.4)-(1.3.5) is a 2×2 system with four unknowns, namely, g, θ, C and T. For a wavefront, which can be defined only in the high frequency limit, the quantities C and T can be expressed in terms of an amplitude w of the wavefront Ω_t. Therefore, to get a determined system of equations, we must add to these equations another evolution equation for w. Such an equation turns out to be a transport equation along a ray which can be derived under high frequency approximation, Prasad (1993, 2001).

§1.4 Weakly Nonlinear Ray Theory (WNLRT)

We consider a two dimensional wavefront propagation due to a small perturbation in polytropic gas which is initially at rest. We assume a constant density ρ_0 and pressure p_0 of the gas initially. Propagation of this wavefront can be studied using KCL discussed in the previous section. As remarked there, KCL is an under determined system and needs one more equation or a relation between the unknowns in order to make it determined. WNLRT derived on the basis of high frequency approximation can be used to find this additional relation. In this section, we briefly discuss the derivation of the relation between the metric g and C in the case of a downstream propagating wavefront Ω_t in a polytropic gas. For detailed discussion, we refer to Prasad (2001).

The perturbation in the physical quantities are given by

$$\rho - \rho_0 = \frac{\rho_0}{a_0} w, \ \boldsymbol{q} = \boldsymbol{n} w, \ p - p_0 = \rho_0 a_0 w, \tag{1.4.1}$$

where a_0 is the sound speed. The ray equations and the transport equation for the amplitude w are given by (Prasad, 2001)

$$\frac{d\boldsymbol{x}}{dt} = \left(a_0 + \frac{\gamma+1}{2} w\right) \boldsymbol{n} \quad , \quad \frac{d\boldsymbol{n}}{dt} = -\frac{\gamma+1}{2} (\nabla - \boldsymbol{n} \langle \boldsymbol{n}, \nabla \rangle) w, \tag{1.4.2}$$

$$\frac{dw}{dt} = \Omega a_0 w, \tag{1.4.3}$$

where $\Omega = -(1/2)\langle \nabla, \boldsymbol{n} \rangle$ is the mean curvature of Ω_t and

$$\frac{d}{dt} = \frac{\partial}{\partial t} + \left(a_0 + \frac{\gamma+1}{2} w\right) \langle \boldsymbol{n}, \nabla \rangle . \tag{1.4.4}$$

From the first equation in (1.4.2), we note $\chi = \left(a_0 + \frac{\gamma+1}{2}\omega\right) \boldsymbol{n}$, so that $T = 0$.

In two dimensions, the normal components of the wavefront are given by $n_1 = \cos\theta$, and $n_2 = \sin\theta$, where θ is the angle between the normal to the wavefront and the x-axis. We non-dimensionalize the x and y coordinates by a typical length L, say the radius of curvature of Ω_0 at a particular point or another length scale in the problem, w by the sound velocity a_0 and the time by L/a_0 and denote the non-dimensional parameters as x, y, t and w itself. Then the equations (1.4.2)-(1.4.3) can be written as

$$\frac{dx}{dt} = \left(1 + \frac{\gamma+1}{2} w\right) \cos\theta, \tag{1.4.5}$$

$$\frac{dy}{dt} = \left(1 + \frac{\gamma+1}{2} w\right) \sin\theta, \tag{1.4.6}$$

$$\frac{d\theta}{dt} = -\frac{\gamma+1}{2} \frac{\partial w}{\partial \lambda}, \tag{1.4.7}$$

$$\frac{dw}{dt} = -\frac{1}{2} w \frac{\partial \theta}{\partial \lambda}, \tag{1.4.8}$$

where

$$\frac{\partial}{\partial \lambda} = \cos\theta \frac{\partial}{\partial y} - \sin\theta \frac{\partial}{\partial x}. \tag{1.4.9}$$

There is no well defined variable λ and therefore we use the ray coordinate system (ξ, t) which will also allow us to use the two conservation laws (1.3.4)-(1.3.5), with $T = 0$ in such a way that $t =$ constant gives the successive positions of the wavefront, $\xi =$ constant gives the family of associated rays in the (x, y)-plane and $g d\xi$ gives an element of length along the wavefront at a given time t, i.e.,

$$g^2 = x_\xi^2 + y_\xi^2, \quad \frac{\partial}{\partial \xi} = g \frac{\partial}{\partial \lambda}.$$

Differentiating the above equation with respect to t and using the equations (1.4.5)-(1.4.8), we get (after simplification)

$$g_t = \frac{-2g\left(1 + \frac{\gamma+1}{2} w\right)}{w} w_t. \tag{1.4.10}$$

Let m be the Mach number of the wave intensity relative to the sound speed a_0 in the undisturbed state, then

$$m = 1 + \frac{\gamma+1}{2} w. \tag{1.4.11}$$

Integrating the equation (1.4.10) with respect to t, we get

$$g = \frac{f(\xi)}{(m-1)^2 e^{2(m-1)}},$$

where $f(\xi)$ is determined from initial data.

Now we choose a new variable $\xi' = \int^{\xi} f(\xi) d\xi$ (which we will denote by ξ itself), then

$$g(m) = (m-1)^{-2} e^{-2(m-1)}. \tag{1.4.12}$$

The equation (1.4.12) can be used as the equation of state with which the KCL with $T = 0$ and $C = m$ becomes a determined system.

The eigenvalues for the system (1.3.6)-(1.3.7) with $C = m$, $T = 0$ and (1.4.12) are given by

$$c_1 = -\sqrt{\frac{m-1}{2g^2}},\ c_2 = \sqrt{\frac{m-1}{2g^2}}. \tag{1.4.13}$$

Hence, the system (1.3.6)-(1.3.7) with $T = 0$, $C = m$ together with the relation (1.4.12) forms a strictly hyperbolic system for $m > 1$ and an elliptic system for $m < 1$. The condition $m > 1$ means that the pressure on the wavefront is greater than the pressure in the ambient medium. In this thesis, we consider only the case when $m > 1$. Once the system (1.3.4)-(1.3.5) with $T = 0$ and (1.4.12) is solved for m, θ and g, the wavefront Ω_t at a given time t can be obtained by solving the ray equation

$$x_t = m\cos\theta,\ y_t = m\sin\theta. \tag{1.4.14}$$

§1.5 Author's Contribution

Kinematical conservation laws (KCL) (Morton, Prasad and Ravindran 1992) in the ray coordinate system govern the evolution of a moving curve in the (x, y)-plane. The moving curve can be a wavefront or a shock front in applications. Prasad and Sangeeta (1996) studied numerically the KCL together with the additional relation (1.4.12) between g and m in the case of polytropic gases, derived in the section 1.4 using weakly nonlinear ray theory, and traced the formation and propagation of kinks on the weakly nonlinear wavefronts. We have derived the additional relation between g and m to study geometrical shapes of the crest-line of a curved long solitary wave on a shallow water. In this case, the relation is different from that obtained in the gas dynamics. So, for a general mathematical study of KCL, we propose a general form of this relation, subject to certain assumptions which has been made after a careful observation of the behaviour of the relations in the above two applications and some other considerations.

In section 1.4, we have seen that the system of KCL is a hyperbolic system for $m > 1$. In this thesis, we consider only the case when $m > 1$. Mathematical analysis of any hyperbolic system of conservation laws starts with the study of Riemann problem, as this problem and the interaction of elementary waves are the building blocks for the solution of any general initial and boundary value problem. Glimm's random choice method (Glimm, 1965) shows that the study of Riemann problem and the interaction of elementary waves for the KCL would serve as basic tools to answer the mathematical questions like existence and uniqueness of a general initial boundary value problem for the KCL.

We have studied in chapter 2 the solution of the Riemann problem for the KCL together with the additional conservation law

$$(gG(m))_t = 0, \tag{1.5.15}$$

where the function G is subjected to certain physically realistic assumptions. This 3×3 system has two genuinely nonlinear characteristic fields and one linearly degenerate characteristic field. As it is well known, a solution of the Riemann problem is basically a self-similar solution which has a combination of three types of elementary waves, namely, a centered rarefaction wave, a shock and a contact discontinuity. We study these elementary waves for the KCL and obtain an admissible domain in which, if the right state lies for a given left state, then the unique solution for the Riemann problem exists. Then, we define an *elementary shape* on a wavefront in the (x, y)-plane which is the image of an elementary wave in the ray coordinate system and study the propagation of these shapes. The geometrical features of a wavefront arising out of a general singularity on it has been studied in detail. This general singularity on the initial wavefront breaks into different combinations of elementary shapes of different families depending on the initial strength of the general singularity. We have justified that the contact discontinuity which appears in the second characteristic field, does not have any significant role in the geometrical shapes of the wavefront and hence with an appropriate choice of the ray coordinate ξ (Prasad, 2001), it can be eliminated by replacing the third conservation law (1.5.15) by a relation between g and m in the form

$$g(\xi, t) = G(m(\xi, t)). \tag{1.5.16}$$

In chapter 3, we have studied all possible interactions of elementary waves of KCL with (1.5.16) and obtained their geometrical features in the (x, y)-plane numerically using discontinuous Galerkin finite element method (Cockburn, et. al. 1989). We presented a brief note on this numerical scheme in the Appendix 1. We categorized the interaction results in two ways, the first category contains those interactions which can be completed in finite time whereas interactions in the second category go on for infinite time. The

justification for the later type of interaction uses the persistence of shock which has been proved by Prasad (1993, 2001).

In chapter 4, we have presented application of KCL to an example of an entirely new class of problems. This example concerns with geometrical shapes of the crest-line of a long two-dimensional solitary wave on the surface of a shallow water. We believe that the method used is quite general and applicable to other solitary waves as well.

The two compatibility conditions of a shock ray theory (SRT) by Prasad (1993) have been put in conservation form by Monica and Prasad (2001), which is discussed in chapter 5. In chapter 6, we have derived new conservation forms of these two compatibility conditions. These conservation forms appear to be more natural and follow a pattern which are valid for each of the infinite set of compatibility conditions for a curved shock of an arbitrary strength. KCL along with these two new conservation laws has been used to study the propagation of an initially square shaped shock front produced by a piston. This simulates a blast wave produced by an explosion of a charge of square shape. We have shown numerically that the nonlinear waves propagating on the shock front make the initially non-circular shock front to almost circular shock front at a finite time. We have also derived an estimate of this time theoretically. Further, we have compared the results obtained from the SRT with the results obtained from Whitham's geometrical shock dynamics (GSD) (1957), WNLRT and also with the results obtained from the numerical solution of the Euler equations. For this, we have first derived appropriate initial and boundary conditions for SRT from those for the Euler equations. The numerical comparison of results show that the SRT results agrees well with the Euler solutions both in the case of acceleration and deceleration of the piston. We have also studied propagation of an initially wedge shaped shock front and an initially periodic shaped shock front. These shocks develop kinks and in the later problem we study numerically complicated interaction of elementary waves. These studies show that SRT results agree very well with those obtained from numerical solution of Euler results, where as the comparison of GSD results are not very good.

Focusing of sonic boom is one of the advanced research problems in the prediction of sonic booms signature from a supersonic aircraft (Plotkin 2002). This focusing occurs in booms produced by an accelerating aircraft or any maneuvering aircraft in which the linear rays tend to converge and form caustic and the linear solutions are singular. The nonlinear diffraction effect causes the maximum focus amplitude to be finite, as observed in flight tests. Hence, from the justifications made in this thesis on the solutions of SRT, we hope that this theory can be effectively used in the calculation of sonic boom signatures for an accelerating aircraft or any maneuvering aircraft. In the final chapter of this thesis, we

have presented an outline of mathematical formulation of this problem for an accelerating aircraft. The shock front emerging from the nose and the tail of the aircraft can be calculated using SRT. For the full signature, we need the family of wavefronts between these two shock fronts. These wavefronts can be calculated using WNLRT. Calculation of these wavefronts using WNLRT, the bow (nose) and the rear (tail) shocks using SRT, and the calculation of the far field sonic boom signature will be pursued in future.

Chapter 2

Riemann Problem for Kinematical Conservation Laws

§2.1 Introduction

A pair of kinematical conservation laws (KCL) in a ray coordinate system (ξ, t) (Morton, Prasad and Ravindran, 1992) given by

$$(g\sin\theta)_t + (m\cos\theta)_\xi = 0 \tag{2.1.1}$$

$$(g\cos\theta)_t - (m\sin\theta)_\xi = 0 \tag{2.1.2}$$

are basic equations governing the evolution of a moving curve in two space-dimensions. In section 1.4, we have seen that the system (2.1.1)-(2.1.2) is closed using an additional relation between the metric g and the wavefront amplitude m given by (1.4.12) in the case of gas dynamics equations.

The KCL can be used more efficiently in many applications like tracing sonic boom signature, finding the shape of the leading wavefront in a blast wave problem produced by a charge confined in a container of arbitrary shape, studying geometrical shapes of the crest-line on a curved solitary wave on a shallow water and so on. In different applications, we may need to solve the KCL with different functions $g = G(m)$ subjected to certain assumptions (see the assumptions **A1-A4** in section 2.2) and with different shapes of the initial wavefront. So, a mathematical theory is needed for KCL with an arbitrary $G(m)$, to have a better understanding of the practical problem. The Riemann problem and interaction of elementary waves are not only interesting mathematical problems, but also important as they are the building blocks for the general mathematical theory and also in numerical study of hyperbolic conservation laws using the well-known random-choice

method proposed by Glimm (1965) and also in Godunov-type difference scheme.

Riemann(1860) proposed and investigated the simplest initial-value problem with discontinuous initial data for isentropic gas dynamics which is known as the *Riemann Problem*. The analysis of the Riemann problem started with the equations of isentropic or adiabatic gas dynamics, because of the need to explain the mathematical aspects of wave interactions and shock tube experiments. The early works done on this topic are reviewed in Courant and Friedrichs (1948). The scalar case was solved by I. Gelfand (1959). The Riemann problem for general genuinely nonlinear strictly hyperbolic systems of conservation laws has been solved by Lax (1957) with the weak wave assumption, i.e., the jump in the initial data is sufficiently small. A comprehensive study of Riemann problem for isothermal adiabatic gas dynamics has been presented in the monograph by Chang and Hsiao (1989). Detail expositions and references on Riemann problem can be found in Smoller (1983), Godlewski and Raviart (1996) and Defermos (2000).

Our aim in this chapter is to study the existence and uniqueness of solutions of the Riemann problem of the KCL (2.1.1)-(2.1.2) with a general expression for $G(m)$ subject to certain assumptions and interprets the results as geometrical features of the moving curve Ω_t (or a nonlinear wavefront). We established an admissible domain of right states for which the Riemann problem has a unique solution. We shall also examine the situation when a relation of the form $g = G(m)$ can be assumed to be uniformly valid i.e., valid across all possible discontinuities. Interaction of elementary waves from KCL will be discussed in the next chapter.

§2.2 Basic Equations, Riemann Invariants and Jump Relations

We write the two basic conservation laws (KCL) (2.1.1)-(2.1.2) and the third relation (in the conservation form) in vector form as

$$(\boldsymbol{H}(\boldsymbol{u}))_t + (\boldsymbol{F}(\boldsymbol{u}))_\xi = 0, \tag{2.2.1}$$

where $\boldsymbol{u} := (\boldsymbol{v}, g)^T = (m, \theta, g)^T$, so that $\boldsymbol{v} = (m, \theta)^T$ and

$$\boldsymbol{H}(\boldsymbol{u}) := (g\sin\theta, g\cos\theta, g/G(m))^T,\ \boldsymbol{F}(\boldsymbol{u}) := (m\cos\theta, -m\sin\theta, 0)^T. \tag{2.2.2}$$

The function $G(m)$ given in (2.2.2) is defined for $m > 1$ and satisfies the following assumptions:

A1. $G(m) \sim \frac{1}{(m-1)^k}$, $k > 0$ for $0 < m - 1 \ll 1$. **A2.** $\lim_{m\to\infty} G(m) = 0$; $G(m) > 0$.
A3. $G'(m) < 0$. **A4.** $G''(m) > 0$.

Note that these properties are satisfied by the function (1.4.12) derived for gas dynamics and also the function (4.1.3) derived in chapter 4 for a crest-line of a curved long solitary wave (also see Baskar and Prasad, 2003). Since, some of the results we use in the section 2.4 and 2.5 and also in the chapter 3 are very difficult to prove (they involve dealing with nonlinear functions), we verify those results numerically. For this purpose, we select a form for $G(m)$ as

$$G(m) = (m-1)^{-k} e^{-n(m-1)},\ k > 0, n > 0, \text{ for all } m > 1. \tag{2.2.3}$$

Since

$$G' = -\frac{k + n(m-1)}{m-1} G(m), \quad G''(m) = \left\{ \frac{k(k+1)}{(m-1)^2} + \frac{2kn}{m-1} + n^2 \right\} G(m),$$

the above four assumptions are satisfied by (2.2.3).

For a smooth solution, the system (2.2.1)-(2.2.2) is equivalent to the following three partial differential equations

$$m_t - \frac{mG}{gG'}\theta_\xi = 0, \quad \theta_t + \frac{1}{g} m_\xi = 0, \quad g_t - m\theta_\xi = 0. \tag{2.2.4}$$

The eigenvalues of the system (2.2.4) are given by

$$c_1 = -\sqrt{\frac{mG}{g^2(-G')}}, \quad c_2 = 0, \quad c_3 = \sqrt{\frac{mG}{g^2(-G')}}. \tag{2.2.5}$$

From the assumption **A3**, it follows that the system (2.2.1)-(2.2.2) is hyperbolic for $m > 1$. For WNLRT in a polytropic gas, $m > 1$ corresponds to the gas pressure on the wavefront Ω_t being greater than the pressure in the ambient medium in which Ω_t is propagating and for a solitary wave on a shallow water, $m > 1$ always holds.

The right eigenvectors corresponding to the eigenvalues (2.2.5) are

$$\boldsymbol{r}^{(1)} = \left(\frac{G}{gG'}, \sqrt{\frac{G}{mg^2(-G')}}, 1 \right)^T, \quad \boldsymbol{r}^{(2)} = (0, 0, 1)^T,$$
$$\boldsymbol{r}^{(3)} = \left(\frac{G}{gG'}, -\sqrt{\frac{G}{mg^2(-G')}}, 1 \right)^T.$$

The c_1 - and c_3 - characteristic fields are genuinely nonlinear, and the c_2-characteristic field is linearly degenerate (see section 1.2 for basic definitions and for more details, we refer to Smoller, 1983 or Prasad, 2001). Thus, there are two families of nonlinear waves and one family of linear waves which propagate on the curve Ω_t in the (x, y)-plane. The elementary wave solutions of the system of conservation laws consist of centered simple waves, shocks and contact discontinuities, which we shall study in the next section.

The linearly independent Riemann invariants corresponding to the ith characteristic fields are denoted by $(\pi_1^{(i)}, \pi_2^{(i)})$ for $i = 1, 2, 3$ and are given by

$$\begin{aligned}
&\pi_1^{(1)} = \theta + L(m),\ \pi_2^{(1)} = \frac{g}{G};\\
&\pi_1^{(2)} = m,\ \pi_2^{(2)} = \theta;\\
&\pi_1^{(3)} = \theta - L(m),\ \pi_2^{(3)} = \frac{g}{G},
\end{aligned} \tag{2.2.6}$$

where

$$L(m) = \int_1^m \sqrt{\frac{-G'}{mG}}dm. \tag{2.2.7}$$

Let the subscripts l and r represent the values of the solution on the left and the right of a discontinuity at $\xi_s(t)$ and s be the discontinuity velocity $s = d\xi_s(t)/dt$. Then, from the R-H (see definition 1.2.2) jump condition for the KCL (2.1.1)-(2.1.2) (see Prasad, 1995), we get

$$\cos(\theta_r - \theta_l) = \frac{m_l g_l + m_r g_r}{m_l g_r + m_r g_l}, \tag{2.2.8}$$

$$s(g_l G(m_r) - g_r G(m_l)) = 0. \tag{2.2.9}$$

The discontinuity velocity speed s is given by

$$s = \frac{(m_r^2 - m_l^2)}{(m_l g_r + m_r g_l)\sin(\theta_r - \theta_l)}. \tag{2.2.10}$$

When $s \neq 0$, (2.2.9) implies

$$g_l G(m_r) - g_r G(m_l) = 0 \tag{2.2.11}$$

and the relation (2.2.8) becomes

$$\cos(\theta_r - \theta_l) = \frac{m_l G(m_l) + m_r G(m_r)}{m_l G(m_r) + m_r G(m_l)}. \tag{2.2.12}$$

We show in Lemma 2.3.1 that the right hand side of (2.2.12) belongs to $(0, 1]$ for $m_r \in [1, \infty)$. Therefore, for a given θ_l, the value of θ_r satisfies

$$-\frac{\pi}{2} < \theta_r - \theta_l < \frac{\pi}{2}. \tag{2.2.13}$$

For this range of value for $\theta_r - \theta_l$, we can write (2.2.12) as

$$\theta_r - \theta_l = \pm\cos^{-1}\left(\frac{m_l G(m_l) + m_r G(m_r)}{m_l G(m_r) + m_r G(m_l)}\right) = \pm h(m_l, m_r)\ \text{(say)}, \tag{2.2.14}$$

where we take only the positive determination of the $\cos^{-1}$ function. However, we shall see later that a shock transition is possible only for $-\pi/2 < \theta_r - \theta_l < 0$.

§2.3 Elementary Wave Solutions

Elementary wave solutions of conservation laws (2.2.1)-(2.2.2) are the non-constant parts of solutions of the form $m(\xi,t) = m(\xi/t)$, $\theta(\xi,t) = \theta(\xi/t)$, $g(\xi,t) = g(\xi/t)$. These are centered rarefaction wave solutions centered at the origin, shocks and contact discontinuity passing through the origin. We shall discuss in this section, all states which can be joined by an elementary wave solution to a state $\boldsymbol{u}_l$ on the left of it. Without loss of generality we shall take $\theta_l = 0$ in all figures of this chapter, so that $\boldsymbol{u}_l = (m_l, 0, g_l)$.

The centered rarefaction waves can exist in the first and third characteristic fields and we denote them as 1-R and 3-R waves. In 1-R wave, the two Riemann invariants $\pi_1^{(1)}$ and $\pi_2^{(1)}$ are constants (see Theorem 1.2.2). Therefore, from (2.2.6), we get

$$\theta^-(m) = \theta_+^* - \int_1^m \sqrt{\frac{-G'(m)}{mG(m)}}dm, \ 1 < m < \infty \tag{2.3.1}$$

with

$$\theta_+^* = \theta_l + \int_1^{m_l} \sqrt{\frac{-G'(m)}{mG(m)}}dm. \tag{2.3.2}$$

Similarly, in 3-R wave, the two Riemann invariants $\pi_1^{(3)}$ and $\pi_2^{(3)}$ are constants (see Theorem 1.2.2) and hence we have from (2.2.6)

$$\theta^+(m) = \theta_-^* + \int_1^m \sqrt{\frac{-G'(m)}{mG(m)}}dm, \ 1 < m < \infty \tag{2.3.3}$$

with

$$\theta_-^* = \theta_l - \int_1^{m_l} \sqrt{\frac{-G'(m)}{mG(m)}}dm. \tag{2.3.4}$$

Assumption **A2** and **A3** implies that the integrands in the two functions (2.3.1) and (2.3.3) are continuous for $m > 1$ and from **A1**, it follows that the integrals exist. The leading order terms of these two functions for $0 < m - 1 \ll 1$ are

$$\theta^- - \theta_+^* = -2k^{1/2}(m-1)^{1/2}, \quad \theta^+ - \theta_-^* = 2k^{1/2}(m-1)^{1/2}.$$

Therefore the curve $\theta = \theta^-(m)$, $m > 1$ in (m,θ)-plane touches the line $m = 1$ at $(1, \theta_+^*)$ and approaches this point as $m \to 1+$ from below. We denote this curve by $R_1(\boldsymbol{v}_l)$ and call it as the *rarefaction curve* of the first family. Similarly, curve $\theta = \theta^+(m)$, $m > 1$ touches the line $m = 1$ at $(1, \theta_-^*)$ and approaches this point as $m \to 1+$ from above. We denote this curve, the *rarefaction curve* of the third family, by $R_3(\boldsymbol{v}_l)$. The above

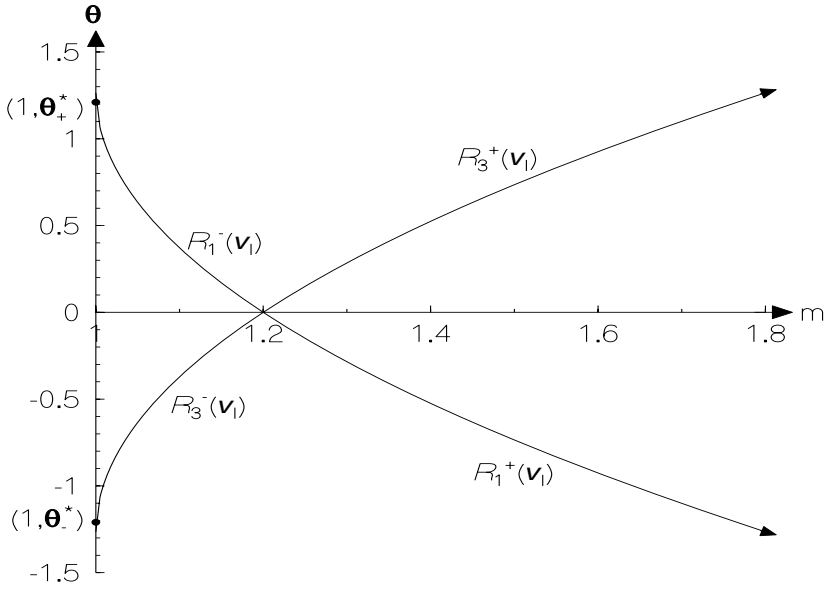

Fig. 2.3.1: *Rarefaction curve* $R_1(\boldsymbol{v}_l) = R_1^+(\boldsymbol{v}_l) \cup R_1^-(\boldsymbol{v}_l) \cup (\boldsymbol{v}_l)$ *of first family and* $R_3(\boldsymbol{v}_l) = R_3^+(\boldsymbol{v}_l) \cup R_3^-(\boldsymbol{v}_l)$ *of third family for* $m_l = 1.2$ *with* $\theta_l = 0$.

approximate expressions for $0 < m - 1 \ll 1$ shows that $R_1(\boldsymbol{v}_l)$ and $R_3(\boldsymbol{v}_l)$ are locally lower and upper parts of the parabolas $m - 1 = \frac{1}{4k}\left(\theta - \theta_+^*\right)^2$ and $m - 1 = \frac{1}{4k}\left(\theta - \theta_-^*\right)^2$ respectively. Each of these two family of curves depend on θ_l and m_l through a single parameter θ_+^* (and θ_-^*). We can also see that, for any point $\boldsymbol{v}'$ in the (m, θ)-plane, $R_1(\boldsymbol{v}_l')$ (and $R_3(\boldsymbol{v}_l')$) can be obtained from $R_1(\boldsymbol{v}_l)$ (and $R_3(\boldsymbol{v}_l)$) simply by translation in the direction of θ axis. Both curves $R_1(\boldsymbol{v}_l)$ and $R_3(\boldsymbol{v}_l)$ pass through the point $\boldsymbol{v}_l = (m_l, \theta_l)$ in (m, θ)-plane as shown in Fig. 2.3.1. It can be directly seen from (2.3.1)-(2.3.4) that the $R_1(\boldsymbol{v}_l)$ and $R_3(\boldsymbol{v}_l)$ curves are strictly monotonic. We note that for a particular G in (2.2.3),

$$\left(\theta^-(m)\right)'' = -\left(\theta^+(m)\right)'' = \frac{1}{2}\frac{(2m-1)k + (m-1)^2 n}{m^{3/2}(m-1)^{3/2}},$$

and k and n are assumed to be strictly positive. For such a G, $R_1(\boldsymbol{u}_l)$ is convex and $R_3(\boldsymbol{u}_l)$ is concave.

Let $\boldsymbol{u}$ be the state on a straight characteristic in 1-R wave and $\boldsymbol{u}_l$ (with $m_l > 1$) be the constant state on the left of it, then from the condition $c_1(\boldsymbol{u}_l) \leq c_1(\boldsymbol{u})$ and $\pi_2^{(1)}(\boldsymbol{u}) = \pi_2^{(1)}(\boldsymbol{u}_l)$, we get

$$g/G(m) = g_l/G(m_l), \tag{2.3.5}$$

and

$$\frac{m_l}{G(m_l)(-G'(m_l))} > \frac{m}{G(m)(-G'(m))}. \tag{2.3.6}$$

Since $G(m)$ and $(-G'(m))$ are decreasing functions of m, $m/(G(m)(-G'(m)))$ is an increasing function of m, the above inequality implies that $m_l > m$. Hence, $\pi_1^{(1)}$=constant in 1-R wave shows that all states in it lie on a part $R_1^-(\boldsymbol{v}_l)$ of a $R_1(\boldsymbol{v}_l)$ in the (m,θ)-plane, where $R_1^-(\boldsymbol{v}_l)$ is given by

$$R_1^-(\boldsymbol{v}_l) = \left\{(m,\theta)/\theta \in \theta^-(m), 1 < m < m_l\right\}. \tag{2.3.7}$$

Thus, on $R_1^-(\boldsymbol{u}_l)$ curve, we have

$$\theta = \theta_l + \int_m^{m_l} \sqrt{\frac{-G'}{mG(m)}}dm, \quad 1 < m < m_l. \tag{2.3.8}$$

The points (m,θ), $1 < m < m_l$ and $\theta_l < \theta < \theta_+^*(\boldsymbol{u}_l)$, on $R_1^-(\boldsymbol{v}_l)$ give the states in a 1-R wave with $\boldsymbol{u}_l$ on the left of this wave (see Fig. 2.3.1). The arguments given above show that for every $\boldsymbol{v}_l$ with $m_l > 1$ and for G satisfying the assumptions **A1-A4** of the section 2.2, the curve $R_1(\boldsymbol{u}_l)$ is uniquely determined. In particular, if $\boldsymbol{v}_r$ lies on the $R_1^-(\boldsymbol{v}_l)$, we get an unique 1-R centered wave joining a constant state $\boldsymbol{v}_l$ on the left and a state $\boldsymbol{v}_r$ on the right.

Consider now a 3-R wave joining a constant state $\boldsymbol{u}_l$ on the left to a state $\boldsymbol{u}_r$ on the right, so that $\pi_1^{(3)}(\boldsymbol{u}_l) = \pi_1^{(3)}(\boldsymbol{u}_r)$ and $\pi_2^{(3)}(\boldsymbol{u}_l) = \pi_2^{(3)}(\boldsymbol{u}_r)$. Since the Riemann invariants $\pi_2^{(1)}$ and $\pi_2^{(3)}$ are the same, the intermediate states $\boldsymbol{u} = (m,\theta,g)$ satisfy the relation (2.3.5) and an additional relation from the constant value of $\pi_1^{(3)}$. Considering the slope of the characteristics of the third family in a 3-R wave (these are straight lines passing through the origin), we deduce as in the previous case $m_l < m \leq m_r$, and therefore the constant value of $\pi_1^{(3)}$ implies that all states in the 3-R wave to lie on $R_3^+(\boldsymbol{v}_l)$ where

$$R_3^+(\boldsymbol{v}_l) = \left\{(m,\theta)/\theta \in \theta^+(m), m_l < m < \infty\right\}. \tag{2.3.9}$$

Thus, on $R_3^+(\boldsymbol{v}_l)$ curve, we have

$$\theta = \theta_l + \int_{m_l}^{m} \sqrt{\frac{-G'}{mG(m)}}dm, \ m_l < m. \tag{2.3.10}$$

This gives a value of θ such that $\theta > \theta_l$ for $m > m_l$. Thus, the set of all states which can be connected to a state (m_l,θ_l) on the left by a 3-R wave is the part $R_3^+(\boldsymbol{v}_l)$ of the rarefaction curve of the third family, i.e. $R_3(\boldsymbol{v}_l)$. The $R_3^+(\boldsymbol{v}_l)$ is above the line $\theta = \theta_l$ with $m > m_l$ (Fig. 2.3.1).

As $\theta^+(m)$ (and also $-\theta^-(m)$) may tend to infinity, θ on these curves may take numerically any large value. From the point of view of physically realistic situations, we need to consider only the strip $-\pi < \theta - \theta_l < \pi$ in the (m,θ)-plane as shown in Fig. 2.3.4, though the part $-\pi < \theta - \theta_l < 0$ cannot be attained by a rarefaction wave. At the end

of the section 2.2, we made relevant comments on the limitations of values of θ through a shock transition. Taking all transitions, we shall see that the points in the (m, θ)-plane which are of interest to our discussion lie in the strip $-\pi < \theta - \theta_l < \pi$. In the Fig. 2.3.4, T denotes the curve represented by (2.3.3) with θ^*_- replaced by $\theta_1 = \theta^*_+(\boldsymbol{v}_l)$ which is also the $R_3^+(\boldsymbol{v}_1)$ curve with $\boldsymbol{v}_1 = (1, \theta_1)$.

The Fig. 2.3.4 has been drawn on the assumption that $\theta^*_+(\boldsymbol{v}_l) < \pi$. However it may turn out that $\theta^*_+(\boldsymbol{v}_l) > \pi$. In that case, the figure has to be modified. $R_1^-(\boldsymbol{v}_l)$ would now intersect the line $\theta = \pi$, the curve T would disappear and we shall get only four domains A, B, C and D where $\boldsymbol{v}_r$ may lie.

Consider now an elementary wave of the second characteristic family in a solution joining two constant states $\boldsymbol{u}_l$ and $\boldsymbol{u}_r$. Since this family is linearly degenerate, the elementary wave solution will be a contact discontinuity moving with the speed zero. Thus, the R-H condition (see Definition 1.2.3) for the third conservation law of the system (2.2.1)-(2.2.2) implies a discontinuity in g. The set of points C in (m, θ)-plane, which can be joined to a point (m_l, θ_l) by a contact discontinuity, consists only of just one point: the point (m_l, θ_l) itself. At a point P of the contact discontinuity on Ω_t, the slope dy/dx of Ω_t is continuous.

Next we consider two states $\boldsymbol{u}_l$ and $\boldsymbol{u}_r$ which satisfy the jump relations (2.2.8) and (2.2.9) with $s \neq 0$. Then the two states are joined by one of two shocks 1-S and 3-S passing through the origin. When we use the expression (2.3.5) in Lax's stability condition (see (1.2.13)) $c_1(\boldsymbol{u}_r) < s < c_1(\boldsymbol{u}_l)$ for 1-S shock, we get

$$\frac{m_l}{m_r} < \frac{G(m_l)(-G'(m_l))}{G(m_r)(-G'(m_r))}. \tag{2.3.11}$$

As in the case of 1-R wave, we can show that this inequality implies $m_l < m_r$. Since $s \neq 0$, (2.2.9) and $m_l < m_r$ gives

$$g_r = \frac{G(m_r)}{G(m_l)} g_l < g_l. \tag{2.3.12}$$

From Lax's stability condition, since we have $s < 0$ for 1-S, it follows from (2.2.10) that $\theta_r < \theta_l$ and therefore from (2.2.13), we have

$$-\frac{\pi}{2} < \theta_r - \theta_l < 0. \tag{2.3.13}$$

Thus, (2.2.14) for 1-S reads

$$\theta_r - \theta_l = -\cos^{-1}\left(\frac{m_l G(m_l) + m_r G(m_r)}{m_l G(m_r) + m_r G(m_l)}\right) = -h(m_l, m_r), \text{ (say)}, \tag{2.3.14}$$

where we take only the positive determination of the $\cos^{-1}$ function.

We first study the properties of the function $h(m_l, m)$ not only for $m \geq m_l$ but also for $1 < m < m_l$.

2.3.1. Lemma *The function*

$$f(m_l, m) = \frac{m_l G(m_l) + mG(m)}{m_l G(m) + mG(m_l)} \tag{2.3.15}$$

has a maximum value 1 at $m = m_l$. It monotinically decreases for $m > m_l$ and tends to zero as $m \to \infty$ and monotonically increases from $1/m_l$ to 1 in $1 < m < m_l$.

Proof. Proof of the Lemma is simple when we note that

$$\frac{df}{dm}(m_l, m) = \frac{(m^2 - m_l^2)G(m_l)G'(m) + m(G^2(m) - G^2(m_l))}{(mG(m_l) + m_l G(m))^2}$$

and G and G' satisfy the assumptions **A1**-**A3** in section 2.2. ∎

Thus, the curve represented by

$$\theta = \begin{cases} \theta_l + h(m_l, m) & \text{if } 1 < m < m_l \\ \theta_l - h(m_l, m) & \text{if } m > m_l, \end{cases} \tag{2.3.16}$$

where we take only the positive determination of $\cos^{-1}$, is a curve with continuously turning tangent and is defined in the whole interval $1 < m < \infty$. We denote this curve by $S_1(\boldsymbol{v}_l)$. $\theta - \theta_l$ decreases continuously from $\lim_{m \to 1+}(\theta - \theta_l) = \cos^{-1}(1/m_l)$ to $-\pi/2$ as m varies from 1 to ∞. $S_1(\boldsymbol{v}_l)$ is called as the *Hugoniot curve of first family.*

We denote the upper part of $S_1(\boldsymbol{v}_l)$, given by $\theta = \theta_l + h(m_l, m)$ for $1 < m < m_l$, by $S_1^-(\boldsymbol{v}_l)$. Since for 1-S shock, $m_l < m_r$, the points on this part cannot be reached by 1-S shock from a state $\boldsymbol{u}_l$ on the left. The lower part $S_1^+(\boldsymbol{v}_l)$ given by $\theta = \theta_l - h(m_l, m), m > m_l$ consists of the points $\boldsymbol{v}_r$ which can be joined to $\boldsymbol{v}_l$ by a shock of the first family. The curve $S_1(\boldsymbol{v}_l)$ has been shown in Fig. 2.3.2 with $\theta_l = 0$.

We denote a shock of the third characteristic family by 3-S shock, with states $\boldsymbol{u}_l$ on the left and $\boldsymbol{u}_r$ on the right. The Lax's entropy condition implies $m_l > m_r$. Thus, for 3-S shock, we have

$$m_l > m_r, \quad g_l < g_r, \quad -\cos^{-1}\left(\frac{1}{m_l}\right) < \theta_r - \theta_l < 0. \tag{2.3.17}$$

The curve $S_3(\boldsymbol{v}_l)$, called as the *Hugoniot curve of third family*, represented by

$$\theta = \begin{cases} \theta_l - h(m_l, m) & \text{if } 1 < m < m_l \\ \theta_l + h(m_l, m) & \text{if } m > m_l \end{cases} \tag{2.3.18}$$

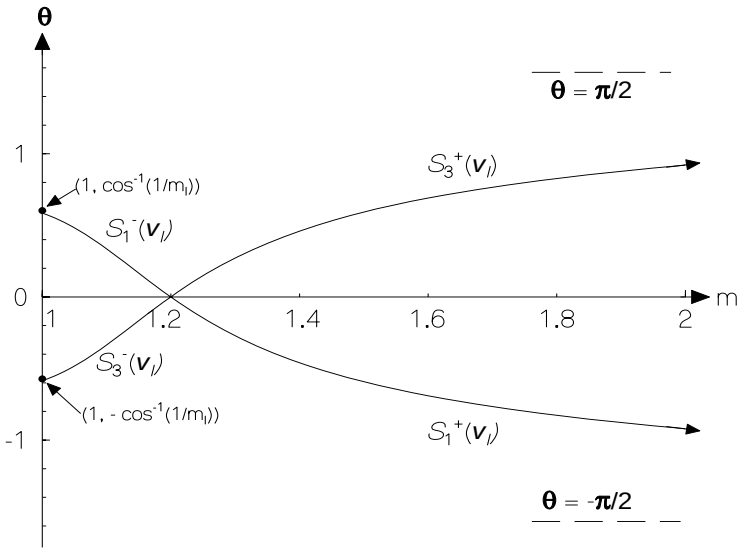

Fig. 2.3.2: *Hugoniot curves $S_1(\boldsymbol{v}_l)$ and $S_3(\boldsymbol{v}_l)$ of first and third families with $m_l = 1.2$, $\theta_l = 0$.*

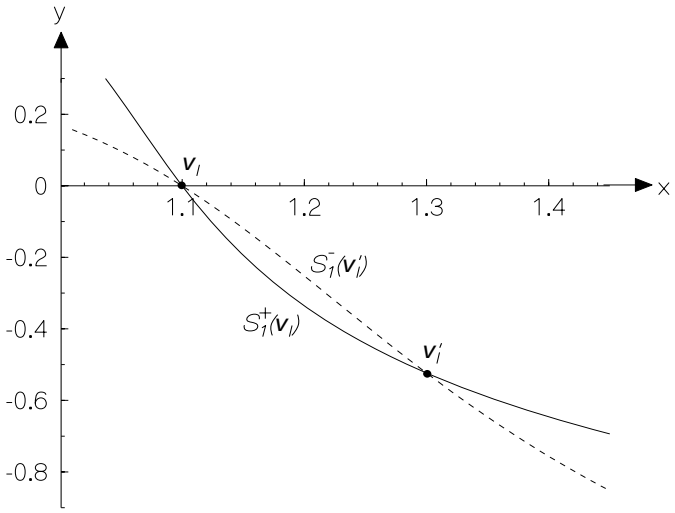

Fig. 2.3.3: *$S_1^+(\boldsymbol{v}_l)$ and $S_1^-(\boldsymbol{v}_l')$ curves meeting at the points $\boldsymbol{v}_l$ and $\boldsymbol{v}_l'$.*

is a reflection of $S_1(\boldsymbol{v}_l)$ in the line $\theta = \theta_l$ as depicted in Fig. 2.3.2 with $\theta_l = 0$. The part $S_3^-(\boldsymbol{v}_l)$ of $S_3(\boldsymbol{v}_l)$ represents the set of points which can be joined to $\boldsymbol{u}_l$ by a 3-S shock. Points on the part $S_3^+(\boldsymbol{v}_l)$ cannot be reached from $\boldsymbol{v}_l$ by a 3-S shock.

The following result is an important property which follows immediately from the fact that $h(m_l, m)$ is symmetric with respect to m_l and m.

2.3.2 Lemma *If $\boldsymbol{v}_l' = (m_l', \theta_l')$ lies on $S_1^+(\boldsymbol{v}_l)$, then (m_l, θ_l) lies on $S_1^-(\boldsymbol{v}_l')$.* ∎

Note that the curves $S_1^-(\boldsymbol{v}_l)$ and $S_1^+(\boldsymbol{v}_l')$ are two distinct curves meeting at the points $\boldsymbol{v}_l$ and $\boldsymbol{v}_l'$ as shown in Fig. 2.3.3. In fact, we can make a less precise statement: if $\boldsymbol{v}_l'$ lies on $S_1(\boldsymbol{v}_l)$, then $\boldsymbol{v}_l$ lies on the curve $S_1(\boldsymbol{v}_l')$. This shows that through $\boldsymbol{v}_l$, an infinity of

S_1 curves other than $S_1(\boldsymbol{v}_l)$ pass. Similar result is true for S_3 curves. However, the one parameter family of curves $R_i(\boldsymbol{v}_l)$, $i = 1$ or 3 is much simpler. If $\boldsymbol{v}_l'$ lies on $R_i(\boldsymbol{v}_l)$, then $R_i(\boldsymbol{v}_l) = R_i(\boldsymbol{v}_l')$. Through each point $\boldsymbol{v}_l$, only one R_i, $i = 1, 3$ curve passes.

The S_i (i=1,3) curve seems to have a point of inflection. Even for the particular function G given in (2.2.3), the second derivative of $h(m_l, m)$ is a complicated function. We numerically compute the derivative $\frac{d}{dm}h(m_l, m)$ for various values of k and n and look for its extremum point with respect to m. This will give the point of inflection of S_i. We find that S_i curves have no point of inflection for $k = 1$, $n = 1$. Without a point of inflection, the curve $S_3(\boldsymbol{v}_l)$ is everywhere concave and the curve $S_1(\boldsymbol{v}_l)$ is everywhere convex. For $k = n$ close to 1, the point of inflection is at a point m_f close to 1. As $k = n$ increase, m_f increases and tends to m_l as $k = n \to \infty$, but does not seem to cross m_l.

In this section *we have studied the curves* $R_1(\boldsymbol{v}_l)$, $R_3(\boldsymbol{v}_l)$, $S_1(\boldsymbol{v}_l)$, *and* $S_3(\boldsymbol{v}_l)$, *and their different parts such as* $R_1^-(\boldsymbol{v}_l)$*; passing through any point* (m_l, θ_l) *in the half plane* $m > 1$ *when* G *satisfies the assumptions* **A1**-**A4** *in the section 2.* Each one of these curves are smooth in spite of the fact that both the denominator and numerator of $\frac{d}{dm}h(m_l, m)$ vanish simultaneously at $m = m_l$.

Dependence of $R_1(\boldsymbol{v}_l)$ (or $R_3(\boldsymbol{v}_l)$) on m_l and θ_l is very simple, as we have described earlier, $R_1(\boldsymbol{v}_l')$ can be obtained from $R_1(\boldsymbol{v}_l)$ by translating $R_1(\boldsymbol{v}_l)$ in θ direction by $\theta_l' - \theta_l + \int_{m_l'}^{m_l} \left\{\frac{-G'(m)}{mG(m)}\right\}^{1/2} dm$. Dependence of $S_1(\boldsymbol{v}_l)$ (or $S_3(\boldsymbol{v}_l)$) on θ_l is also simple: $S_1(\boldsymbol{v}_l, \theta_l)$ can be obtained from $S_1(\boldsymbol{v}_l, \theta_l')$ by translating the later by $\theta_l' - \theta_l$. Even though there are infinity of S_1 curves passing through $\boldsymbol{v}_l$, $S_1(\boldsymbol{v}_l)$ is unique and different from all other $S_1(\boldsymbol{v}_l')$ which pass through $\boldsymbol{v}_l$. The variation of $S_1(\boldsymbol{v}_l)$ on m_l is simple. We first note that when m_l decreases, $\theta_l + \cos^{-1}\frac{1}{m_l}$ decreases to θ_l. Since $f(m_l, m) = f(m, m_l)$, we use Lemma 2.3.1 to deduce

$$f(m, m_{l1}) < f(m, m_{l2}) \text{ for } m_{l1} < m_{l2} < m; f(m, m_{l1}) > f(m, m_{l2}) \text{ for } m < m_{l1} < m_{l2}$$

so that

$$h(m, m_{l1}) > h(m, m_{l2}) \text{ for } m_{l1} < m_{l2} < m \tag{2.3.19}$$

$$h(m, m_{l1}) < h(m, m_{l2}) \text{ for } m < m_{l1} < m_{l2}. \tag{2.3.20}$$

Thus, *the curve* $S_1(m_{l1}, \theta_l)$*, which varies from* $\cos^{-1}\frac{1}{m_{l1}}$ *to* $-\pi/2$*, always lies below the curve* $S_1(m_{l2}, \theta_l)$ *when* $m_{l1} < m_{l2}$. Similarly, it can be shown that $S_3(m_{l1}, \theta_l)$ lies above the curve $S_3(m_{l2}, \theta_l)$ when $m_{l1} < m_{l2}$.

From the properties just discussed, we prove

2.3.1 Theorem *Two members of either R_1 or R_3 or S_1 or S_3 do not intersect when only one of the two variable m_l and θ_l varies.* ∎

This theorem is important as it helps us in solving the Riemann problem.

The set of points in (m, θ)-plane, which can be connected to $\boldsymbol{v}_l$ (with $\theta_l = 0$) by a shock or a centered rarefaction wave, have been shown in Fig. 2.3.4. In addition to that, we have also shown in Fig. 2.3.4 a part T of $R_3^+(m = 1, \theta = \theta_+^*(\boldsymbol{v}_l))$ for $\theta_+^*(\boldsymbol{v}_l) < \theta < \pi$ by a broken curve. The points in (m, θ)-plane relevant to our discussion lie in the domain $1 < m < \infty$, $-\pi < \theta < \pi$. We denote different parts of this domain by A, B, C, D and E as follows:

A: Bounded by $R_1^-(\boldsymbol{v}_l)$, T, $\theta = \pi$ and $R_3^+(\boldsymbol{v}_l)$.

B: Bounded by $R_3^+(\boldsymbol{v}_l)$, $S_1^+(\boldsymbol{v}_l)$ and possibly $\theta = \pi$ (if $R_3^+(\boldsymbol{v}_l)$ intersects $\theta = \pi$).

C: Bounded by $S_3^-(\boldsymbol{v}_l)$, $S_1^+(\boldsymbol{v}_l)$, $\theta = -\pi$ and $m = 1$.

D: Bounded by $m = 1$, $R_1^-(\boldsymbol{v}_l)$ and $S_3^-(\boldsymbol{v}_l)$.

E: Bounded by $m = 1$, $\theta = \pi$ and T.

It is important to note that if $\theta_+^* \geq \pi$, then the set E is a void set.

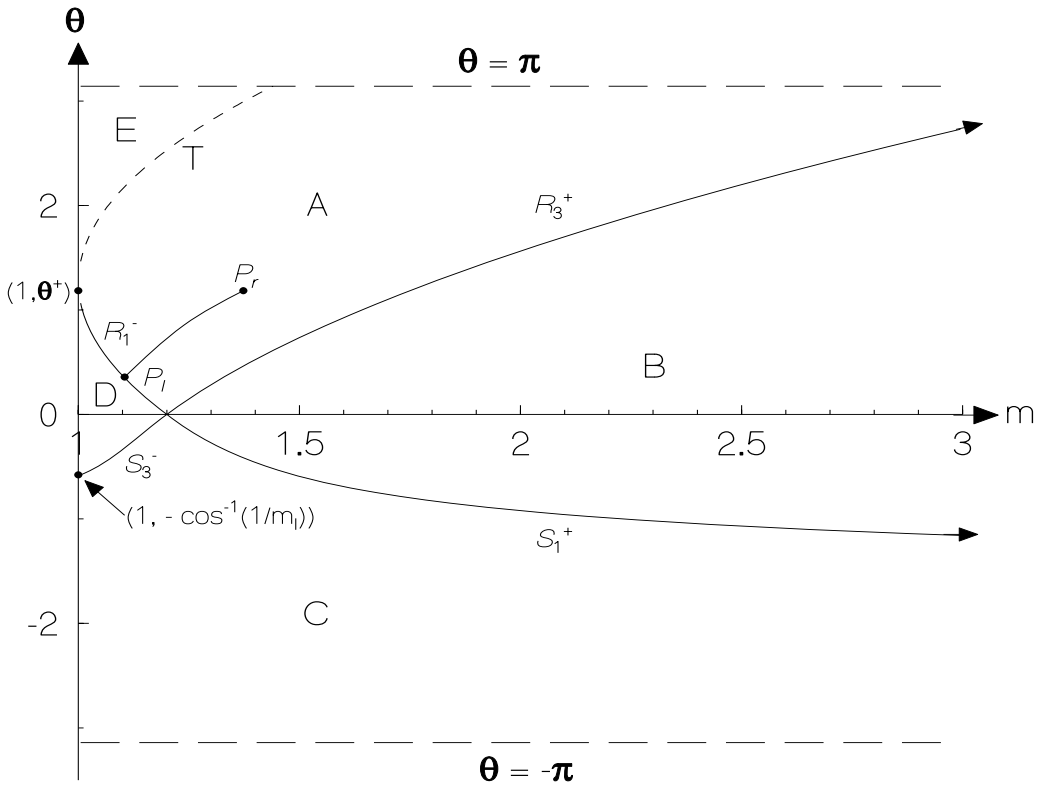

Fig. 2.3.4: *Rarefaction and Hugoniot curves.*

§2.4 Geometrical Features Arising Out of Elementary Waves: Elementary Shapes

A Riemann problem for the system of conservation laws (2.2.1) is to find a weak solution of the system in the upper half plane: $(\xi, t) \in I\!R \times I\!R_+$, satisfying a cauchy data

$$\boldsymbol{u}(x,0) = \begin{cases} \boldsymbol{u}_l, & \text{if } \xi < 0, \text{ with } \theta_l = 0 \\ \boldsymbol{u}_r, & \text{if } \xi \geq 0, \end{cases} \tag{2.4.1}$$

where $\boldsymbol{u}_l$ and $\boldsymbol{u}_r$ are two constant states and for this system we can choose $\theta_l = 0$ without any loss of generality. Since g is the metric along the wavefront Ω_t, the initial position Ω_0 of the front is obtained by integrating the equation (see equation 1.3.3)

$$x_\xi = -g\sin\theta, \quad y_\xi = g\cos\theta \tag{2.4.2}$$

with g and θ as given in (2.4.1). Thus $\Omega_0 : (x_0(\xi), y_0(\xi))$ is

$$(x_0(\xi), y_0(\xi)) = \begin{cases} (0, g_l\xi) & , \text{ if } \xi \leq 0 \\ (\xi g_r \sin\theta_r, \xi g_r \cos\theta_r) & , \text{ if } \xi > 0 \end{cases} \tag{2.4.3}$$

which has a singularity at the origin $(0,0)$ joining two straight parts. This singular point is not necessarily a kink unless $\boldsymbol{v}_r$ lies either on $S_1^+(\boldsymbol{v}_l)$ or $S_3^-(\boldsymbol{v}_l)$ as discussed in section 2.3. Once the Riemann problem is solved in the (ξ,t)-plane, the mapping from (ξ,t)-plane to (x,y)-plane is obtained by integrating the ray equations (1.4.14) for a fixed value of ξ,

$$x(\xi,t) = x_0(\xi) + \int_0^t m(\xi,\tau)\cos(\theta(\xi,\tau))d\tau, \tag{2.4.4}$$

$$y(\xi,t) = y_0(\xi) + \int_0^t m(\xi,\tau)\sin(\theta(\xi,\tau))d\tau. \tag{2.4.5}$$

A ray starting from (x_0, y_0) is given by (2.4.4)-(2.4.5) when ξ is kept fixed. The wavefront Ω_t at any point is again given by (2.4.4)-(2.4.5) when t is kept fixed and ξ varies.

Now we consider the structure of a 1-R wave in (ξ,t)-plane and the geometrical shape $\mathcal{R}_1$, of the wavefront Ω_t associated with this solution. To get a 1-R wave as a solution of the Riemann problem, we choose the state $\boldsymbol{v}_r$ to lie on $R_1^-(\boldsymbol{v}_l)$ curve and $g_l G(\boldsymbol{v}_r) = g_r G(\boldsymbol{v}_l)$.

If $g_l \neq g_r$, there must be a contact discontinuity along $\xi = 0$, hence we first solve m as a function of ξ/t from

$$\frac{mG(m)}{g^2(-G'(m))} = \left(\frac{\xi}{t}\right)^2, \; g = \frac{g_l G(\boldsymbol{v})}{G(\boldsymbol{v}_l)}; c_1(\boldsymbol{u}_l) < \frac{\xi}{t} \leq c_1(\boldsymbol{v}_r, g_L), \tag{2.4.6}$$

where

$$g_L = \left.\frac{g_l G(m)}{G(m_l)}\right|_{\xi/t = c_1(\boldsymbol{u}_r)}. \tag{2.4.7}$$

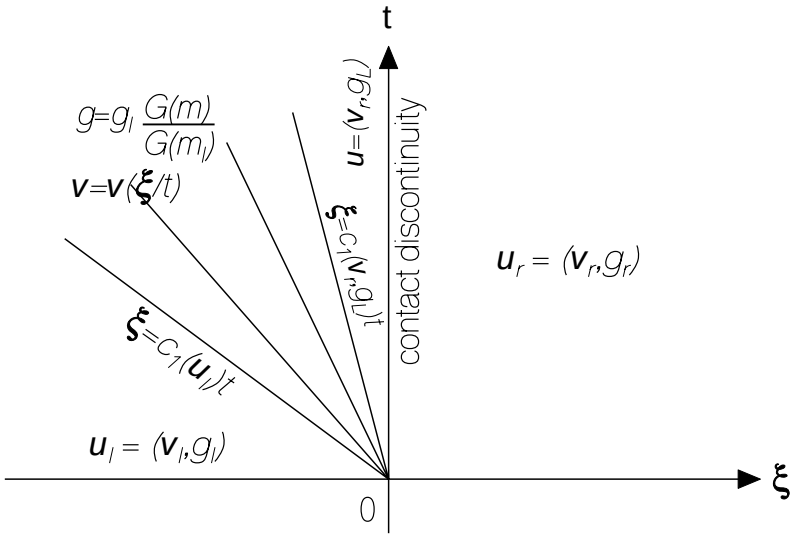

Fig. 2.4.1 : *Solution of the Riemann problem when* $\boldsymbol{v}_r \in R_1^-(\boldsymbol{v}_l)$.

Since $\frac{m}{-G'}$ is a monotonically increasing function, the solution $m = m(\xi/t)$ exists uniquely.

Then the solution is given by (see Fig. 2.4.1)

$$\boldsymbol{u} = \boldsymbol{u}_l, \qquad \text{if } -\infty < \xi \le c_1(\boldsymbol{u}_l)t \tag{2.4.8}$$

$$= \begin{cases} m, \\ \theta = \theta_l + \int_m^{m_l} \sqrt{\frac{(-G')}{mG}}\, dm, \\ g = g_l \frac{G(m)}{G(m_l)}, \end{cases} \quad \text{if } c_1(\boldsymbol{u}_l)t < \xi \le c_1(\boldsymbol{v}_r, g_L)t \tag{2.4.9}$$

$$= \begin{cases} m_r, \\ \theta_r, \\ g = g_L, \end{cases} \qquad \text{if } c_1(\boldsymbol{u}_L)t < \xi \le 0 \tag{2.4.10}$$

$$= \boldsymbol{u}_r, \qquad \text{if } 0 < \xi < \infty. \tag{2.4.11}$$

The 1-R solution is completely determined. Fig. 2.4.2 shows the geometry of the wavefront Ω_t associated with this solution. The wavefront Ω_t contains a curved part $\mathcal{R}_1$ of the wavefront, which we call an *elementary shape* $\mathcal{R}_1$. Ω_t and rays can be determined with the help of (2.4.4)-(2.4.5) as explained there. We note that the elementary shape $\mathcal{R}_1$ propagates downwards on Ω_t. The rays starting from the points below the singularity at $\xi = 0$ on Ω_0 enter $\mathcal{R}_1$ zone in the (x, y)-plane from below, curve upward and finally emerge out of this zone again as straight lines.

As in the case of $\mathcal{R}_1$ above, we define *an elementary shape on* Ω_t *to be the image in* (x, y)*-plane of an elementary wave solution of the system of conservation laws.* We denote

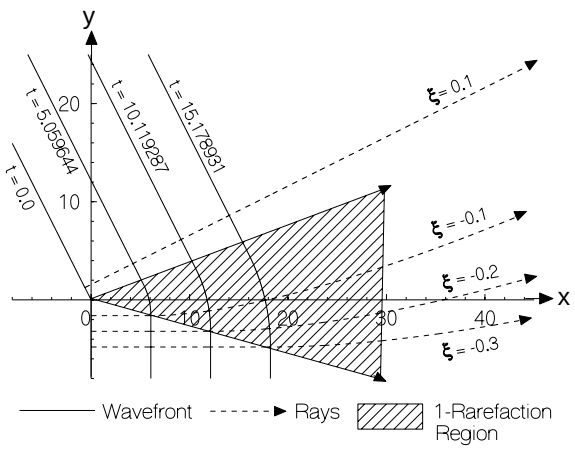

Fig. 2.4.2: $\mathcal{R}_1$ *elementary shape with* $m_l = 1.2$, $m_r = 1.08$.

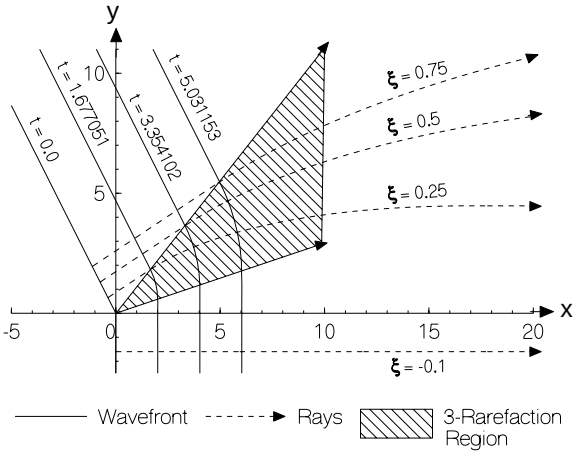

Fig. 2.4.3: $\mathcal{R}_3$ *elementary shape with* $m_l = 1.2$, $m_r = 1.4$.

these elementary shapes by $\mathcal{R}_1$, $\mathcal{R}_3$, $\mathcal{C}$, $\mathcal{K}_1$, and $\mathcal{K}_3$ where $\mathcal{R}_3$ corresponds to 3-R wave, $\mathcal{C}$ to a contact discontinuity, $\mathcal{K}_1$ to a 1-S shock and $\mathcal{K}_3$ to a 3-S shock. Note that $\mathcal{C}$, $\mathcal{K}_1$ and $\mathcal{K}_3$ are point singularities on Ω_t.

As the case of 1-R solution, we can discuss the structure of 3-R centered wave and the associated elementary shape $\mathcal{R}_3$. They have been shown in Fig. 2.4.3. $\mathcal{R}_3$ is also convex, but unlike $\mathcal{R}_1$, the elementary shape $\mathcal{R}_3$ moves upwards on Ω_t and the rays starting from the points on the upper part of Ω_0, enter $\mathcal{R}_3$ zone from above and finally emerge out of this zone as straight lines.

It is easy to derive the boundary lines of a $\mathcal{R}_1$ zone (or $\mathcal{R}_3$ zone) in the (x, y)-plane. Let us do this for the $\mathcal{R}_1$ zone. The two characteristic lines which bound the 1-R wave in the (ξ, t)-plane are $\xi = c_1(\boldsymbol{u}_l)t$, and $\xi = c_1(\boldsymbol{u}_r)t$. (see Fig. 2.4.1) Since the lower part of Ω_0 is the lower half of the y-axis, a point on the image of $\xi = c_1(\boldsymbol{u}_l)t$ can be reached by a ray starting from $(0, g_l\xi)$, $\xi < 0$ and moving with the velocity m_l in x-direction. Hence, the equation of the lower boundary of the image of (2.4.9) in (x, y)-plane is given parametrically in terms of t as

$$x = m_l t, \; y = g_l\xi = g_l c_1(\boldsymbol{u}_l)t \tag{2.4.12}$$

or since

$$\frac{g_l c_1(\boldsymbol{u}_l)}{m_l} \;=\; -\sqrt{\frac{G(m_l)}{m_l(-G'(m_l))}},$$

this lower boundary of R_1-zone is

$$y = -x\sqrt{\frac{G(m_l)}{m_l(-G'(m_l)}}. \tag{2.4.13}$$

To get the image of $\xi = c_1(\boldsymbol{u}_r)t$, i.e., the upper boundary of $\mathcal{R}_1$-zone, we refer to the Fig. 2.4.1 in (ξ, t)-plane, which is pre-image of the Fig. 2.4.2. A point $(c_1(\boldsymbol{u}_r), t)$ in Fig. 2.4.1, which can be reached from the origin first moving vertically up along the t-axis and then moving horizontally in negative ξ direction. Thus, a point on the upper boundary of 1-R region in (x, y)-plane can be reached from the origin by moving along the ray with velocity $(m_r \cos\theta_r, m_r \sin\theta_r)$ and then moving along the wavefront Ω_t. The second movement correspond to a displacement $(-g_L\xi \sin\theta_r, g_L\xi \cos\theta_r)$ in the Fig. 2.4.2 from the point $(m_r t \cos\theta_r, m_r t \sin\theta_r)$. Therefore, the image of $\xi = c_1(\boldsymbol{u}_r)t$ is given by

$$x = -g_L\xi \sin\theta_r + m_r t \cos\theta_r, y = g_L\xi \cos\theta_r + m_r t \sin\theta_r \tag{2.4.14}$$

or using $\xi = c_1(\mathbf{u}_r)t$, we write it as

$$y = \left(\frac{g_L c_1(\boldsymbol{u}_r)\cos\theta_r + m_r \sin\theta_r}{-g_L c_1(\boldsymbol{u}_r)\sin\theta_r + m_r \cos\theta_r}\right) x. \tag{2.4.15}$$

We note that the lower boundary of $\mathcal{R}_1$-zone always has a negative slope, the upper boundary may slope upward, for example for $0 < \theta_r < \pi/2$, if

$$\frac{g_r}{g_L}\sqrt{\frac{m_r(-G'(m_r))}{G(m_r)}} < \cot\theta_r, \tag{2.4.16}$$

where g_L is given by (2.4.7).

Consider now a solution $\boldsymbol{u}$ with constant $\boldsymbol{v} = (m_l, \theta = 0)$ in the whole of (ξ, t)-plane and a contact discontinuity along $\xi = 0$ across which $[g] \neq 0$. Since m on Ω_t is constant equal to m_l and $\theta = 0$, the wavefront Ω_t is a straight line $x = m_l t$ parallel to y-axis and the elementary shape $\mathcal{C}$ corresponding the contact discontinuity consists of points on the ray $\xi = 0$ i.e., $y = 0$. This elementary shape is not observable on the wavefront. However, if a contact discontinuity appears in a solution in which Ω_t is not a straight line and g is not constant on Ω_t (with a jump on $\mathcal{C}$), then the second derivatives $x_{\xi\xi}$ and $y_{\xi\xi}$ obtained from (2.4.2) show that though the tangent direction of Ω_t is continuous, its curvature may be discontinuous across $\mathcal{C}$.

When the Riemann data (2.4.1) is such that $(m_r, \theta_r) \in S_1^+(\boldsymbol{v}_l)$, and (2.3.12) is satisfied, the solution contains only one elementary wave solution, namely 1-S shock. The shock starts from the origin in (ξ, t)-plane and moves with a negative velocity (2.2.10), since

$\theta_r < 0$. The image of the 1-S shock in (ξ, t)-plane is a $\mathcal{K}_1$-kink in (x, y)-plane, its path i.e., the kink path is

$$y = x\left(\frac{m_r - m_l\cos\theta_r}{m_l\sin\theta_r}\right) \tag{2.4.17}$$

(see the expression (3.3.33) for the kink slope S in Prasad, 2001). A ray starting from the lower part of Ω_0 (i.e., with $\xi_0 < 0$) moves parallel to the x-axis, intersects the kink path and then changes its direction so as to make an angle $\theta_r < 0$ with the x-axis, as depicted in Fig. 2.4.4.

Similarly, we can consider a Riemann data which leads to the elementary wave 3-S. The image of this shock is an elementary shape $\mathcal{K}_3$-kink. The geometry of the wavefront Ω_t, rays and the kink path corresponding to this solution has been shown in Fig. 2.4.5.

Suppose now that the state $\boldsymbol{u}_r$ be such that (m_r, θ_r) lies either on R_1^-, or R_3^+ or S_1^+ or S_3^- but without satisfying the relation (2.3.5), then the solution of the Riemann problem consists of either a 1-R wave or a 3-R wave or 1-S wave or 3-S wave respectively and in addition there will be a contact discontinuity on $\xi = 0$. When (m_r, θ_r) lies on $R_3^+(\boldsymbol{v}_l)$, the contact discontinuity will be on the left of 3-R wave and when (m_r, θ_r) lies on $S_1^+(\boldsymbol{v}_l)$ the contact discontinuity will be on the right of 1-S shock and so on.

The solution of the Riemann problem when (m_r, θ_r) is an arbitrary point in (m, θ)-plane, have been presented in the next section. Here we first analyze whether we can take $g/G(m)$ to be the same constant on two sides of a 1-S or 3-S shock. This question was raised by Whitham, in his heuristic theory of shock dynamics. The answer to the question follows immediately from the jump relation (2.2.9) with $s \neq 0$. Hence across both shocks, $g/G(m)$ has the same value and in a smooth solution $g/G(m) =$ constant is an integral

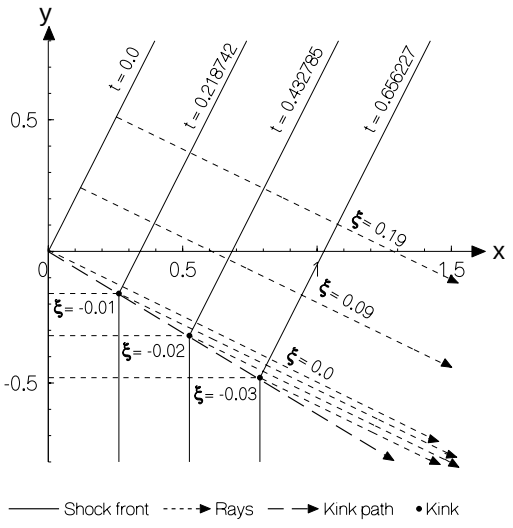

Fig. 2.4.4: $\mathcal{K}_1$ *with* $m_l = 1.2$, $m_r = 1.4$.

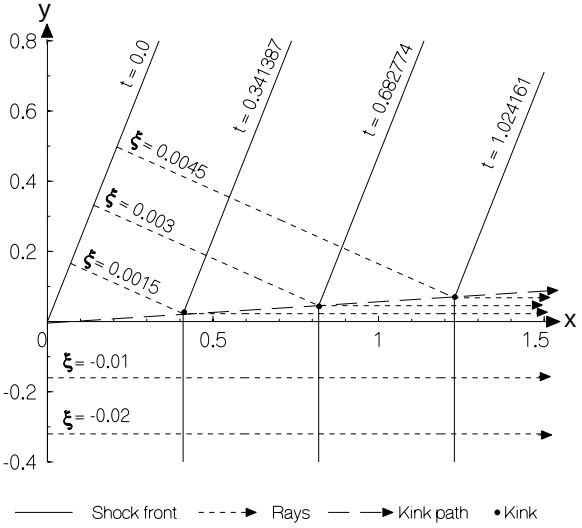

Fig. 2.4.5: $\mathcal{K}_3$ *with* $m_l = 1.2$, $m_r = 1.08$.

of the third conservation law in the system (2.2.1). Thus, it is possible to take $g/G(m)$ to be the same constant in the solution in (ξ, t)-plane on the two sides of a shock.

Next, we analyze whether we can replace the system of three conservation laws (2.2.1)-(2.2.2) simply by a system of two conservation laws (2.1.1)-(2.1.2) with a given expression for $g = G(m)$, as done by Prasad and Sangeeta (1999) for solutions which are continuous but piecewise smooth in (ξ, t)-plane. We consider an initial value for the system of conservation laws (2.1.1)-(2.1.2):

$$\boldsymbol{u}(\xi, 0) = \boldsymbol{u}_0(\xi), \tag{2.4.18}$$

such that

$$g_0(\xi) = G(m_0(\xi)). \tag{2.4.19}$$

We can always achieve (2.4.19) in an initial data by replacing ξ by a new function of ξ (Prasad, 2001, page 209). For a smooth solution, we can integrate the third equation of the system (2.2.1) to get $g/G(m)$ as a function of ξ which is identically equal to 1, since $g_0/G(m_0) = 1$ from (2.4.19). Hence

$$g(\xi, t) = G(m(\xi, t)). \tag{2.4.20}$$

If the solution $\boldsymbol{u}(\xi, t)$ is continuous but piecewise smooth due to the presence of simple waves or more complex solutions in some subdomains of $\mathbb{R} \times \mathbb{R}_+$, then across the common boundaries of these subdomains the relation (2.4.20) remains valid. When 1-S and 3-S shocks appear in the solution, $g_l/G(m_l) = g_r/G(m_r)$ being the common jump relation for both shocks, we find that g/G remains continuous across these shock paths. Thus, we note that a constant value of $g/G(m)$ is carried along lines $\xi =$ constant as t evolves as long as the solution is continuous and after meeting a shock, same value of g/G crosses over and is again maintained afterward along $\xi =$ constant lines. Thus, (2.4.19) implies (2.4.20) in all continuous piecewise smooth solutions. This justifies the use of the relation (2.4.20) and the KCL (2.1.1)-(2.1.2), provided we choose the initial data satisfying (2.4.19) as done by Prasad and Sangeeta (1999). With such a choice of ξ, since m is continuous across a contact discontinuity, g is also continuous across it i.e., the contact discontinuity disappears. For a Riemann initial data (2.4.1), this would mean a suitable choice of ξ i.e., a choice of g on the two sides of $\xi = 0$ such that $g_l/G(m_l) = g_r/G(m_r) = 1$. Thus we have justified the use of the relation (2.4.20) along with the KCL (2.1.1)-(2.1.2) to discuss the propagation of a nonlinear wavefront even for the initial data (2.4.1) which is discontinuous at $\xi = 0$ but otherwise smooth. However, a trace of a contact discontinuity on Ω_t will still be seen as a discontinuity in the curvature of Ω_t at the elementary shapes $\mathcal{C}$. But a discontinuity in the curvature of Ω_t may exist even in a piecewise C^1 solution of (2.1.1)-(2.1.2) with (2.4.20) due to discontinuity in the derivatives of m, for example across a curve in (ξ, t)-plane which forms the boundary of a simple wave.

§2.5 Geometrical Shapes Arising Out of a General Singularity on Ω_t

In this and the next section, we shall use the relation (2.4.20) instead of the third conservation law in the system (2.2.1). Our governing equations are then the KCL (2.1.1)-(2.1.2) with (2.4.20). We shall first study the general Riemann problem, when the point $\boldsymbol{v}_l = (m_l, \theta_l = 0)$ is given and $\boldsymbol{v}_r = (m_r, \theta_r)$ is an arbitrary point in (m, θ)-plane. This problem can be easily solved with the help of Fig. 2.3.4 (or a slightly modified figure when $\theta_+^* > \pi$ as mentioned in the section 2.3).

Let $P_r(m_r, \theta_r)$ be a point in the domain A. The solution of the Riemann problem exists because $R_3^-(\boldsymbol{v}_r)$ being below T, it always meets $R_1^-(\boldsymbol{v}_l)$ and in this case it consists of the state $(m_l, 0)$ on the left of a 1-R wave continuing up to an intermediate constant state $P_i(m_i, \theta_i)$, which ends into a 3-R wave to the right of which we get the final state (m_r, θ_r). This intermediate state (m_i, θ_i) is the point of intersection P_i of the curves $R_1^-(\boldsymbol{v}_l)$ and $R_3^-(\boldsymbol{v}_r)$ which is unique because of the geometry of these curves (see Fig. 2.3.4) as discussed in section 2.3. Existence of the unique point of intersection can also be proved by using fixed point method, but it appears that it is unnecessary because of very clear geometrical arguments. It is important to note that, since $R_3(\boldsymbol{v})$ for $\boldsymbol{v} \neq \boldsymbol{v}_l$ is just a translation of $R_3(\boldsymbol{v}_l)$ in θ direction, $R_3^-(\boldsymbol{v}_r)$ can never intersect $R_3^+(\boldsymbol{v}_l)$. This argument ensures the existence of the intermediate point $P_i(m_i, \theta_i)$ as the point of intersection of the $R_1^-(\boldsymbol{v}_l)$ and $R_3^-(\boldsymbol{v}_r)$ curves if $(m_r, \theta_r) \in A$. The above argument is equivalent to saying that there exists a unique point $P_i(m_i, \theta_i)$ on the $R_1^-(\boldsymbol{v}_l)$ curve such that $R_3^+(\boldsymbol{v}_i)$ passes through P_r. The shape of the wavefront at $t = 0$ and at times $t > 0$ is depicted in Fig. 2.5.1.

If we have considered the third conservation law in the system (2.2.1) instead of the relation (2.4.20), we would have got a contact discontinuity along $\xi = 0$, but this would not have affected the geometry of the wavefront depicted in Fig. 2.5.1. We describe this result symbolically as

$$(m_r, \theta_r) \in A \rightarrow \mathcal{R}_1\mathcal{R}_3, \tag{2.5.1}$$

which means that, when (m_r, θ_r) is in the domain A, the resultant wavefront has an elementary shape $\mathcal{R}_1$ propagating below on Ω_t, and $\mathcal{R}_3$ propagating above and these two are separated by a plane (straight) section of the front.

Similarly, we get the result

$$(m_r, \theta_r) \in B \rightarrow \mathcal{K}_1\mathcal{R}_3, \tag{2.5.2}$$

and the geometrical shape of the wavefront at different times is shown in Fig. 2.5.2.

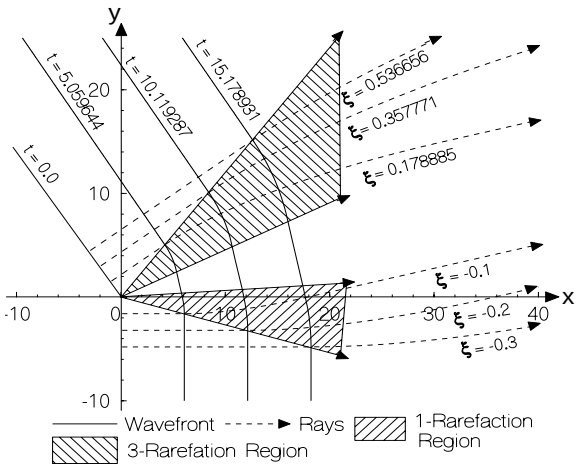

Fig. 2.5.1: $\boldsymbol{v}_r \in A$ *with* $m_l = 1.2$, $m_r = 1.25$.

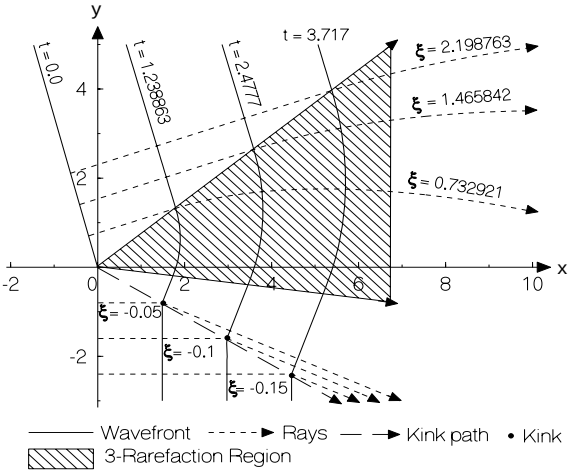

Fig. 2.5.2: $\boldsymbol{v}_r \in B$ *with* $m_l = 1.2$, $m_r = 1.7$.

Let $\boldsymbol{v}_r = (m_r, \theta_r) \in C$. We expect the result $\boldsymbol{v}_r \in C \to \mathcal{K}_1\mathcal{K}_3$ but we face a difficulty now. When the point $\boldsymbol{v}_r$ is close to the curve $S_3^-(\boldsymbol{v}_l)$, then the curve $S_3^+(\boldsymbol{v}_r)$ enters into the domain D. Therefore, it looks as if the curve $S_3^+(\boldsymbol{v}_r)$ may intersect the curve $R_1^-(\boldsymbol{v}_l)$ instead of $S_1^+(\boldsymbol{v}_l)$. But this does not happen. Consider a point $P_r'(m_r, \theta_r')$ on $S_3^-(\boldsymbol{v}_l)$ above the point $P_r(m_r, \theta_r)$. By Lemma 2.3.2, the curve $S_3^+(m_r, \theta_r')$ passes through $\boldsymbol{v}_l = (m_l, 0)$. But the curve $S_3^+(m_r, \theta_r)$ is obtained by translating the curve $S_3^+(m_r, \theta_r')$ in the negative direction of θ-axis by a distance $\theta_r - \theta_r'$ and hence will meet $S_1^+(\boldsymbol{v}_l)$ at a point $P_i(m_i, \theta_i)$. Thus, we get the following result

$$(m_r, \theta_r) \in C \to \mathcal{K}_1\mathcal{K}_3. \tag{2.5.3}$$

The geometrical shape of Ω_t if $(m_r, \theta_r) \in C$ is shown in Fig. 2.5.3.

Similar arguments as above can be made to show the result depicted in Fig. 2.5.4. i.e.,

$$(m_r, \theta_r) \in D \to \mathcal{R}_1\mathcal{K}_3. \tag{2.5.4}$$

Finally, let $(m_r, \theta_r) \in E$. Then $\theta_r > \theta_+^* + \int_1^{m_r} \sqrt{\frac{-G'(m)}{mG(m)}}\, dm$, where θ_+^* is given by (2.3.2), and hence $R_3^-(\boldsymbol{v}_r)$ touches the line $m = 1$ at $\theta > \theta_+^*$. This shows that there exist no intermediate state which joins $\boldsymbol{u}_l$ on the left and $\boldsymbol{u}_r$ on the right. Thus, we get the following theorem.

2.5.1 Theorem *When $P_r \in E$, there is no solution for the Riemann problem. For every pair m_l and m_r, and m_r sufficiently close to 1; there exists an angle $\theta_c(m_l, m_r)(0 < \theta_c < \pi)$ such that if $\theta_r > \theta_c(m_l, m_r)$, the solution fails to exist.*

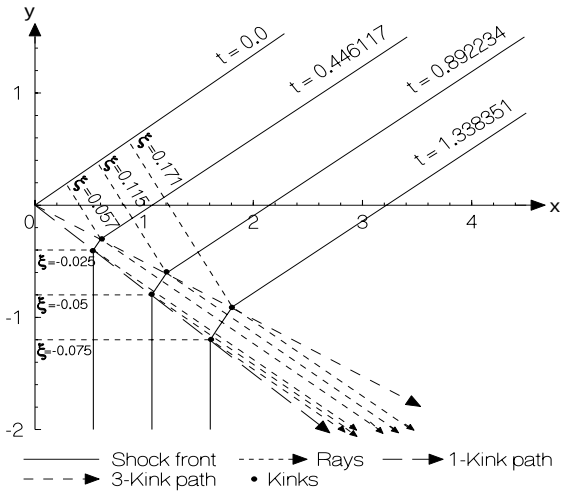

Fig. 2.5.3: $\boldsymbol{v}_r \in C$ *with* $m_l = 1.2$, $m_r = 1.3$.

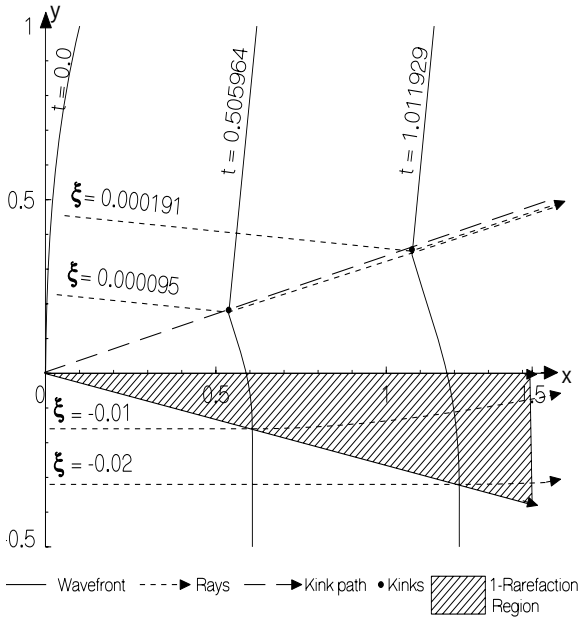

Fig. 2.5.4: $\boldsymbol{v}_r \in D$ *with* $m_l = 1.2$, $m_r = 1.02$.

We have not examined so far the case $m \to 1+$. We notice from the assumption **A1** in section 2.2, that $G(m) \to \infty$ as $m \to 1+$. As $gd\xi = G(m)d\xi$ represents an element of length dl along the wavefront Ω_t, it follows that between two given rays corresponding to ξ and $\xi + \delta\xi$, the distance $\delta l = G(m)(\delta\xi)$ tends to infinity as $m \to 1+$. It means that the energy flux $F(m) = 1/G(m)$ along a ray tends to zero as $m \to 1+$. The situation is similar to that encountered in gas dynamics where the mass density $\rho \to 0$ implies appearance of a vacuum (Courant and Friedrichs, 1948) in a piston problem when the piston is withdrawn sufficiently rapidly giving a complete simple wave (see also Prasad, 2001, section 3.1.1). In our theory, a *vacuum* with vanishing energy flux appears on the wavefront Ω_t wherever $m \to 1+$.

We have not studied the way in which this limiting process takes place but we can quickly write down the consequences of KCL in the degenerate case when $m = 1$:

$$\theta_t = 0 \quad , \quad g_t = \theta_\xi. \tag{2.5.5}$$

The first equation states that the rays are straight lines given by $x_t = \cos\theta, y_t = \sin\theta$. The second one is the usual relation of the convergence of rays with the ray tube area. Thus, $m = 1$ corresponds to the linear theory. It is an important and difficult problem to study mathematically. The transition from linear to weakly nonlinear results are first experimentally observed by Sturtevant and Kulkarni (1976).

Chapter 3

Interaction of Elementary Shapes

§3.1 Introduction

In the previous chapter, we solved the Riemann problem for kinematical conservation laws (KCL) in a ray coordinate system (ξ, t) (Morton, Prasad and Ravindran, 1992) given by

$$(g\sin\theta)_t + (m\cos\theta)_\xi = 0, \tag{3.1.1}$$

$$(g\cos\theta)_t - (m\sin\theta)_\xi = 0 \tag{3.1.2}$$

and we justified that the additional conservation law $(gG(m))_t = 0$ can be integrated and for a suitable choice of the ray coordinate ξ, this conservation law can be written as

$$g = G(m), \tag{3.1.3}$$

where the function G is subjected to certain assumptions as stated in section 2.2. We studied the solution involving centered rarefaction waves and shock waves which are called the *elementary waves*. We also studied the geometrical features of the *elementary shapes* which are the images on (x, y)-plane of the elementary waves in the (ξ, t)-plane, under the transformation given by the equations

$$x_t = m\cos\theta, \quad y_t = m\sin\theta.$$

Interaction of elementary waves of (3.1.1)-(3.1.3) in the (ξ, t)-plane gives rise to new emerging elementary waves, which are essential in establishing the existence theorem for a general initial value problem (Glimm, 1965 and Liu, 1977). It also provides a very detailed picture of solutions with rich geometric structure both in the (ξ, t)-plane and in the (x, y)-plane, and interesting techniques of numerical computation like random choice method developed by Glimm (1965) which has been implemented as a successful numerical scheme

by Chorin (1976) and front tracking algorithm proposed by Dafermos (1972), which is used by Bressan and his coworkers in the mathematical analysis of system of hyperbolic conservation laws in one space variable (2000) (see N. H. Risebro, 1993, H. Holden and N. H. Risebro, 2002 for implementation). Moreover, it has its own significance in some other practical applications, for instance in the understanding of shock tube experiments (See Courant and Friedrichs, 1948).

In this chapter, we use the results obtained in the previous chapter to study the interaction of elementary waves of KCL (3.1.1)-(3.1.2) with the relation (3.1.3), where G is subjected to the assumptions (**A1**)-(**A4**) discussed in section 2.2. We also study numerically, the geometrical features of the wavefront as a result of interaction of the elementary shapes in the (x, y)-plane. For numerical computations, we use discontinuous Galerkin finite element method (see Cockburn, et. al., 1989) which we have discussed in Appendix 1.

§3.2 Interaction of Elementary Shapes

We consider two elementary shapes separated by a straight part on a wavefront Ω_t in the (x, y)-plane, which correspond to the initial stages of the solution of the system (3.1.1)-(3.1.3) with the following initial data

$$\boldsymbol{v}(\xi, 0) = \begin{cases} \boldsymbol{v}_l = (m_l, 0) & , \quad -\infty < \xi \leq 0 \\ \boldsymbol{v}_0 = (m_0, \theta_0) & , \quad 0 < \xi \leq \xi_r \\ \boldsymbol{v}_r = (m_r, \theta_r) & , \quad \xi_r < \xi \leq \infty \end{cases} \tag{3.2.1}$$

for an appropriate choice of $\boldsymbol{v}_0$ and $\boldsymbol{v}_r$ in terms of $\boldsymbol{v}_l$ and for any non-zero $\xi_r \in I\!R$. With the above initial data, we have two Riemann problems locally as shown in Fig. 3.2.1.

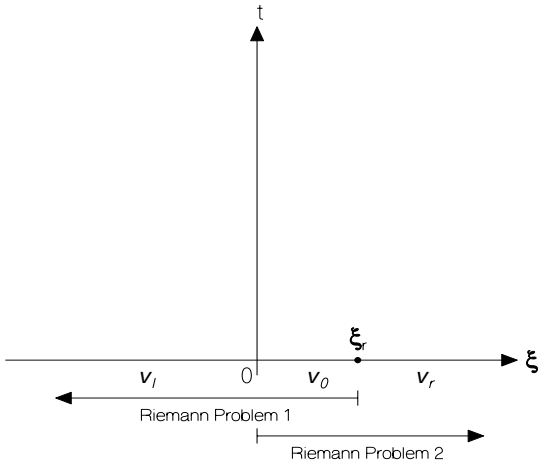

Fig. 3.2.1: *Initial condition in the (ξ, t)-plane.*

An elementary shape of the first Riemann problem may interact with the elementary shape of the second Riemann problem. The process of interaction if it takes place, may take finite or infinite time depending on the nature as well as the relative strengths of the two corresponding elementary waves in the (ξ, t)-plane. Although, it is not possible to compute the shape of Ω_t during the process of interaction without a full numerical solution of the system (3.1.1)-(3.1.3), we shall see that we can make a very good prediction of the final results qualitatively.

When the interaction period is finite, we show that the final results will again consist of a pair of elementary shapes. All these geometrical features of Ω_t can be studied from the corresponding results on the interaction of simple waves and shock waves in (ξ, t)-plane. For the interaction of elementary waves from Euler's equations of one-dimensional unsteady gas flow, see Courant and Friedrichs (1948), Smoller (1983).

In order to describe the result of interaction, we use a notation $\mathcal{E}_i\mathcal{E}_j$ to denote a state of Ω_t corresponding to an elementary shape $\mathcal{E}_i$ joining states $\boldsymbol{v}_l$, $\boldsymbol{v}_0$ and $\mathcal{E}_j$ joining $\boldsymbol{v}_0$ and $\boldsymbol{v}_r$ on Ω_t. Thus, $\mathcal{R}_1\mathcal{K}_1 \to \mathcal{K}_1\mathcal{R}_3$ means that interaction of $\mathcal{R}_1$ elementary shape and $\mathcal{K}_1$ elementary shape will give $\mathcal{K}_1$ kink and $\mathcal{R}_3$ shape. Interactions are of two type, namely interaction of elementary shapes from different families and interaction of elementary shapes from same family. All possible interaction of elementary shapes from different families are : $\mathcal{K}_3\mathcal{R}_1$, $\mathcal{R}_3\mathcal{K}_1$, $\mathcal{K}_3\mathcal{K}_1$, and $\mathcal{R}_3\mathcal{R}_1$. Possible interaction of elementary shapes from same family are: $\mathcal{K}_1\mathcal{K}_1$, $\mathcal{K}_3\mathcal{K}_3$, $\mathcal{R}_1\mathcal{K}_1$, $\mathcal{K}_1\mathcal{R}_1$, $\mathcal{R}_3\mathcal{K}_3$ and $\mathcal{K}_3\mathcal{R}_3$. We note here that the $\mathcal{R}_1\mathcal{R}_1$ and $\mathcal{R}_3\mathcal{R}_3$ interactions are not possible.

All figures have been drawn by taking

$$G(m) = (m-1)^{-2}e^{-2(m-1)}.$$

§3.2.1 Interaction of Elementary Shapes From Different Family

(i) $\mathcal{K}_3\mathcal{R}_1$ **interaction:** We consider the initial value problem (3.1.1)-(3.2.1) in such a way that $\boldsymbol{v}_0 \in S_3^-(\boldsymbol{v}_l)$ and $\boldsymbol{v}_r \in R_1^-(\boldsymbol{v}_0)$ as shown in Fig. 3.2.2. In other words, for a given $\boldsymbol{v}_l$, we choose $\boldsymbol{v}_0$ and $\boldsymbol{v}_r$ in such a way that

$$m_l > m_0,\ \theta_0 = -\cos^{-1}\left(\frac{m_lG(m_l)+m_0G(m_0)}{m_lG(m_0)+m_0G(m_l)}\right) = -h(m_l, m_0),$$

$$1 < m_r < m_0,\ \theta_r = \theta_0 + \int_{m_r}^{m_l}\sqrt{\frac{-G'(m)}{mG(m)}}dm.$$

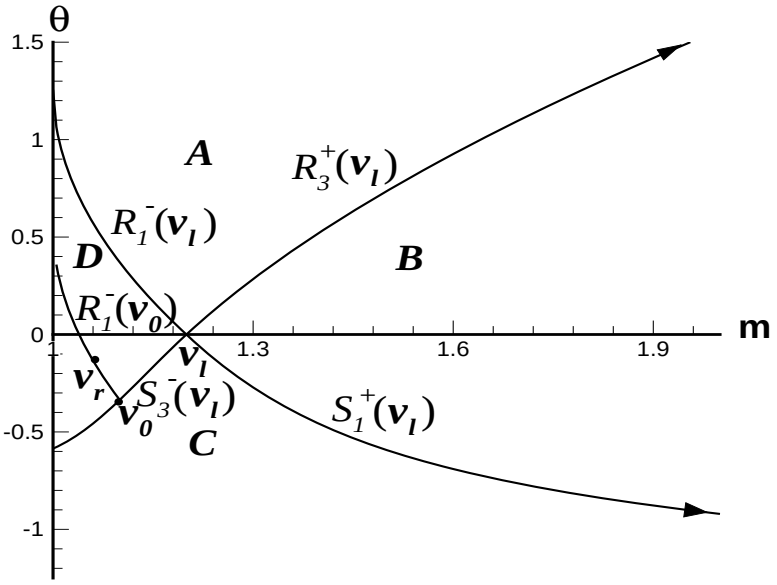

Fig. 3.2.2: *For $\mathcal{K}_3\mathcal{R}_1$ interaction, the point $\boldsymbol{v}_0 \in S_3^-(\boldsymbol{v}_l)$ and $\boldsymbol{v}_r \in R_1^-(\boldsymbol{v}_0)$, resulting $\boldsymbol{v}_r \in D$.*

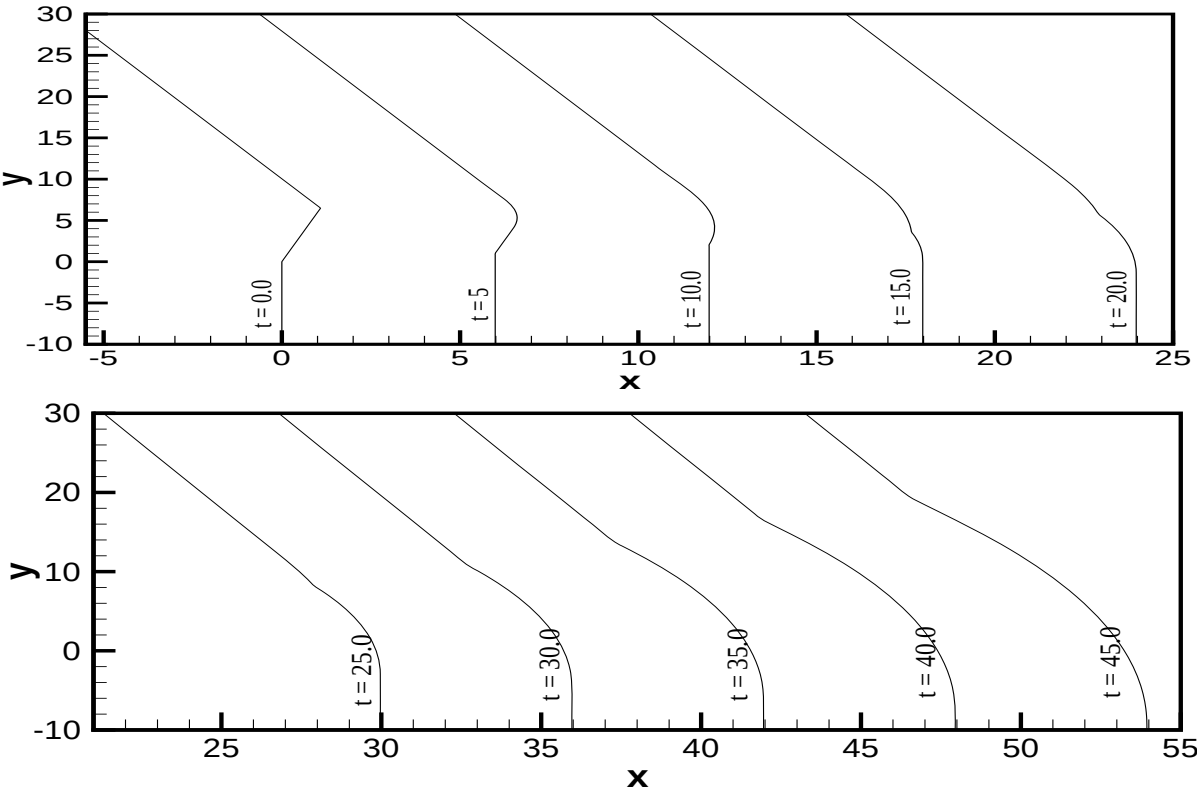

Fig 3.2.3: *Propagation of elementary shapes in the (x, y)-plane for $\mathcal{K}_3\mathcal{R}_1$ interaction with $m_l = 1.2$, $\theta_l = 0$; $m_0 = 1.15$, $\theta_0 = -0.166033$; $m_r = 1.05$, $\theta_r = 0.296956$.*

Since $m_0 < m_l$, the curve $R_1^-(\boldsymbol{v}_0)$ lies entirely in the domain D and hence, the interaction result (see section 2.5) is

$$\mathcal{K}_3\mathcal{R}_1 \to \mathcal{R}_1\mathcal{K}_3. \tag{3.2.2}$$

After the interaction, shapes $\mathcal{R}_1$ and $\mathcal{K}_3$ are separated by a straight part with $m = m_i$, $\theta = \theta_i$. The successive positions and the different shapes of Ω_t at various times is depicted in Fig. 3.2.3.

(ii) $\mathcal{R}_3\mathcal{K}_1$ **interaction:** Here $\boldsymbol{v}_0 \in R_3^+(\boldsymbol{v}_l)$ and $\boldsymbol{v}_r \in S_1^+(\boldsymbol{v}_0)$ as shown in Fig. 3.2.4. That is, for a given $\boldsymbol{v}_l$, we choose $\boldsymbol{v}_0$ and $\boldsymbol{v}_r$ such that

$$m_l < m_0,\ \theta_0 = \int_{m_l}^{m_0} \sqrt{\frac{-G'(m)}{mG(m)}}dm,$$
$$m_0 < m_r,\ \theta_r = \theta_0 - \cos^{-1}\left(\frac{m_rG(m_r) + m_0G(m_0)}{m_rG(m_0) + m_0G(m_r)}\right) = \theta_0 - h(m_0, m_r).$$

Since $S_1^+(\boldsymbol{v}_0)$ and $S_1^+(\boldsymbol{v}_l)$ are asymptotic to $\theta = \theta_0 - \pi/2$ and $\theta = \theta_l - \pi/2$ respectively and $\theta_0 > \theta_l$, we have $\boldsymbol{v}_r \in B$. This argument, for $\boldsymbol{v}_r \in B$ is not rigorous because we have not proved that the curve $S_1^+(\boldsymbol{v}_0)$ would not go below $S_1^+(\boldsymbol{v}_l)$ and then again come up above it i.e., those two curves would not intersect one another even number of times. However, we accept without proof that the two curves do not intersect and $\boldsymbol{v}_r \in B$. Then, it follows (see section 2.5) that

$$\mathcal{R}_3\mathcal{K}_1 \to \mathcal{K}_1\mathcal{R}_3. \tag{3.2.3}$$

The successive positions and the different shapes of Ω_t at various times is shown in Fig. 3.2.5.

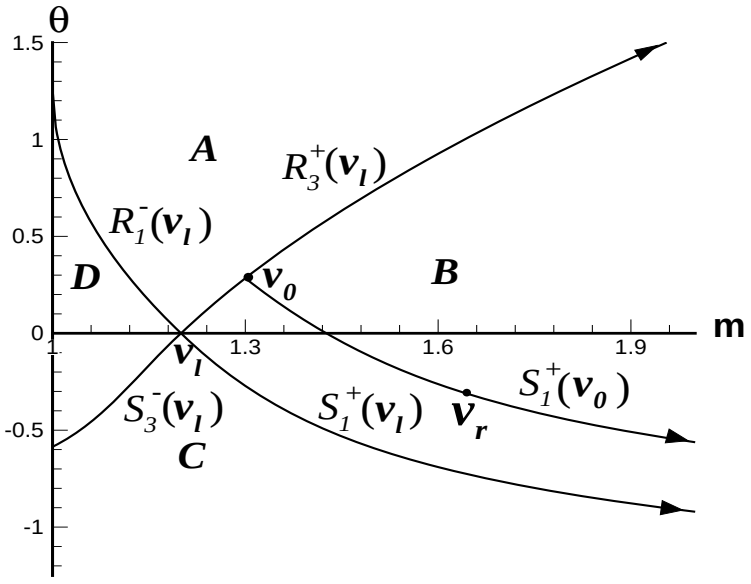

Fig. 3.2.4: *For $\mathcal{R}_3\mathcal{K}_1$ interaction, the point $\boldsymbol{v}_0 \in R_3^+(\boldsymbol{v}_l)$ and $\boldsymbol{v}_r \in S_1^+(\boldsymbol{v}_0)$, resulting $\boldsymbol{v}_r \in B$.*

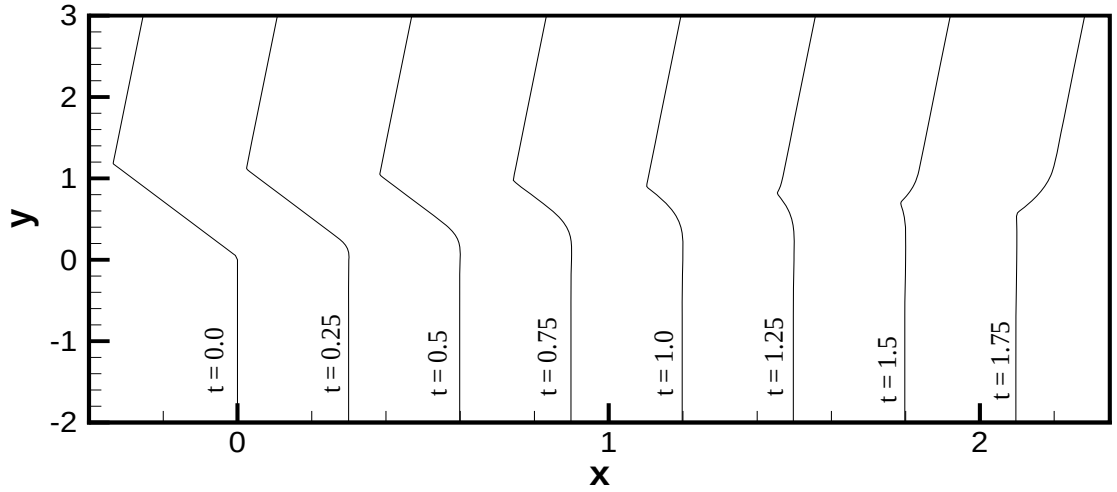

Fig. 3.2.5: *Propagation of elementary shapes in the (x, y)-plane for $\mathcal{R}_3\mathcal{K}_1$ interaction with $m_l = 1.2$, $\theta_l = 0$, $m_0 = 1.3$, $\theta_0 = 0.284282$, $m_r = 1.4$, $\theta_r = 0.051417$.*

(iii) $\mathcal{K}_3\mathcal{K}_1$ **interaction:** Here $\boldsymbol{v}_0 \in S_3^-(\boldsymbol{v}_l)$ and $\boldsymbol{v}_r \in S_1^+(\boldsymbol{v}_0)$ as shown in Fig. 3.2.6. In other words, for a given $\boldsymbol{v}_l$, we choose $\boldsymbol{v}_0$ and $\boldsymbol{v}_r$ such that

$$m_0 < m_l,\ \theta_0 = -\cos^{-1}\left(\frac{m_l G(m_l) + m_0 G(m_0)}{m_l G(m_0) + m_0 G(m_l)}\right) = -h(m_l, m_0),$$
$$m_0 < m_r,\ \theta_r = \theta_0 - \cos^{-1}\left(\frac{m_r G(m_r) + m_0 G(m_0)}{m_r G(m_0) + m_0 G(m_r)}\right) = \theta_0 - h(m_0, m_r),$$

so that $\boldsymbol{v}_r \in C$. As in the previous case, there is no rigorous proof here and we accept that $\boldsymbol{v}_r \in C$. Hence, (see section 2.5) we get

$$\mathcal{K}_3\mathcal{K}_1 \to \mathcal{K}_1\mathcal{K}_3. \tag{3.2.4}$$

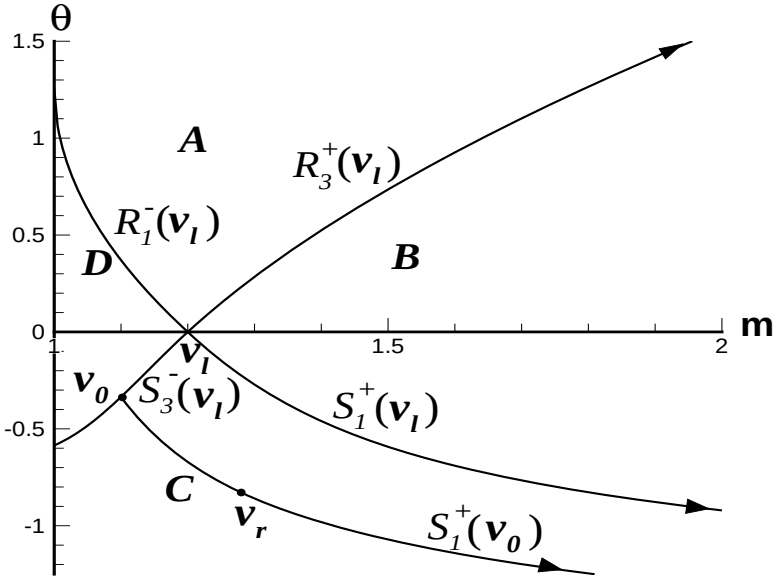

Fig. 3.2.6: *For $\mathcal{K}_3\mathcal{K}_1$ interaction, the point $\boldsymbol{v}_0 \in S_3^-(\boldsymbol{v}_l)$ and $\boldsymbol{v}_r \in S_1^+(\boldsymbol{v}_0)$, resulting $\boldsymbol{v}_r \in C$.*

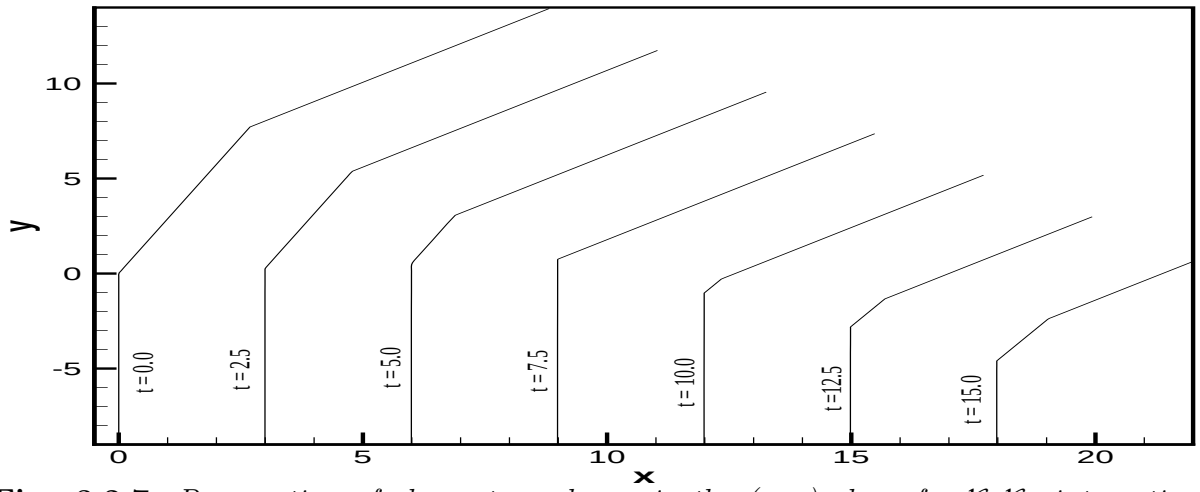

Fig. 3.2.7: *Propagation of elementary shapes in the (x, y)-plane for $\mathcal{K}_3\mathcal{K}_1$ interaction $m_l = 1.2$, $\theta_l = 0$; $m_0 = 1.1$, $\theta_0 = -0.335657$; $m_r = 1.25$, $\theta_r = -0.776916$.*

The propagation of the elementary shapes on Ω_t in the (x, y)-plane is depicted in Fig. 3.2.7.

(iv) $\mathcal{R}_3\mathcal{R}_1$ **interaction:** This interaction takes place when $\boldsymbol{v}_0 \in R_3^+(\boldsymbol{v}_l)$ and $\boldsymbol{v}_r \in R_1^-(\boldsymbol{v}_0)$, i.e.,

$$m_l < m_0,\ \theta_0 = \int_{m_l}^{m_0} \sqrt{\frac{-G'(m)}{mG(m)}}dm$$

$$1 < m_r < m_0,\ \theta_r = \theta_0 + \int_{m_r}^{m_l} \sqrt{\frac{-G'(m)}{mG(m)}}dm$$

as shown in Fig. 3.2.8. This interaction will always be complete since the trailing end of 3-R wave has a positive velocity (bounded below) in (ξ, t)-plane and that of 1-R wave has a negative velocity (bounded above). Since $\boldsymbol{v}_0 \in R_3^+(\boldsymbol{v}_l)$ except when $m_l = 1$, the case for which our theory is not valid, $R_1^-(\boldsymbol{v}_0)$ may intersect either the curve T or the boundary $\theta = \pi$. Hence there exists a $\delta_4(m_l, m_0)$ such that for

$$m_r - m_0 = \delta_4(m_l, m_0),\ \boldsymbol{v}_r \in T \text{ or the line } \theta = \pi \tag{3.2.5}$$

We now give an equation to determine $\delta_4(m_l, m_0)$ when $\boldsymbol{v}_r \in T$. Since $\boldsymbol{v}_0 \in \mathcal{R}_3^+(\boldsymbol{v}_l)$ with $\theta_l = 0$, and $\boldsymbol{v}_r \in \mathcal{R}_1^-(\boldsymbol{v}_0)$, we get

$$\theta_0 = \int_{m_l}^{m_0} \sqrt{\frac{-G'(m)}{mG(m)}}dm,\ \theta_r = \theta_0 + \int_{m_r}^{m_0} \sqrt{\frac{-G'(m)}{mG(m)}}dm.$$

On the other hand, since $\boldsymbol{v}_r \in T$, the expression of the curve T gives

$$\theta_r = \theta_+^* + \int_1^{m_r} \sqrt{\frac{-G'(m)}{mG(m)}}dm.$$

Since θ is monotonically increasing function of the curve T and is monotonically decreasing on $R_1^-(\boldsymbol{v}_0)$, these two curves will intersect at a unique point. This point of intersection can be obtained by equating the above two expressions for θ_r, which gives after simplification

$$\int_1^{m_r} \sqrt{\frac{-G'(m)}{mG(m)}}dm = \int_{m_l}^{m_0} \sqrt{\frac{-G'(m)}{mG(m)}}dm. \tag{3.2.6}$$

Once the function G is given explicitly, M (where we have written M for m_r), can be obtained from the above expression and hence δ_4 can be calculated using the formula $\delta_4 = m_0 - M$. This leads to the following result

(a) If $m_0 - m_r < \delta_4(m_l, m_0)$, $\boldsymbol{v}_r \in A$ and we have

$$\mathcal{R}_3\mathcal{R}_1 \to \mathcal{R}_1\mathcal{R}_3. \tag{3.2.7}$$

(b) When $m_0 - m_r = \delta_4$, then $\boldsymbol{v}_r \in T$, and therefore, the 1-R wave ends up at the point $\boldsymbol{v}_r$ on T - this point can be joined to $\boldsymbol{v}_l$ by a 1-R wave on the left and a 3-R wave on the right through the point ($m = 1,\ \theta = \theta_+^*$), which represents a vacuum with vanishing energy flux. This is not an acceptable solution as the ray coordinate formulation breaks down. Our theory does not provide any information on the result of this interaction.

(c) when $m_0 - m_r > \delta_4$, then the point $\boldsymbol{v}_r \in E$ and our theory again provides no information on the result of this interaction.

(d) When $\boldsymbol{v}_r$ lies on the line $\theta = \pi$, we get a limiting case of the wavefront folding on itself. This degenerate case does not seem to be physically realistic.

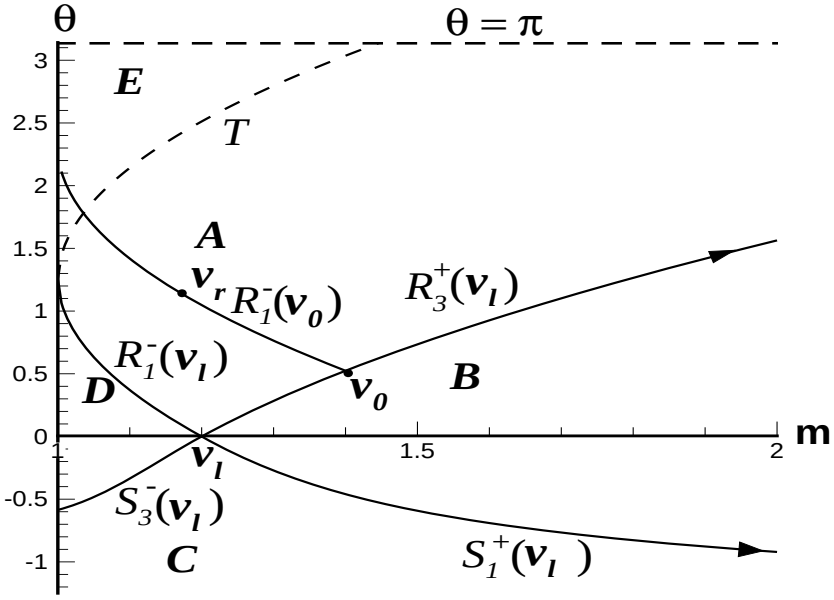

Fig. 3.2.8: *For $\mathcal{R}_3\mathcal{R}_1$ interaction, the point $\boldsymbol{v}_0 \in R_3^+(\boldsymbol{v}_l)$ and $\boldsymbol{v}_r \in R_1^-(\boldsymbol{v}_0)$, resulting $\boldsymbol{v}_r \in A$ for a sufficiently weak 1-R wave.*

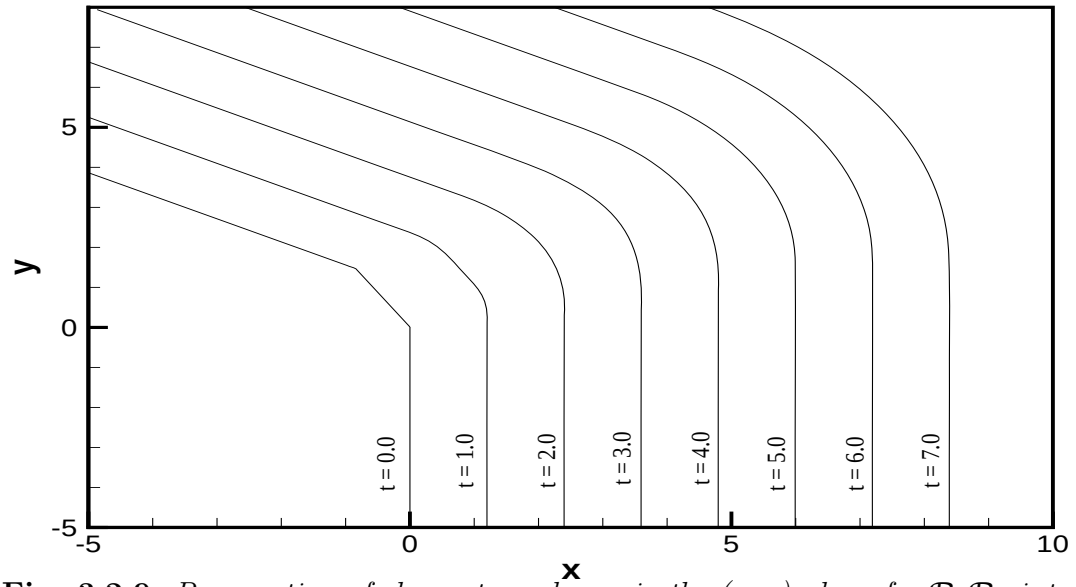

Fig. 3.2.9: *Propagation of elementary shapes in the (x, y)-plane for $\mathcal{R}_3\mathcal{R}_1$ interaction with $m_l = 1.2$, $\theta_l = 0$; $m_0 = 1.3$, $\theta_0 = 0.284282$; $m_r = 1.1$, $\theta_r = 0.939048$.*

The successive positions and the different shapes of Ω_t at various times is shown in Fig. 3.2.9.

We have now completed the interaction analysis of elementary shapes of different characteristic families. We note (from Figures 3.2.2, 3.2.4, 3.2.6 and 3.2.8) that if any of the elementary shape is weak before the interaction, the corresponding transmitted wave is also weak (measured in terms of jump in m).

§3.2.2 Interaction of Elementary Shapes From Same Family

(v) $\mathcal{K}_1\mathcal{K}_1$ **interaction:** We consider the initial value problem (3.1.1)-(3.2.1) in such a way that $\boldsymbol{v}_0 \in S_1^+(\boldsymbol{v}_l)$ and $\boldsymbol{v}_r \in S_1^+(\boldsymbol{v}_0)$. In other words, for a given left state $\boldsymbol{v}_l$, the intermediate state $\boldsymbol{v}_0$, and the right state $\boldsymbol{v}_r$ are chosen such that

$$m_l < m_0,\ \theta_0 = -\cos^{-1}\left(\frac{m_l G(m_l) + m_0 G(m_0)}{m_l G(m_0) + m_0 G(m_l)}\right) = -h(m_l, m_0),$$
$$m_0 < m_r,\ \theta_r = \theta_0 - \cos^{-1}\left(\frac{m_0 G(m_0) + m_r G(m_r)}{m_0 G(m_r) + m_r G(m_0)}\right) = \theta_0 - h(m_0, m_r).$$

It is one of the difficult cases where we are unable to prove whether $S_1^+(\boldsymbol{v}_0)$ which starts from $\boldsymbol{v}_0$, enters into the domain C or the domain B. We take help of drawing the curves $S_1^+(\boldsymbol{v}_0)$ by numerical computation for a large number of values of the parameters k and n in (2.2.3) and m_0, and verify that the point $\boldsymbol{v}_r$ remains entirely in C. This result as $m \to \infty$ is true, as can be seen from the fact that θ on $S_1^+(\boldsymbol{v}_l)$ tends to $-\pi/2$ and θ on $S_1^+(\boldsymbol{v}_0)$ tends to $\theta_0 - \pi/2$ with $\theta_0 < 0$. Once we accept that $S_1^+(\boldsymbol{v}_0)$ lies entirely in the

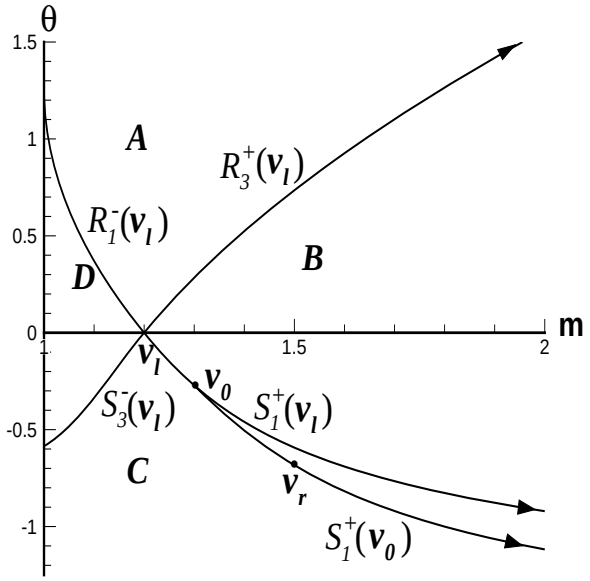

Fig. 3.2.10: *For $\mathcal{K}_1\mathcal{K}_1$ interaction, the point $\boldsymbol{v}_0 \in S_1^+(\boldsymbol{v}_l)$, $\boldsymbol{v}_r \in S_1^+(\boldsymbol{v}_0)$, resulting $\boldsymbol{v}_r \in C$.*

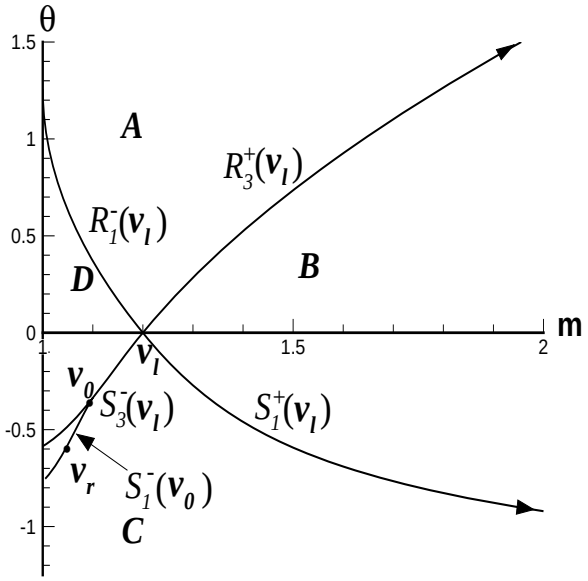

Fig. 3.2.11: *For $\mathcal{K}_3\mathcal{K}_3$ interaction, the point $\boldsymbol{v}_0 \in S_3^-(\boldsymbol{v}_l)$, $\boldsymbol{v}_r \in S_3^-(\boldsymbol{v}_0)$, resulting $\boldsymbol{v}_r \in C$.*

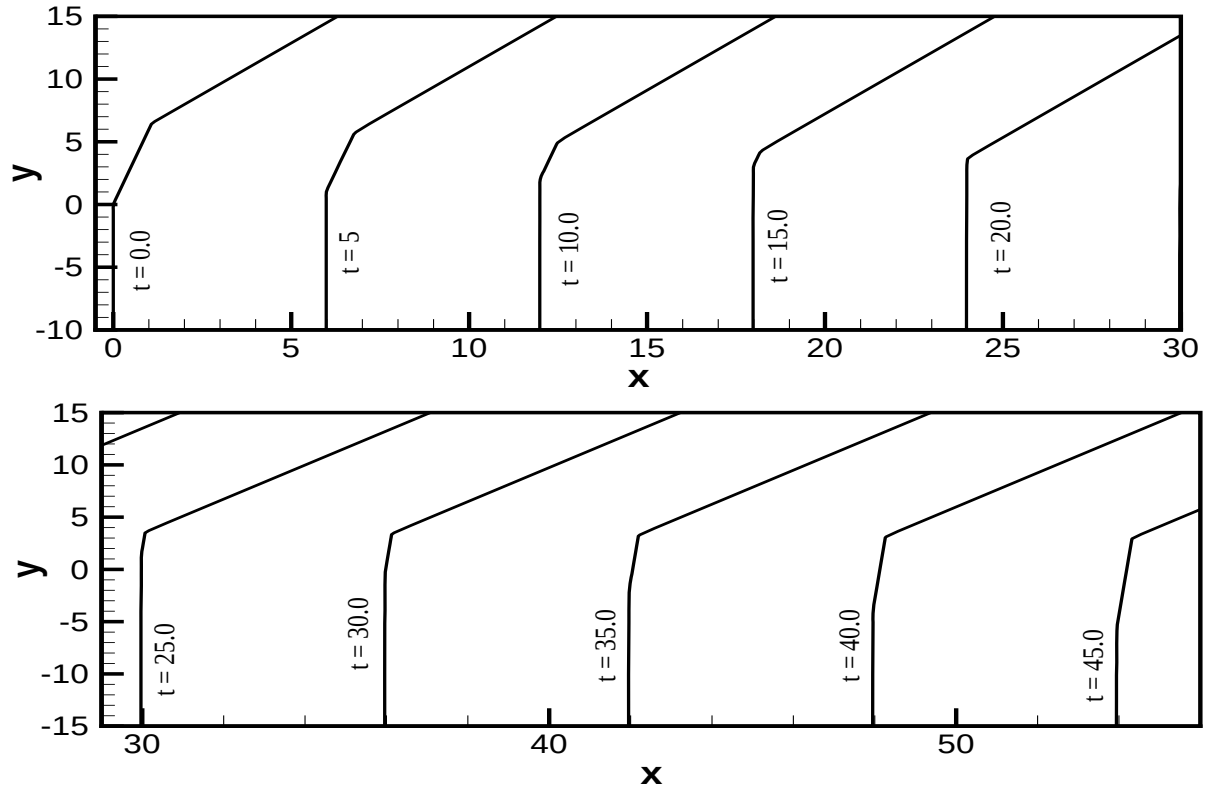

Fig. 3.2.12: *Propagation of elementary shapes in the (x, y)-plane for $\mathcal{K}_3\mathcal{K}_3$ interaction with $m_l = 1.2$, $\theta_l = 0$; $m_0 = 1.15$, $\theta_0 = -0.166033$; $m_r = 1.05$, $\theta_r = -0.550454$.*

domain C, we get the result

$$\mathcal{K}_1\mathcal{K}_1 \to \mathcal{K}_1\mathcal{K}_3. \tag{3.2.8}$$

Note that $\mathcal{K}_1\mathcal{K}_1$ interaction generates a reflected kink $\mathcal{K}_3$. From Fig. 3.2.10, since $S_1^+(\boldsymbol{v}_l)$ and $S_1^+(\boldsymbol{v}_0)$ are quite close, it follows that the reflected $\mathcal{K}_3$ is weak compared to the $\mathcal{K}_1(\boldsymbol{v}_0, \boldsymbol{v}_r)$ before the interactions. Further, the resulting $\mathcal{K}_1$ kinks after interaction increases its strength significantly if $\mathcal{K}_1(\boldsymbol{v}_0, \boldsymbol{v}_r)$ is not weak. The above results are also observed in the numerical datas given in Table. 3.2.1.

Table 3.2.1

Table for $m-1$ before interaction and the strength of the emerging $\mathcal{K}_1$ and $\mathcal{K}_3$ kinks with respect to m after interaction. We take $m_l = 1.2$ and $\theta_l = 0$.

$m_0 - 1$	$m_r - 1$	$\mathcal{K}_1$	$\mathcal{K}_3$
0.25	0.3	0.10195	0.00195
0.25	0.35	0.15538	0.00538
0.25	0.4	0.20977	0.00977
0.25	0.45	0.26473	0.01473
0.25	0.5	0.32001	0.02001

The geometry of the wavefront Ω_t associated with the above interaction result are similar to that in the case of $\mathcal{K}_3\mathcal{K}_3$ interaction shown in Fig. 3.2.12.

(vi) $\mathcal{K}_3\mathcal{K}_3$ **interaction:** $\mathcal{K}_3\mathcal{K}_3$ interaction takes place when $\boldsymbol{v}_0 \in S_3^-(\boldsymbol{v}_l)$ and $\boldsymbol{v}_r \in S_3^-(\boldsymbol{v}_0)$. In other words, if $\boldsymbol{v}_l$ is given, we choose $\boldsymbol{v}_0$ and $\boldsymbol{v}_r$ such that

$$\begin{aligned} &m_l > m_0,\ \theta_0 = -\cos^{-1}\left(\frac{m_l G(m_l) + m_0 G(m_0)}{m_l G(m_0) + m_0 G(m_l)}\right) = -h(m_l, m_0), \\ &m_0 > m_r,\ \theta_r = \theta_0 - \cos^{-1}\left(\frac{m_0 G(m_0) + m_r G(m_r)}{m_0 G(m_r) + m_r G(m_0)}\right) = \theta_0 - h(m_0, m_r). \end{aligned}$$

As discussed in the previous case, we find that the curve $S_3^-(\boldsymbol{v}_0)$ lies entirely in C as shown in Fig. 3.2.11. Therefore, we get the result

$$\mathcal{K}_3\mathcal{K}_3 \to \mathcal{K}_1\mathcal{K}_3. \tag{3.2.9}$$

The geometry of the wavefront Ω_t associated with the above interaction result is shown in Fig. 3.2.12. We note that the reflected $\mathcal{K}_1$ kink would, *in general*, be weak compared to the incident $\mathcal{K}_3(\boldsymbol{v}_0, \boldsymbol{v}_r)$ kink. We have used "in general" because $S_3^-(\boldsymbol{v}_l)$ and $S_3^-(\boldsymbol{v}_0)$ curves have points of inflections.

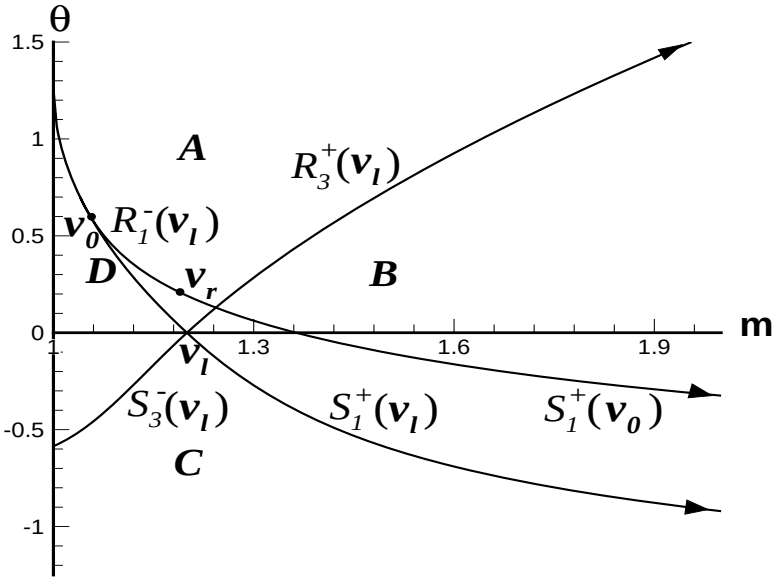

Fig. 3.2.13: *For $\mathcal{R}_1\mathcal{K}_1$ interaction, the point $\boldsymbol{v}_0 \in R_1^-(\boldsymbol{v}_l)$ and $\boldsymbol{v}_r \in S_1^+(\boldsymbol{v}_0)$, resulting $\boldsymbol{v}_r$ lies in A or in B depending on the strength of the 1-S shock.*

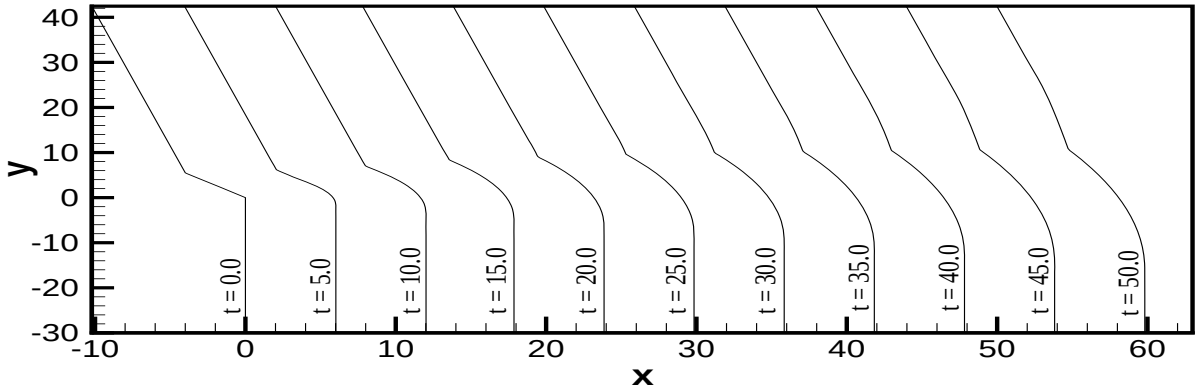

Fig. 3.2.14: *Propagation of elementary shapes in the (x, y)-plane for $\mathcal{R}_1\mathcal{K}_1$ interaction when $\boldsymbol{v}_r \in A$ with $m_l = 1.2$, $\theta_l = 0$; $m_0 = 1.05$, $\theta_0 = 0.632456$; $m_r = 1.19$, $\theta_r = 0.166588$.*

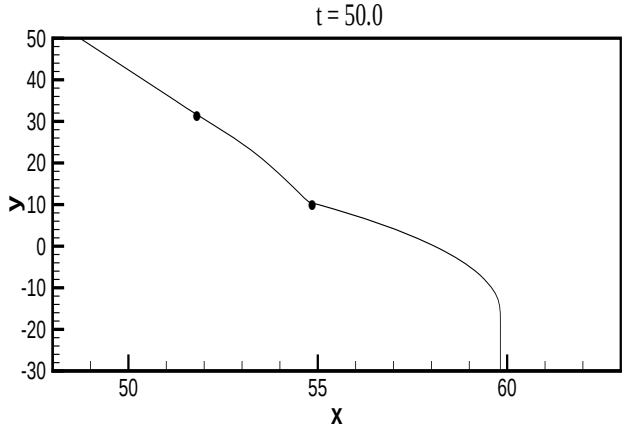

Fig. 3.2.15: *$\mathcal{R}_1\mathcal{K}_1$ interaction. Wavefront at t =50 with a weak reflected $\mathcal{R}_3$ elementary shape between the two dots.*

(vii) $\mathcal{R}_1\mathcal{K}_1$ **interaction:** We now consider the case when the shock of the first family in the second Riemann problem overtakes the rarefaction wave of the first family in the first Riemann problem. This situation occurs when $\boldsymbol{v}_0 \in R_1^-(\boldsymbol{v}_l)$ and $\boldsymbol{v}_r \in S_1^+(\boldsymbol{v}_0)$ as shown in Fig. 3.2.13. That is, for a given $\boldsymbol{v}_l$, we choose $\boldsymbol{v}_0$ and $\boldsymbol{v}_r$ in such a way that

$$1 < m < m_l,\ \theta_0 = \int_{m_0}^{m_l} \sqrt{\frac{-G'(m)}{mG(m)}}dm,$$
$$m_0 < m_r,\ \theta_r = \theta_0 - \cos^{-1}\left(\frac{m_0G(m_0) + m_rG(m_r)}{m_0G(m_r) + m_rG(m_0)}\right) = \theta_0 - h(m_0, m_r).$$

This is a case where the interaction is not completed in finite time when the strength of the 1-S wave is sufficiently small.

From numerical observations, we take $S_1^+(\boldsymbol{v}_0)$ to be above $R_1^-(\boldsymbol{v}_l)$ i.e., in the domain A for small values of $m_r - m_0$. Then, there exists a value $\delta_7(m_l, m_0)$ say, such that for $m_r - m_0 = \delta_7(m_l, m_0)$, the point $\boldsymbol{v}_r \in R_3^+(\boldsymbol{v}_l)$. The value δ_7 is given by $\delta_7(m_l, m_0) = m_0 - M$, where M can be obtained as the solution of the equation

$$\int_{m_l}^{M} \sqrt{\frac{-G'}{mG(m)}} = \theta_0 - h(m_0, M) \tag{3.2.10}$$

(a) When $m_r - m_0 = \delta_7(m_l, m_0)$, the interaction will continue for infinite time and we get $\mathcal{R}_1\mathcal{K}_1 \to \mathcal{R}_3$. From the theorem on the persistence of a shock (Prasad, 2001, p 35, see also Prasad, 1993)), $\mathcal{K}_1$ cannot disappear in finite time. In this case both, 1-R wave and 1-S shock keep on interacting with diminishing strengths and we get

$$\mathcal{R}_1\mathcal{K}_1 \to \mathcal{R}_1\mathcal{K}_1\mathcal{R}_3, \quad \lim_{t\to\infty} \mathcal{R}_1\mathcal{K}_1\mathcal{R}_3 = \mathcal{R}_3 \tag{3.2.11}$$

In (ξ, t)-plane, the state at any time t on the left of the 3-R wave will tend to $\boldsymbol{v}_l$ as $t \to \infty$. This is a very interesting case, when two waves of the first family interact and give rise to a wave of the third family after the interaction and complete annihilation of one another. At any finite time we have a shape represented by $\mathcal{R}_1\mathcal{K}_1\mathcal{R}_3$ (see Fig. 3.2.15). The reflected $\mathcal{R}_3$ shape is small compared to both incident shapes $\mathcal{R}_1$ and $\mathcal{K}_1$ - a result which is true also in the case (b) below.

(b) When $m_r - m_0 < \delta_7$, $\boldsymbol{v}_r \in A$ and we may think that $\mathcal{R}_1\mathcal{K}_1 \to \mathcal{R}_1\mathcal{R}_3$, which is not strictly correct. The theorem on the persistence of a shock implies that the 1-S shock cannot disappear to form a 1-R wave. The correct result at any finite time is $\mathcal{R}_1\mathcal{K}_1 \to \mathcal{R}_1\mathcal{K}_1\mathcal{R}_3$. In (ξ, t)-plane, the 1-R wave on the left continues to interact indefinitely with the 1-S shock (the shock is unable to penetrate the 1-R wave fully), and there appears asymptotically a constant state $\boldsymbol{v}_i$ which is the state behind the 1-S shock and into which

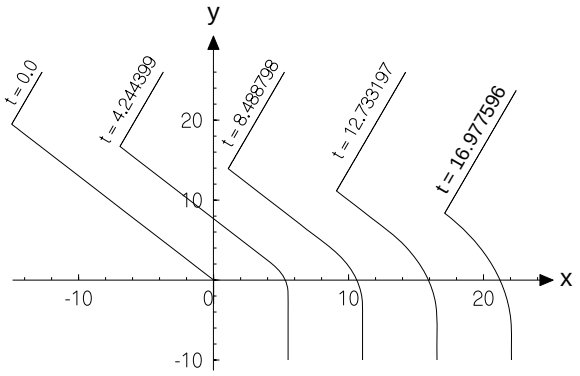

Fig. 3.2.16(a): *From initial to final time of interaction.*

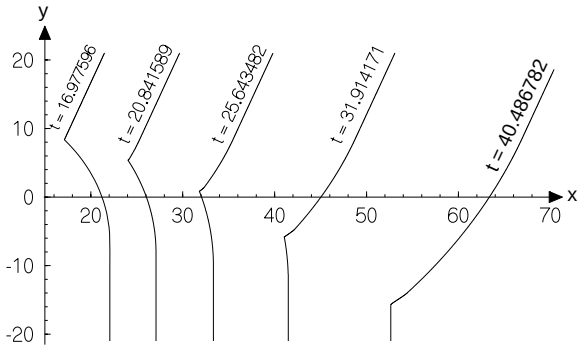

Fig. 3.2.16(b): *Up to the time of interaction.*

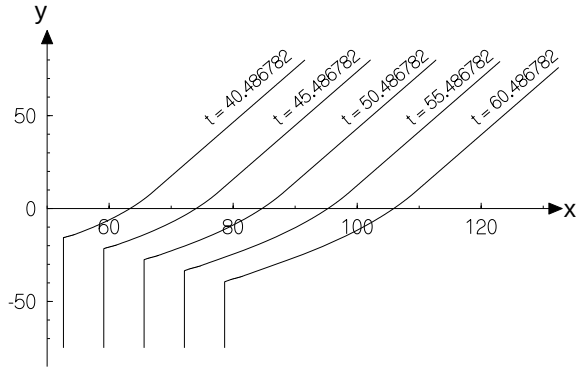

Fig. 3.2.16(c): *After interaction.*

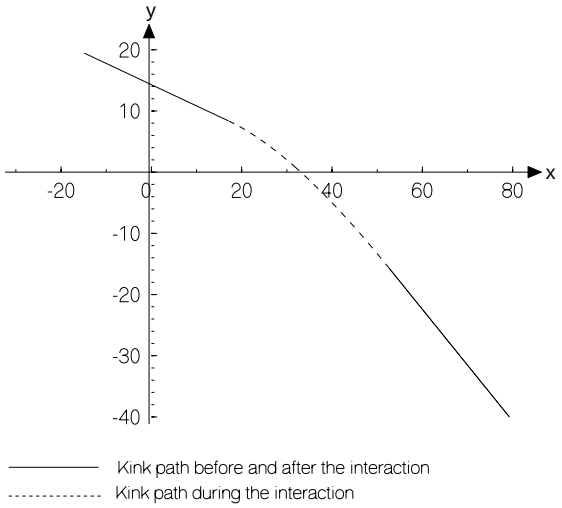

Fig. 3.2.16(d): *Kink path.*

Fig. 3.2.16: *Propagation of elementary shapes in the (x, y)-plane for $\mathcal{R}_1\mathcal{K}_1$ interaction with $m_l = 1.2$, $\theta_l = 0$; $m_0 = 1.1$, $\theta_0 = 0.370484$; $m_r = 1.3$, $\theta_r = -0.153058$.*

the 3-R wave ends on its left. The strength of 1-S shock tends to zero but the two expansion waves 1-R and 3-R will have finite strength confirming

$$\lim_{t\to\infty} \mathcal{R}_1\mathcal{K}_1\mathcal{R}_3 = \mathcal{R}_1\mathcal{R}_3$$

a result which we get from the fact that $\boldsymbol{v}_r \in A$. Thus, we get

$$\mathcal{R}_1\mathcal{K}_1 \to \mathcal{R}_1\mathcal{K}_1\mathcal{R}_3, \quad \lim_{t\to\infty} \mathcal{R}_1\mathcal{K}_1\mathcal{R}_3 = \mathcal{R}_1\mathcal{R}_3 \tag{3.2.12}$$

This result is depicted geometrically in Fig. 3.2.14, in which the wavefront up to time t=50 has been plotted. We observe that the process of interaction continues beyond this time. The wavefront at t=50 has been enlarged in Fig. 3.2.15 in order to show the elementary shape as a bending of the wavefront above the 1-kink which corresponds to the image of the reflecting 3-R wave.

(c) When $m_r - m_0 > \delta_7(m_l, m_0)$, $\boldsymbol{v}_r \in B$. The shock $S_1(\boldsymbol{v}_0, \boldsymbol{v}_r)$, where the bracket now indicates that the 1-S shock joins a state $\boldsymbol{v}_0$ on the left and $\boldsymbol{v}_r$ on the right in (ξ, t)-plane, is strong compared to the simple wave $R_1(\boldsymbol{v}_l, \boldsymbol{v}_0)$ and hence traverses through this simple wave in finite time. The diagram in (m, θ)-plane, which we have been using so far, does not describe the process of interaction but from our understanding of shock propagation we can describe qualitatively the process of interaction. When the 1-S shock overtakes from the right the trailing end of the 1-R wave, a 3-R wave (reflected wave) starts getting generated. The 1-S shock becomes weaker (note $m_0 < m_l$ so that $m_r - m_0 > m_r - m_l$) and after the completion of the interaction in finite time it joins the state $\boldsymbol{v}_l$ on the left and a new constant state $\boldsymbol{v}_i$ on the right. The 3-R wave generated by the interaction is $R_3(\boldsymbol{v}_i, \boldsymbol{v}_r)$. The final result is given by the position of $\boldsymbol{v}_r \in B$ in (m, θ)-plane. Symbolically the result is represented by

$$\mathcal{R}_1\mathcal{K}_1 \to \mathcal{K}_1\mathcal{R}_3. \tag{3.2.13}$$

The propagation of the elementary shapes in the (x, y) plane is shown in Fig. 3.2.16 along with the kink path. We again note that the reflected $\mathcal{R}_3$ shape is weak compared to $\mathcal{K}_1$ shape before interaction, but not necessarily weak compared to the incident $\mathcal{R}_1$ shape.

(viii) $\mathcal{K}_1\mathcal{R}_1$ **interaction:** Here $\boldsymbol{v}_0 \in S_1^+(\boldsymbol{v}_l)$ and $\boldsymbol{v}_r \in R_1^-(\boldsymbol{v}_0)$. In other words, for a given $\boldsymbol{v}_l$, we choose $\boldsymbol{v}_0$ and $\boldsymbol{v}_r$ such that

$$m_l < m_0, \ \theta_0 = -\cos^{-1}\left(\frac{m_0 G(m_0) + m_l G(m_l)}{m_0 G(m_l) + m_l G(m_0)}\right) = -h(m_l, m_0) \tag{3.2.14}$$

$$m_r < m_0, \ \theta_r = \theta_0 + \int_{m_r}^{m_0} \sqrt{\frac{-G'(m)}{mG(m)}}\, dm \tag{3.2.15}$$

We have observed from extensive numerical computation that the curve $R_1^-(\boldsymbol{v}_0)$ is above

the curve $S_1^+(\boldsymbol{v}_l)$ as shown in the Fig. 3.2.17. Then, there exists a function $\delta_8(m_l, m_0) = m_0 - M$, where M is obtained uniquely by solving the equation

$$\int_{m_l}^{M} \sqrt{\frac{-G'(m)}{mG(m)}}dm + \int_{m_0}^{M} \sqrt{\frac{-G'(m)}{mG(m)}}dm = \theta_0 \tag{3.2.16}$$

such that when $m_0 - m_r = \delta_8(m_l, m_0)$, the state $\boldsymbol{v}_r \in R_3^+(\boldsymbol{v}_l)$. As in the last case, three cases arise.

(a) When $m_r > m_0 - \delta_8(m_l, m_0)$, the point $\boldsymbol{v}_r$ is in the domain B and we get the result

$$\mathcal{K}_1\mathcal{R}_1 \to \mathcal{K}_1\mathcal{R}_3. \tag{3.2.17}$$

The kink $\mathcal{K}_1$ is sufficiently strong to annihilate the elementary shape $\mathcal{R}_1$. The new elementary shape $\mathcal{R}_3$ produced as a result of the interaction is separated from the kink $\mathcal{K}_1$ by a straight portion represented by a constant state $\boldsymbol{v}_i$. Since, the curve $R_1(\boldsymbol{v}_0)$ runs very close to $S_1^+(\boldsymbol{v}_l)$, the reflected R_3 is small compared to both incident shapes $\mathcal{K}_1$ and $\mathcal{R}_1$. This result is true also for the case (b) below.

(b) When $m_r = m_0 - \delta_8(m_l, m_0)$, as in the case (vii)-(a), the kink $\mathcal{K}_1$ annihilates the elementary shape $\mathcal{R}_1$ in infinite time but asymptotically the strength of the kink $\mathcal{K}_1$ also vanishes as $t \to \infty$. Thus, we get

$$\mathcal{K}_1\mathcal{R}_1 \to \mathcal{K}_1\mathcal{R}_1\mathcal{R}_3, \quad \lim_{t\to\infty} \mathcal{K}_1\mathcal{R}_1\mathcal{R}_3 = \mathcal{R}_3. \tag{3.2.18}$$

(c) When the elementary shape $\mathcal{R}_1$ is sufficiently strong, there exists a function $\delta_8'(m_l, m_0) = m_0 - M'$, where M' is the solution of the equation

$$\int_{1}^{m_l} \sqrt{\frac{-G'(m)}{mG(m)}}dm + \int_{1}^{M'} \sqrt{\frac{-G'(m)}{mG(m)}}dm = \theta_0 + \int_{M'}^{m_0} \sqrt{\frac{-G'(m)}{mG(m)}}dm, \tag{3.2.19}$$

such that for $m_0 - m_r = \delta_8'(m_l, m_0)$, the state $\boldsymbol{v}_r$ is on the curve T. For $1 < m_r < m_0 - \delta_8(m_l, m_0)$, the point $\boldsymbol{v}_r \in A$. The kink $\mathcal{K}_1$ is unable to annihilate the elementary shape $\mathcal{R}_1$ but in this process the strength of $\mathcal{K}_1$ tends to zero as $t \to \infty$ and we get the result

$$\mathcal{K}_1\mathcal{R}_1 \to \mathcal{K}_1\mathcal{R}_1\mathcal{R}_3, \quad \lim_{t\to\infty} \mathcal{K}_1\mathcal{R}_1\mathcal{R}_3 = \mathcal{R}_1\mathcal{R}_3. \tag{3.2.20}$$

In this case, $\mathcal{R}_3$ shape is weak compared to $\mathcal{R}_1$ shape.

(d) When $m_r < m_0 - \delta_8'(m_l, m_0)$, and the point $\boldsymbol{v}_r \in T$ or the domain E, as discussed in (iv)-(b) and (c), we draw no conclusion.

The propagation of the elementary shape in the (x, y)-plane is similar to the case of $\mathcal{K}_3\mathcal{R}_3$ interaction which is depicted in Fig. 3.2.20.

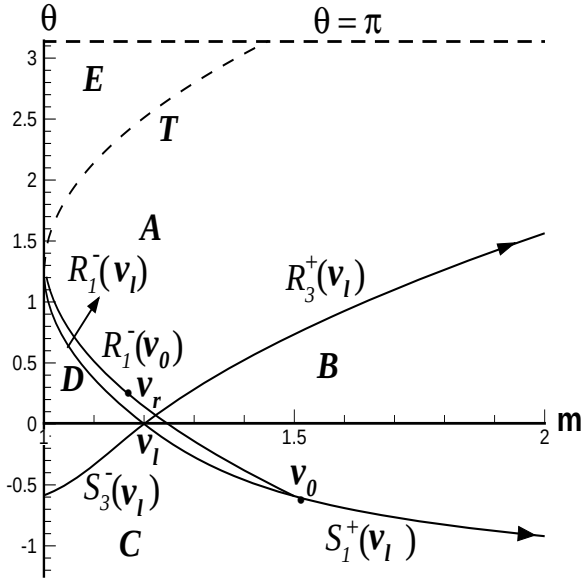

Fig 3.2.17: *For $\mathcal{K}_1\mathcal{R}_1$ interaction, the point $\boldsymbol{v}_0 \in S_1^+(\boldsymbol{v}_l)$, $\boldsymbol{v}_r \in R_1^-(\boldsymbol{v}_0)$, resulting $\boldsymbol{v}_r$ lies in B or in A depending on the strength of the 1-R wave.*

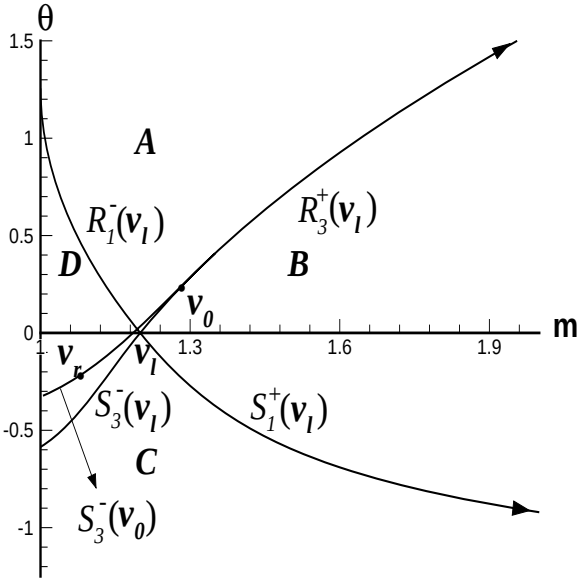

Fig 3.2.18: *For $\mathcal{R}_3\mathcal{K}_3$ interaction, the point $\boldsymbol{v}_0 \in R_3^+(\boldsymbol{v}_l)$, $\boldsymbol{v}_r \in S_3^-(\boldsymbol{v}_0)$, resulting $\boldsymbol{v}_r$ lies in A or in D depending on the strength of the 3-S shock.*

(ix) $\mathcal{R}_3\mathcal{K}_3$ **interaction:** The $\mathcal{R}_3\mathcal{K}_3$ interaction takes place when $\boldsymbol{v}_0 \in R_3^+(\boldsymbol{v}_l)$ and $\boldsymbol{v}_r \in S_3^-(\boldsymbol{v}_0)$. That is, for a given $\boldsymbol{v}_l$, we choose $\boldsymbol{v}_0$ and $\boldsymbol{v}_r$, in such a way that

$$\begin{aligned} m_l < m_0,\ \theta_0 &= \int_{m_l}^{m_0} \sqrt{\frac{-G'(m)}{mG(m)}}dm \\ m_r < m_0,\ \theta_r &= \theta_0 - \cos^{-1}\left(\frac{m_0G(m_0)+m_rG(m_r)}{m_0G(m_r)+m_rG(m_0)}\right) = \theta_0 - h(m_0,m_r) \end{aligned}$$

We see from numerical results that $S_3^-(\boldsymbol{v}_0)$ is above $R_3^+(\boldsymbol{v}_l)$ as seen in Fig. 3.2.18. Therefore, there exists a $\delta_9(m_l,m_0) = m_0 - M$, where M satisfies the equation

$$\int_M^{m_l} \sqrt{\frac{-G'(m)}{mG(m)}}dm = \theta_0 - \cos^{-1}\left(\frac{m_0G(m_0)+MG(M)}{m_0G(M)+MG(m_0)}\right), \tag{3.2.21}$$

such that if $m_0 - m_r = \delta_9(m_l,m_0)$, the point $\boldsymbol{v}_r \in R_1^-(\boldsymbol{v}_l)$. The following cases arise

(a) When the kink $\mathcal{K}_3$ is strong compared to the elementary shape $\mathcal{R}_3$ i.e., $m_0 - m_r > \delta_9(m_l,m_0)$, which implies $m_r < m_0 - \delta_9(m_l,m_0)$, the point $\boldsymbol{v}_r \in D$ and

$$\mathcal{R}_3\mathcal{K}_3 \to \mathcal{R}_1\mathcal{K}_3. \tag{3.2.22}$$

The interaction is of finite duration and the strength of the reflected $\mathcal{R}_1$ shape is small compared to the incident $\mathcal{K}_3$ kink. This conclusion is also in case (b) below. Fig. 3.2.18 shows in detail this case of the $\mathcal{R}_3\mathcal{K}_3$ interaction.

(b) When $m_r = m_0 - \delta_9(m_l, m_0)$, the interaction between $\mathcal{K}_3$ and $\mathcal{R}_3$ continues indefinitely, both ultimately become infinitesimally weak and we have

$$\mathcal{R}_3\mathcal{K}_3 \to \mathcal{R}_1\mathcal{R}_3\mathcal{K}_3, \quad \lim_{t\to\infty} \mathcal{R}_1\mathcal{R}_3\mathcal{K}_3 = \mathcal{R}_1. \tag{3.2.23}$$

(c) When $m_r > m_0 - \delta_9(m_l, m_0)$, $\boldsymbol{v}_r \in A$. The interaction of $\mathcal{R}_3$ with $\mathcal{K}_3$ continues indefinitely during which process strength of $\mathcal{K}_3$ decays to zero and we get

$$\mathcal{R}_3\mathcal{K}_3 \to \mathcal{R}_1\mathcal{R}_3\mathcal{K}_3, \quad \lim_{t\to\infty} \mathcal{R}_1\mathcal{R}_3\mathcal{K}_3 = \mathcal{R}_1\mathcal{R}_3. \tag{3.2.24}$$

The strength of reflected $\mathcal{R}_1$ shape is small compared to $\mathcal{R}_3$ and $\mathcal{K}_3$ shapes.

The propagation of the elementary shape in the (x, y)-plane is similar to the case of $\mathcal{R}_1\mathcal{K}_1$ interaction which is depicted in Fig. 3.2.14-3.2.16.

(x) $\mathcal{K}_3\mathcal{R}_3$ **interaction:** Here $\boldsymbol{v}_0 \in S_3^-(\boldsymbol{v}_l)$ and $\boldsymbol{v}_r \in R_3^+(\boldsymbol{v}_0)$ as shown in Fig. 3.2.19. That is, for a given $\boldsymbol{v}_l$, we choose $\boldsymbol{v}_0$ and $\boldsymbol{v}_r$, such that

$$1 < m_0 < m_l, \ \theta_0 = -\cos^{-1}\left(\frac{m_0G(m_0) + m_lG(m_l)}{m_0G(m_l) + m_lG(m_0)}\right) = -h(m_l, m_0),$$

$$m_0 < m_r, \ \theta_r = \theta_0 + \int_{m_0}^{m_r} \sqrt{\frac{-G'(m)}{mG(m)}}dm$$

On the basis of numerical results, we take $R_3^+(\boldsymbol{v}_0)$ to lie above $S_3^-(\boldsymbol{v}_l)$. Therefore, there exists a function $\delta_{10}(m_l, m_0) = M - m_0$,where M is the solution of the equation

$$\int_M^{m_l} \sqrt{\frac{-G'(m)}{mG(m)}}dm = \theta_0 + \int_{m_0}^{M} \sqrt{\frac{-G'(m)}{mG(m)}}dm. \tag{3.2.25}$$

such that, when $m_r - m_0 = \delta_{10}(m_l, m_0)$, the point $\boldsymbol{v}_0 \in R_3^+(\boldsymbol{v}_l)$. We again get three cases.

(a) When $m_r < m_0 + \delta_{10}(m_l, m_0)$, $\boldsymbol{v}_r \in D$, the $\mathcal{K}_3$ annihilates $\mathcal{R}_3$ in finite time and we get

$$\mathcal{K}_3\mathcal{R}_3 \to \mathcal{R}_1\mathcal{K}_3. \tag{3.2.26}$$

The strength of the reflected $\mathcal{R}_1$ shape is small compared to both incident $\mathcal{K}_3$ and $\mathcal{R}_3$ shapes. This result is true also for the case (b) below.

(b) When $m_r = m_0 + \delta_{10}(m_l, m_0)$, we get

$$\mathcal{K}_3\mathcal{R}_3 \to \mathcal{R}_1\mathcal{K}_3\mathcal{R}_3, \quad \lim_{t\to\infty} \mathcal{R}_1\mathcal{K}_3\mathcal{R}_3 = \mathcal{R}_1. \tag{3.2.27}$$

(c) When $m_r > m_0 + \delta_{10}(m_l, m_0)$, $\boldsymbol{v}_r \in A$. We finally have

$$\mathcal{K}_3\mathcal{R}_3 \to \mathcal{R}_1\mathcal{K}_3\mathcal{R}_3, \quad \lim_{t\to\infty} \mathcal{R}_1\mathcal{K}_3\mathcal{R}_3 = \mathcal{R}_1\mathcal{R}_3. \tag{3.2.28}$$

The propagation of the elementary shapes in the (x, y)-plane is presented in Fig. 3.2.20.

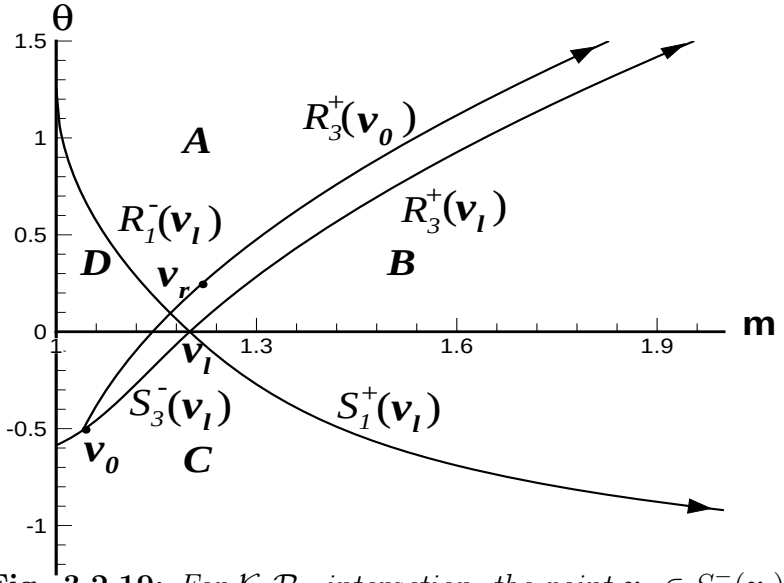

Fig. 3.2.19: *For $\mathcal{K}_3\mathcal{R}_3$ interaction, the point $\boldsymbol{v}_0 \in S_3^-(\boldsymbol{v}_l)$ and $\boldsymbol{v}_r \in R_3^+(\boldsymbol{v}_0)$, resulting $\boldsymbol{v}_r$ lies in A or in D depending on the strength of the 1-R wave.*

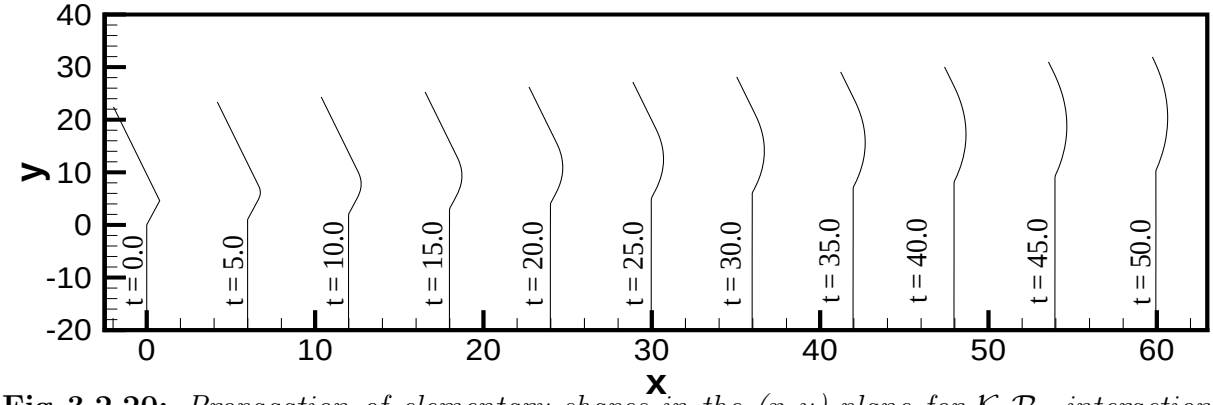

Fig 3.2.20: *Propagation of elementary shapes in the (x, y)-plane for $\mathcal{K}_3\mathcal{R}_3$ interaction with $m_l = 1.2$, $\theta_l = 0$; $m_0 = 1.15$, $\theta_0 = -0.166033$; $m_r = 1.25$, $\theta_r = 0.152735$.*

Chapter 4

Kinematical Conservation Laws Applied to Study Geometrical Shapes of a Solitary Wave

§4.1 Introduction

Considerable amount of research has been done on the stability (both longitudinal and transverse) of solitary waves in the last 30 years (Bridges, 2001). In this chapter, we have considered geometrical shapes of stable curved solitary waves in shallow water of constant depth. By a curved solitary wave, we mean a wave whose extent in the transverse direction (i.e., a direction perpendicular to the direction of propagation) is very large compared to its extent in normal direction (i.e., the direction of propagation) and the shape of the wave in a normal section is locally a solitary wave. This allows us to define at any time a crest-line Ω_t, the locus of the highest points of the local solitary waves in the normal sections. Our aim in this chapter is to study the successive positions of Ω_t and its geometric shape starting from its initial configuration. When the amplitude of the wave on the crest-line vary slowly (compared to the variation of the amplitude in the local solitary wave), transverse waves are induced which propagate along the crest-line. The slow amplitude variation is coupled to the variation in the normal direction of the crest-line.

Propagation of waves (or shock waves) along the crest-line have been discussed by Ostrovsky and Shrira (1976), Miles (1977), Shrira (1980), Zakharov (1986) and Pederson (1994), some of these use Whitham's equations. Quite exhaustive results have been obtained by these authors. But one needs to fit each kink (shock-shock as usually called by these authors) on the crest-line individually, since Whitham's equations are not in

conservation form. Thus, long term solution of the problem becomes quite cumbersome. We shall write the basic equations for the propagation of the crest-line in physically realistic conservation forms, which are true for any propagating curve Ω_t in a plane. These are kinematical conservation laws (KCL), first derived by Morton, Prasad and Ravindran, 1992, for an appropriately defined velocity m of Ω_t, the Mach number of curve and angle θ which normal to Ω_t makes with the x-axis in terms of an appropriately defined ray coordinate system (ξ, τ). Here τ = constant give the successive positions of Ω_t (or Ω_τ) and ξ = constant are rays - in this case orthogonal to Ω_t. Let g be the metric associated with the variable ξ, then the KCL are

$$(g \sin\theta)_\tau + (m \cos\theta)_\xi = 0, \tag{4.1.1}$$

$$(g \cos\theta)_\tau - (m \sin\theta)_\xi = 0. \tag{4.1.2}$$

A brief note on the derivation of the KCL is presented in the section 1.3.

Whitham's equations follow from these equations. The system (4.1.1)-(4.1.2) is an under-determined system of equations for three dependent variables, the dynamics of the propagating curve appears in additional partial differential equations (Monica and Prasad, 2001) or an additional relation $g = G(m)$, where G is a known function (see chapter 2 and Baskar and Prasad, 2002). We shall use the local solitary wave solution to determine G in the form

$$G(m) = (m-1)^{-3/2}\, e^{-(3/2)(m-1)} \tag{4.1.3}$$

For $0 < m-1 << 1$, to which our theory applies $g(m) = (m-1)^{-3/2}$, which is equivalent to the closure relation used by Miles (1977)(see his equations (2.3a,b)) and Ostrovsky and Shrira (1976). Miles deduced this relation from the expression for the solution of solitary wave in water wave problem in a channel of slowly varying breadth. We deduce (4.1.3) by a method which will be applicable to solitary waves in all physical systems in which an equation for curved solitary waves can be obtained.

Use of KCL provides a new understanding of the phenomenon of kinks - it shows that the kinks are basically geometric shocks in a ray coordinate system. KCL makes computation of the successive positions of the crest-line not only very easy but very robust - the method of numerical solution can be continued for a very long time even if there are more than one kink, which interact among themselves and also with more complicated solutions than simple wave solutions. This is because, the whole range of sophisticated methods of numerical solution of hyperbolic conservation laws (Prasad and Sangeeta 1999, and Monica and Prasad 2001) are applicable to KCL.

In chapter 2 (also see Baskar and Prasad, 2002), we have studied existence and uniqueness of the solution of Riemann problem for KCL with a general form of the metric function

$g = G(m)$ and discussed all possible geometric shapes of the propagating curve Ω_t. We also studied the interaction of elementary shapes on a propagating wavefront in chapter 3. We note that the function (4.1.3) satisfies the assumptions **A1**-**A4** stated in section 2.2 on $G(m)$. Thus, the results obtained in chapter 2 and 3 are applicable to the crest-line of a curved solitary waves in a shallow water.

§4.2 Multi-Dimensional KdV Equation

First we briefly mention various length and time scales and non-dimensional quantities involved in discussion of waves in shallow water.

H = a length scale characterizing the depth of the undisturbed water,
λ = wave length of the waves,
A = a measure of the maximum height of the wave, it has the dimension of length.

$$\epsilon = (H/\lambda)^2 \quad , \quad \delta = A/H \quad , \quad \bar{h} = Hh \ , \ \bar{\eta} = H\delta\eta \tag{4.2.1}$$

$$\left.\begin{array}{rcl} (\bar{x}, \bar{y}, \bar{z}) & = & (\lambda x,\, \lambda y,\, Hz) \ , \ \bar{t} = \epsilon^{-1/2}(H/g)^{1/2} t \\ (\bar{u}, \bar{v}, \bar{w}) & = & \delta(gH)^{1/2}(u, v, \epsilon^{1/2} w) \ , \ \bar{p} = \bar{\rho} g H p \end{array}\right\} \tag{4.2.2}$$

where $(\bar{u}, \bar{v}, \bar{w})$ are components of the velocity in $\bar{x}, \bar{y}, \bar{z}$ directions, the undisturbed free surface is $\bar{z} = 0$, $\bar{z} = \bar{\eta}(\bar{x}, \bar{y})$ is the disturb free surface, $\bar{h}$ is the constant depth, $\bar{p}$ is the excess pressure above the atmospheric pressure and $\bar{\rho}$ is the constant density.

The water wave is dispersive, but in the long wave limit $\epsilon \to 0$ (without small amplitude assumption), it is well known that it supports non-dispersive waves and is governed by a system of hyperbolic equations (e.g., see Prasad and Ravindran, 1977, equations (2.28) - (2.30)). These are equations in variables $\eta, \tilde{u}$ and $\tilde{v}$ where $\tilde{u}$ and $\tilde{v}$ are defined as velocity components in x, y directions respectively up to order ϵ terms but after carefully removing z-dependent parts from the velocity components. This system supports nonlinear non-dispersive curved waves with eigenvalues

$$c_1 = \sqrt{h + \delta\eta} - \delta(n_1\tilde{u} + n_2\tilde{v}) \ , \ c_2 = \sqrt{h + \delta\eta} \ , \ c_3 = \sqrt{h + \delta\eta} + \delta(n_1\tilde{u} + n_2\tilde{v}) \tag{4.2.3}$$

where $n_1 = \cos\theta$ and $n_2 = \sin\theta$ are components of the unit normal to the wavefront. The system can have simple wave solution of third family propagating in a fixed direction (n_1, n_2) (section 3.1.3, Prasad 2001). The simple wave is a non-stationary phenomenon, it cannot reduce to a steady solution in any frame of reference. The stationary nature of a solitary wave results from the balance of the nonlinear effects in the simple wave by dispersion. The balance is beautifully described by the KdV equation under small

amplitude assumption, however this balance takes place in certain situations - in one case when

$$\delta = \epsilon^{1/3} = \epsilon_1 \tag{4.2.4}$$

where ϵ_1 is a short length scale characterizing a neighbourhood of the wavefront over which the disturbance is concentrated (see Prasad and Ravindran, 1977, result (3.17)). Derivation of the KdV equation requires that in the small amplitude perturbations ($\delta << 1$) $\delta\eta$, $\delta\tilde{u}$ and $\delta\tilde{v}$ are related by

$$\tilde{u} = n_1\eta/\sqrt{h}\ ,\ \ \tilde{v} = n_2\eta/\sqrt{h}. \tag{4.2.5}$$

As is well known, the solitary wave is a solution of the KdV equation. The most important point to note is that the velocity of propagation of the solitary wave is not given by the eigenvalue c_3.

The plane KdV equation with wavefront normal in (n_1, n_2)-direction can be modified by taking (n_1, n_2) to very slowly over a length scale L such that

$$H << \lambda << L. \tag{4.2.6}$$

Let $\phi(x, y, t)$ is the phase function such that $\phi = 0$ is the curved wavefront , and approximate the equations of surface water waves in propagation space (i.e., equations (2.31) - (2.33) of Prasad and Ravindran, 1977) in an ϵ_1 neighbourhood of $\phi = 0$. This leads to the modified KdV equation for the propagation of curved waves on a shallow water from the equation (4.5) of Prasad and Ravindran (1977) in the form

$$\frac{d\eta}{dt} - \sqrt{h}\eta\Omega + \frac{h}{6}\left\{(\phi_x^2 + \phi_y^2)\right\}^{3/2}\eta_{sss} = 0 \tag{4.2.7}$$

where

$$\frac{d}{dt} = \frac{\partial}{\partial t} + \left(\sqrt{h} + \frac{3}{2\sqrt{h}}\delta\eta\right)\left(n_1\frac{\partial}{\partial x} + n_2\frac{\partial}{\partial y}\right), \tag{4.2.8}$$

$$\Omega = -\frac{1}{2}\left(\frac{\partial n_1}{\partial x} + \frac{\partial n_2}{\partial y}\right) \tag{4.2.9}$$

and s is the fast variable defined by

$$s = \phi(x, y, t)/\epsilon. \tag{4.2.10}$$

Note that we do not wish to replace ϕ by the linear phase function ϕ_0 as done in Prasad and Ravindran (1977) and do not wish to go up to the equation (4.17) there.

The function ϕ satisfies the Eikonal equation

$$\phi_t + \left(\sqrt{h} + \frac{3}{2\sqrt{h}}\delta\eta\right) |\nabla\phi| = 0,\ \nabla = \left(\frac{\partial}{\partial x}, \frac{\partial}{\partial y}\right)$$

and $(n_1, n_2) = \nabla\phi/|\nabla\phi|$. This means that the derivative $\frac{d}{dt}$ is along the paths given by the corresponding ray equations,

$$\frac{dx_\alpha}{dt} = \left(\sqrt{h} + \frac{3\delta\eta}{2\sqrt{h}}\right) n_\alpha \ ,\ \ \frac{dn_\alpha}{dt} = -\frac{3\delta}{2\sqrt{h}} L\eta \tag{4.2.11}$$

where

$$L = \nabla - \mathbf{n}\langle\mathbf{n}, \nabla\rangle. \tag{4.2.12}$$

The equations (4.2.7), and (4.2.11) are coupled together. Unlike the purely non-dispersive problem (where the last term in (4.2.7) is absent) as in chapter 6 Prasad (2001), numerical solution of the system (4.2.7), (4.2.11) and (4.2.12) appears to be extremely complex. However, unlike the well known KP (Kadomstev and Petvaishvili) equation this system is a true generalization of the KdV equation to multi-dimensions for the propagation of a curved dispersive waves in high frequency approximation. Our aim in this chapter is to study propagation not of a general dispersive wave but only a curved solitary wave. In the next section, we shall use the equation (4.2.7) to determine the function g which appears in (4.1.3).

§4.3 Equation for the Average Flux of Energy

Consider now a point on the crest-line of a curved solitary wave such that at $t = 0$, the point coincides with a point $P(x_p, y_p)$. In a two-dimensional neighbourhood N_p in (x, y)-plane, of P of linear dimension ϵ_1, we can write

$$\phi = n_1(x - x_p) + n_2(y - y_p) - \sqrt{h}t + O(\epsilon_1^2).$$

Let $\tilde{x} = (x - x_p)/\epsilon_1,\ \tilde{y} = (y - y_p)/\epsilon_1$, then $\tilde{x}$ and $\tilde{y}$ are of order one in N_p. Then

$$\tilde{\Omega} = -\frac{1}{2}\left(\frac{\partial n_1}{\partial\tilde{x}} + \frac{\partial n_2}{\partial\tilde{y}}\right) = -\frac{\epsilon}{2}\left(\frac{\partial n_1}{\partial x} + \frac{\partial n_2}{\partial y}\right) = \epsilon\Omega,$$

where Ω is of order one. Hence, when we consider the equation (4.2.7) locally in the neighbourhood N_p with

$$s = \tilde{s} = \{n_1(x - x_p) + n_2(x - y_p) - \sqrt{h}t\}/\epsilon_1 \tag{4.3.1}$$

the curvature term can be neglected and it reduces locally to the KdV equation

$$\eta_{t'} + \frac{3}{2\sqrt{h}}\eta\eta_{\tilde{s}} + \frac{h}{6}\eta_{\tilde{s}\tilde{s}\tilde{s}} = 0 \tag{4.3.2}$$

where

$$\frac{\partial}{\partial t'} = \frac{\partial}{\partial t} + \sqrt{h}\left(n_1\frac{\partial}{\partial x} + n_2\frac{\partial}{\partial y}\right). \tag{4.3.3}$$

The local solitary wave satisfying (4.3.2) is

$$\eta_0 = 3c\alpha\sec h^2\left(\frac{\sqrt{c}}{2}(s-\beta ct)/\beta\right) \tag{4.3.4}$$

where

$$\alpha = 2^{2/3}3^{-4/3}h^{4/3}\ ,\ \beta = 6^{-1/3}h^{5/6}. \tag{4.3.5}$$

(4.3.4) gives the amplitude A of the solitary wave $A = \delta\max_{I\!R}\eta_0 \equiv \delta\eta_c = 3c\alpha\delta$. Its normal velocity C (which is also the velocity of the crest-line), is given by $s - \beta ct =$ constant i.e., $C = \sqrt{h} + \beta c\delta$. We define the Mach number of the crest-line as $m = C/\sqrt{h}$ and hence the relation between m and the amplitude A at the point P is

$$m - 1 = \frac{\beta\delta_c}{\sqrt{h}} = \frac{\beta A}{3\alpha\sqrt{h}} = \frac{A}{2h}. \tag{4.3.6}$$

As mentioned after the relation (4.2.5), the most important influence of the balance between the nonlinearity and dispersion in maintenance of the solitary wave shape is that the crest-line velocity is not the same as eigenvalue $c_3 = \sqrt{h} + \{3/(2\sqrt{h})\}\delta\eta_c$ but it is equal to

$$C = \sqrt{h} + \{\beta/(3\alpha)\}\,\delta\eta_c = \sqrt{h} + \left\{1/(2\sqrt{2})\right\}\delta\eta_c \tag{4.3.7}$$

which results in the relation (4.3.6).

The ray velocity of the solitary wave (i.e., also that of the crest-line) is $C(\cos\theta, \sin\theta)$. Hence the time rate of change, $\frac{d}{dT}$, when we move with the crest-line is

$$\frac{d}{dT} = \frac{\partial}{\partial t} + C\left(n_1\frac{\partial}{\partial x} + n_2\frac{\partial}{\partial y}\right). \tag{4.3.8}$$

Rearranging terms in the multi-dimensional KdV equation (4.2.7), we get

$$\frac{d\eta}{dT} - \sqrt{h}\eta\Omega + \left\{\frac{3}{2\sqrt{h}}\delta\eta - C\right\}\left(n_1\frac{\partial}{\partial x} + n_2\frac{\partial}{\partial y}\right)\eta + \frac{h}{6}\left\{h(\phi_x^2 + \phi_y^2)\right\}^{3/2}\eta_{sss} = 0. \tag{4.3.9}$$

Multiplying this by 2η we write another relation

$$\frac{d\eta^2}{dT} - 2\sqrt{h}\eta\Omega + \left\{\frac{3}{\sqrt{h}}\delta\eta^2 - \eta C\right\}\eta_s + \frac{h}{3}\{h(\phi_x^2+\phi_x^2)\}^{3/2}\eta\eta_{sss} = 0. \tag{4.3.10}$$

Since C, n_1 and n_2 can be treated as constants in N_p, the operator $\frac{d}{dT}$ and integration with respect to s or $\zeta = \phi_0 - \beta\delta ct$ commute. Further, both integrations $\int_{-\infty}^{\infty}(\eta_0 - \eta_c\eta_0)\eta_{0s}ds$ and $\int_{-\infty}^{\infty}\eta_0\eta_{0sss}ds$ vanish. Hence, integrating (4.3.10) with respect to s from $-\infty$ to ∞, we get

$$\frac{dD_2}{dT} - 2\sqrt{h}\Omega D_2 = 0 \tag{4.3.11}$$

where

$$D_2 = \int_{-\infty}^{\infty}\eta_0^2(s')ds' \ , \ s' = s - \beta ct. \tag{4.3.12}$$

(4.3.11) is a very important relation and implies that the product of D_2 and the ray tube area $\mathcal{A}$ (which for the propagating curve Ω_t in (x,y)-plane may be taken to be g) associated with the crest-line is constant (see (2.2.23) in Prasad, 2001 and also Whitham, 1974). Using the expressions (4.3.4) we get

$$D_2 = 24c^{3/2}\alpha^2\beta, \tag{4.3.13}$$

so that (4.3.6) and (4.3.11) give

$$\frac{dm}{dT} = \frac{4}{3}\sqrt{h}\Omega(m-1). \tag{4.3.14}$$

Now, we define a new time variable $\tau = t/\sqrt{h}$ and use the ray coordinate system (ξ,τ) in which the time rate of change is denoted by the partial derivative $\frac{\partial}{\partial\tau}$, so that $\frac{d}{dT} = \sqrt{h}\frac{\partial}{\partial\tau}$. The ray equations for the crest-line are

$$x_\tau = m\cos\theta \ \ , \ \ y_\tau = m\sin\theta. \tag{4.3.15}$$

From (4.1.1)-(4.1.2) we get the time rate of change of θ and g along the rays in the form

$$\theta_\tau = -\frac{1}{g}m_\xi \ , \ g_\tau = m\theta_\xi \tag{4.3.16}$$

(see also equation (3.3.15, 16 and 19) Prasad, 2001). Since $\Omega = -\frac{1}{2g}\frac{\partial\theta}{\partial\xi}$, elimination of θ from the above equations gives

$$m_\tau = -\{2(m-1)/(3mg)\}g_\tau, \tag{4.3.17}$$

which finally leads to the expression (4.1.3) for g. Note that the constant of integration in (4.3.17) can be chosen to be one by suitable choice of ξ.

We have now a complete formulation of the problem. Given initial position of the crest-line in terms of a parameter $\xi : x|_{\tau=0} = x_0(\xi)$, $y|_{\tau=0} = y_0(\xi)$ and amplitude distribution $m_0(\xi)$ on it, we determine initial value of g from (4.1.3). Then we first solve the system of conservation laws (4.1.1)-(4.1.2) and next we use the (4.3.15) to get the position of the crest-line at any time $t = \sqrt{h}\,\tau$ (for details, see chapter 6 in Prasad, 2001)

Since the local KdV has infinity of conservation laws, we can get as many transport equations as we wish, like (4.3.11). In fact, starting with equation (4.2.7), we shall get $G(m) = (m-1)^{-1}e^{-(m-1)}$. But only one of these, namely (4.1.3) appears to be physically realistic. We first notice that $\delta\eta$ is proportional to the potential energy of the water per unit surface area of the water and $\frac{1}{2}\{(\delta\tilde{u})^2 + (\delta\tilde{v})^2\}$ is proportional to the corresponding kinetic energy. Therefore, to the first order in δ, the total energy density is $\delta\eta$ and the flux of the energy density crossing the lines parallel to the crest-line is proportional to

$$\{\delta(n_1\tilde{u} + n_2\tilde{v}\}\{\delta\eta\} + O(\delta^3) = (\delta^2/h)\eta^2 + O(\delta^3) \tag{4.3.18}$$

However, at the micro-scale of order ϵ_1, $\eta^2\mathcal{A} = \eta^2 g$ is not constant due to the presence of the dispersion term in (4.3.2). D_2 is proportional to the integral of the square of the flux at the micro-scale. Thus, (4.3.11) is the physically realistic transport equation along the rays associated with the crest-line. Result (4.1.3) is valid for $0 < m - 1 << 1$, in which case we get $g(m) \simeq (m-1)^{-3/2}$. It is interesting to note that it agrees with the A-M relation used by Ostrovsky and Shrira (1976) and Miles (1977).

§4.4 Geometrical Shapes of the Crest-Line

Consider the parametric representation of the initial wavefront in the (x, y)-plane to be

$$x(\xi, 0) = \begin{cases} 0 & \text{if} \quad \xi < 0 \\ \\ -\xi g_r \sin\theta_r & \text{if} \quad \xi > 0 \end{cases} \tag{4.4.1}$$

$$y(\xi, 0) = \begin{cases} g_l\xi & \text{if} \quad \xi < 0 \\ \\ \xi g_r \cos\theta_r & \text{if} \quad \xi > 0 \end{cases} \tag{4.4.2}$$

which is equivalent to the initial data

$$(m, \theta)(\xi, 0) = \begin{cases} (m_l, 0) & \text{if} \quad \xi < 0 \\ \\ (m_r, \theta_r) & \text{if} \quad \xi > 0 \end{cases} \tag{4.4.3}$$

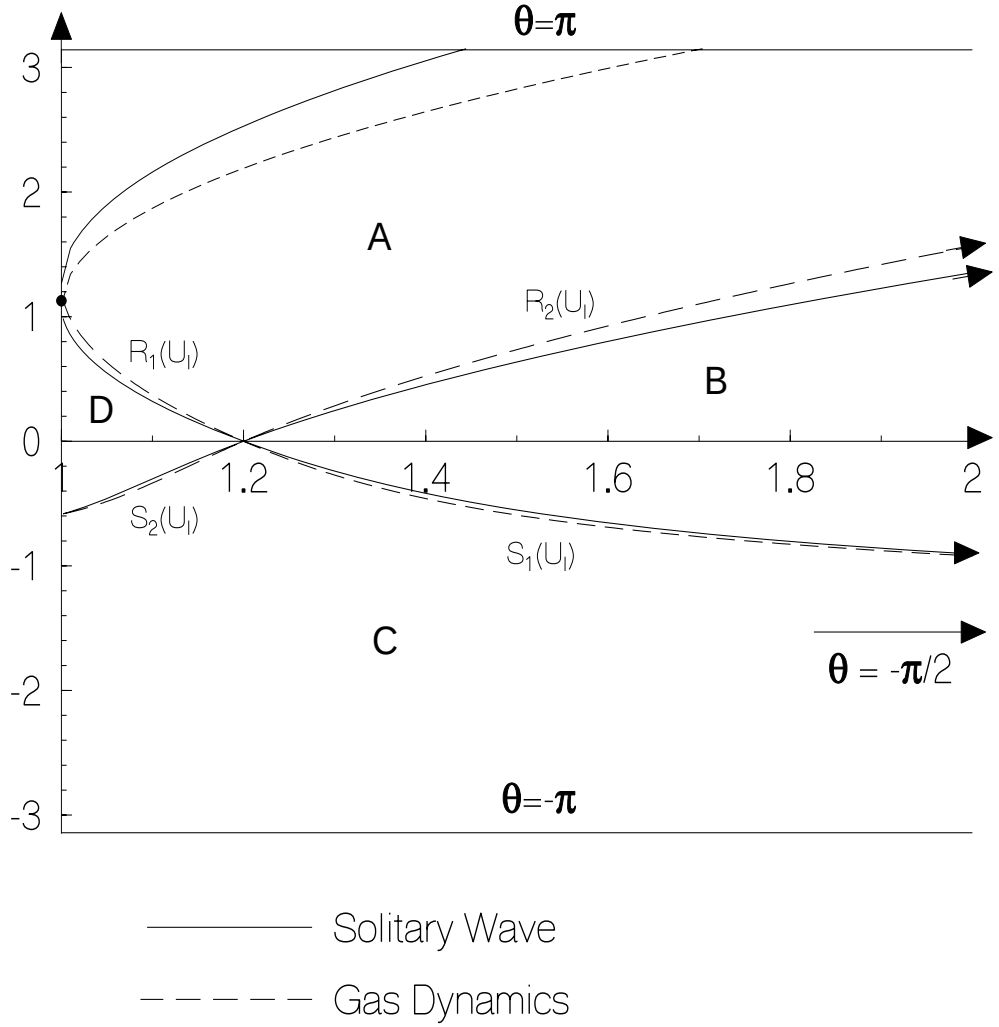

Fig. 4.4.1: *Domain A, B, C, D in (m, θ)-plane with $m_l = 1.2$ and $\theta_l = 0$. When (m_r, θ_r) belong to these domains, we get different geometrical shapes.*

for the system (4.1.1)-(4.1.2) in the (ξ, t)-plane, where m_l, m_r and θ_r are constant, $g_l = G(m_l)$ and $g_r = G(m_r)$ with g as defined in (4.1.3).

The initial value problem (4.1.1)-(4.1.2) together with the initial data (4.4.3) has been studied in chapter 2 (also see Baskar and Prasad, 2002) in the case of a general metric g satisfying a set of assumptions and shapes of the curve Ω_t for $t > 0$ has been computed for $g = G(m) = (m-1)^{-2} e^{-2(m-1)}$, which appears for a front in weakly nonlinear ray theory in gas dynamics. As discussed in this work, the $(m > 1, \theta)$-plane is divided into four regions A, B, C and D (as shown in Fig. 4.4.1) by four curves $R_i(U_l), S_i(U_l), i = 1, 2$, which are given by

$$R_1(U_l) = \left\{ (m, \theta) | \begin{array}{l} 1 < m \leq m_l, \\ \theta = \sqrt{6(m_l - 1)} - \sqrt{6(m-1)} \end{array} \right\} \tag{4.4.4}$$

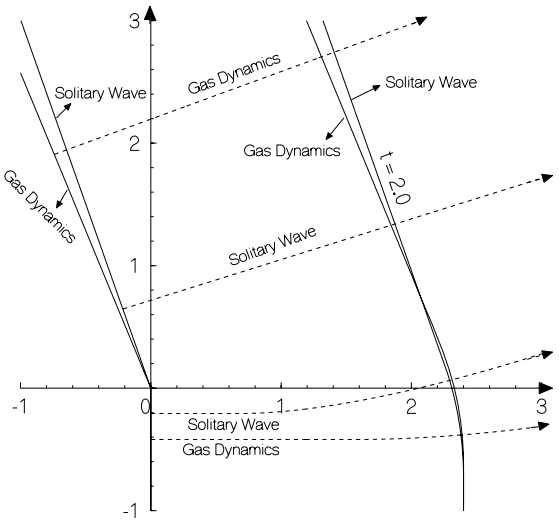

Fig. 4.4.2a: *Comparison of $\mathcal{R}_1$ elementary shape.*

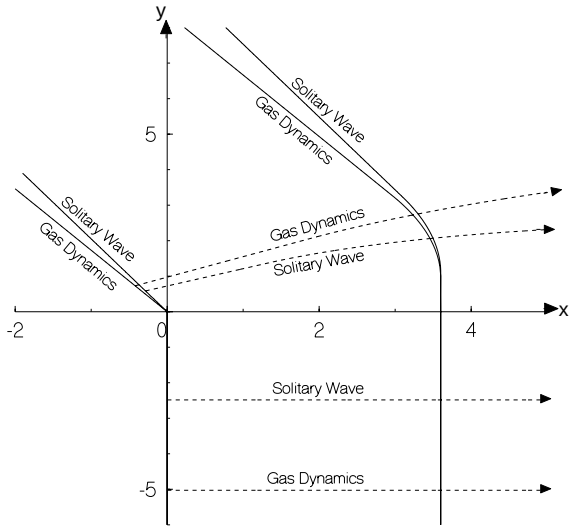

Fig. 4.4.2b: *Comparison of $\mathcal{R}_2$ elementary shape.*

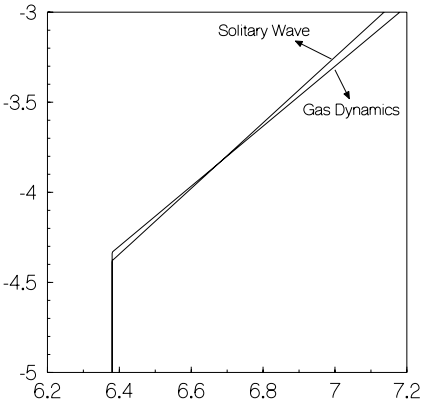

Fig. 4.4.3a: *Comparison of $\mathcal{K}_1$ elementary shape.*

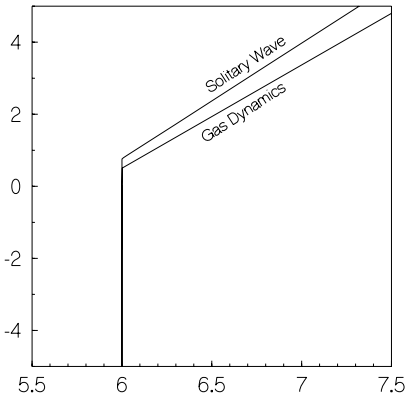

Fig. 4.4.3b: *Comparison of $\mathcal{K}_2$ elementary shape.*

$$R_2(U_l) = \left\{ (m,\theta)| \begin{array}{l} m_l \le m < \infty \\ \theta = \sqrt{6(m-1)} - \sqrt{6(m_l-1)} \end{array} \right\} \tag{4.4.5}$$

$$S_1(U_l) = \left\{ (m,\theta)| \begin{array}{l} m_l \le m < \infty \\ \theta = -\cos^{-1}\left(\frac{m_l g_l + m g(m)}{m g_l + m_l g(m)}\right) \end{array} \right\} \tag{4.4.6}$$

$$S_2(U_r) = \left\{ (m,\theta)| \begin{array}{l} 1 < m \le m_l \\ \theta = -\cos^{-1}\left(\frac{m_l g_l + m g(m)}{m g_l + m_l g(m)}\right) \end{array} \right\}, \tag{4.4.7}$$

the line $\theta = -\pi$ and the curve

$$\theta = \begin{cases} \sqrt{6(m_l-1)} + \sqrt{6(m-1)}, & \text{for} \quad \sqrt{6(m_l-1)} < \theta < \pi \\ \\ \pi, & \text{elsewhere} \end{cases} \tag{4.4.8}$$

where we have taken the positive determination of $\cos^{-1}$. The existence and uniqueness of the intermediate state through which the left state can be joined to the right state has been discussed in chapter 2 (also see Baskar and Prasad, 2002). Their results with general function g show that qualitatively the shapes of Ω_t with *similar* initial conditions are the same. Since the curves R_1, R_2, S_1 and S_2 differ by a small quantity for two expressions for g, we do not expect much quantitative change also.

If the right state (m_r, θ_r) lies on $R_i(U_l), i = 1, 2$, then the singularity on the initial wavefront will be resolved and the wavefront becomes smooth for $t > 0$. This smooth part denoted as elementary shape $\mathcal{R}_i$ $(i = 1, 2)$, on the wavefront is the image of the rarefaction region in the (ξ, t)-plane. These are depicted in Fig. 4.4.2 along with the results for the nonlinear wavefront in gas dynamics.

If the right state (m_r, θ_r) lies on $S_i(U_l), i = 1, 2$ then the singularity on Ω_0 remains unresolved and propagates on Ω_t as a $\mathcal{K}_i$ $(i = 1, 2)$, elementary shape which is a kink. A comparison between the crest-line of the solitary wave and nonlinear wavefront in gas dynamics is shown in Fig. 4.4.3.

In all the above cases the shape of a propagating crest-line is qualitatively same as that of a nonlinear wavefront in the gas dynamics. In fact, had we taken the initial position and initial shapes to be the same (which can be easily done) we would not have found much difference in the graphs. Therefore we omit the detailed discussion of different shapes except showing their graphs in Fig. 4.4.4. of the Ω_t in the present case when the right state (m_r, θ_r) lies in the regions A, B, C and D. For the full details, we refer to Baskar and Prasad, 2002.

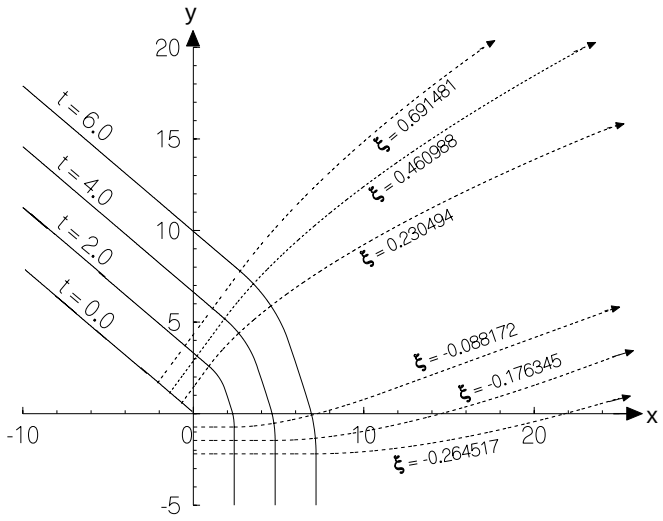

Fig. 4.4.4a: *Propagation of the crest-line when* $(m_r, \theta_r) \in A$ *with* $m_l = 1.2$, $m_r = 1.3, \theta_r = 0.9$.

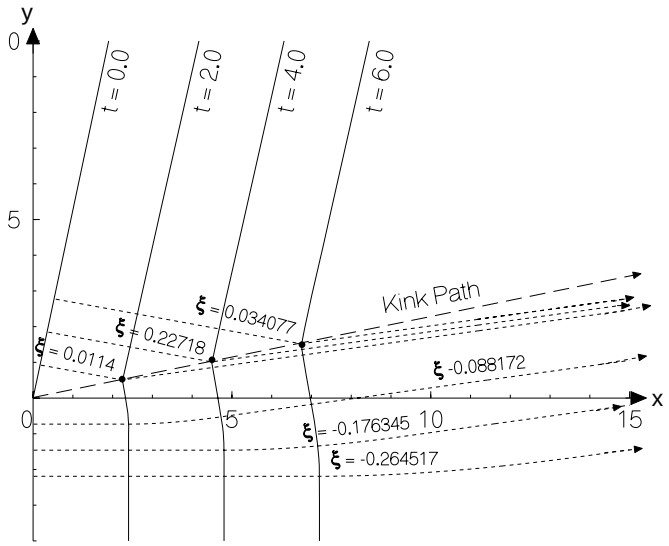

Fig. 4.4.4b: *Propagation of the crest-line when* $(m_r, \theta_r) \in B$ *with* $m_l = 1.2$, $m_r = 1.7, \theta_r = 0.5$.

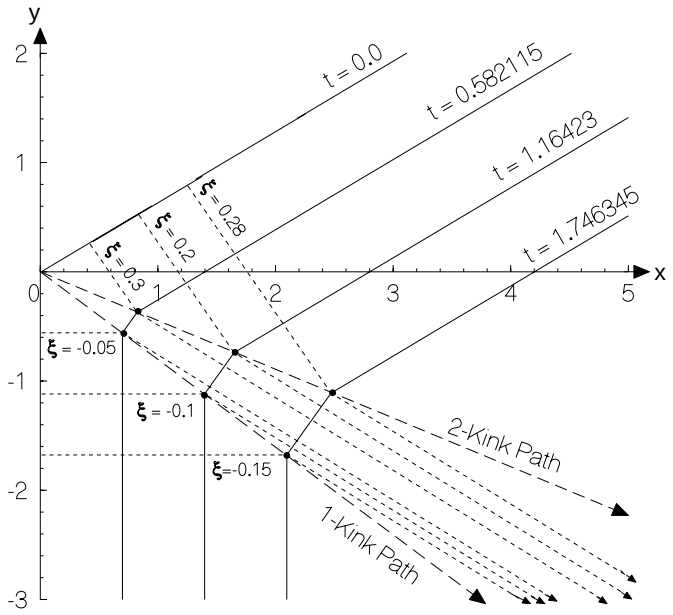

Fig. 4.4.4c: *Propagation of the crest-line when* $(m_r, \theta_r) \in C$ *with* $m_l = 1.2$, $m_r = 1.3, \theta_r = -0.9$.

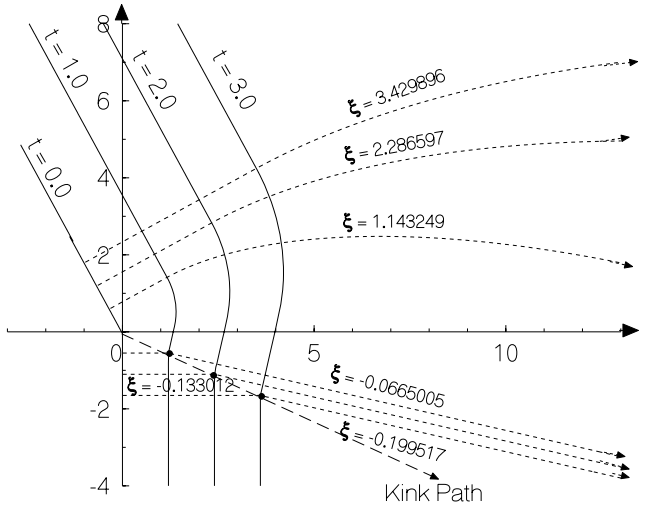

Fig. 4.4.4d: *Propagation of the crest-line when* $(m_r, \theta_r) \in D$ *with* $m_l = 1.2$, $m_r = 1.05, \theta_r = -0.2$.

Chapter 5

Shock Ray Theory

§5.1 Introduction

A system of equations for shock ray theory (SRT) consists of the ray equations derived from a shock manifold partial differential equation (SME) by Prasad (1982) and an infinite system of compatibility conditions along a shock ray (Grinfel'd, 1978, Maslov, 1978). An idea of SME can also be seen in the work of Kluwick (1971). However, the system of equations for successive compatibility conditions become too complex to be of any use. Suitable truncation of these equations in nth compatibility conditions leads to a finite system of equations, which leads to a new theory of shock dynamics (NTSD) developed by Ravindran and Prasad (1990) and it has been shown that only two compatibility conditions works well for a weak shock (Monica and Prasad, 2001). When we refer to the SRT in this thesis, we mean the ray equations with two compatibility conditions and with suitable truncation in the second compatibility condition for a weak shock.

In the first section of this chapter, we present briefly the NTSD for a scalar conservation law. Derivation of the equations for a weak shock ray theory (SRT) using WNLRT is briefly sketched in the section 5.2 in order to make the material self content. A more detailed discussion on these topics are available in the recent book by Prasad (2001). As mentioned in the chapter 1, the basic equations for studying the evolution of the shock front will be the kinematical conservation laws (KCL) and for the additional relation in order to make the KCL determined, we use the two compatibility conditions obtained after using NTSD. Conservation form for these two compatibility conditions were first obtained by Monica and Prasad (2001). We have obtained here a new formulation of the conservation form of the two compatibility conditions used in SRT. These conservation forms appear to be more natural and follow a pattern which are valid for each of the infinite set of compatibility conditions for a curved shock of an arbitrary strength.

§5.2 New Theory of Shock Dynamics

In this section, we derive the infinite system of compatibility conditions and discuss the new theory of shock dynamics for single conservation law

$$u_t + \left(\frac{1}{2}u^2\right)_x = 0, \quad (x,t) \in I\!R \times I\!R^+ \tag{5.2.1}$$

with initial condition

$$u(x,0) = u_0(x), \quad x \in I\!R \tag{5.2.2}$$

such that the solution is sufficiently smooth, except for a single shock curve

$$\Omega : x = X(t), \quad t \in I\!R^+. \tag{5.2.3}$$

The solution can be represented in the form

$$u(x,t) \;=\; u_l(x,t) + H(s)(u_r(x,t) - u_l(x,t)), \;\; s = x - X(t) \tag{5.2.4}$$

where H is the Heaviside function, and u_l and u_r are sufficiently smooth functions defined on $I\!R \times I\!R^+$. The state u_r on the right of the shock ($s > 0$), the state u_l on the left of the shock ($s < 0$) and the shock path $X(t)$ are uniquely determined by the initial condition (5.2.2). The jump condition across the shock can be written as (see Prasad, 2001)

$$\frac{dX(t)}{dt} \;=\; \frac{1}{2}\{u_l(X(t),t) + u_r(X(t),t)\} \equiv C, \text{ say} \tag{5.2.5}$$

The solution on the left of the shock $x < X(t)$ satisfies the partial differential equation

$$u_t + uu_x = 0, \tag{5.2.6}$$

which we write in the form

$$\frac{\partial u_l}{\partial t} + \frac{1}{2}(u_l + u_r)\frac{\partial u_l}{\partial x} = \frac{1}{2}(u_r - u_l)\frac{\partial u_l}{\partial x}$$

Taking the limit of this equation as $x \to X(t) - 0$, we get

$$\frac{du_l(X(t),t)}{dt} \;=\; \frac{1}{2}\{u_r(X(t),t) - u_\ell(X(t),t)\}\frac{\partial u_l}{\partial x}|_\Omega \tag{5.2.7}$$

where

$$\frac{d}{dt} \;=\; \frac{\partial}{\partial t} + C\frac{\partial}{\partial x}. \tag{5.2.8}$$

(5.2.7)-(5.2.8) is the first compatibility condition along the shock path. This equation giving the time-rate of change of u_l along the shock path contains $\frac{\partial u_l}{\partial x}|_\Omega$. To get an

equation for this new quantity $\frac{\partial u_l}{\partial x}|_\Omega$, we need to derive the second compatibility condition. We differentiate (5.2.6) with respect to x and write the result in the form

$$\frac{\partial}{\partial t}\left(\frac{\partial u_l}{\partial x}\right)+\frac{1}{2}(u_l+u_r)\frac{\partial}{\partial x}\left(\frac{\partial u_l}{\partial x}\right)=-\left(\frac{\partial u_l}{\partial x}\right)^2+\frac{1}{2}(u_r-u_l)\frac{\partial^2 u_l}{\partial x^2}$$

Taking the limit as $x \to X(t)-0$, we get the second compatibility condition

$$\frac{d}{dt}\left(\frac{\partial u_l}{\partial x}|_\Omega\right) = -\left(\frac{\partial u_l}{\partial x}|_\Omega\right)^2 + \frac{1}{2}\left\{(u_r-u_l)\frac{\partial^2 u_l}{\partial x^2}\right\}\Big|_\Omega, \tag{5.2.9}$$

which also contains a new quantity, namely, $\frac{\partial^2 u_l}{\partial x^2}\Big|_\Omega$

To derive the ith compatibility conditions, we differentiate (5.2.6) i times, arrange the terms appropriately and take the limit as $x \to X(t)-0$ to get

$$\frac{d}{dt}\left(\frac{\partial^i u_l}{\partial x^i}\Big|_\Omega\right)=\frac{1}{2}\left\{(u_r-u_l)\frac{\partial^{i+1}u_l}{\partial x^{i+1}}\right\}\Big|_\Omega-\left\{\sum_{j=1}^{i}{}^iC_j\frac{\partial^j u_l}{\partial x^j}\,\frac{\partial^{i-j+1}u_l}{\partial x^{i-j+1}}\right\}\Big|_\Omega \tag{5.2.10}$$

where ${}^iC_j = i!/(j!(i-j)!)$. The number of compatibility conditions which we can derive on the shock path depends on the degree of smoothness of the solution in the left subdomain of the shock. For solutions which are infinitely differentiable, we get an infinite system of compatibility conditions.

Let us denote the value of the ith spatial derivative at the shock divided by $i!$ by $v_i(t)$ i.e.,

$$v_i(t) = \frac{1}{i!}\,\frac{\partial^i u}{\partial x^i}\Big|_\Omega\ ,\ i=1,2,3,\ldots \tag{5.2.11}$$

and let $u_0(t) = u_l(X(t),t)$ represent the state just behind the shock. The equation for the shock path and the compatibility conditions are

$$\frac{dX}{dt} = \frac{1}{2}(u_0+u_r), \tag{5.2.12}$$

$$\frac{du_0}{dt} = -\frac{1}{2}(u_0-u_r)v_1 \tag{5.2.13}$$

and

$$\frac{dv_i}{dt} = -\frac{(i+1)}{2}(u_0-u_r)v_{i+1}-\frac{i+1}{2}\sum_{j=1}^{i}v_jv_{i-j+1},\ i=1,2,3,\ldots. \tag{5.2.14}$$

In the derivation of the second term on the right hand side of (5.2.14), we have used the identity

$$\sum_{j=1}^{i}(i-j+1)v_jv_{i-j+1} = \frac{i+1}{2}\sum_{j=1}^{i}v_jv_{i-j+1} \tag{5.2.15}$$

The compatibility conditions (5.2.13)-(5.2.14) were derived independently by Grinfel'd (1978) and Maslov (1980). The shock position $X(t)$, the shock strength u_0 and the spatial derivatives $i!v_i$, $i \geq 1$ can be obtained if we can solve the infinite system of ordinary differential equations (5.2.12)-(5.2.14).

The initial values of X, u_0 and v_i are given by the initial data (5.2.2)

$$\left.\begin{aligned} X(0) \quad &= X_0 \quad ; \quad u_0(0) \;=\; \varphi(X_0 - 0) \equiv u_{00}, \text{ say} \\ v_i(0) \quad &= \lim_{x \to X_0 - 0} \left\{ \tfrac{1}{i!} \tfrac{d^i \varphi}{dx^i} \right\} \equiv v_{i0}, \text{ say}, \; i = 1, 2, 3, \ldots \end{aligned}\right\} \tag{5.2.16}$$

where X_0 is the value of x at which $\varphi(x)$ has the discontinuity.

Equations (5.2.13)-(5.2.14) form a coupled system. The ith equation for $i!\, v_i$ contains $(i+1)!v_{i+1}$ and hence is coupled to the next equation. The coupling coefficient in the equation, namely $-\frac{1}{2}(u_0 - u_r)$ is the same for all equations. The theory of an infinite system of ordinary differential equations (an infinite-dimensional problem) is not necessarily simpler than that of a partial differential equation. However, unlike in the original initial value problem (5.2.1)-(5.2.2), we have to deal only with smooth functions in the new initial value problem for (5.2.12)-(5.2.14). The coupling coefficient is small for a weak shock. The existence and uniqueness of the solution of the infinite system have been discussed in Prasad (2001).

If we set $v_{n+1} = 0$ in the nth equation in (5.2.14), then the first $(n+1)$ equations in (5.2.13)-(5.2.14) form a closed system. Let $\bar{X}(t), \bar{u}_0(t), \bar{v}_i(t)$, $i = 1, 2, 3, \ldots, n$ is the solution of the truncated system of $n+2$ equations.

$$\frac{d\bar{X}}{dt} = \frac{1}{2}(\bar{u}_0 + u_r), \;\; u_r = u_r(\bar{X}, t) \tag{5.2.17}$$

$$\frac{d\bar{u}_0}{dt} = -\frac{1}{2}(\bar{u}_0 - u_r)\bar{v}_1 \tag{5.2.18}$$

$$\frac{d\bar{v}_i}{dt} = -\frac{i+1}{2}(\bar{u}_0 - u_r)\bar{v}_{i+1} - \frac{(i+1)}{2}\sum_{j=1}^{i} \bar{v}_j \bar{v}_{i-j+1}, i = 1, 2, \ldots, n-1 \tag{5.2.19}$$

and

$$\frac{d\bar{v}_n}{dt} = -\frac{(n+1)}{2}\sum_{j=1}^{n} \bar{v}_j \bar{v}_{n-j+1} \tag{5.2.20}$$

with initial conditions for these $n+2$ quantities as in (5.2.16), i.e.,

$$\bar{X}(0) = X_0, \;\; \bar{u}_0(0) = u_{00}, \;\; \bar{v}_i(0) = v_{i0}, \;\; i = 1, 2, 3, \ldots, n \tag{5.2.21}$$

Assuming the function $u_r(\bar{X}, t)$ to be analytic in a neighbourhood of $(X_0, 0)$, we can use Cauchy's existence theorem to prove the existence of a unique analytic solution of the

initial value problem (5.2.17)-(5.2.20) valid in a neighbourhood of $t = 0$. This solution can be expressed in the form

$$\bar{X}(t) = \sum_{j=0}^{\infty} \frac{\bar{X}_j}{j!} t^j, \bar{u}_0(t) = \sum_{j=0}^{\infty} \frac{\bar{u}_{0j}}{j!} t^j, \bar{v}_i(t) = \sum_{j=0}^{\infty} \frac{\bar{v}_{ij}}{j!} t^j, i = 1, 2, 3, \ldots, n \tag{5.2.22}$$

Having obtained the solution of the problem (5.2.17)-(5.2.21), we construct a function $\bar{u}(x, t)$ by

$$\begin{array}{rcll} \bar{u}(x,t) & = & \bar{u}_0(t) + \sum\limits_{i=1}^{n} \bar{v}_i(t)(x - X(t))^i, & x < \bar{X}(t) \\ & = & u_r(x,t), & x > \bar{X}(t) \end{array} \tag{5.2.23}$$

It has been proved by Prasad (2001) that this function is an approximate solution of the partial differential equation (5.2.1) in the left subdomain $x < X(t)$. A non-homogeneous partial differential equation has been obtained (see Prasad, 2001) for the error function which depends on both the space variable x and the time variable t. The following theorem (Prasad, 2001) gives a more precise statement for small t, regarding the manner in which the function $\bar{u}(x, t)$ given by (5.2.23) tends to the actual solution of the equation (5.2.1).

5.2.1. Theorem For small t, the analytic solution of the initial value problem (5.2.17)-(5.2.21) tends to the analytic solution of the initial value problem (5.2.12)-(5.2.14) and (5.2.16) as n tends to infinity.

We call the procedure of constructing the function $\bar{u}(x, t)$ by (5.2.23) after solving the initial value problem (5.2.17)-(5.2.21), the *"new theory of shock dynamics* (NTSD)". Theorem 5.2.1 shows that the new theory of shock dynamics will certainly give a good approximate solution for small t and it has also been shown by Prasad (2001) that this approximate solution is quite likely to remain a good approximation near the shock even for large values of t. The numerical comparison between the results of NTSD and the exact solution of the initial value problem (5.2.1)-(5.2.2) given in Prasad (2001) shows that the NTSD gives a good approximation when compared to the Whitham's theory of shock dynamics.

§5.3 Governing Equations of SRT

A system of equations of shock ray theory consists of the ray equations derived from a shock manifold partial differential equation (Prasad, 1982) and an infinite system of compatibility conditions along these ray (Grinfel'd (1978), Maslov, (1978)). However, the system of equations for successive compatibility conditions become too complex to be of any use. Suitable truncation of these equations in nth compatibility conditions leads

to a finite system of equations (NTSD), which simplify considerably for a weak shock (Prasad, 1993, Monica and Prasad (2001)). In this section, we present a derivation of these equations for a weak shock (Prasad, 2000) from the equations of WNLRT, derived under short wave or high frequency assumption.

Consider a weak shock front propagating into a polytropic gas at rest ahead of it. Then the shock will be followed by a one parameter family of nonlinear waves belonging to the same characteristic field (or mode). Each one of these wavefronts will catch up with the shock, interact with it and then disappear. A nonlinear wave, while interacting with the shock will be instantaneously coincident with it in the short wave assumption. The ray equations of the WNLRT in three-space-dimensions for a particular nonlinear wavefront in notations of $\epsilon a_0\tilde{w}$ for w, are (Prasad, 2001)

$$\frac{d\boldsymbol{x}}{dt} = \boldsymbol{n}a_0\left(1+\epsilon\frac{\gamma+1}{2}\tilde{w}\right) \tag{5.3.1}$$

and

$$\frac{d\boldsymbol{n}}{dt} = -\epsilon\frac{\gamma+1}{2}a_0\mathbf{L}\tilde{w} \tag{5.3.2}$$

where $\epsilon\tilde{w}$ represents the amplitude of the wave in terms of which perturbations due to the waves in the density ρ, fluid velocity $\boldsymbol{q}$ and pressure p are given by

$$\rho-\rho_0 = \epsilon\rho_0\tilde{w}\ ,\ \ \boldsymbol{q} = \epsilon\boldsymbol{n}a_0\tilde{w}\ ,\ \ p-p_0 = \epsilon\rho_0 a_0^2\tilde{w} \tag{5.3.3}$$

The transport equation (1.4.3) for the amplitude $\tilde{w}$ on the nonlinear wavefront is

$$\frac{d\tilde{w}}{dt} = \left\{\frac{\partial}{\partial t}+a_0\left(1+\epsilon\frac{\gamma+1}{2}\right)\tilde{w}\langle\boldsymbol{n},\nabla\rangle\right\}\tilde{w} = -\frac{1}{2}a_0\langle\nabla,\boldsymbol{n}\rangle\tilde{w} \tag{5.3.4}$$

We denote the unit normal to the shock front by $\boldsymbol{N}$. For the linear wavefront just ahead of the shock and instantaneously coincident with it (this is actually a linear wavefront moving with the ray velocity $\boldsymbol{N}$ multiplied by the local sound velocity a_0), $\tilde{w}$=0 and the bicharacteristic velocity is $\boldsymbol{N}a_0$. For the nonlinear wavefront just behind the shock and instantaneously coincident with it, we denote the amplitude $\tilde{w}$ by μ. Then, μ is the shock amplitude of the weak shock under consideration. Using Theorem 9.2.1 of Prasad (2001), and the results (5.3.1) and (5.3.2) with $\boldsymbol{n}=\boldsymbol{N}$, we get for a point $\boldsymbol{X}$ on the shock ray

$$\frac{d\boldsymbol{X}}{dT} = \frac{1}{2}\left\{a_0\boldsymbol{N}+\boldsymbol{N}a_0\left(1+\epsilon\frac{\gamma+1}{2}\mu\right)\right\} = \boldsymbol{N}a_0\left(1+\epsilon\frac{\gamma+1}{4}\mu\right) \tag{5.3.5}$$

$$\frac{d\boldsymbol{N}}{dT} = -\frac{1}{2}\left\{0+\epsilon\frac{\gamma+1}{2}a_0\mathbf{L}\mu\right\} = -\epsilon\frac{\gamma+1}{4}a_0\mathbf{L}\mu \tag{5.3.6}$$

where T is the time measured while moving along a shock ray. We take $\tilde{w}=\mu$ and $\boldsymbol{n}=\boldsymbol{N}$ in (5.3.4) and write it as

$$\frac{d\mu}{dT} \equiv \left\{\frac{\partial}{\partial t}+a_0\left(1+\epsilon\frac{\gamma+1}{4}\mu\right)\langle\boldsymbol{N},\nabla\rangle\right\}\mu = -\frac{1}{2}a_0\langle\nabla,\boldsymbol{N}\rangle\mu-\epsilon\frac{\gamma+1}{4}\mu\langle\boldsymbol{N},\nabla\rangle\tilde{w} \tag{5.3.7}$$

The equation (5.3.7) leads to the first compatibility condition along a shock ray

$$\frac{d\mu}{dT} = \Omega_s \mu - \frac{\gamma+1}{4}\mu\mu_1 \tag{5.3.8}$$

where

$$\bar{\Omega}_s = -\frac{1}{2}a_0\langle\nabla, \boldsymbol{N}\rangle \tag{5.3.9}$$

is the value of the mean curvature of the nonlinear wavefront instantaneously coincident with the shock from behind and

$$\mu_1 = \epsilon\{\langle \boldsymbol{N}, \nabla\rangle\, \tilde{w}\}|_{\text{shock front}}. \tag{5.3.10}$$

The second compatibility condition along a shock is given by (Prasad, 2001)

$$\frac{d\mu_1}{dT} = \bar{\Omega}_s\mu_1 - \frac{\gamma+1}{4}\mu_1^2 - \frac{\gamma+1}{4}\mu\mu_2 \tag{5.3.11}$$

where

$$\mu_2 = \epsilon^2 \left\{\langle \boldsymbol{N}, \nabla\rangle^2 \tilde{w}\right\}|_{\text{shock front}} \tag{5.3.12}$$

Similarly, higher order compatibility conditions can be derived. Thus, for the Euler's equations, we have derived the infinite system of compatibility conditions for a weak shock just from the dominant terms of WNLRT. Since the shock ray theory (SRT) can be derived from the WNLRT, the latter is more general than SRT. However, the results obtained by SRT are quantitatively different from those by WNLRT (see Chapter 6).

Unlike the well known geometrical optics theory, the shock ray theory is an exact theory (weak shock assumption is another independent assumption) but since there are infinite number of compatibility conditions on it, it is impossible to use it for computing shock propagation. We now use the new theory of shock dynamics (NTSD) according to which the system of equations (5.3.5), (5.3.6), (5.3.8) and (5.3.11) can be closed by dropping the term containing μ_2 in the equation (5.3.11). For more details on the NTSD and SRT, and their justifications, we refer to Prasad (2001).

The final equations of the SRT, which we use in this thesis, for the propagation of a weak shock propagation are (5.3.5), (5.3.6), (5.3.8) and (5.3.11) with the third term on the right hand side of (5.3.11) omitted.

§5.4 Conservation Form of the Equations of SRT

Let us consider a cylindrical shock propagating into a polytropic gas at rest and in uniform state $(\rho, \boldsymbol{q}, p) = (\rho_0, 0, p_0)$, where ρ is density, $\boldsymbol{q} = (q_1, q_2)$ velocity and p is the pressure.

Let a be the sound velocity in the medium : $a^2 = \gamma p/\rho$, where γ is the ratio of specific heats. Propagation of such a shock can be studied in (x, y)-plane. We assume the shock to be produced by the motion of a curved piston. Before proceeding further, we introduce a non-dimensional coordinate system with the help of a length L and the sound velocity a_0 in the uniform state. We choose L to be a length of the order of the linear dimension of the piston. We denote the non-dimensional coordinates also by the same symbol (x, y, t). The basic equations from which the equations in this section have been derived are Euler equations which have been written in the section 6.3.

We assume the piston to be at rest for $t < 0$ and then start moving suddenly with a small non-zero velocity at $t = 0$ and with a small acceleration. This produces a shock front initially coincident with the piston. The shock will be followed by a one parameter family of nonlinear wavefronts between the piston and the shock. For a small distance behind the shock, the high frequency (or the short wave approximation) is valid so that *the unit normal to the shock front and that of any one of the nonlinear wavefronts are the same.*

Let $\boldsymbol{N} = (\cos\Theta, \sin\Theta)$ be the unit normal of the shock front. Assuming the shock to be weak, the perturbations in density ρ, fluid velocity $\boldsymbol{q}$ and pressure p up to a short distance behind the shock are given by (5.3.3) with $\boldsymbol{n} = \boldsymbol{N}$. We denote the value of $\tilde{w}$ on the shock front by μ and the Mach number of the shock by M

$$\mu = \tilde{w}|_{\text{shock front}}, \quad M = 1 + \epsilon\frac{\gamma+1}{4}\mu \tag{5.4.1}$$

Under a short wave assumption $\langle \boldsymbol{N}, \nabla\rangle\tilde{w}$ is assumed to be $O(\epsilon^{-1})$. We define now a quantity V by (from equation (5.3.10))

$$V = \frac{\gamma+1}{4}\mu_1 = \frac{\gamma+1}{4}\epsilon\{\langle N, \nabla\rangle\tilde{w}\}|_{\text{shock front}}. \tag{5.4.2}$$

Note that this quantity was denoted by N by Prasad (2001) and Monica and Prasad (2001).

We introduce a ray coordinate system (ξ, t) such that $\xi =$ constant are shock rays in the (x, y)-plane and $t =$ constant are successive positions of the shock. Let G be the metric associated with ξ, and (X, Y) be a point on the shock at time t. The equations of SRT for a weak shock can be derived from the equation (5.3.5), (5.3.6), (5.3.8) and (5.3.11) and are given by

$$X_t = M\cos\Theta, \quad Y_t = M\sin\Theta \tag{5.4.3}$$

$$\Theta_t + \frac{1}{G}M_\xi = 0 \tag{5.4.4}$$

$$M_t + \frac{M-1}{2G}\Theta_\xi + (M-1)V = 0 \tag{5.4.5}$$

$$V_t + \frac{V}{2G}\Theta_\xi + 2V^2 = 0 \tag{5.4.6}$$

$$G_t - M\Theta_\xi = 0 \tag{5.4.7}$$

If we eliminate Θ_ξ between (5.4.5) and (5.4.7), we get the equation

$$\frac{2M}{M-1}M_t + \frac{G_t}{G} + 2VM = 0 \tag{5.4.8}$$

In order to discuss the shocks in the solutions of the above equations in (ξ, t)-plane, we need conservation form of the equations (5.4.4) - (5.4.7). Two physically realistic conservation laws, representing conservation of distance in two independent directions and equivalent to (5.4.4) and (5.4.7) for differentiable functions M, Θ and G, are the KCL

$$(G\sin\Theta)_t + (M\cos\Theta)_\xi = 0 \tag{5.4.9}$$

$$(G\cos\Theta)_t + (M\sin\Theta)_\xi = 0 \tag{5.4.10}$$

We derive now two more new conservation form of equations, which not only follow a general pattern valid for all compatibility conditions but are particular cases for a shock of arbitrary strength (Prasad, 2003). We notice in the equation (5.4.5) for the shock strength $M-1$ and (5.4.6) for the gradient V behind the shock that the second terms have a coefficient $\frac{1}{2G}\Theta_\xi$, which represents geometric amplification of decay of the corresponding quantities $M-1$ and V respectively. To derive a conservation law involving $M-1$ we eliminate Θ_ξ between (5.4.5) and (5.4.7). This leads to (5.4.8), which gives a combination $\{F'(h)/F(h)\}h_t + G_t/G$ where $h = M-1$ and F is a known function of h, or more specifically $F(h) = h^2e^{2h}$, leading to the conservation form

$$\{G(M-1)^2e^{2(M-1)}\}_t + 2M(M-1)^2e^{2(M-1)}GV = 0 \tag{5.4.11}$$

Similarly, eliminating Θ_ξ between (5.4.6) and (5.4.7) we get an equation which we rewrite as

$$V_t + \frac{V}{2G}G_t + \frac{V}{2}\left(\frac{1}{M} - 1\right)\frac{G_t}{G} + 2V^2 = 0$$

We use (5.4.8) to replace G_t/G in the third term by $G_t/G = -2MM_t/(M-1) - 2VM$ (note $M_t = (M-1)_t$) and write this equation as

$$\{ln(V^2G) + 2(M-1)\}_t + (M+1)V = 0$$

which gives the conservation form

$$\{GV^2e^{2(M-1)}\}_t + GV^3(M+1)e^{2(M-1)} = 0 \tag{5.4.12}$$

The conservation forms (5.4.11) and (5.4.12) of the compatibility conditions (5.4.6) and (5.4.7) respectively appear to be physically realistic. In linear theory the energy conservation along with a ray tube is represented by $\{G(M-1)^2\}_t = 0$. Nonlinearity seems to bring in a factor $e^{2(M-1)}$ as seen in Section 1.4 on WNLRT (also see Prasad (2001) or Prasad and Sangeeta (1999)). Any other form containing an expression $\{f(GF(h))\}_t$, where $f : I\!R \to I\!R$ is a monotonic function also appears gives appropriate geometrical decay or amplification of h.

In this case, a jump relation across a shock:

$$G_r F(h_r) = G_l F(h_l) \Leftrightarrow f(G_r F(h_r)) = f(G_l F(h_l)),$$

where l and r represents the states on the two sides of a shock.

The system of four equations (5.4.4) - (5.4.7) are hyperbolic for $M > 1$, which is true for a shock. Thus, we get a system of 4 equations in conservation form: (5.4.9) - (5.4.12), which is hyperbolic. Given a solution of this system, we solve (5.4.3) as ordinary differential equations for each value of $\xi : (X = X(\xi, t), Y = (\xi, t))$ which give the position of the shock front at a fixed time t and a ray for a fixed ξ. Given an initial position of a shock $\Omega_0 : (X_0(\xi), Y_0(\xi))$ so that we can compute $\Theta_0(\xi)$, initial shock strength $M_0(\xi)$ and initial gradient $V_0(\xi)$ of the flow behind Ω_0; we can set up an initial value problem of SRT equations (5.4.3) and (5.4.9) - (5.4.12)

$$\begin{aligned} &X(\xi, 0) = X_0(\xi), Y(\xi, 0) = Y_0(\xi), \\ &\Theta(\xi, 0) = \Theta_0(\xi), M(\xi, 0) = M_0(\xi), V(\xi, 0) = V_0(\xi) \end{aligned} \tag{5.4.13}$$

The problem of finding successive positions of a shock front is reduced from a 3-dimensional problem of solving the Euler equations in (x, y, t)-space to that of solving the SRT equations in (ξ, t)-plane. This reduction of one dimension leads to a considerable computational efficiency. In fact, in the case of problems we have solved in the Chapter 6, SRT takes only less than 10% of time required for solving Euler's equations. Moreover, since we need to solve a system of a hyperbolic equation in conservation form, we can use highly sophisticated and powerful numerical schemes. In this thesis, we used discontinuous Galerkin finite element scheme (Cockburn, et. al., 1989) to solve the system of conservation laws (5.4.9) - (5.4.12). We used source term splitting method to handle the nonhomogeneous part present in the equations (5.4.11) and (5.4.12) as explained in the Appendix 1.

Chapter 6

Propagation of Curved Shock Fronts Using Shock Ray Theory and Comparison With Other Theories

§6.1 Introduction

We consider the propagation of a cylindrical shock described in the (x, y)-plane and study blast waves produced by an explosion of a charge of finite size, which is initially in a non-circular shape. The initial shape will be non-circular not only because the explosive may be packed in a non-circular container but also because all parts of the explosive would not burn simultaneously. After a long time, when the leading shock has traveled a large distance compared to the linear dimensions of the explosive, the shock front will be almost circular even according to the linear theory. However, nonlinearity present in the Euler's equations of motion (we consider propagation of the shock front in a polytropic gas) will tend to smoothen the geometry of the shock front due to nonlinear waves propagating on the shock front itself and the shock front may become almost circular much earlier. We shall like to investigate this phenomenon by the shock ray theory (SRT) which has been derived for a weak shock by Prasad (1993) and later by Monica and Prasad (2001),(see Prasad, 2001) from a weakly nonlinear ray theory (WNLRT). The SRT is ideally suited for this investigation since

(i) it provides the shock as a well defined curve in computational results,

(ii) it requires very small computational time to give successive positions of the shock - in fact only a fraction of the time required for computing shock position by numerical solution of Euler's equations,

(iii) it gives a critical time t_c, an estimate of the time when the shock curve is very nearly a circle and

(iv) it gives results very close to those obtained by solving Euler's equations.

We recall from Section 5.3 that, by the governing equations of SRT in this thesis, we mean the ray equations with two compatibility conditions and with suitable truncation in the second compatibility condition for a weak shock. Kevlahan (1996) provided evidence for the property (iv) for SRT by comparison of its results with some known exact solutions, experimental and some numerical solutions of Euler's equations. Since, Kevlahan did not have the conservation form of the equations of SRT, his comparison with Euler's results is only for a limited time. In this chapter, we show that there is an excellent agreement of the results of SRT with Euler's results through an extensive numerical computation even for those cases in which there is some doubt for the validity of SRT i.e. when the curved piston is accelerating.

In section 5.4, we presented a new formulation of the conservation forms of the two compatibility conditions used in SRT. These conservation forms appear to be more natural and follow a pattern which are valid for each of the infinite set of compatibility conditions for a curved shock of an arbitrary strength. In section 6.2, we derive the initial conditions to set up the initial value problem for the equations of the SRT appropriate to the flow produced by the motion of a curved piston. In the subsequent sections we present the results of three problems solved by SRT and comparison of the results of SRT, numerical solutions of Euler's equations (NSEE) and results of Whitham's geometrical shock dynamics (GSD).

Since no estimation of error of the shock ray theory, specially for curved shocks, seems to be possible and theory is very important from the point of view of applications, for example for sonic boom and in aviation to shock wave lithotripsy to treat kidney stone disease, it is important to compare the results of SRT with Euler's results. This has become more important because the GSD have been used to predict finer results of the shape of shock fronts in some limiting cases (Schwendeman (2002) and Apazidis, Lasser, Tillmark and Johnson (2002)). Even if a theory has only 5% error, the limiting results may be completely wrong. Hence, the comparison of the results by SRT, GSD and Euler's equations, which we have presented are needed. We find an excellent agreement between the results of SRT and Euler's results, where as those between GSD and Euler's result is not so good. We also notice some limitations in application of WNLRT, GSD and SRT for solving piston problem with a convex corner.

§6.2 Initial conditions for SRT equations for a piston problem

When shock is produced by an impulsive motion of a piston, as described in the beginning of the section 5.4, the shock initially coincides with the piston. Hence the parameter ξ which appears in the ray coordinate description of the shock, may be taken to describe the initial geometry of the piston. In fact, we choose ξ to be the arc length along the boundary of the piston.

Let the shape of the moving piston be given by

$$(x, y) = (x_p(\xi, t),\ \ y_p(\xi, t)), \tag{6.2.1}$$

where ξ is a variable which varies along the piston at a fixed time t.

The fluid flow between the shock front $(x, y) = (X(\xi, t), Y(\xi, t))$ and the piston is generated by the one parameter family of nonlinear wavefronts (mentioned in section 5.4) and is given by (5.3.3). The normal $\boldsymbol{n}_p$ of the piston is obtained from (6.2.1) is different from $\boldsymbol{N}$ for $t > 0$ but in the limit $t \to 0+$ we have $\boldsymbol{N} = \boldsymbol{n}_p$.

Since

$$X_0(\xi) = x_p(\xi, 0),\ \ Y_0(\xi) = y_p(\xi, 0) \tag{6.2.2}$$

we can calculate $\Theta_0(\xi)$ from the initial shape of the piston. Now, we proceed to calculate $M_0(\xi)$ and $V_0(\xi)$. We note that the boundary condition at the piston in an inviscid flow is given by *"the fluid speed on the piston in the normal direction is equal to the piston speed in the normal direction"*. This gives

$$\epsilon\tilde{w}(\boldsymbol{x}_p(\xi, t), t) \equiv \langle \boldsymbol{n}_p(\xi, t), \boldsymbol{q}(\boldsymbol{x}_p(\xi, t), t)\rangle = \langle \boldsymbol{n}_p(\xi, t), \boldsymbol{x}_{pt}(\xi, t)\rangle. \tag{6.2.3}$$

From (5.4.1) and (6.2.3), we get

$$M_0(\xi) = 1 + \frac{\gamma + 1}{4}\langle \boldsymbol{n}_p(\xi, 0), \boldsymbol{x}_{pt}(\xi, 0)\rangle. \tag{6.2.4}$$

The transport equation for the amplitude $\tilde{w}$ (from WNLRT, equation (10.1.4), Prasad 2001) takes the form

$$\frac{\partial\tilde{w}}{\partial t} + \left(1 + \epsilon\frac{\gamma + 1}{2}\tilde{w}\right)\langle \boldsymbol{N}, \nabla\rangle\tilde{w} = \Omega\tilde{w}, \tag{6.2.5}$$

where $\Omega = -\frac{1}{2}\langle\nabla, \boldsymbol{N}\rangle$ is the mean curvature of a nonlinear wavefront behind the shock front in the short wave limit. Taking its limit as we approach the piston, we get

$$\left.\frac{\partial\tilde{w}}{\partial t}\right|_p + \left(1 + \epsilon\frac{\gamma + 1}{2}\tilde{w}|_p\right)\{\langle \boldsymbol{n}_p(\xi, t), \nabla\rangle\tilde{w}\}|_p = \Omega\tilde{w}|_p.$$

Using (6.2.3) in this equation, we get

$$\left.\frac{\partial \tilde{w}}{\partial t}\right|_p + \left\{1 + \frac{\gamma+1}{2}\langle \boldsymbol{n}_p(\xi,t),\ \boldsymbol{x}_{pt}(\xi,t)\rangle\right\}\langle \boldsymbol{n}_p(\xi,t), \nabla\rangle \tilde{w}|_p = \Omega \tilde{w}|_p. \tag{6.2.6}$$

We shall now encounter two types of partial derivatives with respect to t, one when x is kept fixed and another when ξ is kept fixed. The result (6.2.3) is valid for all $t > 0$ and taking its derivative with respect to t, we get

$$\epsilon\left\{\tilde{w}_t|_p + (\langle \boldsymbol{x}_{pt}, \nabla\rangle \tilde{w})|_p\right\} = \langle \boldsymbol{n}_{pt}(\xi,t), \boldsymbol{x}_{pt}(\xi,t)\rangle + \langle \boldsymbol{n}_p(\xi,t), \boldsymbol{x}_{ptt}(\xi,t)\rangle. \tag{6.2.7}$$

Taking projection of the vector $\boldsymbol{x}_{pt}(\xi,0)$ on the tangent vector

$$\boldsymbol{T}_0 = \{\boldsymbol{X}_\xi\}|_{t=0} = \frac{\boldsymbol{X}_{0\xi}}{|\boldsymbol{X}_{0\xi}|}$$

or

$$\boldsymbol{T}_0 \equiv \frac{\boldsymbol{x}_{p\xi}(\xi,0)}{|\boldsymbol{x}_{p\xi}(\xi,0)|}$$

and the normal vector

$$\boldsymbol{n}_{p0} = \frac{(x_{2p\xi}(\xi,0), -x_{1p\xi}(\xi,0))}{|\boldsymbol{x}_{p\xi}(\xi,0)|},$$

we get

$$\boldsymbol{x}_{pt}(\xi,0) = \langle \mathbf{x}_{pt}(\xi,0), \boldsymbol{n}_{p0}\rangle \boldsymbol{n}_{p0} + \langle \boldsymbol{x}_{pt}(\xi,0), \boldsymbol{T}_0\rangle \boldsymbol{T}_0. \tag{6.2.8}$$

The relation (6.2.7) at $t = 0$ becomes

$$\begin{aligned} \epsilon\tilde{w}_t|_{p,t=0} \quad &+ \quad \epsilon\langle \boldsymbol{x}_{pt}(\xi,0), \boldsymbol{n}_{p0}\rangle\langle \boldsymbol{n}_{p0}, \nabla\rangle \tilde{w}|_{p,t=0} \\ &= \quad -\epsilon\langle \boldsymbol{x}_{pt}(\xi,0), \boldsymbol{T}_0\rangle\langle \boldsymbol{T}_0, \nabla\rangle \tilde{w}|_{p,t=0} + \\ &\quad \left\{\langle \boldsymbol{n}_{pt}(\xi,0), \boldsymbol{x}_{pt}(\xi,0)\rangle + \langle \boldsymbol{n}_p(\xi,0), \boldsymbol{x}_{ptt}(\xi,0)\rangle\right\}. \end{aligned} \tag{6.2.9}$$

Setting $t = 0$ in (6.2.6) and eliminating $\tilde{w}_t|_{p,t=0}$ between (6.2.6) and (6.2.9), we get (we note $\boldsymbol{n}_p(\xi,0) = \boldsymbol{n}_{p0}$ and $\Omega_{t=0}$ = mean curvature of the piston at $t = 0$ is equal to $\Omega_p|_{t=0}$)

$$\begin{aligned} \epsilon\left\{\left(1 + \epsilon\frac{\gamma+1}{2}\tilde{w}|_{p,t=0}\right) - \langle \boldsymbol{x}_{pt}(\xi,0), \boldsymbol{n}_{p0}\rangle\right\}\{\langle \boldsymbol{n}_{p0}, \nabla\rangle \tilde{w}|_{p,t=0}\} \\ = \epsilon\left(\Omega_p|_{t=0}\tilde{w}|_{p,t=0}\right) + \epsilon\langle \boldsymbol{x}_{pt}(\xi,0), \boldsymbol{T}_{p0}\rangle\langle \boldsymbol{T}_0, \nabla\rangle \tilde{w}|_{p,t=0} \\ - \left\{\langle \boldsymbol{n}_{pt}(\xi,0), \boldsymbol{x}_{pt}(\xi,0)\rangle + \langle \boldsymbol{n}_{p0}(\xi,0), \boldsymbol{x}_{ptt}(\xi,0)\rangle\right\}. \end{aligned} \tag{6.2.10}$$

We now use (6.2.3) in (6.2.10) and note (5.4.2) to derive the initial value $V(\xi,0) = V_0(\xi)$. Collecting (6.2.3) and this result together, we finally get, using

$$\langle \boldsymbol{T}_0, \nabla\rangle = \frac{1}{|\boldsymbol{x}_{p\xi}|}\frac{\partial}{\partial\xi}$$

$$V_0(\xi) = \frac{\gamma+1}{4\{1+\frac{\gamma-1}{2}\langle \boldsymbol{n}_{p0}, \boldsymbol{x}_{pt}(\xi,0)\rangle\}} \left[\Omega_p|_{t=0}\langle \boldsymbol{n}_{p0}, \boldsymbol{x}_{pt}(\xi,0)\rangle \right.$$
$$+\frac{1}{|\boldsymbol{x}_{p\xi}|_{t=0}}\epsilon\langle \mathbf{x}_{pt}(\xi,0), \boldsymbol{T}_0\rangle \frac{\partial}{\partial\xi}\langle \boldsymbol{n}_{p0}, \boldsymbol{x}_{pt}(\xi,0)\rangle$$
$$\left. -\{\langle \boldsymbol{n}_{pt}(\xi,0), \boldsymbol{x}_{pt}(\xi,0)\rangle + \langle \boldsymbol{n}_{p0}, \boldsymbol{x}_{ptt}(\xi,0)\rangle\}\right]. \tag{6.2.11}$$

Note that the values $M_0(\xi)$ and $V_0(\xi)$ are completely determined by (6.2.4) and (6.2.11) in terms of the initial shape and initial motion of the curved piston.

The initial value $G_0 = G(\xi, 0)$ is obtained from the initial geometry of the shock front, which is the same as that of the piston. Hence

$$G(\xi,0) = |\boldsymbol{x}_{p\xi}(\xi,0)| \tag{6.2.12}$$

The expression (6.2.11) is quite complicated. In this work, we shall use very simple geometrical forms of the piston, which will be either a symmetrically expanding square or a curve made of a number of straight segments and moving as a rigid line in the direction of a symmetry. In this case $\boldsymbol{n}_{p0}$ is piecewise constant i.e., $\Omega_p = 0$ except for a set S of isolated points, so that

$$\frac{\partial}{\partial\xi}(\langle \boldsymbol{n}_{p0}, \boldsymbol{x}_{pt}(\xi,0)\rangle) = 0$$

and $\boldsymbol{n}_{pt} = 0$ except for S. In this case, the expression for $V_0(\xi)$ simplifies considerably to

$$V_0(\xi) = -\frac{\gamma+1}{4\{1+\frac{\gamma-1}{2}\langle \boldsymbol{n}_{p0}, \boldsymbol{x}_{pt}(\xi,0)\rangle\}}\langle \boldsymbol{N}_0(\xi), \boldsymbol{x}_{ptt}(\xi,0)\rangle. \tag{6.2.13}$$

§6.3 Other Theories

In this section, we shall describe some other theories, with which we shall compare the results of SRT. The simplest of these is the linear theory. This is a well known theory, in which rays in a uniform medium are straight lines and the wavefront is given by Huygens method.

Weakly nonlinear ray theory (WNLRT) This theory has been discussed in section 1.4. When we consider a shock front behind which the flow satisfies high frequency or short wave length approximation, the shock front is followed by a one parameter family of nonlinear waves. These waves, when weak, follow the weak shock front, catch up with the shock, interact and then disappear from the flow. The evolution of any one of these wavefronts is also governed by the KCL (See, Prasad 2001)

$$(g\sin\theta)_t + (m\cos\theta)_\xi = 0, \tag{6.3.1}$$
$$(g\cos\theta)_t - (m\sin\theta)_\xi = 0, \tag{6.3.2}$$

where m is the Mach number of the weakly nonlinear wavefront, θ the angle between the normal to the wavefront and the x-axis and the metric g associated with the coordinate ξ is given by

$$g = (m-1)^{-2} e^{-2(m-1)} \tag{6.3.3}$$

provided the variable ξ is chosen suitably.

As discussed in section 1.4, the system (6.3.1) and (6.3.2) is hyperbolic if $m > 1$, which due to the relation

$$m = 1 + \epsilon \frac{\gamma+1}{2} \tilde{w} \tag{6.3.4}$$

and (5.3.3) implies that the pressure p on the wavefront is greater than that in the ambient medium. We only consider the case when $m > 1$. Once we get a solution of (6.3.1) -(6.3.3) : $m = m(\xi, t), \theta = \theta(\xi, t)$; the position of the wavefront can be obtained by solving

$$x_t = m\cos\theta \quad , \quad y_t = m\sin\theta. \tag{6.3.5}$$

The system of equations (6.3.1) - (6.3.3) and (6.3.5) forms the WNLRT and gives the complete history of weakly nonlinear waves which may be continuously produced by a piston. A weakly nonlinear wave, which instantaneously coincide with the shock front, heading the disturbance in the piston problem, is produced by the piston not at the time $t = 0$ when the shock is produced but at a later time. Thus, there is not much gain in comparing the history of a nonlinear wave front and that of the shock but we do this because (i) the evolution of both are qualitatively same and (ii) the geometrical shock dynamics (GSD) is almost the same as the WNLRT except that the relation (6.3.6) is replaced by (5.4.1). In this chapter, we shall discuss only one nonlinear wavefront, the one which was produced by the piston at the same time as the shock was produced - but this is done only as an academic exercise because it is annihilated by the shock as soon as it is produced. We only calculate its geometry and position without bothering that it really does not exist. The initial condition for θ for this weakly nonlinear wavefront are the same as those for Θ in the section 3 (i.e., $\theta(\xi, 0) = \theta_p$) and that for m is

$$m(\xi, 0) = 1 + \epsilon \frac{\gamma+1}{2} \tilde{w}_p = m_0, \text{ say.} \tag{6.3.6}$$

Whitham's geometrical shock dynamics

The KCL (5.4.9) and (5.4.10) governs the evolution of any moving curve in a plane. The additional closure equations such as (5.4.5) and (5.4.6) in SRT or (6.3.3) for WNLRT come from the dynamics of the curve. Whitham did not have the KCL but derived its

differential form (5.4.4) and (5.4.7) and then using his valuable insight into the physics of the problem provided a closure relation (now well known as A - M relation) which for a weak shock becomes

$$G(M) = (M-1)^{-2} \tag{6.3.7}$$

provided we again choose the variable ξ suitably. The two relations (6.3.3) and (6.3.7) agree up to the first term in the expansion of the right hand side of (6.3.3) for small $m-1$. Whitham's intuition, which led to (6.3.7), clearly show the self-propagation property of weakly nonlinear wavefronts (Prasad (1995), see Prasad (2001)) but was used for a shock front. By GSD, we shall mean only the differential form of equations by Whitham but use KCL (5.4.9) and (5.4.10) along with (5.4.3) and (6.3.7). One of our main aim in this chapter is to compare the results of SRT and GSD with NSEE.

Euler equations of motion

Conservation form of the Euler equations of motion of a polytropic gas are

$$\boldsymbol{H}_t + \langle \nabla, \boldsymbol{F} \rangle = 0 \tag{6.3.8}$$

with

$$\boldsymbol{H} = \begin{bmatrix} \rho \\ \rho q_1 \\ \rho q_2 \\ \rho\left(\frac{p}{(\gamma-1)} + \frac{1}{2}\boldsymbol{q}^2\right) \end{bmatrix}, \mathbf{F} = \begin{bmatrix} \rho\boldsymbol{q} \\ \rho(q_1^2 + p, q_1 q_2) \\ \rho(q_1 q_2, \boldsymbol{q}^2 + p) \\ \rho\boldsymbol{q}\left(\frac{\gamma p}{\gamma-1} + \frac{1}{2}\boldsymbol{q}^2\right) \end{bmatrix}. \tag{6.3.9}$$

We have already commented on non-dimensionalization of space and time coordinates in the section 5.4. We include that and additional non-dimensional variables (with $'$)

$$\rho' = \rho/\rho_0, \boldsymbol{q}' = \boldsymbol{q}/a_0, p' = p(\gamma p_0), \rho' = \rho/\rho_0, \boldsymbol{x}' = \boldsymbol{x}/L, t' = a_0 t/L \tag{6.3.10}$$

and then drop $'$ from the non-dimensional variables in the transformed equations. The non-dimensional form of the Euler equations remains the same as (6.3.8) and (6.3.9).

The equilibrium state ahead of the shock (or the nonlinear wavefront) is $(\rho_0, \mathbf{q}_0, p_0) = (1, 0, \frac{1}{\gamma})$, so that the perturbation (5.3.3) becomes

$$\rho = 1 + \epsilon\tilde{w}, \;\; \mathbf{q} = \epsilon\mathbf{N}\tilde{w}, \;\; p = \frac{1}{\gamma} + \epsilon\tilde{w} \tag{6.3.11}$$

and the shock and nonlinear wavefront Mach numbers are given by (5.4.1) and (1.4.11) (with $w = \epsilon\tilde{w}$). Given the piston motion and its geometry in the form (6.2.1), we can use

(6.2.4) and (6.2.11) (or (6.2.13)) to set up initial value problem for SRT; (6.2.4) alone for GSD and

$$m(\xi,0) = 1 + \frac{\gamma+1}{2}\langle \mathbf{n}_p(\xi,0), \mathbf{x}_{pt}(\xi,t)\rangle \tag{6.3.12}$$

for WNLRT

Before we close this section, we discuss a superficial relation between the WNLRT and SRT. The solution of an initial value problem of the equations (5.4.9) - (5.4.12) for small time t tend to the solutions with the same initial values of the equations (5.4.9) - (5.4.10) and

$$\{G(M-1)^2e^2(m-1)\}_t = 0, \;\; \{GV^2e^{2(M-1)}\}_t = 0. \tag{6.3.13}$$

With a proper choice of ξ i.e. initial value of G, the first of these two give us $G = (M-1)^{-2}e^{-2(M-1)}$. Therefore, it appears that for a small time the SRT shock is governed by the equations of the WNLRT but this is only a superficial relation because it is the difference in the initial values in (6.2.4) for $M_0(\xi)$ and (6.3.12) for $m_0(\xi)$ which makes a nonlinear wavefront and a shock front to be distinct propagating curves. As discussed in section 5.3, SRT equations can be derived from the WNLRT equations (also see Monica and Prasad, 2001). However, if we approximate $(M-1)^{-2}e^{-2(M-1)}$ by $(M-1)^2$ for small $M-1$, then it follows that initially, near the source of creation of the shock, the SRT shock is governed approximately by GSD equations.

§6.4 Piston Problem When the Shape of the Piston is a Wedge

Consider a wedge shaped piston which starts moving with velocity u_0+u_1t in the direction of the symmetry, assumed to be the direction of the x-axis as shown in Fig. 6.4.1. Let ξ

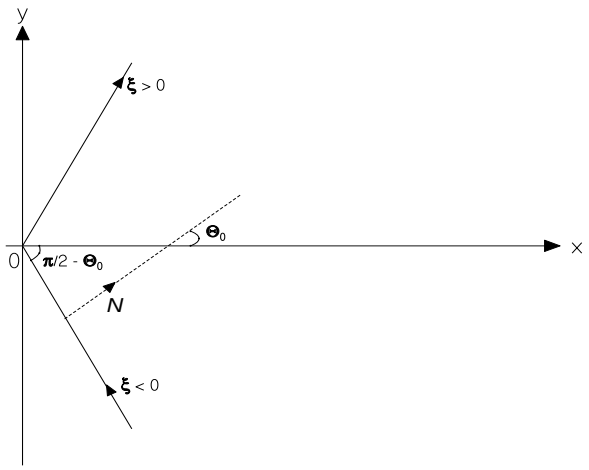

Fig 6.4.1: *Initially wedge shaped shock front.*

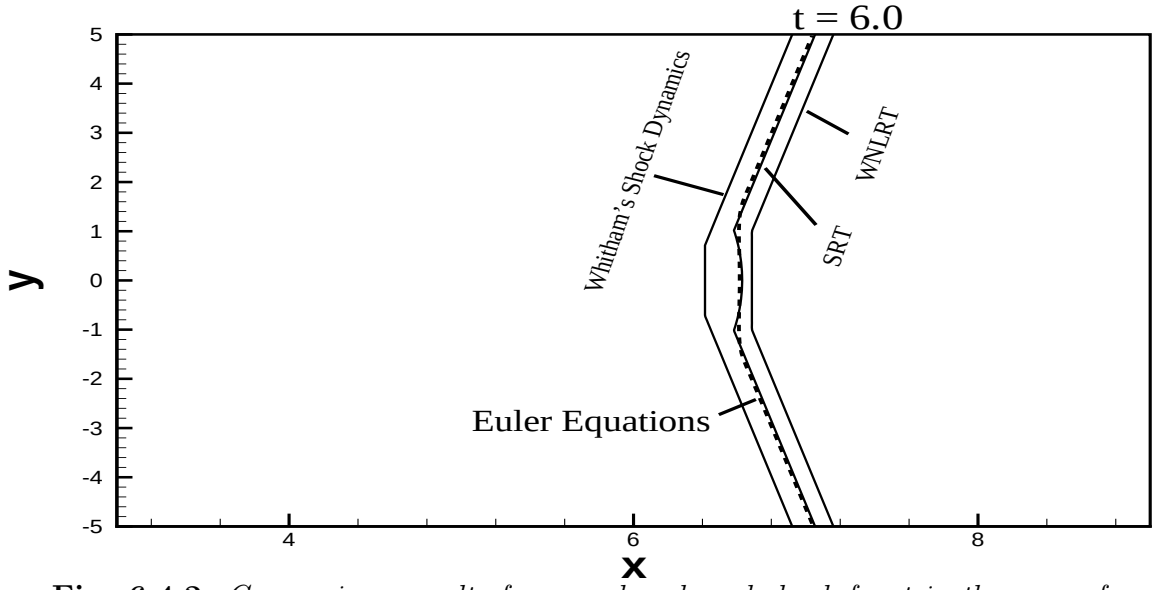

Fig. 6.4.2: *Comparison results for a wedge shaped shock front in the case of an accelerating piston with acceleration 0.15.*

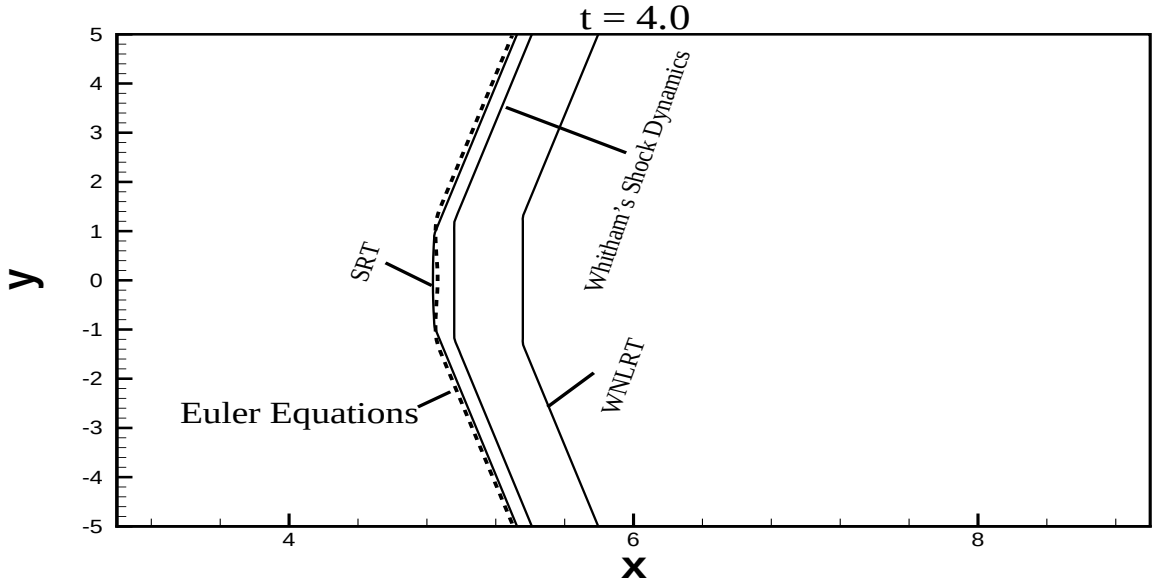

Fig. 6.4.3: *Comparison results for a wedge shaped shock front in the case of an decelerating piston with deceleration -0.15.*

be the distance along the piston measured from the vertex. Then for $t > 0$

$$x_p(\xi, t) = \begin{cases} -\xi \sin\Theta_0 + (u_0 t + \frac{1}{2} u_1 t^2), & \xi > 0 \\ \xi \sin\Theta_0 + u_0 t + \frac{1}{2} u_t t^2, & \xi < 0 \end{cases} \tag{6.4.1}$$

and

$$y_p(\xi, t) = \xi \cos\Theta_0.$$

For the piston motion, we get the following initial values for SRT

$$M_0(\xi) = 1 + \frac{\gamma + 1}{4} u_0 \cos\Theta_0, \tag{6.4.2}$$

$$V_0(\xi) = -\frac{(\gamma + 1) u_1 \cos\Theta_0}{4\left\{1 + \frac{\gamma - 1}{2} u_0 \cos\Theta_0\right\}} \tag{6.4.3}$$

and

$$G_0(\xi) = 1. \tag{6.4.4}$$

The initial value for the WNLRT is

$$m_0(\xi) = 1 + \frac{\gamma + 1}{2} u_0 \cos\Theta. \tag{6.4.5}$$

In order that the relation (1.4.12) is satisfied, we need to choose a new ξ in (6.4.1), which we denote by ξ_{new} and is given by $\xi_{\text{new}} = \frac{1}{(m_0 - 1)^{-2} e^{-2(\xi_0 - 1)}} \xi$.

Let us assume that this has been done for WNLRT. It is easy to find the solution of the KCL together with the relation (1.4.12) satisfying

$$\left.\begin{array}{lcl} m(\xi, 0) & = & m_0(\xi) \ , \ -\infty < \xi < \infty \\ \text{and} & & \\ \theta(\xi, 0) & = & \left\{ \begin{array}{lll} -\Theta_0 & , & \xi > 0 \\ \Theta_0 & , & \xi < 0 \end{array} \right. \end{array}\right\} \tag{6.4.6}$$

(see expression (6.2.15) in Prasad (2001)). Successive positions of the nonlinear wavefront now consist of a pair of kinks joining three straight parts as shown in Fig. 6.4.2 and 6.4.3. We call the central part between the two kinks as 'disk', which is perpendicular to the axis of symmetry i.e. the x-axis. The outer straight parts, we call them as 'wings' are parallel to the two sides of the wavefront at $t = 0$.

The initial value for GSD is same as (6.4.2). However, to use the expression (6.3.7) for $G(m)$, we need to use a new ξ in (6.4.1) as in the case of WNLRT above. There is an exact solution of this problem also and the graph of the position of the GSD shock front

is shown in Fig. 6.4.2 and Fig. 6.4.3. The general feature of a straight disc joined by two straight wings for a nonlinear wavefront is also present in a GSD shock at $t > 0$.

Since an exact solution of the equations of the SRT and Euler's equations are not possible, we compute the SRT shock numerically using discontinuous Galerkin finite element method (Cockburn et. al. 1989) explained in Appendix 1 and compare them with shocks by NSEE (using discontinuous Galerkin finite element method with dimension splitting method explained in Appendix 1) and plot them in the same Fig. 6.4.2 and Fig. 6.4.3. We make following observations from Fig. 6.4.2 and Fig. 6.4.3.

(i) The shock fronts by SRT and NSEE are very close - almost not distinguishable at these times.

(ii) The shock by GSD lags very much behind that of NSEE at $t = 0.6$. The results in Fig. 6.4.2 and Fig. 6.4.3 correspond to an accelerating and decelerating pistons respectively. Initially the shocks and nonlinear wavefront start from the same position. However, since the GSD does not take into account the acceleration of the piston, GSD shock starts falling behind the SRT and NSEE shocks which are pushed a head by the acceleration of the piston in Fig. 6.4.2. In the case of a decelerating piston, the GSD shock is ahead of the piston.

(iii) The difference between the positions of GSD and SRT will rapidly increase in the case of a decelerating piston because the shock strength of the SRT shock will decrease due to the deceleration of the piston, i.e. due to interaction of the shock with nonlinear waves (of decreasing amplitude) coming from the piston at a later time (see the detailed results in Monica and Prasad (2001)).

(iv) The nonlinear wavefront by WNLRT starts with a larger velocity compared to the shocks by the same piston motion and is always ahead of them. However, the piston acceleration will ultimately push the SRT and NSEE shocks so much that they will tend to catch up with the nonlinear wavefront, which is self-propagating i.e., it remains unaffected by the piston acceleration.

(v) Successive positions of the shock front by SRT have been shown in Fig. 6.4.4.

The central disc of SRT and NSEE shock is convex when observed from the medium ahead of it. This is a very interesting result - has not been observed in GSD shock (or the wavefront by WNLRT) but has been observed also in the numerical results of Sturtevant (1989). This important result was not clear in the work of Kevlahan (1996). The results of this section from the concave piston problem, show that SRT is an excellent theory to discuss this type of problems - not only there is a very good agreement with NSEE but it reproduces a very important effect seen in the experiments.

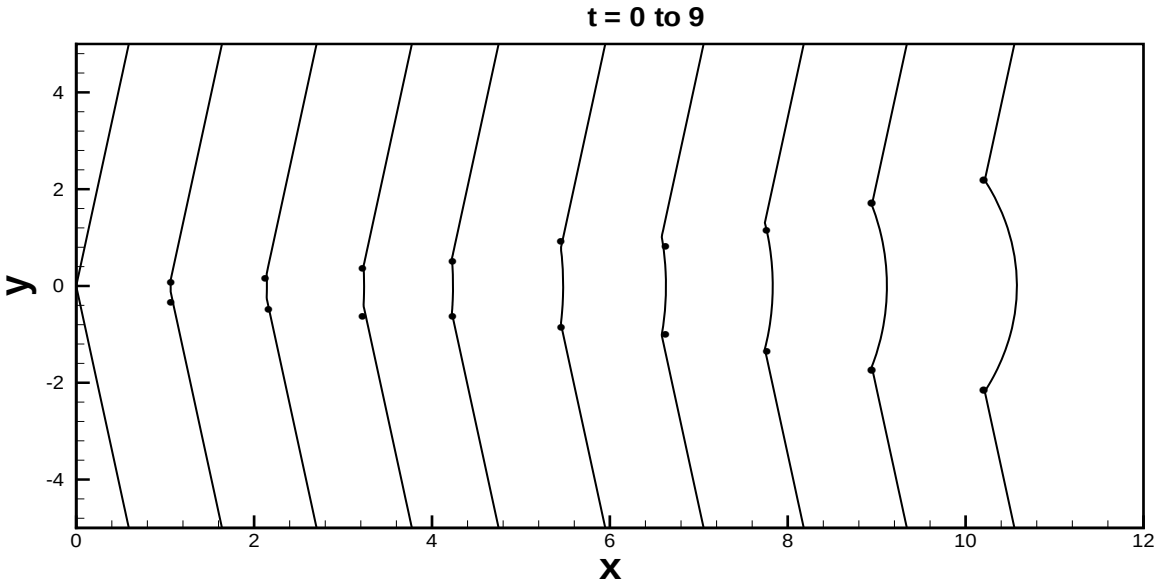

Fig. 6.4.4: *Successive positions of a wedge shaped shock front using SRT at a time interval 0.01.*

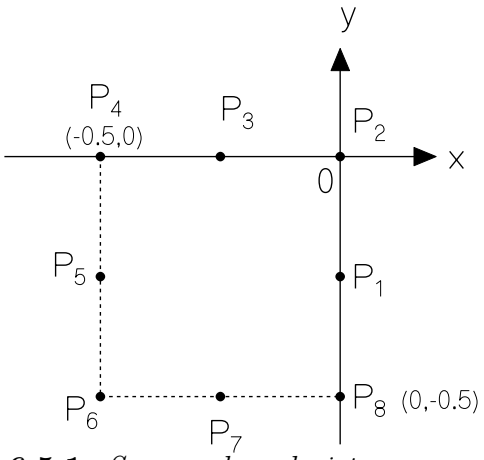

6.5.1: *Square shaped piston.*

§6.5 Blast Wave From a Square Shaped Container

Let us assume that the explosion of the charge in the container produces a shock front which is initially a square (Fig. 6.5.1) and which has a uniform shock strength. Just behind this initial shock, we shall have a nonlinear wavefront of the same shape and same uniform intensity $\tilde{w}$. For this problem, it is sufficient to set up an initial value problem for one half of the square (in fact a smaller part of square will do). In order to see the salient features of the shock front at $t > 0$, we first use WNLRT to trace the nonlinear wavefront, for which we can get an exact solution for small time.

Before we start further discussion, we first give the initial position of the square piston

as

$$(x_p(\xi,0), y_p(\xi,0)) = \begin{cases} (0,y) & , \quad -0.5 < y < 0 \\ (x,0) & , \quad -0.5 < x < 0 \\ (-1,y) & , \quad -0.5 < y < 0 \\ (x,-1) & , \quad -0.5 < x < 0 \end{cases} \tag{6.5.1}$$

The length of a side of the piston is 0.5.

We assume each side of the piston to suddenly start moving with a speed u_0 and acceleration u_1.

WNLRT Solution The Mach number of the piston is given by $m_0 = 1 + \frac{\gamma+1}{2}u_0$. Considering the symmetry in the shape of the piston, it is sufficient for numerical solution if we consider a portion of the initial piston from P_1 to P_3 (or equivalently, from P_3 to P_5) in Fig. 6.5.1. But to be more presice in the geometry of the shock front (or wavefront), we consider the portion P_1 to P_5 of the piston in Fig. 6.5.1 and the following initial value for the system (6.3.1) - (6.3.3)

$$\begin{aligned} m(\xi,0) &= m_0, -\xi_0 < \xi < 3\xi_0 \\ \theta(\xi,0) &= \begin{cases} 0 & , \quad -\xi_0 < \xi < 0 \\ \pi/2 & , \quad 0 < \xi < 2\xi_0 \\ \pi & , \quad 2\xi_0 < \xi < 3\xi_0 \end{cases} \end{aligned} \tag{6.5.2}$$

where ξ_0 is so chosen such that when ξ varies in $(-\xi_0, 0)$, the point $(x_p(\xi,0), y_p(\xi,0))$ moves on the line $x = 0$ from P_1 to P_2; and when ξ varies in $(0, 2\xi_0)$ the points move on the line $y = 0$ from P_2 to P_4.

$$\xi_0 = \frac{1}{4(m_0-1)^{-2}e^{-2(m_0-1)}} = \frac{1}{4g_0}. \tag{6.5.3}$$

If s is the arc length along the initial boundary measured from the point P_2, then $\xi = 4\xi_0 s$.

In a neighbourhood (lying in the upper half $t > 0$) of the point $(\xi = 0, t = 0)$, the solution of (6.3.1) - (6.3.3) with initial value $(m, \theta) = (m_0, 0)$ for $\xi < 0$ and $(m, \theta) = (m_0, \pi/2)$ for $\xi > 0$ is a solution of a Riemann problem. From Baskar and Prasad (2002), it follows that, if the solution exists, it will contain two centered simple waves separated by a constant state $(m_i, \pi/4)$ where m_i can be easily determined. The consideration that $m_i > 1$ leads to a critical value m_c given by

$$m_c = 1 + \frac{\pi^2}{128} \tag{6.5.4}$$

such that when $m_0 > m_c$ we have $m_i > 1$. Thus, *a necessary and sufficient condition for the existence of the solution is that* $m > m_c$. Equation (6.5.4) gives a magic number because even though the solution of the square piston problem exists for all values of m_0,

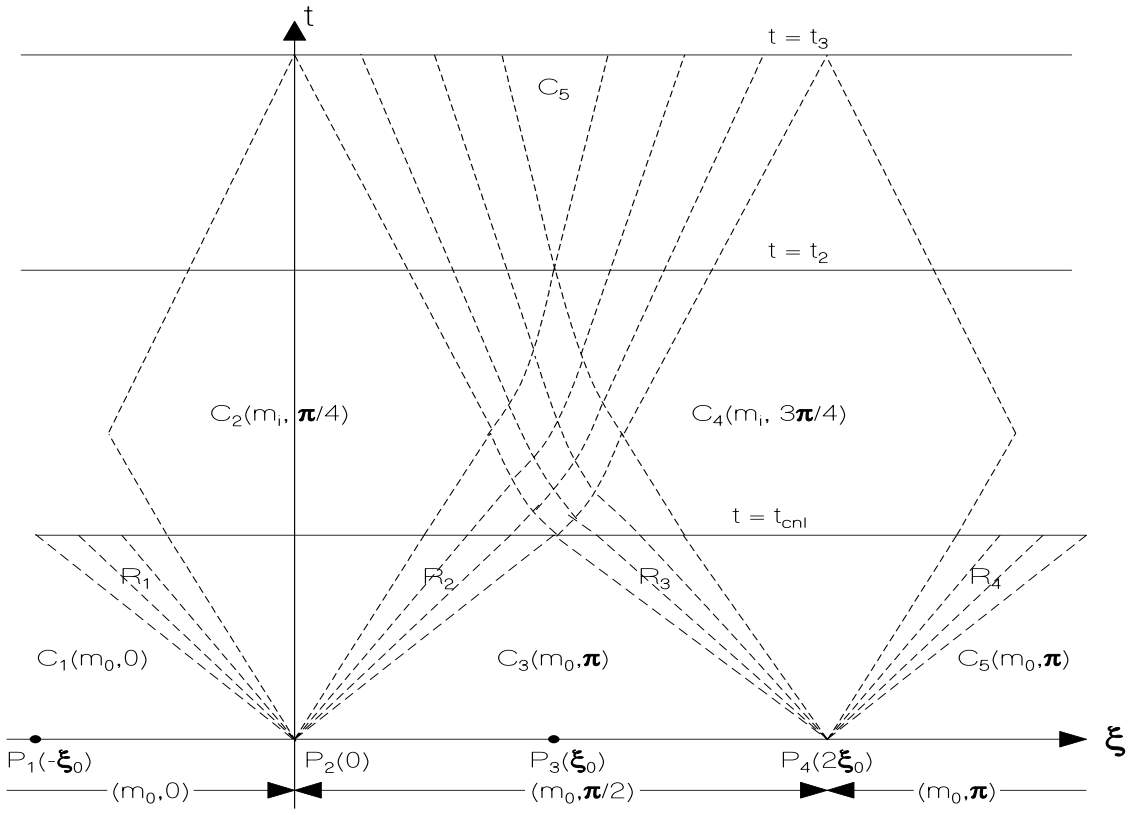

Fig 6.5.2: *When $m > m_c$ and $t < t_{cnl}$, the solution by WNLRT consists of a number of centered simple waves R_1, R_2, R_3, ... separated by constant state regions C_1, C_2, C_3, ...*

the WNLRT is not applicable for $m_0 < m_c$. We have shown in the end of the section 5 that *for small time, the SRT solution will tend to the solution of the corresponding homogeneous system i.e. the WNLRT, therefore this type of restriction will be applicable to the SRT also.*

When $m > m_c$, we can find an exact solution of the problem for $t < t_{cnl}$, where t_{cnl} is the time when the waves moving on the nonlinear wavefront from the two corners P_2 and P_4 meet. This is in fact the time when the leading end of the central simple wave of the positive characteristic family meet the line $\xi = \xi_0$ in the (ξ, t)-plane (see Fig 6.5.2). For $t < t_{cnl}$, the solution in (ξ, t)-plane consists of isolated rarefaction waves R_1, R_2, R_3, ... (of same strength) separated by a constant state (m_i, θ_i), with $m_i < m_0$ and from symmetry it follows that $\theta_i = \frac{\pi}{4}, \frac{3\pi}{4}, \ldots$. It is easy to determine an equation which would determine m_i. For $t > t_{cnl}$, no exact solution of the problem can be found and we need to solve the problem numerically. From $t = t_{cnl}$, the two rarefaction waves R_2 and R_3 (of different families as shown in Fig. 6.5.2) start interacting, this interaction will be of finite duration from time t_{cnl} to t_2 leading again to two rarefaction waves of two different families. Meanwhile, the newly generated rarefaction waves from interactions will bound

the constant state regions between R_1 and R_2 etc up to time t_3 (which may be either greater than t_2 or less than t_2). The solution beyond t_3 will again consist of non-constant regions and constant state regions between the two rarefaction waves produced as a result of interaction of R_2 and R_3 etc such as C_5. The shape of a weakly nonlinear wavefront at $t = 1.6, (t_2 < 1.6 < t_3)$ is shown in Fig. 6.5.6.

Using the characteristic velocity $\sqrt{\frac{m-1}{2g^2}}$, we find the value of $t_{cnl} = \xi_0/\sqrt{\frac{m-1}{2g^2}}$ so that

$$t_{cnl} = \frac{1}{\sqrt{8(m_0 - 1)}}. \tag{6.5.5}$$

GSD Solutions The main difference in WNLRT and GSD theory is that in the expressions (6.3.3) and (6.3.6), the metric g and Mach number m are replaced by the expressions (6.3.7) and (5.4.1) for G and M respectively. All other features of the solution by WNLRT are to be seen in that by GSD.

Interpretation of the initial conditions for the WNLRT, GSD and SRT

The above features of the solutions by WNLRT and GSD will also be present in the solution by SRT in a modified form. However, are these common features from all the three theories shared by the solution of the original problem i.e. numerical solution of the Euler (NSEE) ? This question becomes important because *there appears to be more than one initial data for Euler's equations which lead to the same initial value problem for any one of the three theories: WNLRT, GSD and SRT.*

Consider the following two blast wave problems produced by a piston initially in the

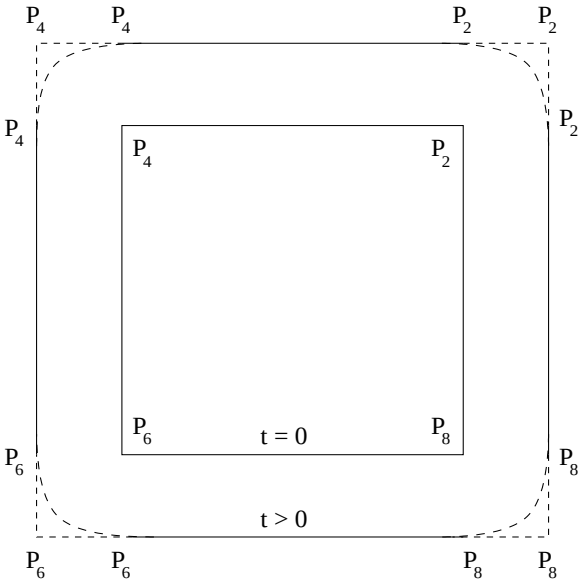

Fig. 6.5.3: *Piston motion: (a) sides of the square have fixed length and they simply move leaving 4 gaps $P_2''P_2'$, $P_4''P_4'$ etc.*

form of a square. The position of the piston is shown in Fig. 6.5.3. (a) In the first problem the lengths of the sides remain fixed as they move with same speed, at a later time $t > 0$ we get a punctured square with gaps $P_2''P_2', P_4'P_4'', P_6''P_6', P_8'P_8''$ at the corners. (b) The lengths of all sides increase as they move so that at a time $t > 0$, we get a bigger square $P_2'''P_4'''P_6'''P_8'''$. We can have one more problem in which the corners of the expanding square are rounded as shown in the Fig. 6.5.3. All these problems lead to the same initial data for WNLRT or GSD or SRT but for NSEE we need to prescribe different boundary conditions. In the problem (a), a vacuum is created in the gap and suitable boundary conditions are to be provided for Euler's equations. Similarly, in case (b) the fluid at the corners is continuously pushed and a different type of boundary conditions are required. The two problems (a) and (b) have different solutions but the corresponding problem either for WNLRT, GSD or SRT has a unique solution.

The WNLRT shows that at the corner P_2, we shall have elementary shapes (images of elementary waves) corresponding to R_1 and R_2 elementary waves separated by a straight part carrying the value m_i (i.e. a perturbation amplitude $\epsilon w_i = \frac{2}{\gamma+1}(m_i - 1)$, see relation (6.3.6)) and having normal direction given by $\theta_i = \pi/4$. What should be the correct boundary condition at the piston corresponding to this solution of WNLRT? We note that WNLRT is valid for small $m-1$ but there is a critical value m_c (slightly greater than 1, as seen from (6.5.4)) which is the lowest value of m_0 and for this $m_i = 1$ or $w_i = 0$. For other admissible values of m_0 (see Table 6.5.1)

Table 6.5.1

m_0	1.1	1.15	1.2	1.25
m_i	1.001486	1.012016	1.028742	1.049426

the value of $m_i - 1$ is quite small. Moreover, for small piston speed, the boundary conditions for NSEE is applied on the fixed piston having initial position. Hence, we think that the most appropriate boundary value at P_2 (and hence at other corners) is zero velocity of the fluid (and hence the piston) and zero acceleration. At all other points we can prescribe the initial fluid speed $1 + \epsilon\tilde{w}$ which is the same as the initial piston speed $|(x_{pt}(\xi, 0), y_{pt}(\xi, 0)|$.

Comparison of the NSEE and solutions by GSD and SRT

As discussed above, we apply the appropriate boundary conditions for NSEE on the initial position of the square piston and solve the Euler's equations. Given the piston motion, we then evaluate the initial values for the equations of SRT from (6.2.4) and (6.2.13). For SRT we take ξ to be the arc length from P_2 and hence $G_0 = G(\xi, 0) = 1$.

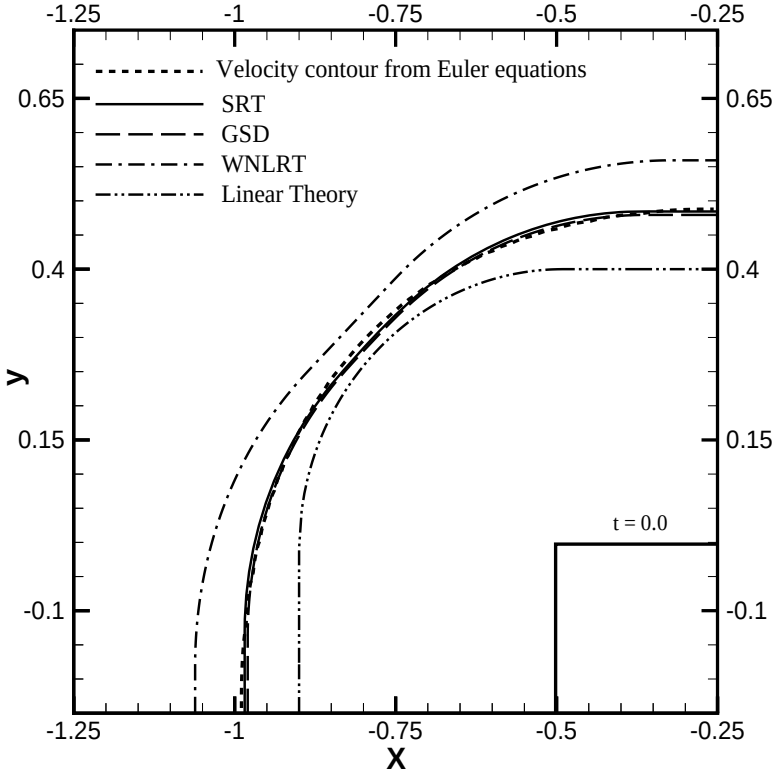

Fig. 6.5.4: *Comparison of results at time $t = 0.4$ in the case of a blast wave with an accelerating piston with acceleration 0.5.*

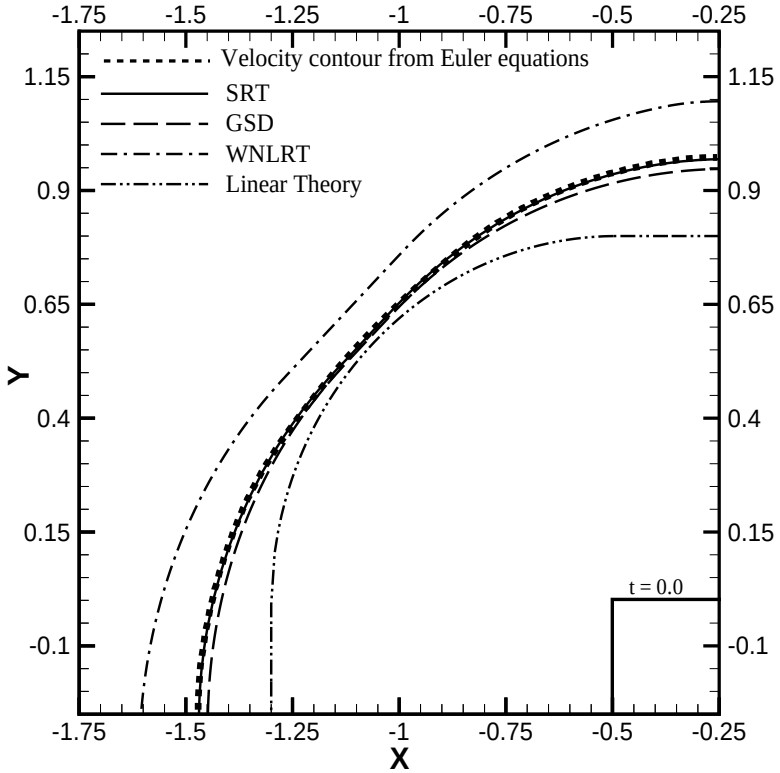

Fig. 6.5.5: *Comparison of results at time $t = 0.8$ in the case of a blast wave with an accelerating piston with acceleration 0.5.*

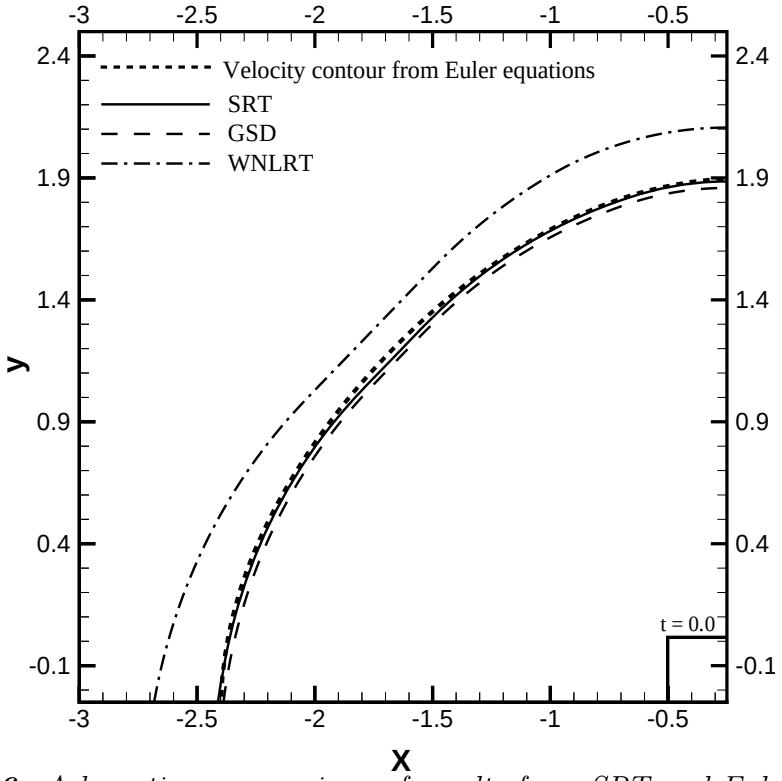

Fig. 6.5.6: *A long time comparison of results from SRT and Euler equations at time t = 1.6 in the case of an accelerating piston with acceleration 0.5.*

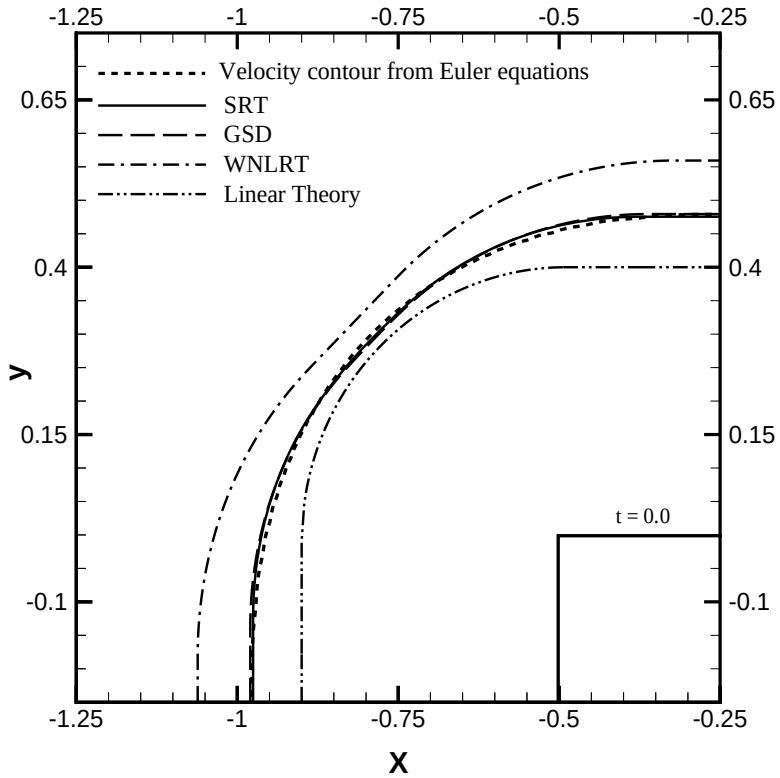

Fig. 6.5.7: *Comparison of results at time t = 0.4 in the case of a blast wave with a deceleration piston with deceleration -0.5.*

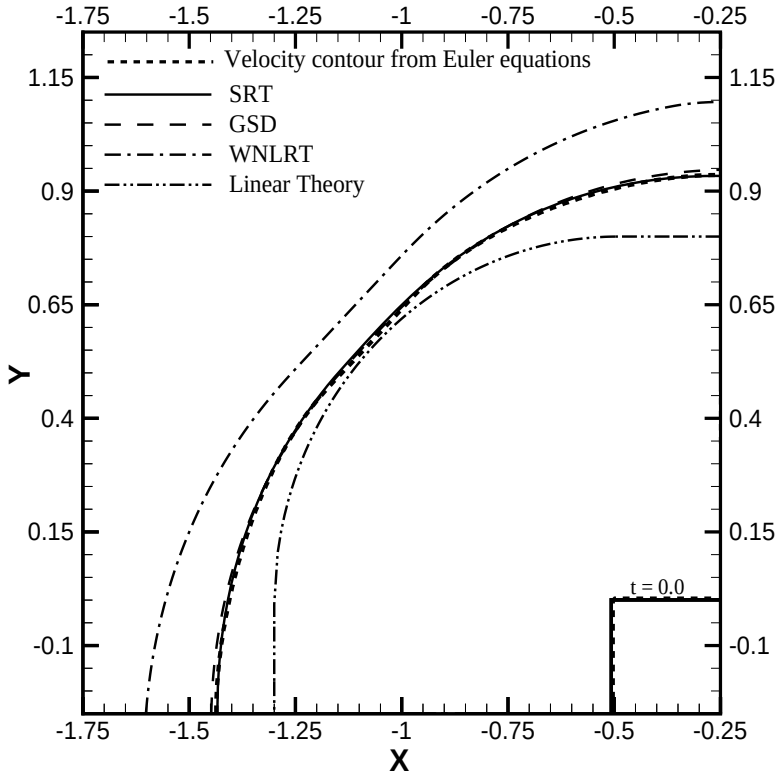

Fig. 6.5.8: *Comparison of results at time $t = 0.8$ in the case of a blast wave with a deceleration piston with deceleration -0.5.*

Before we discuss the comparison of the results, we calculate t_{cs}, the time when the waves from the corners P_2 and P_4 (Fig. 6.5.1) reach the point P_3 according to SRT. The relevant eigenvalue (or characteristic velocity) of the system (5.4.4) - (5.4.7) is $\sqrt{\frac{M-1}{2G^2}}$ in (ξ, t)-plane. Since the wave from P_2 moves into the constant state with $M = M_0$ and $G_0 = 1$, it reaches the point P_3 at a distance $\frac{1}{4}$ in time

$$t_{cs} = \frac{1}{\sqrt{8(M_0 - 1)}} = (0.89\ldots \text{ for } M_0 = 1.2). \tag{6.5.6}$$

Since $0 < M_0 - 1 < m_0 - 1$, it follows from (6.5.5) and (6.5.6) that

$$t_{cnl} < t_{cs}. \tag{6.5.7}$$

For the value $M_0 = 1.2$, we find $t_{cs} = 0.79057$. This gives an order of time when we may consider the shock front to be approximately circular. We shall comment on this later in this section.

Fig. 6.5.4 - Fig. 6.5.8 contain graphical depiction of the results by all 5 theories mentioned in this chapter. Though we have drawn the graphs of results by the WNLRT and linear theory also, the important comparison is between the results by SRT, GSD and NSEE. Fig. 6.5.4 - Fig. 6.5.6 contain results for an accelerating piston at time

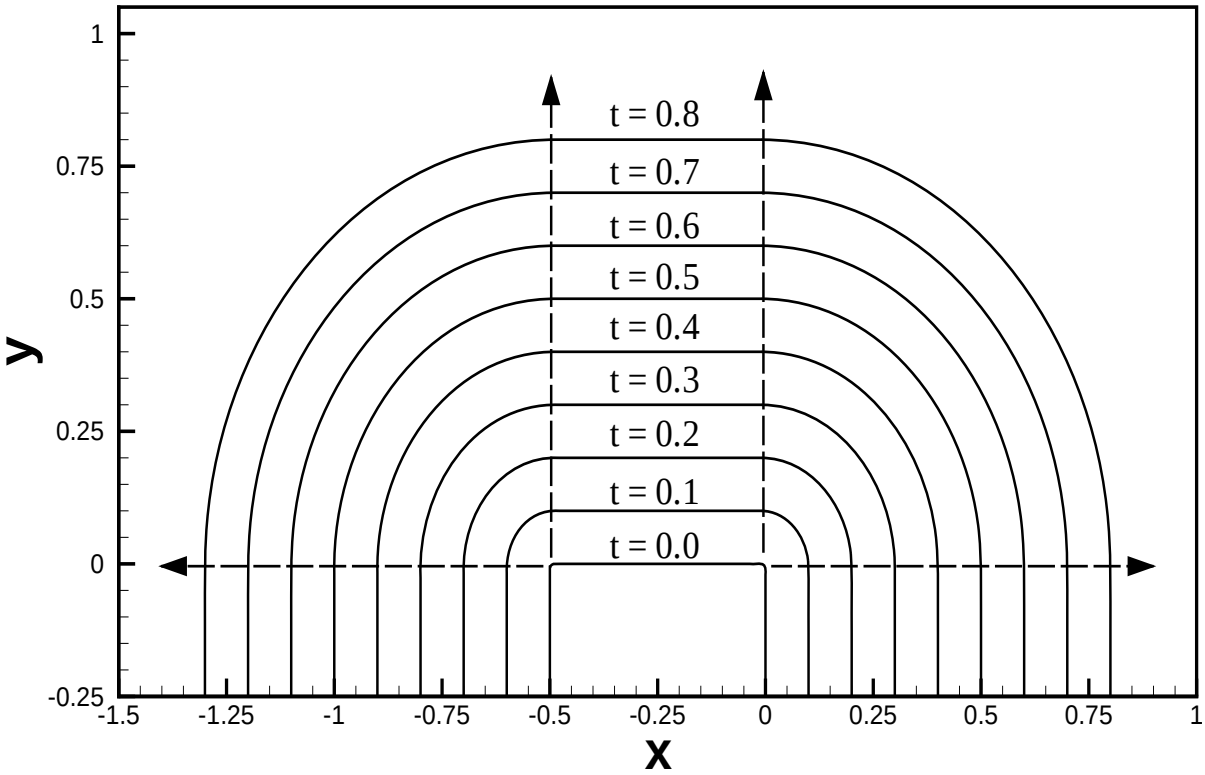

Fig. 6.5.9: *Successive positions at times t of a leading wavefront from a blast wave due to a square shaped source using linear theory.*

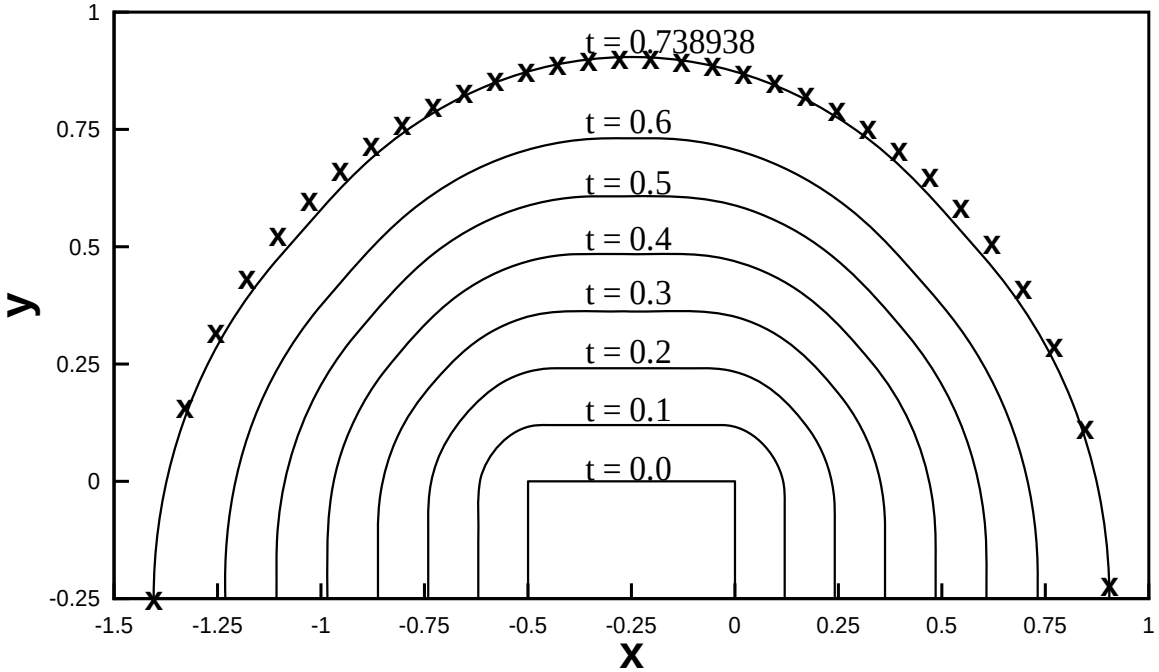

Fig. 6.5.10: *Successive positions of a leading shock front (at different times t) from a blast wave due to a square shaped source using SRT. A circle of same radius has been shown at t_c by X*

$t = 0.4, t = 0.8$ and $t = 1.6$. All three shocks start with same piston and same velocity and hence for small t, they almost overlap. At time $t = 0.4$, Fig 6.5.4 shows that all three curves representing the results by the three theories almost overlap but the SRT curve occupies overall a middle position of the GSD and NSEE curve. At $t = 0.8$ (Fig 6.5.5), the SRT and NSEE overlap as at $t = 0.4$ but the GSD curve now lags behind and this effect becomes more pronounced at $t = 1.6$. For an accelerating piston, energy is fed into the flow at an increasing rate but this increasing input of the energy is not taken into account by GSD. This causes the GSD shock to lag behind. The comparison has been stopped at $t = 1.6$ since our scheme for NSEE could not continue beyond this time. There is not much reason to continue solution beyond this time because as t increases GSD result is bound to differ significantly from that of SRT. Fig. 6.5.7 and Fig. 6.5.8 contain results of a decelerating piston at $t = 0.4$ and $t = 0.8$ respectively. At both times, all three results are very close but the SRT curve lies almost in the middle of the other two curves. In the decelerating piston case, the energy is fed into the flow at a decreasing rate. Till the time we have presented our results, the deceleration has not sufficiently affected the relative positions of shocks and this has caused GSD shock to be only little ahead of the SRT and NSEE shocks. It is well known that GSD does give good result in some cases (see Whitham, 1974) but it is only accidental (Prasad, Ravindran and Sau (1991)). What is important for us is to note that SRT gives consistently good result, very close to Euler's solutions not only in this case but also for the wedged shaped piston problem discussed in the previous section. This agrees with the conclusion of Kevlahan (1996), who compared the results of the SRT with NSEE and found an excellent agreement between the two results. He also found excellent agreement of the results of SRT with experimental results of Sturtevant and Kulkarni (1976) and some known exact solutions.

Evolution toward a circular shock

We now discuss the main aim of this chapter. The shock front (more precisely the linear wavefront) produced by a square piston, when calculated according to the linear theory will tend to a circle as $t \to \infty$. At any finite time, it will have four straight parts joined by circular arcs as shown in the Fig. 6.5.9. If a is the length of the side of the square at $t = 0$, the ratio of total length of the straight parts of the linear wavefront to that of the circular arcs is $2a/(\pi t)$. Here $a = 0.5$ and, therefore, at $t = 0.8$, this ratio in Fig. 6.5.9 is approximately $1/3$. The linear wavefront may be treated as almost circular, when this ratio is $\frac{1}{10}$ i.e $t = O\left(\frac{2a}{\pi}\right)$ which is equal to ≈ 3. Fig. 6.5.10 shows the successive positions of the SRT shock up to a time 0.738938 which is quite close to t_c. At this time, a circle (shown by the symbol "x") has been drawn with its center at the center of the square. The shock and the circle are almost coinciding. This evolution almost into a circle of an initially square shock has taken place at t_c which is just $\frac{1}{3}$ of the time when

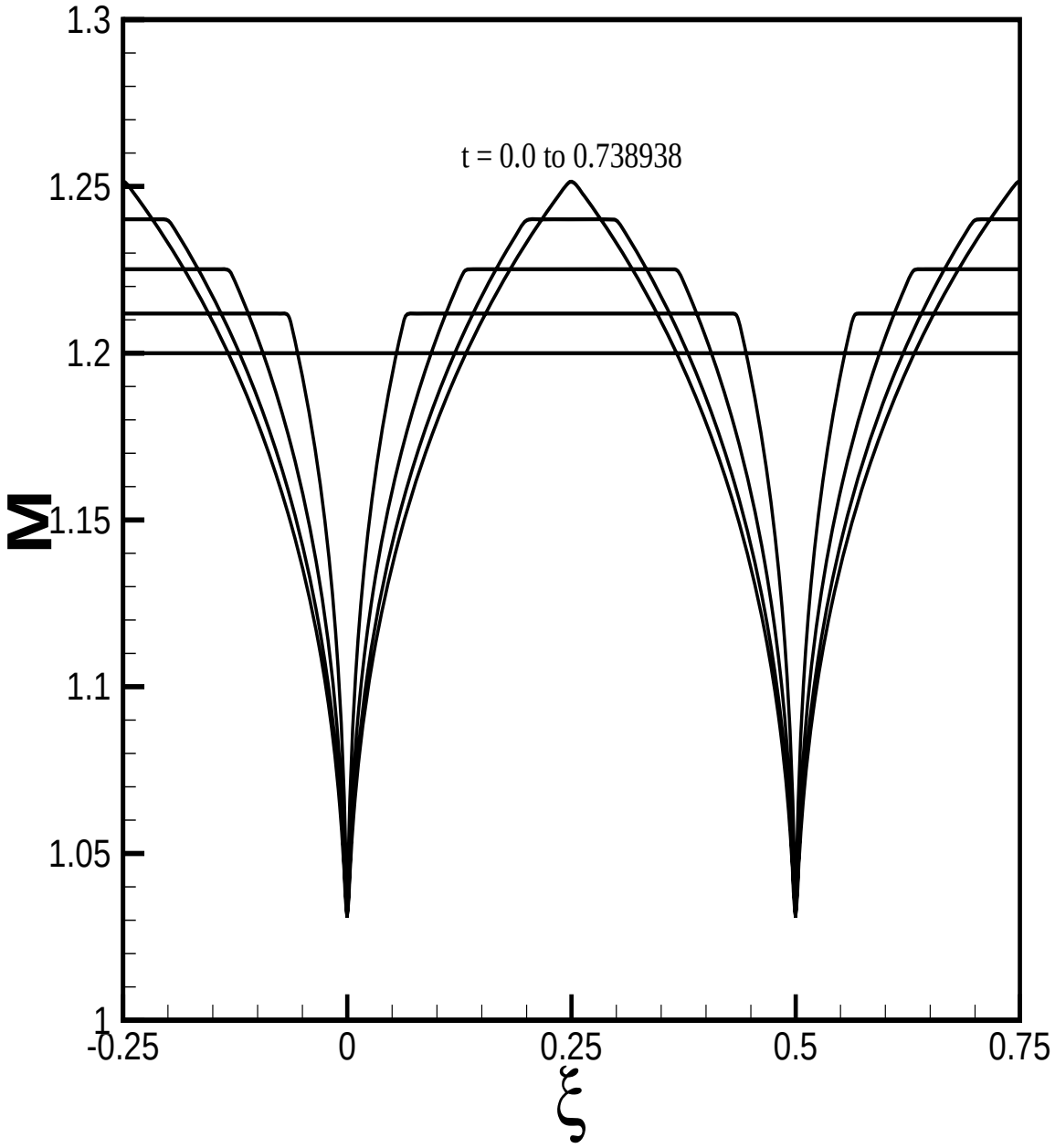

Fig. 6.5.11a: *Variation in M with respect to ξ in the case of a blast wave from a square shaped source using SRT. Inner most curves correspond to the results at $t = 0$ and outermost ones to those at $t = 0.738938$.*

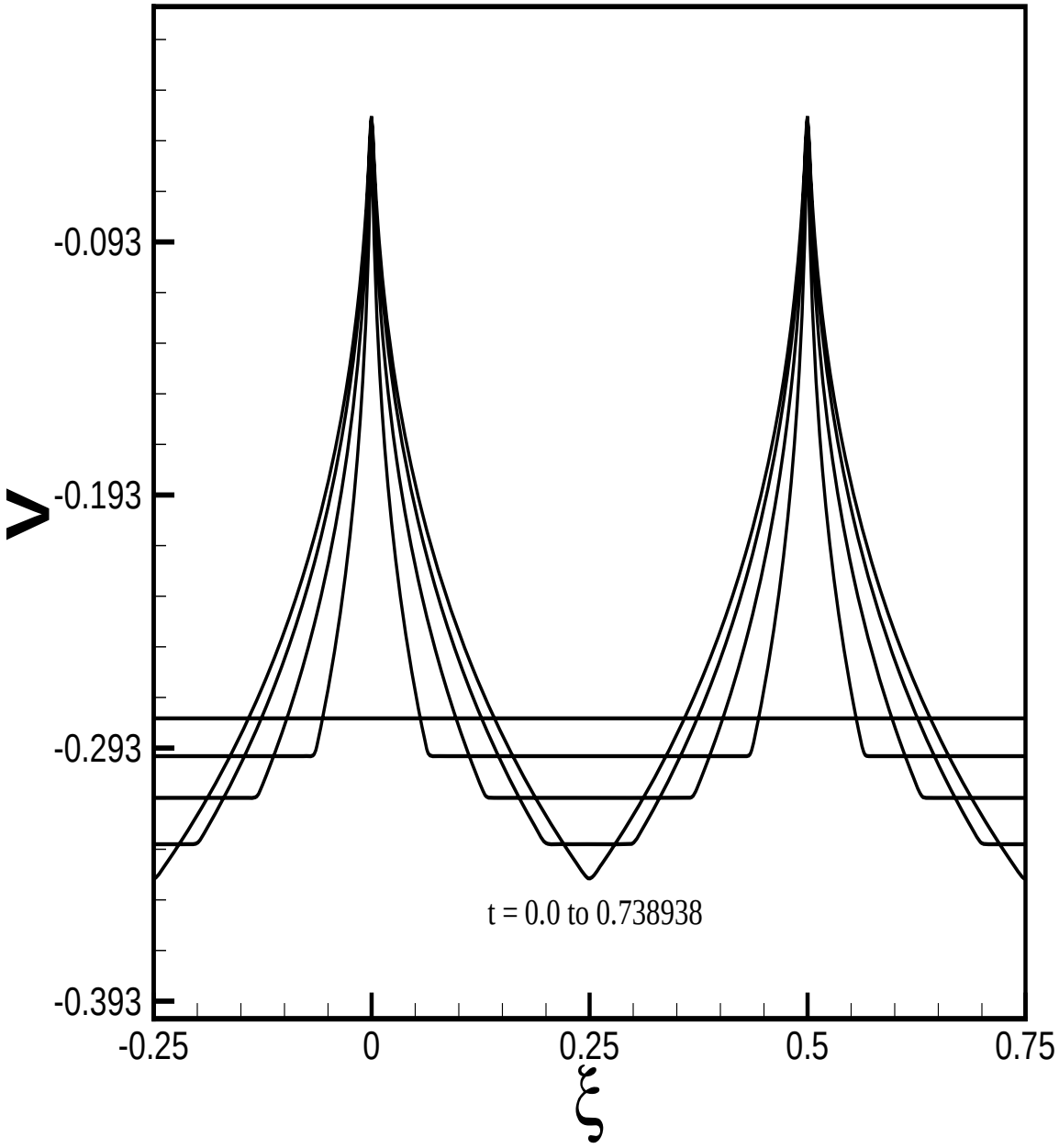

Fig. 6.5.11b: *Variation in V with respect to ξ in the case of a blast wave from a square shaped source using SRT. Inner most curves correspond to the results at $t = 0$ and outermost ones to those at $t = 0.738938$.*

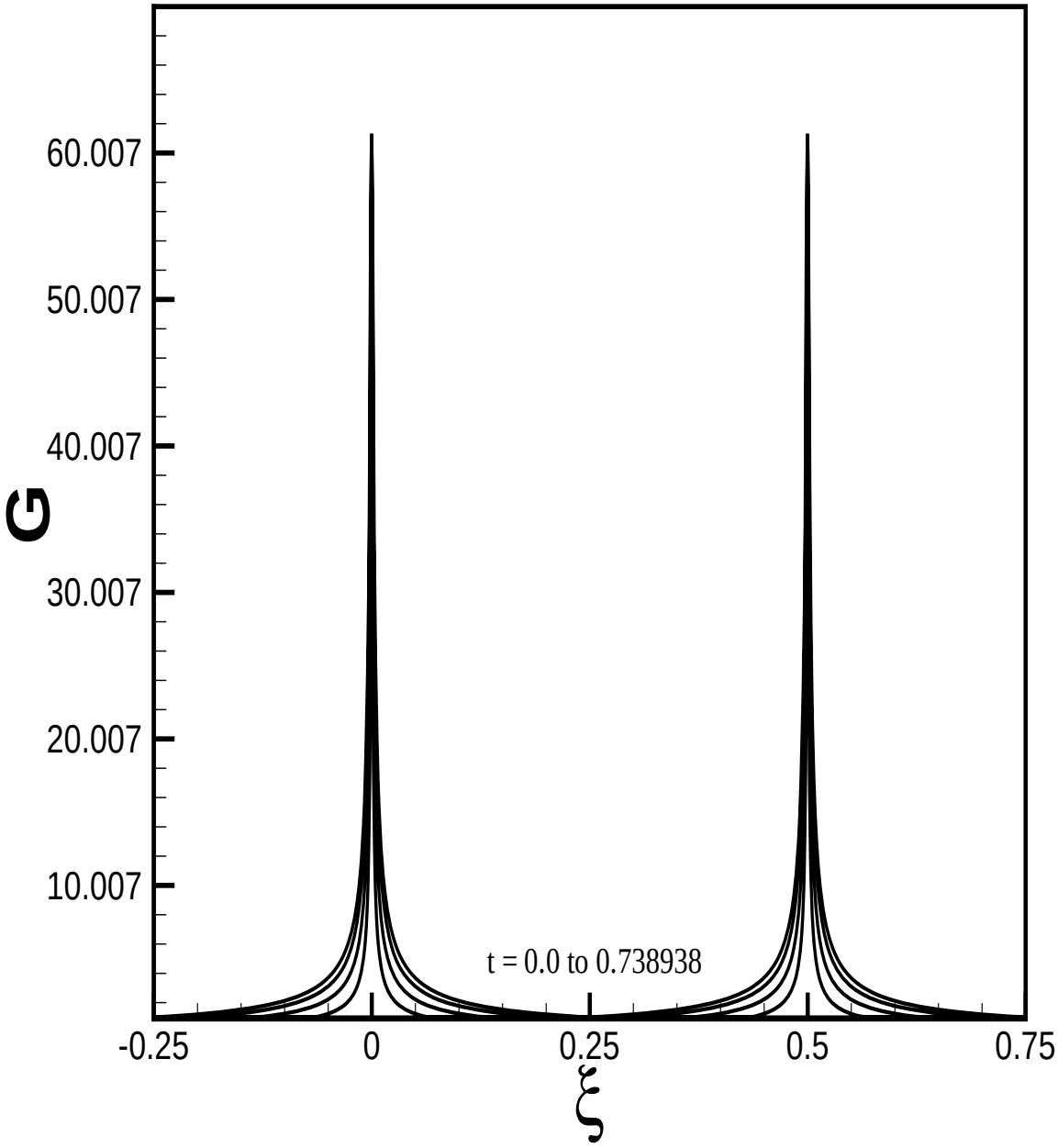

Fig. 6.5.11c: *Variation in G with respect to ξ in the case of a blast wave from a square shaped source using SRT. Inner most curves correspond to the results at $t = 0$ and outermost ones to those at $t = 0.738938$.*

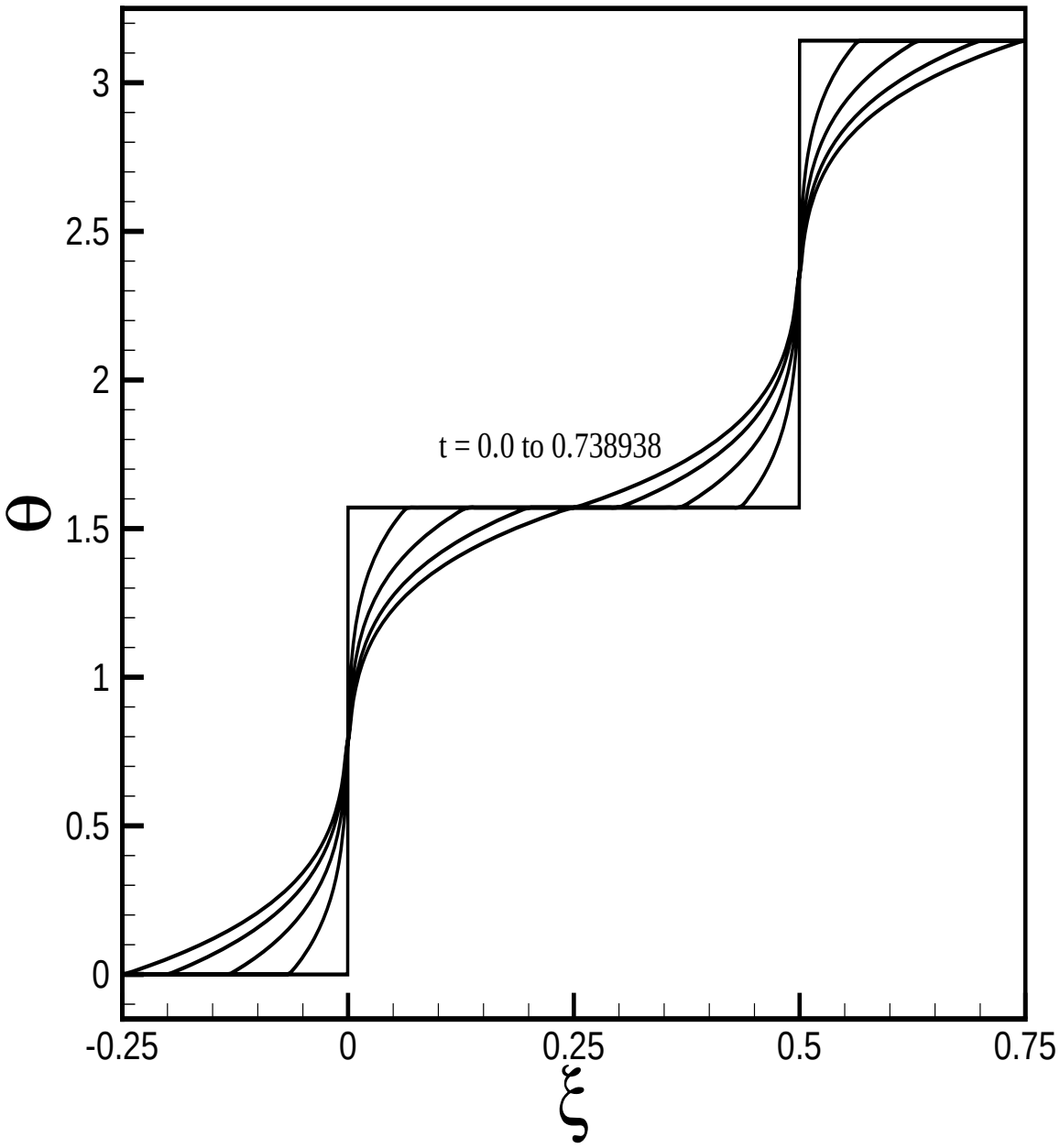

Fig. 6.5.11d: *Variation in* Θ *with respect to* ξ *in the case of a blast wave from a square shaped source using SRT. Inner most curves correspond to the results at* $t = 0$ *and outermost ones to those at* $t = 0.738938$.

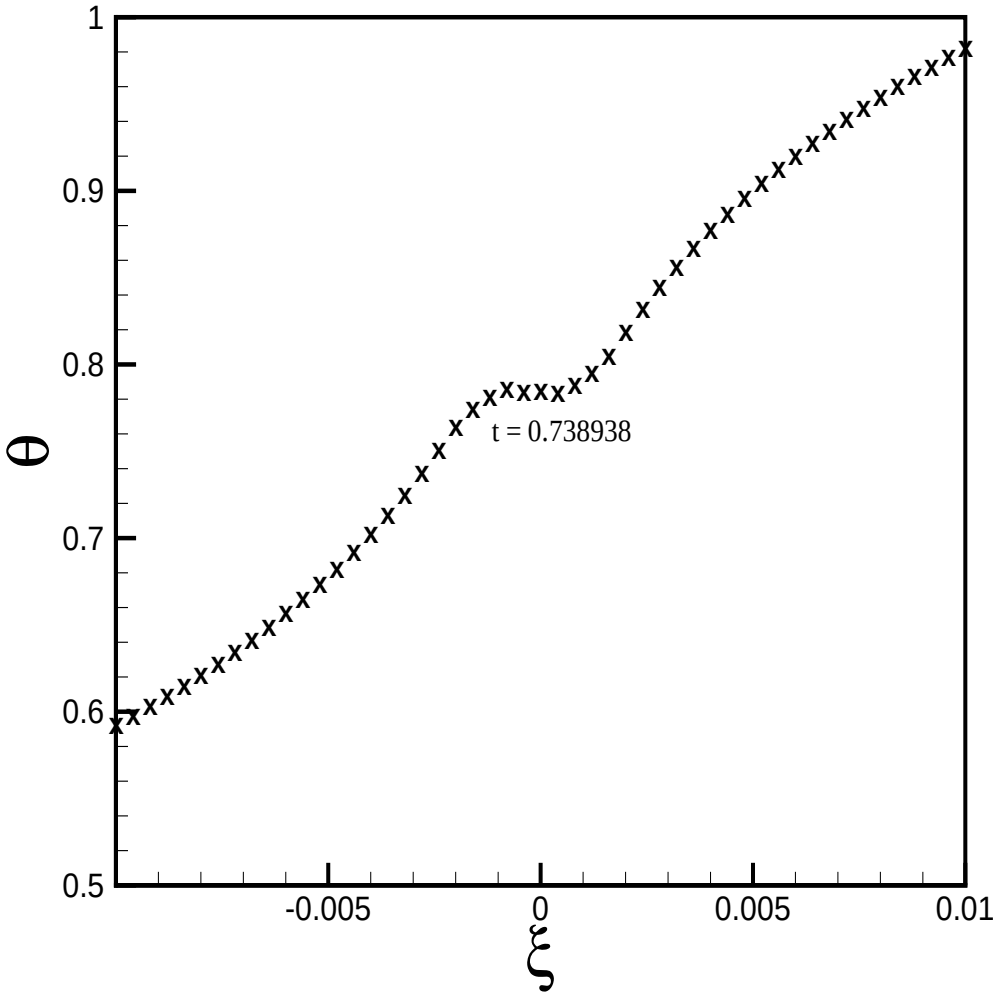

Fig. 6.5.12: *An enlarged* Θ *graph presented in Fig. 6.5.11d.*

the linear wavefront may be treated as a circle. The cause for the shock to tend to become a circle are the nonlinear waves on the shock, which move with the characteristic velocities (or eigenvalues) of the hyperbolic system (5.4.4) - (5.4.8). This tendency for the shock front is nothing but corrugation stability of a plane shock front (Monica and Prasad, 2001).

Some characteristic properties of the shock produced by a square piston have been shown graphically in Fig. 6.5.11 and Fig. 6.5.12. Fig. 6.5.11 does not give a good resolution of a very small constant regions at the original four corners, which has been shown by a graph Θ with ξ at $\xi = 0$ in Fig. 6.5.12. This corresponds to the constant region $C_2(m_i, \frac{\pi}{4})$ in Fig 6.5.2. Fig 6.5.11d shows that the value of G is very large in a small neighbourhood of $\xi = 0$, which implies that a very small neighbourhood of $\xi = 0$ where Θ is constant gets mapped onto a straight part of the shock as seen in Fig. 6.5.10, where the circle deviates a little from the shock front. Such a deviation would disappear at $t = 1.6$.

§6.6 Shock Produced by a Wavy Piston

Interesting results on the propagation of a shock initially in a periodic shape have been discussed by Monica and Prasad (2001). In this section, we shall present only two results but before we do that, we give an extension of the result (6.5.4). Consider the initial position of a nonlinear wavefront, which consists of two infinite straight parts meeting at a point. Let (m, θ) on the lower part be $(m_0, 0)$ and that on the upper part be (m_0, θ_r) with $0 < \theta_r < \pi$. The extension of the result (6.5.4) is the existence of a critical number m_c:

$$m_c = 1 + \frac{\theta_r}{32}, \tag{6.6.1}$$

such that if $m_0 > m_c$, the solution of the Riemann problem for equations (6.3.1) - (6.3.3) with initial condition $(m, \theta) = (m_0, 0)$ for $\xi < 0$ and $(m, \theta) = (m_0, \theta_r)$ for $\xi > 0$ exists and is unique. m_c increases monotonically from 0 to $\pi^2/32 = 0.3084$ as θ varies from 0 to π.

Consider now a piston whose shape is in the form of a periodic curve which is formed by periodically extending in y-direction a finite wedge given by

$$x = \begin{cases} x_0 + y \tan\Theta_0, & -x_0 \cot\Theta_0 < y < 0 \\ x_0 - y \tan\Theta_0, & 0 < y < x_0 \cot\Theta_0, \end{cases} \tag{6.6.2}$$

where Θ_0 is a constant, $0 < \Theta_0 < \pi/2$. We choose ξ to be arc length along the piston measured from the corner $(x_0, 0)$ of the piston. Then, the corners of the piston above $(x_0, 0)$ in one period are at $(0, x_0 \cos\Theta_0)$ and $(x_0, 2x_0 \cos\Theta_0)$ and correspond to $\xi = x_0(1 + \cos^2\Theta_0)^{1/2} = \xi_1$ say, and $\xi = 2\xi_1 = \xi_2$ say. Similarly the corners of the piston below $(x_0, 0)$ in the lower period are at $(0, -x_0 \cos\Theta_0)$ and $(x_0, 2x_0 \cos\Theta_0)$ and correspond to $-\xi_1$ and ξ_2.

The shock front produced by the piston, will initially coincide with the piston so that the change in the angle of the normal at the corner $(x_0, 0)$ is $2\Theta_0$. Therefore, the value of M_0 the constant Mach number of the shock given by (6.2.4) should satisfy $M_0 > 1 + \Theta_0^2/8$ by (6.6.1).

The angle between the normal to the shock front and the x-axis Θ is initially given by

$$\Theta(\xi, 0) = \begin{cases} \Theta_0 & , \quad \text{if } -\xi_2 < \xi \le -\xi_1 \\ -\Theta_0 & , \quad \text{if } -\xi_1 < \xi \le 0 \\ \Theta_0 & , \quad \text{if } 0 < \xi \le \xi_1 \\ -\Theta_0 & , \quad \text{if } \xi_1 < \xi \le \xi_2 \end{cases} \tag{6.6.3}$$

and periodically extended for $\xi < -\xi_2$ and $\xi > \xi_2$.

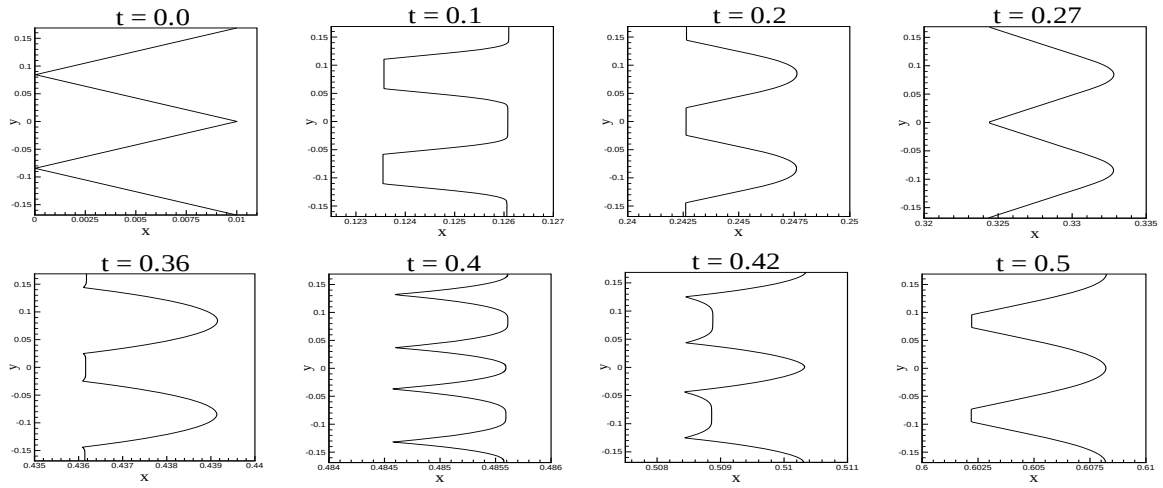

6.6.1: *Successive positions of a periodic shock front using SRT.*

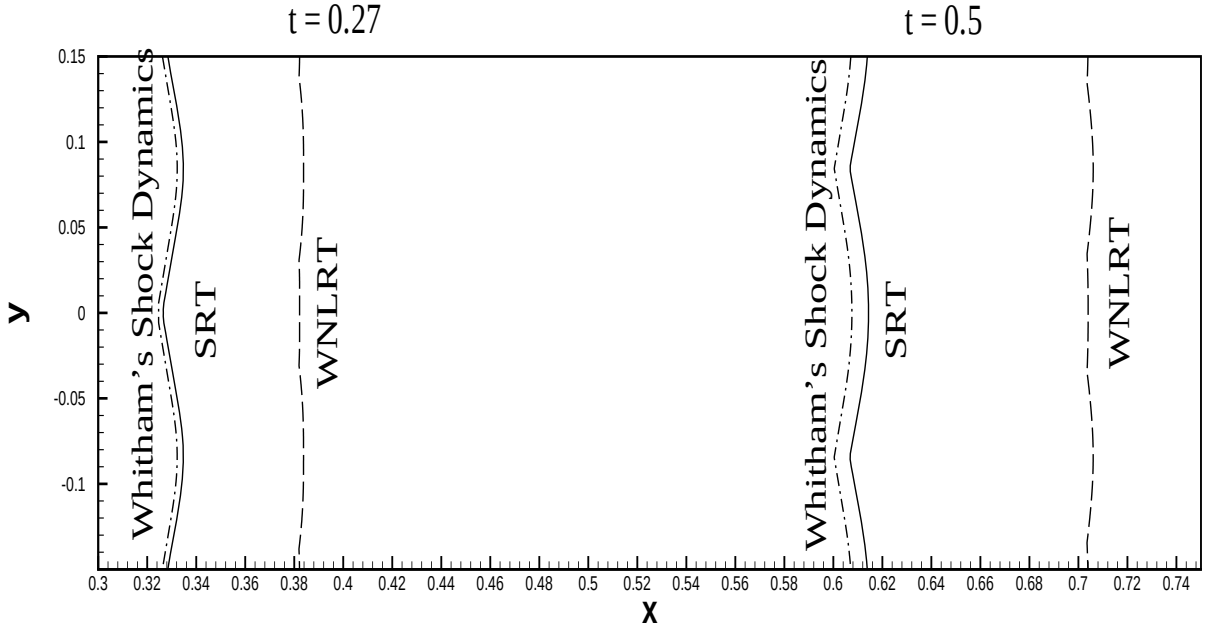

6.6.2: *Comparison of results in the case of a periodic shock front.*

The above initial condition corresponds to three Riemann problems for the non-homogeneous system (5.4.9)-(5.4.12) in the intervals

1. $(-\xi_2, -\xi_1)$ and $(-\xi_1, 0)$,
2. $(-\xi_1, 0)$ and $(0, \xi_1)$,
3. $(0, \xi_1)$ and (ξ_1, ξ_2).

The solution of the non-homogeneous system (5.4.9)-(5.4.12) for small time approximates the solution of the corresponding system of four conservation laws obtained from the system by omitting the source terms in (5.4.11) and (5.4.12). To the reduced system, analysis of Baskar and Prasad (2002) of the Riemann problem for the KCL would apply.

Later on, the centered waves, which emerge out of the reduced equations as shown in Fig. 6.5.2, would get modified by the source terms and waves from other periods would come and interact. This would result in corrugational stability leading to the formation of a smooth shock front at a large time (Monica and Prasad, 2001). From the corners in the center of the convex parts (such as that at $\xi = 0$) two centered rarefaction waves would emerge. Similarly, from the corners in the concave parts (such as those at $-\xi_1$ and ξ_1), two shocks emerge. Later on they go through multiple interactions leading to complex shapes of the shock as the time t increases as shown in Fig. 6.6.1.

In fig. 6.6.2, we have shown the comparison between the GSD, SRT and the WNLRT. As observed in the previous cases, the shock front from GSD remains behind and the wavefront from WNLRT travels ahead of the shock front from SRT. From the comparison results with Euler equations of the previous sections, we see that NSEE and SRT would be close so that although qualitatively the shape of the shock front from GSD is same, the shock position remains behind the shock from SRT and therefore from full gas dynamics equations. It is also observed that when we increase the acceleration of the piston, the shock front from SRT comes closer to the wavefront obtained from WNLRT and hence travels much ahead of GSD.

Conclusion

We have derived a new set of conservation form of the first two compatibility conditions of SRT for a weak shock. These conservation forms are more natural and follow a pattern which can be easily extended for each one of the infinite set of compatibility conditions for a weak shock. Hence it is possible to write conservation form of higher order SRT with three or more compatibility conditions. We have carried out intensive numerical calculation and found that:

(i) SRT gives results which agrees very well with NSEE compared to the agreement of results of GSD with those obtained by NSEE.

(ii) The results of SRT show that nonlinear waves on the shock front helps a non-circular shock to evolve into a circular one quite rapidly.

(iii) We theoretically show that there are limitations on the applicability of WNLRT, GSD and SRT to a piston problem when the piston has a corner making an obtuse angle to the flow: it may move with a small velocity to produce a weak shock but its velocity should not be too small.

(iv) The difference in the solution of GSD and NSEE may become more significant for a strong shock with large values of V. The SRT for a strong shock has been just formulated (Prasad, 2003) and we hope to make such comparison in near future.

The comparison and limitations discussed in this chapter are very important. GSD and SRT with kinematical conservation laws (KCL) are now very powerful theories to solve many practical problems and they also take considerably less time compared to NSEE. As mentioned in the introduction, attempts have been made to discuss some finer limiting results of the shape of a shock front by GSD. Such results are acceptable only if it can be shown that the error between the GSD results and the solution (not numerical but exact) of the Euler's equations are much smaller than those involved in the finer structures. What we see from the comparison of the results is, that GSD will certainly fail in the case of many limiting results. One may use SRT with caution or probably higher order SRT.

Chapter 7

A Note on Application of Shock Ray Theory to Sonic Boom

§7.1 Introduction

When an aircraft moves in supersonic speed, two conical shock surfaces extending behind the aircraft nose and tail are generated. The region between the two conical surfaces is the entire region of pressure disturbance at a given instant. This pressure disturbance propagates from the aircraft to the ground. The wave starting from the nose will give rise to a sudden pressure jump in the atmosphere which decreases linearly till it reaches the tail (or rear) wave. A sudden recompression takes place at the tail wave and the pressure will be restored to its normal value. Generally, the strength of the nose and tail shocks are same and we get an N-shaped wave which is commonly known as *N-wave* far from the body. An observer on the ground will recognize this pressure variation like a boom, which is called as *sonic boom*. This undesirable effect of supersonic flight are regarded as a society problem.

Sonic boom analysis is generally divided into three parts, namely, generation, propagation and evolution.

A supersonic aircraft generates several (a one parameter family of) wavefronts in between the bow (nose) and the rear (tail) shock front, which causes pressure disturbance in the atmosphere. For slender vehicles or projectiles, this disturbance soon after the generation, called as near field disturbance, is governed by linearized supersonic flow theory (W. D. Hayes, 1947) and it was studied using supersonic area rule methods (R. T. Whitcomb and T. L. Fischetti, 1953). In this near field, the disturbance is sufficiently weak and it behaves according to the acoustic (linear) approximation. For blunt bodies

(e.g. Space Shuttle Orbiter) the aerodynamic flow is inherently nonlinear, and the near field is more complex than slender body (linear) theory mentioned above.

The disturbance generated by the supersonic aircraft propagates to the ground through the real atmosphere and this propagation has been computed by the method of geometrical acoustics developed by Blokhintzev (1946). Because the basic acoustic propagation follows the rules of geometrical acoustics, it is possible for waves to converge and focus.

Although the signature shape produced by the vehicle is weak, it evolves as it propagates from the near field to the far field and the nonlinear effects plays role. Due to this nonlinear effect, the signature develops shocks at the far-field and become an N-wave. The procedure for computing the formation of shock was developed by Whitham (1952, 1956), and is considered as a fundamental theory of sonic booms. In this theory, first the amplitude is calculated by linear theory using linear rays and nonlinear effect is incorporated by Whitham's nonlinearization technique.

Hayes, Haefeli and Kulsrud (1969) has implemented the fundamental theory of sonic boom which is referred as ARAP program. The program begins with an Whitham's F-function (see Whitham, 1974) source and implements a formulation of ray tracing analytically derived from Fermat's principle. The next worth noticing program was due to Thomas (1972). Thomas computed ray paths by direct numerical integration of the Eikonal equation and applied Whitham's rule via the analytic waveform parameter method, whereas Hayes et al. (1969) derived the ray paths analytically using Fermat's principle and applied Whitham's rule via the concept of an age parameter. The above mentioned implementation of fundamental theory are the most commonly used programs till now for arbitrarily maneuvering aircraft in arbitrary horizontally stratified atmospheres with wind.

One of the advanced phenomena in sonic boom is the focused boom (Plotkin, 2002). The linear rays from the nose (for instance) of an accelerating aircraft for different instance of time tend to converge since the Mach angle decreases as the Mach number increases and thus form a caustic (or a focus line) which is the envelop of the rays as shown in Fig. 7.1.1. The solution calculated from the linear theory becomes singular in the caustic region. But, from extensive flight tests (J. C. L. Wanner, et. al., 1972), it has been observed that the nonlinear effect and the diffraction cause the maximum focus amplitude to be finite and due to diffraction effect, we get a U-shaped wave with the shocks peaked. Gill and Seebass (1975) obtained a numerical solution for focus at a caustic. The only code available today for calculating full sonic boom signature solution at foci is PCBoom3 due to Plotkin (1998), which uses Guiraud's scaling law to extend the Thomas code to apply Gill and Seebass (1975) approximate solution at focal zones.

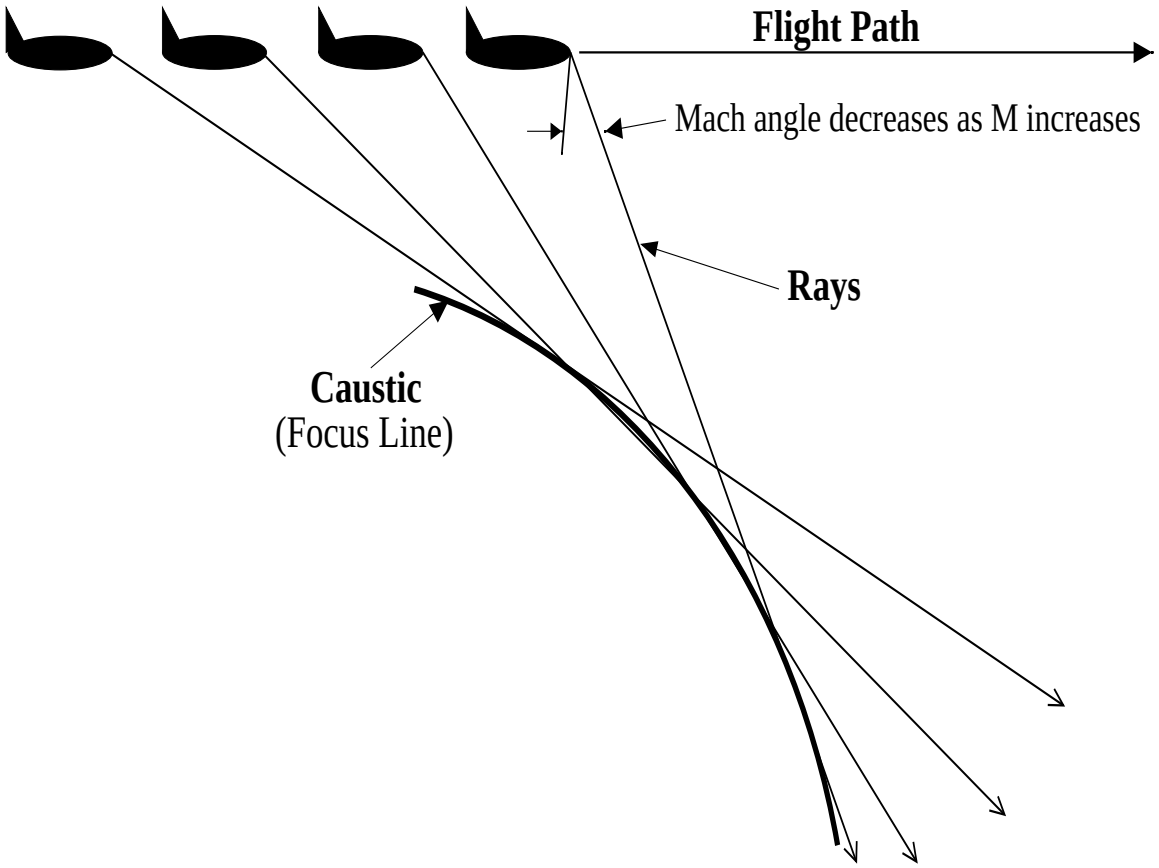

Fig 7.1.1: Formation of caustic from an accelerating aircraft.

Shock ray theory (SRT) developed by Prasad (1982, 2001) discussed in chapter 5, is well suited for studying the propagation of the shock front emerging from the nose and the tail of an accelerating aircraft, as it is evident from the results discussed in the chapter 6. But, to get the full sonic boom signature in the far-field, we need to calculate the wavefronts in between the bow and the rear shocks, which can be obtained using weakly nonlinear ray theory (WNLRT) discussed in Section 1.4. For this procedure of obtaining the pressure signature, we need appropriate initial and boundary conditions both for the shock fronts and the wavefronts. In this chapter, we explain the physical problem which we are interested in. The formulation of the problem which involves the derivation of the initial conditions for calculating the leading and rear shock front using SRT will be pursued in future. Once the correct initial conditions are obtained, the system of conservation laws (5.4.9) - (5.4.12) for SRT discussed in chapter 5 can be solved numerically. Calculation of the wavefronts in between the leading and the rear shock fronts and the calculation of the full sonic boom signature are more advanced as they involve careful mathematical formulation which properly balance the two theories (SRT and WNLRT) in the calculation as well as the boundary conditions. This work will also be pursued in future.

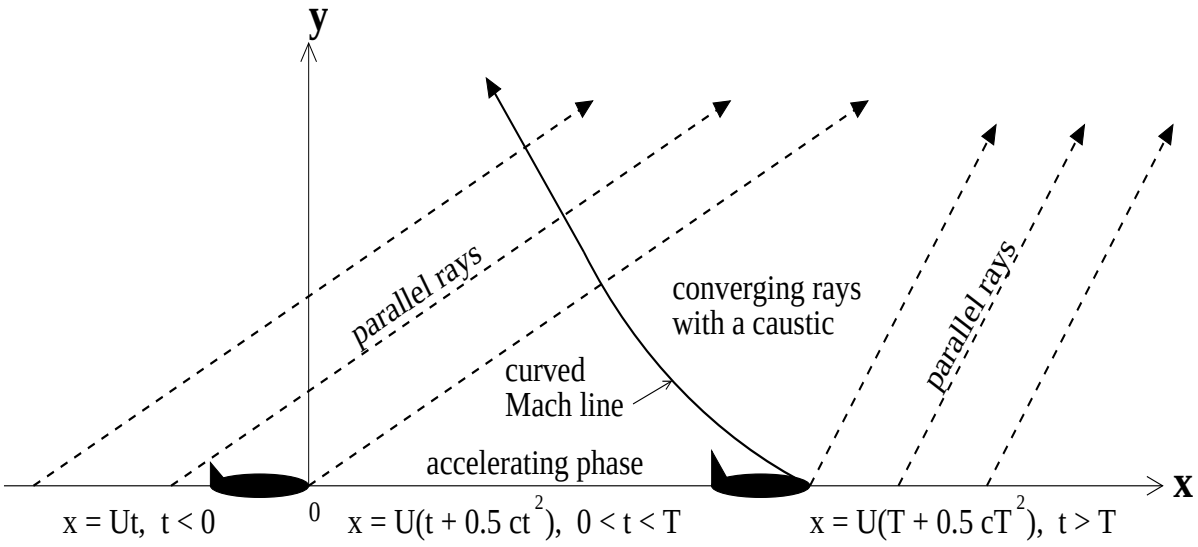

Fig. 7.2.1: Physical model.

§7.2 **Physical Problem**

Consider a two-dimensional thin aerofoil of length d and thickness b such that

$$\epsilon = \frac{b}{d} \ll 1 \tag{7.2.1}$$

which moves with steady supersonic velocity U (constant) till the time $t = t_0$, then it accelerates in the interval $t_0 < t < t_1$ and from $t > t_1$ it again starts moving with the constant velocity. Without loss of generality, we assume $t_0 = 0$. We take the x-axis along the path of the aircraft and the y-axis to be vertically upward. Let the upper part of the aerofoil at $t = 0$ be given by

$$y = b_u(x), \quad -d \leq x \leq 0 \tag{7.2.2}$$

and the position s of the front edge of the aerofoil be given by

$$\boldsymbol{u}(x,0) = \begin{cases} Ut, & t \leq 0 \\ U\left(t + \frac{1}{2}At^2\right), & 0 < t < t_1 \\ U\left(t_1 + \frac{1}{2}At_1^2\right), & t \geq t_1 \end{cases} \tag{7.2.3}$$

where the acceleration $A = AU$ is taken to be a function of time.

Since the aircraft moves with constant velocity in the intervals $t < 0$ and $t > t_1$, the rays emerging from these intervals are parallel to each other in the corresponding domain in (x, y)-plane. The slope of the rays starting from the interval $x < 0$ are less than those of the rays from the interval $x > Ut_1 + \frac{1}{2}At_1^2$. The slope of rays from $0 < x < Ut_1 + \frac{1}{2}At_1^2$ continuously increases. Thus, the slope of the rays increases continuously as shown in Fig. 7.2.1. Hence, if the rays under consideration are linear, then they tend to converge and form a caustic beyond which the linear theory ceases to be valid.

Appendix 1

§0.1 Discontinuous Galerkin Method in One Space Dimension

In this section, we discuss in details, the discontinuous Galerkin finite element method for solving conservation laws, following Cockburn et. al. (1989).

Let Ω be an open subset of $\mathbb{R}^n$. Consider a system of hyperbolic conservation laws

$$\boldsymbol{u}_t + \boldsymbol{f}(\boldsymbol{u})_x = 0,\ x \in \mathbb{R}, t > 0, \tag{0.1.1}$$

where $\boldsymbol{u} = (u_1, ..., u_n)^T \in \Omega$ and $\boldsymbol{f} : \Omega \to \mathbb{R}^n$ is a smooth function, together with an initial condition

$$\boldsymbol{u}(x, 0) = \mathbf{u}_0(x) \tag{0.1.2}$$

for some $\boldsymbol{u}_0 \in \Omega$. We shall first discretize in the spatial variable x. Let

1. $I_j := (x_{j-1/2}, x_{j+1/2})$, $I = \cup_j I_j$ be a partition of the real line,
2. $\Delta x_j := x_{j+1/2} - x_{j-1/2}$, $h := \sup_j \Delta x_j$.

The finite element method which we are going to use is a Galerkin method for which

$$\boldsymbol{V}_h^k := \left\{ \boldsymbol{p} \in (BV \cap L^1)^n / \text{each component of } \boldsymbol{p}|_{I_j} \in P^k(I_j) \right\}, \tag{0.1.3}$$

where $P^k(I_j)$ is the space of polynomials of degree $\leq k$ on I_j. Since V_h^k contains the functions that are allowed to have jumps at the interfaces $x_{j+1/2}$, this method is called a *discontinuous Galerkin method*.

We choose the Legendre polynomials over I_j as a local orthogonal basis over I_j given by

$$v_0^{(j)}(x) = 1, v_1^{(j)}(x) = x - x_j, v_2^{(j)}(x) = (x - x_j)^2 - \frac{1}{12}\Delta x_j^2, ... \tag{0.1.4}$$

satisfying

$$\int_{I_j} v_l(x) v_k(x) dx = 0, \text{ for all } l \neq k. \tag{0.1.5}$$

We define the approximation $\boldsymbol{u}^h(x,t)$ to the solution $\boldsymbol{u}(x,t)$ of the IVP (0.1.1)-(0.1.2) in V_h^k as

$$\boldsymbol{u}^h(x,t) = \sum_{l=0}^{k} a_l \boldsymbol{u}_j^{(l)}(t) v_l^{(j)}(x),\ x \in I_j, \tag{0.1.6}$$

where we define the degree of freedom as

$$\boldsymbol{u}_j^{(l)} = \boldsymbol{u}_j^{(l)}(t) = \frac{1}{\Delta x_j^{l+1}} \int_{I_j} \boldsymbol{u}(x,t) v_l^{(j)}(x) dx, \quad l = 0, 1, ..., k \tag{0.1.7}$$

and the coefficients are defined as

$$a_l = \frac{\Delta x_j^{l+1}}{\int_{I_j} (v_l^{(j)}(x))^2 dx}, \quad l = 0, 1, ..., k. \tag{0.1.8}$$

Note that $a_0 = 1$, $a_1 = \frac{12}{\Delta x_j}$, $a_2 = \frac{180}{\Delta x_j^2}$ and so on.

From (0.1.6), we can see that if the degrees of freedom $\boldsymbol{u}_j^{(l)}$ are determined, then the approximate solution $\boldsymbol{u}^h$ can be determined. Multiplying (0.1.1) by $v \in P^k(I_j)$, integrating over I_j, and replacing the exact solution $\boldsymbol{u}$ by its approximation $\boldsymbol{u}^h$, we get

$$\int_{I_j} (\boldsymbol{u}^h(x,t))_t v(x) dx + \int_{I_j} (\boldsymbol{f}(\boldsymbol{u}^h(x,t)))_x v(x) dx = 0, \text{ for all } v \in P^k(I_k).$$

Using integration by parts, we get

$$\begin{aligned} &\int_{I_j} (\boldsymbol{u}^h(x,t))_t v(x) dx + (\boldsymbol{f}(\boldsymbol{u}^h(x_{j+1/2},t)) v(x_{j+1/2}) - \boldsymbol{f}(\boldsymbol{u}^h(x_{j-1/2},t)) v(x_{j-1/2})) \\ - &\int_{I_j} \boldsymbol{f}(\boldsymbol{u}^h(x,t))(v(x))_x dx = 0, \text{ for all } v \in P^k(I_j). \end{aligned} \tag{0.1.9}$$

Since v_0, v_1, ...,$v_k \in P^k(I_j)$, (0.1.9) is true for these functions also. Hence, from (0.1.6), (0.1.9) and (0.1.5), we get for $v = v_0$,

$$\int_{I_j} (\boldsymbol{u}_j^{(0)}(t))_t dx + (\boldsymbol{f}(\boldsymbol{u}^h(x_{j+1/2},t)) v_0(x_{j+1/2}) - \boldsymbol{f}(\boldsymbol{u}^h(x_{j-1/2},t)) v_0(x_{j-1/2})) = 0$$

or

$$\Delta x_j \frac{d}{dt} \boldsymbol{u}_j^{(0)} + (\boldsymbol{f}(\boldsymbol{u}^h(x_{j+1/2},t)) - \boldsymbol{f}(\boldsymbol{u}^h(x_{j-1/2},t))) = 0.$$

Using some monotone flux (which we will choose later) $\boldsymbol{h}(.,.)$ in the place of $\boldsymbol{f}(.,.)$ with the consistency condition $\boldsymbol{h}(\boldsymbol{u},\boldsymbol{u}) = \boldsymbol{f}(\boldsymbol{u})$, we get

$$\frac{d}{dt} \boldsymbol{u}_j^{(0)} = -\frac{1}{\Delta x_j} [\boldsymbol{h}_{j+1/2} - \boldsymbol{h}_{j-1/2}]. \tag{0.1.10}$$

Here $\boldsymbol{h}_{j-1/2} = \boldsymbol{h}(\boldsymbol{u}_{j-1/2}^-, \boldsymbol{u}_{j-1/2}^+)$ with $\boldsymbol{u}_{j-1/2}^{\pm} = \boldsymbol{u}^h(x_{j-1/2}^{\pm}, t)$.

For $v = v_1$, we get

$$\int_{I_j} \left(\frac{12}{\Delta x_j} \boldsymbol{u}_j^{(1)}(t)(x - x_j) \right)_t (x - x_j)dx + (\boldsymbol{f}(\boldsymbol{u}^h(x_{j+1/2}, t))v_1(x_{j+1/2}) - \boldsymbol{f}(\boldsymbol{u}^h(x_{j-1/2}, t))v_1(x_{j-1/2})) - \int_{I_j} \boldsymbol{f}(\boldsymbol{u}^h(x, t))dx = 0.$$

This implies

$$\frac{12}{\Delta x_j} \frac{d}{dt} \boldsymbol{u}_j^{(1)}(t) \int_{I_j} (x - x_j)^2 dx + \left(\boldsymbol{f}(\boldsymbol{u}^h(x_{j+1/2}, t)) + \boldsymbol{f}(\boldsymbol{u}^h(x_{j-1/2}, t)) \right) \frac{\Delta x_j}{2} - \int_{I_j} \boldsymbol{f}(\boldsymbol{u}^h(x, t))dx = 0.$$

But

$$\int_{I_j} (x - x_j)^2 dx = \frac{\Delta x_j^3}{12}.$$

Therefore, we have

$$(\Delta x_j)^2 \frac{d}{dt} \boldsymbol{u}_j^{(1)}(t) + \left(\boldsymbol{f}(\boldsymbol{u}^h(x_{j+1/2}, t)) + \boldsymbol{f}(\boldsymbol{u}^h(x_{j-1/2}, t)) \right) \frac{\Delta x_j}{2} - \int_{I_j} \boldsymbol{f}(\boldsymbol{u}^h(x, t))dx = 0.$$

Replacing the flux $\boldsymbol{f}$ by the monotone flux $\boldsymbol{h}$ chosen above, we get

$$\frac{d}{dt} \boldsymbol{u}_j^{(1)} = -\frac{1}{2\Delta x_j} (\boldsymbol{h}_{j+1/2} + \boldsymbol{h}_{j-1/2}) + \frac{1}{\Delta x_j^2} \int_{I_j} \boldsymbol{f}(\boldsymbol{u}^h(x, t))dx \tag{0.1.11}$$

and so on. The integration in (0.1.9) can be approximated by a suitable quadrature (see Cockburn, et. al. 1989). For $k = 1$ Simpson's rule can be used.

Note that, for

1. $k = 0$ (First Order), $\boldsymbol{u}_{j+1/2}^- = \boldsymbol{u}_{j-1/2}^+ = \boldsymbol{u}_j^{(0)}$ (which is the cell average of $\boldsymbol{u}$ in I_j).
2. $k = 1$ (Second Order), $\boldsymbol{u}_{j+1/2}^- = \boldsymbol{u}_j^{(0)} + 6\boldsymbol{u}_j^{(1)}$, $\boldsymbol{u}_{j-1/2}^+ = \boldsymbol{u}_j^{(0)} - 6\boldsymbol{u}_j^{(1)}$,

and so on. Here we note that, for $k = 0$, if we use the Euler forward time marching method, then the present scheme reduces to the famous MUSCL type finite difference scheme by Osher (1985).

To achieve total variation stability, we need to modify $\boldsymbol{u}_{j+1/2}^{\pm}$ by some local projection limiter which we will do as follows: We write

$$\boldsymbol{u}_{j+1/2}^- = \boldsymbol{u}_j^{(0)} + \tilde{\boldsymbol{u}}_j, \quad \boldsymbol{u}_{j-1/2}^+ = \boldsymbol{u}_j^{(0)} - \tilde{\tilde{\boldsymbol{u}}}_j, \tag{0.1.12}$$

where from (0.1.6), we get

$$\tilde{\boldsymbol{u}}_j = \sum_{l=1}^{k} a_l \boldsymbol{u}_j^{(l)} v_l^{(j)}(x_{j+1/2}), \quad \tilde{\tilde{\boldsymbol{u}}}_j = \sum_{l=1}^{k} a_l \boldsymbol{u}_j^{(l)} v_l^{(j)}(x_{j-1/2}). \tag{0.1.13}$$

Thus, we have

1. For $k = 0$, $\tilde{\boldsymbol{u}}_j = \tilde{\tilde{\boldsymbol{u}}}_j = 0$.
2. For $k = 1$, $\tilde{\boldsymbol{u}}_j = \tilde{\tilde{\boldsymbol{u}}}_j = 6\boldsymbol{u}_j^{(1)}$ and so on.

To achieve total variation diminishing (TVD) property, we define

$$\tilde{\boldsymbol{u}}_j^{(mod)} = \boldsymbol{m}(\tilde{\boldsymbol{u}}_j, \Delta_+ \tilde{\boldsymbol{u}}_j^{(0)}, \Delta_- \tilde{\boldsymbol{u}}_j^{(0)}), \tag{0.1.14}$$

$$\tilde{\tilde{\boldsymbol{u}}}_j^{(mod)} = \boldsymbol{m}(\tilde{\tilde{\boldsymbol{u}}}_j, \Delta_+ \tilde{\boldsymbol{u}}_j^{(0)}, \Delta_- \tilde{\boldsymbol{u}}_j^{(0)}), \tag{0.1.15}$$

where $\boldsymbol{m}$ is a vector minmod function for TVD correction:

$$\boldsymbol{m}(\boldsymbol{a}_1, \boldsymbol{a}_2, ..., \boldsymbol{a}_n) = \begin{pmatrix} m(a_{11}, a_{21}, ..., a_{n1}) \\ ... \\ ... \\ ... \\ m(a_{1m}, a_{2m}, ..., a_{nm}) \end{pmatrix} \tag{0.1.16}$$

where $\boldsymbol{a}_i = (a_{i1}, a_{i2}, ..., a_{im})^T$ and

$$m(b_1, b_2, ..., b_n) = \begin{cases} s \min_{1 \le i \le n} |b_i|, & \text{if } sgn(b_1) = ... = sgn(b_n) = s \\ 0 & \text{otherwise.} \end{cases} \tag{0.1.17}$$

We use the local Lax-Friedrichs flux

$$\boldsymbol{h}_{j+1/2} = \frac{1}{2}[\boldsymbol{f}(\boldsymbol{u}_{j+1/2}^-) + \boldsymbol{f}(\boldsymbol{u}_{j+1/2}^+) - \alpha_{j+1/2}(\boldsymbol{u}_{j+1/2}^+ - \boldsymbol{u}_{j+1/2}^-)] \tag{0.1.18}$$

with

$$\alpha_{j+1/2} = \max_{1 \le p \le m} \left(|\lambda_{j+1/2}^{(p)+}|, |\lambda_{j+1/2}^{(p)-}| \right) \text{[local Lax-Friedrichs]} \tag{0.1.19}$$

or

$$\alpha_{j+1/2} = \max_{j,p} \left(|\lambda_{j+1/2}^{(p)\pm}| \right) \text{[Lax-Friedrichs]}, \tag{0.1.20}$$

where $\lambda_{j+1/2}^{(p)+}$, $p = 1, 2, ..., m$ are the m real eigenvalues of the Jacobian of the flux vector $\boldsymbol{f}$.

Finally, for time discretization we use TVD Runge-Kutta type method which is given below.

We first rewrite (0.1.9) in a concise ODE form,

$$\frac{d}{dt}\boldsymbol{u}^h = \boldsymbol{L}_h(\boldsymbol{u}^h, t),$$

and apply the high-order TVD Runge-Kutta methods

$$(\boldsymbol{u}^h)^{(i)} = \sum_{l=0}^{i-1} \left[\beta_{il}(\boldsymbol{u}^h)^{(l)} + \gamma_{il}\Delta t \boldsymbol{L}_h((\boldsymbol{u}^h)^{(l)}, t^n)\right],\ i = 1, 2, ..., r, \tag{0.1.21}$$

$$(\boldsymbol{u}^h)^{(0)} = (\boldsymbol{u}^h)^n, (\boldsymbol{u}^h)^{(r)} = (\boldsymbol{u}^h)^{n+1}, \tag{0.1.22}$$

where for second order accuracy, i.e., $r = 2$, the coefficients are given by

$$\beta_{10} = \gamma_{10} = 1, \quad \beta_{20} = \beta_{21} = \gamma_{21} = 0.5, \quad \gamma_{20} = 0, \quad \text{CFL} = 1. \tag{0.1.23}$$

We will now apply the above TVD Runge-Kutta method (0.1.21)-(0.1.23) to the ODE's (0.1.10)-(0.1.11).

First, let $k = 0$. Then the scheme becomes first order i.e., $r = 1$. Thus, we have from (0.1.6),

$$\boldsymbol{u}^h(x, t) = \boldsymbol{u}_j^{(0)}(t).$$

From (0.1.10),(0.1.21)-(0.1.23), we have

$$(\boldsymbol{u}^h(x,t))^{n+1} = (\boldsymbol{u}_j^{(0)})^{n+1} = (\boldsymbol{u}_j^{(0)})^n - \frac{\Delta t_n}{\Delta x_j}[\boldsymbol{h}_{j+1/2}^n - \boldsymbol{h}_{j-1/2}^n], \tag{0.1.24}$$

where $\boldsymbol{h}_{j+1/2}^n$ denotes $\boldsymbol{h}$ evaluated at $(\boldsymbol{u}_j^{(0)})^{(0)} = (\boldsymbol{u}_j^{(0)})^n$.

For $k = 1$, the scheme becomes second order and therefore $r = 2$. Thus from (0.1.6), we have

$$\boldsymbol{u}^h(x, t) = \boldsymbol{u}_j^{(0)}(t) + \frac{12}{\Delta x_j}(x - x_j)\boldsymbol{u}_j^{(1)}(t).$$

From (0.1.10),(0.1.21)-(0.1.23), we get

$$(\boldsymbol{u}_j^{(0)})^{(1)} = (\boldsymbol{u}_j^{(0)})^n - \frac{\Delta t_n}{\Delta x_j}[\boldsymbol{h}_{j+1/2}^n - \boldsymbol{h}_{j-1/2}^n], \tag{0.1.25}$$

$$(\boldsymbol{u}_j^{(1)})^{(1)} = (\boldsymbol{u}_j^{(1)})^n - \frac{\Delta t_n}{2\Delta x_j}[\boldsymbol{h}_{j+1/2}^n + \boldsymbol{h}_{j-1/2}^n] + \frac{\Delta t_n}{\Delta x_j^2}\int_{I_j}(\boldsymbol{f}(\boldsymbol{u}^h(x,t)))^n dx, \tag{0.1.26}$$

$$(\boldsymbol{u}^h)^{(1)} = (\boldsymbol{u}_j^{(0)})^{(1)} + \frac{12}{\Delta x_j}(\boldsymbol{u}_j^{(1)})^{(1)}(x - x_j). \tag{0.1.27}$$

Similarly, we have

$$(\boldsymbol{u}_j^{(0)})^{(2)} = \frac{1}{2}\left[(\boldsymbol{u}_j^{(0)})^n + (\boldsymbol{u}_j^{(0)})^{(1)} - \frac{\Delta t_n}{\Delta x_j}[\boldsymbol{h}_{j+1/2}^{(1)} - \boldsymbol{h}_{j-1/2}^{(1)}]\right], \tag{0.1.28}$$

$$(\boldsymbol{u}_j^{(1)})^{(2)} = \frac{1}{2}\left[(\boldsymbol{u}_j^{(1)})^n + (\boldsymbol{u}_j^{(1)})^{(1)} - \frac{\Delta t_n}{2\Delta x_j}[\boldsymbol{h}_{j+1/2}^{(1)} + \boldsymbol{h}_{j-1/2}^{(1)}] + \frac{\Delta t_n}{\Delta x_j^2}\int_{I_j}(\boldsymbol{f}(\boldsymbol{u}^h(x,t)))^{(1)}dx\right], \tag{0.1.29}$$

$$(\boldsymbol{u}^h)^{n+1} = (\boldsymbol{u}^h)^{(2)} = (\boldsymbol{u}_j^{(0)})^{(2)} + \frac{12}{\Delta x_j}(\boldsymbol{u}_j^{(2)})^{(1)}(x - x_j). \tag{0.1.30}$$

The above scheme is applied componentwise. Unfortunately, this scheme do show wriggles. To avoid this, we need to apply the scheme characteristicwise which we will do now.

STEP: 1 Let

$$\boldsymbol{u}_{j+1/2} = \frac{\boldsymbol{u}_j^{(0)} + \boldsymbol{u}_{j+1}^{(0)}}{2}. \tag{0.1.31}$$

Let $\lambda_{j+1/2}^{(p)}$, $\boldsymbol{l}_{j+1/2}^{(p)}$, $\boldsymbol{r}_{j+1/2}^{(p)}$ are the eigenvalues, left and right eigenvectors respectively of the pth characteristic field evaluated at $\boldsymbol{u}_{j+1/2}$. We normalize the left eigenvector in such a way that

$$\boldsymbol{l}_{j+1/2}^{(p)} \cdot \boldsymbol{r}_{j+1/2}^{(p)} = \delta_{pq}.$$

STEP: 2 We first project everything to the eigenspace of the Jacobian of the flux vector, which we represent as $A_{j+1/2}$ using the transformation

$$a^{(p)} = \boldsymbol{l}_{j+1/2}^{(p)} \cdot \boldsymbol{a}, \tag{0.1.32}$$

where we take $\boldsymbol{a} = \tilde{\boldsymbol{u}}_j$, $\tilde{\tilde{\boldsymbol{u}}}_{j+1}$, $\boldsymbol{u}_j^{(0)}$, $\boldsymbol{u}_{j+1}^{(0)}$, $\Delta_-\boldsymbol{u}_j^{(0)}$, $\Delta_+\boldsymbol{u}_j^{(0)}$, $\Delta_+\boldsymbol{u}_{j+1}^{(0)}$.

STEP: 3 We then apply the local projection limiting in each characteristic field:

$$(\tilde{u}_j)^{(p)(mod)} = m(\tilde{u}_j)^{(p)}, (\Delta_+ u_j^{(0)})^{(p)}, (\Delta_- u_j^{(0)})^{(p)}), \tag{0.1.33}$$

$$(\tilde{\tilde{u}}_{j+1})^{(p)(mod)} = m(\tilde{\tilde{u}}_{j+1})^{(p)}, (\Delta_+ u_{j+1}^{(0)})^{(p)}, (\Delta_- u_{j+1}^{(0)})^{(p)}), \tag{0.1.34}$$

and form

$$(u_{j+1/2}^-)^{(p)} = (u_j^{(0)})^{(p)} + (\tilde{u}_j)^{(p)(mod)}, \quad (u_{j+1/2}^+)^{(p)} = (u_j^{(0)})^{(p)} - (\tilde{\tilde{u}}_{j+1})^{(p)(mod)}. \tag{0.1.35}$$

Hence we got $\boldsymbol{u}$ characteristicwise.

STEP: 4 We use the transformation

$$\boldsymbol{a} = \sum_{p=1}^{m} a^{(p)} \boldsymbol{r}^{(p)}_{j+1/2}, \tag{0.1.36}$$

and get $\boldsymbol{a} = \boldsymbol{u}^{\pm}_{j+1/2}$ componentwise, and then compute $\boldsymbol{f}^{\pm}_{j+1/2} = \boldsymbol{f}(\boldsymbol{u}^{\pm}_{j+1/2})$.

STEP: 5 Use step: 2 to convert $\boldsymbol{f}^{\pm}_{j+1/2}$ characteristicwise and hence get $(f^{\pm}_{j+1/2})^{(p)}$.

STEP: 6 Use any scalar monotone flux in the pth characteristic field, $p = 1, 2, ..., m$. For example, we may use the local Lax-Friedrichs flux

$$h^{(p)}_{j+1/2} = \frac{1}{2}\left[(f^{+}_{j+1/2})^{(p)} + (f^{-}_{j+1/2})^{(p)} - \alpha^{(p)}_{j+1/2}((u^{+}_{j+1/2})^{(p)} - u^{-}_{j+1/2})^{(p)})\right] \tag{0.1.37}$$

with

$$\alpha^{(p)}_{j+1/2} = \max(|\lambda^{(p)}_{j}|, |\lambda^{(p)}_{j+1}|). \tag{0.1.38}$$

STEP: 7 We finally get $\boldsymbol{h}_{j+1/2}$ using Step: 4 with $\boldsymbol{a} = \boldsymbol{h}_{j+1/2}$.

§0.2 Multi-Dimensional Case: Dimensional Splitting Method

In this section we are concerned with the numerical methods for solving nonlinear systems of hyperbolic conservation laws in multidimensions. For the sake of simplicity we consider the equation in two space dimension given by

$$\boldsymbol{u}_t + \boldsymbol{f}(\boldsymbol{u})_x + \boldsymbol{g}(\boldsymbol{u})_y = 0, \ x, y \in I\!R, t > 0, \tag{0.2.1}$$

where $\boldsymbol{f}$ and $\boldsymbol{g}$ are vectors of fluxes in the x and y directions respectively. There are at least two commonly used ways to solve (0.2.1) numerically, namely, *dimensional splitting method* and *finite volume method*. The dimensional splitting method (also called as *fractional step method*) is a simple extension of the one-dimensional method which we will introduce now.

Consider the two dimensional nonlinear system (0.2.1) together with the initial condition

$$\boldsymbol{u}(x, y, t^n) = \boldsymbol{u}^n, \tag{0.2.2}$$

where the initial data at a time t^n is given by the set $\boldsymbol{u}^n$ of discrete cell values $(\boldsymbol{u}^i_j)^n$.

The dimensional splitting approach replaces (0.2.1)-(0.2.2) by a pair of one-dimensional initial value problems as given below:

$$\left.\begin{array}{l} \boldsymbol{u}_t + \boldsymbol{f}(\boldsymbol{u})_x = 0 \\ \boldsymbol{u}(., y_j, t^n) = \boldsymbol{u}^n \end{array}\right\} \Longrightarrow \boldsymbol{u}^{n+\frac{1}{2}} \tag{0.2.3}$$

and

$$\left.\begin{array}{l} \boldsymbol{u}_t + \boldsymbol{g}(\boldsymbol{u})_y = 0 \\ \boldsymbol{u}(x_i, ., t^n) = \boldsymbol{u}^{n+\frac{1}{2}} \end{array}\right\} \Longrightarrow \boldsymbol{u}^{n+1}. \tag{0.2.4}$$

In the first problem (0.2.3), we solve a one-dimensional problem in the x-direction for a time step Δt by keeping y fixed (i.e., for each j). This is called the x *sweep* and its solution is denoted by $\boldsymbol{u}^{n+\frac{1}{2}}$. In the next problem (0.2.4), we solve another one-dimensional problem in the y-direction for a time step Δt by keeping x fixed (i.e., for each i) by keeping the solution $\boldsymbol{u}^{n+\frac{1}{2}}$ of the first problem as the initial condition. This is called the y *sweep*. It can be proved that the final solution obtained by the above method is indeed an approximate solution for the initial value problem (0.2.1) and (0.2.2) (see Crandall and Majda, 1980) . The above method is of first order accurate, when the scheme used to solve the above two initial value problems are at least of first order accurate. Strang (1968) suggested a splitting which gives second order accuracy, in which we solve the first problem (0.2.3) with the time step $\Delta t/2$, keep the solution of this problem as an initial condition and solve the second problem (0.2.4) with the time step Δt and finally keep the solution of this second problem as the initial condition and solve the first problem with time step $\Delta t/2$. For more details on the dimension splitting method, we refer to Toro (1997).

§0.3 Inhomogeneous Equations: Source Term Splitting Method

Consider the nonlinear system of hyperbolic conservation laws with source terms

$$\boldsymbol{u}_t + \boldsymbol{f}(\boldsymbol{u})_x = \boldsymbol{S}(\boldsymbol{u}),\ x \in I\!R, t > 0, \tag{0.3.1}$$

where $\boldsymbol{S}$ is a vector of sources. This problem can be solved numerically using source term splitting method which we will explain briefly in this section. More details of this method may be found in Toro (1997).

Given the initial value problem (0.3.1) together with the initial data

$$\boldsymbol{u}(x, t^n) = \boldsymbol{u}^n. \tag{0.3.2}$$

We split the initial value problem (0.3.1)-(0.3.2) into homogeneous part and solve the equation using any standard numerical scheme available for solving system of homogeneous hyperbolic conservation laws with time step Δt. Keeping the solution obtained from this homogeneous equation as an initial data, solve the equation

$$\frac{d\boldsymbol{u}}{dt} = \boldsymbol{S}(\boldsymbol{u}), \tag{0.3.3}$$

which is a system of ordinary differential equations using any standard scheme such as Runge-Kutta method of second order (two stage) or fourth order (four stage).

We summarize this splitting method as follows:

$$\left.\begin{array}{l} \boldsymbol{u}_t + \boldsymbol{f}(\boldsymbol{u})_x = 0 \\ \boldsymbol{u}(x, t^n) = \boldsymbol{u}^n \end{array}\right\} \Longrightarrow \bar{\boldsymbol{u}}^{n+1} \tag{0.3.4}$$

and

$$\left.\begin{array}{l} \frac{d\boldsymbol{u}}{dt} = \boldsymbol{S}(\boldsymbol{u}) \\ \boldsymbol{u}(x, t^n) = \bar{\boldsymbol{u}}^{n+1} \end{array}\right\} \Longrightarrow \boldsymbol{u}^{n+1}. \tag{0.3.5}$$

As in the case of dimensional splitting method, the above splitting method is first order accurate in time when the schemes used are at least first order in time. To get a second order accuracy, we solve the problem (0.3.4) for the time step $\Delta t/2$, keeping the solution obtained by this problem as an initial data, we solve the problem (0.3.5) with time step Δt and finally, keeping this solution as an initial data, we solve the problem (0.3.4) with time step $\Delta t/2$.

It can be easily proved (Toro, 1997) that the solution obtained by the source term splitting method solves the inhomogeneous equation (0.3.1).

§0.4 Implementation Details

In Chapter 3 and Chapter 5 of this thesis, we have solved numerically, the kinematical conservation laws (KCL) (see section 1.3), which forms a 2×2 system of hyperbolic equations (when the wavefront Mach number is greater than 1) in one space variable. For this, we used the discontinuous Galerkin finite element method (characteristicwise) explained in section 0.1 with $k = 1$ in (0.1.6), which is a second order scheme. To verify the code developed for solving this problem, we compared the numerical results with the exact solution for the Riemann problem of KCL in all possible cases discussed in Chapter 2. We found that the numerical solution matches exactly with the exact solution for 200 mesh points on the space variable.

We solved the conservation form of the governing equations of shock ray theory (SRT) discussed in Chapter 5, which is a 4×4 inhomogeneous system of hyperbolic equations (when the shock front Mach number is greater than 1) in one space variable. For this, we used the discontinuous Galerkin finite element method (characteristicwise) with $k = 1$ in (0.1.6) and the source term splitting method explained in section 0.3. For the verification

of the code, we solved the scalar equation

$$u_t + \left(\frac{1}{2}u^2\right)_x = ku, \ k = \text{constant} \tag{0.4.6}$$

and compared the numerical solution with the analytical solution.

A numerical comparison between the results of the SRT and the Euler equations of motion have been done in Chapter 6. For this, we solved the Euler equations of motion (see (6.3.8)-(6.3.9)) in two-space dimensions using the discontinuous Galerkin finite element method (characteristicwise) with $k = 1$ in (0.1.6) together with the dimension splitting method explained in section 0.2. To verify the code, we performed the cylindrical explosion test problem (see Toro, 1997, section 17.1.1 for details) and obtained a very good comparison.

All the above problems are coded in ANCII C programming language and run in intel machine with Pentium 4, 1.7 GHz processor and 512 RAM.

References

1. Apazidis, N., Lesser, M. B., Tillmark, N. and Johanson, B. (2002), An experimental and theoretical study of converging polygonal shock waves, *Shock Waves*, **12**, 39-58.

2. Baskar, S. and Prasad, P. (2003), *Kinematical conservation laws applied to study geometrical shapes of a solitary wave*, Wind Over Waves II: Forecasting and Fundamentals of Applications, ed. S. Sajjadi and J. Hunt., 189-200.

3. Baskar, S. and Prasad, P. (2002) Riemann problem for kinematical conservation laws and geometrical features of nonlinear wavefront, Preprint, January 2002, Department of Mathematics, Indian Institute of Science, Bangalore - 560 012 (to appear in *IMA J. Appl. Math.*).

4. Betelu, S. I. and Aronson, D. G. (2001), Focusing of noncircular self-similar shock waves, *Phys. Rev. Lett.*, **87(7)**, 3058-3068.

5. Blokhintzev, D. I. (1946), The propagation of sound in an inhomogeneous and moving medium I, *J. Acoust. Soc. Am.*, **18**, 322-328.

6. Bressan, A. (2000), *Hyperbolic Systems of Conservation Laws*, Oxford Univ. Press, Oxford.

7. Bressan, A., Liu, T. P. and Yang, T. (1999), L^1 stability estimates for $n \times n$ conservation laws, *Arch. Rat. Mech. Anal.*, **149**, 1-22.

8. Bridges, T. J. (2001), Transverse instability of solitary-wave states of the water-wave problem, *J Fluid Mech.*, **439**, 255-278.

9. Chang, T. and Hsiao, L. (1989), *The Riemann Problem and Interaction of Waves in Gas Dynamics*, Longman, Harlow.

10. Chorin, A. J. (1976), Random choice solution of hyperbolic systems, *J. Comp. Phys.*, **22**, 517-533.

11. Cockburn, B., San, Y. L. and Shu, C. W. (1989), TVB Runge-Kutta local projection discontinuous Galerkin finite element method for conservation laws III: one-dimensional systems, *J. Compu. Phys.*, **84**(1), 90-113.

12. Courant, R. and Friedrichs, K. O. (1948), *Supersonic Flow and Shock Saves*, Interscience Publishers, New York.

13. Crandall, M. and Majda, A. (1980), The method of fractional steps for conservation laws, *Numer. Math.*, **34**, 285-314.

14. Dafermos, C. M. (1972), Polygonal approximations of solutions of the initial value problem for a conservation law, *J. Math. Anal. Appl.*, **38**, 33-41.

15. Dafermos, C. M. (2000), *Hyperbolic Conservation Laws in Continuum Physics*, Springer-Verlag, New York.

16. DiPerna, R. J. (1983 a), Convergence of approximate solutions to conservation laws, *Arch. Rational Mech. Anal.*, **82**, 27-70.

17. DiPerna, R. J. (1983 b), Convergence of the viscosity method for isentropic gas dynamics, *Comm. Math. Phys.*, **91**, 1-30.

18. Gelfand, I. (1959), Some problems in the theory of quasilinear equations, *Usp. Mat. Nauk.*, **14**, 87-158; English transl. in *Amer. Math. Soc. Transl.* ser 2, **29** (1963), 295-381.

19. Gill, P. M. and Seebass, A. R. (1975), Nonlinear acoustic behaviour at a caustic: An approximate solution, *AIAA Progress in Astronautics and Aeronautics*, ed. Nagamatsu, H. J. T., MIT, Cambridge.

20. Glimm, J. (1965), Solutions in the large for nonlinear hyperbolic systems of equations, *Comm. Pure Appl. Math.*, **18**, 697-715.

21. Glimm, J and Lax, P. D. (1970), *Decay of solutions of systems of nonlinear hyperbolic conservation laws*, Amer. Math. Soc. Memoir, No. **101**, American Mathematical Society, Providence, RI.

22. Godlewski, E. and Raviart, P. A. (1991), *Hyperbolic Systems of Conservation Laws*, Ellipses, Paris.

23. Godlewski, E. and Raviart, P. A. (1996), *Numerical Approximation of Hyperbolic Systems of Conservation Laws*, Springer, New York.

24. Goodman, J. B. and Xin, Z. (1992), Viscous limits for piecewise smooth solutions to systems of conservation laws, *Arch. Rat. Mech. Anal.*, **121**, 235-265.

25. Grinfel'd, M. A. (1978), Ray method for calculating the wavefront intensity in nonlinear elastic material, *PMM J. Appl. Math. and Mech.*, **42**, 958-977.

26. Hayes, W. D. (1947), *Linearized Supersonic Flow*, Thesis, California Institute of Technology; reprinted as North American Aviation Report AL-222; Available as Princton University AMS Report **852**.

27. Hayes, W. D., Haefeli, R. C. and Kulsrud, H. E. (1969), Sonic boom propagation in a stratified atmosphere, with computer program, *NASA CR* - **1299**.

28. Henshaw, W. D., Smyth, N. F. and Schwendeman D. W. (1986), Numerical shock propagation using geometrical shock dynamics, *J. Fluid. Mech.*, **171**, 519-545.

29. Holden, H. and Risebro, N. H. (2002), *Front Tracking for Hyperbolic Conservation Laws*, Springer-Verlag, New York.

30. James, F., Peng, Y. J. and Perthame, B. (1995), Kinetic formulation for chromatography and some other hyperbolic systems, *J. Math. Pures Appl.*, **74**, 367-385.

31. Kesavan, S. (1989), *Topics in Functional Analysis and Applications*, Wiley Eastern Limited, India.

32. Kevlahan, N. K. R. (1996), The propagation of weak shocks in non-uniform flow, *J. Fluid Mech.* **327**, 167-197.

33. Kluwick, A. von (1971), Zur Ausbreitung schwacher stoesse in dreidimensionalen instationaeren stroemungen, *Z Angew. Math. Mech.*, **51**, 225-232.

34. Kruskov, S. (1970), First-order quasi-linear equations with several space variables, *Mat. Sb.,* **123**, 228-255; English transl. in *Math. USSR Sb.,* **10**, 217-273.

35. Lax, P. D. (1954), Weak solutions of nonlinear hyperbolic equations and their numerical computation, *Comm. Pure Appl. Math.*, **7**, 159-193.

36. Lax, P. D. (1957), Hyperbolic system of conservation laws II, *Comm. Pure Appl. Math.*, **10**, 537-566.

37. Lax, P. D. (1973), *Hyperbolic Systems of Conservation Laws and the Mathematical Theory of Shock Waves*, CBMS Regional Conference Series in Mathematics No. **11**. Philadelphia: SIAM.

38. Liu, T. P. (1977), The deterministic version of the Glimm scheme, *Comm. Math. Phys.*, **57**, 135-148.

39. Maslov, V. P. (1980), Propagation of shock waves in an isentropic non-viscous gas, *J. Sov. Math.*, **13**, 119-163 (Russian publication 1978).

40. Miles, J. W. (1977), Diffraction of solitary waves, *J. Appl. Math and Phy.* (ZAMP), **28**, 889-902.

41. Monica, A. and Prasad, P. (2001), Propagation of a curved weak shock front, *J. Fluid Mech.*, **434**, 119-151.

42. Morton, K. W., Prasad, P. and Ravindran, R. (1992), *Conservation form of nonlinear ray equations*, Technical report 2. Department of Mathematics, Indian Institute of Science, Bangalore.

43. Oleinik, O. (1957), Discontinuous solutions of nonlinear differential equations, *Usp. Mat. Nauk. (N. S)*, **12**, 3-73; English transl. in *Amer. Math. Soc. Transl. Ser. 2*, **26**, 95-172.

44. Osher, S. (1985), Convergence of generalized MUSCL schemes, *SIAM J. Numer. Anal.*, **2**, 947-961.

45. Ostrovsky, L. A. and Shrira, V. I. (1976), Instability and self refraction of solitons, *Sov. Phys. JETP*, **44**, No.4, 738-743.

46. Pederson, G. (1994), Nonlinear modulations of solitary waves, *J. Fluid. Mech.*, **267**, 83-108.

47. Pilon, A. and Lyrintzis, A. (1995), *A Data-Parallel TVD Method for Sonic Boom Calculations*, Preprint 95-003, University of Minnesota, Minnesota.

48. Plotkin, K. J. (1998), *PCBoom3 Sonic Boom Prediction Model, Version 1.0e*, Wyle Research Report WR **95-22E**.

49. Plotkin, K. J., (2002), State of the art of sonic boom modeling, *J. Acoust. Soc. Am.* **111** (1), 530 - 536.

50. Prasad, P. (1975), Approximation of perturbation equations in a quasilinear hyperbolic system in the neighbourhood of a bicharacteristic, *J. Math. Anal. Appl.*, **50**, 470-482.

51. Prasad, P. (1982), Kinematics of a multi-dimensional shock of arbitrary strength in an ideal gas, *Acta Mechanica*, **45**, 163-176.

52. Prasad, P. (1993), *Propagation of a Curved Shock and Nonlinear Ray Theory*, Pitman Researches in Mathematics Series, No. 292, Longman, Essex.

53. Prasad, P. (1995), Formation and propagation of singularities on a nonlinear wavefront and a shock front, *J. of Indian Inst. of Sci.*, **75**, 517-535.

54. Prasad, P. (2000), An asymptotic derivation of weakly nonlinear ray theory, *Proc. Indian Acad. Sci. Math. Sci.*, **110**, 4, 431-447.

55. Prasad, P. (2001), *Nonlinear Hyperbolic Waves in Multi-Dimensions*, Chapman and Hall/CRC, Monographs and Surveys in Pure and Applied Mathematics - 121.

56. Prasad, P. (2003), Propagation of a curved shock of arbitrary strength, in preparation.

57. Prasad, P. and Ravindran, R. (1977), A theory of nonlinear waves in multi-dimensions with special reference to surface water waves, *J. Inst. Math. Applics.* **20**, 9-20.

58. Prasad, P., Ravindran, R. and Sau, A. (1991), On the characteristic rule for shocks *Appl. Math. Lett.*, **4**, 5-8.

59. Prasad, P. and Sangeeta, K. (1999), Numerical simulation of converging nonlinear wavefronts, *J. Fluid Mech.*, **385**, 1-20.

60. Ravindran, R. and Prasad, P. (1990), A new theory of shock dynamics, Part-I: analytic considerations, *Appl. Math. Lett.*, **3**, 77-81.

61. Riemann, B. (1860), Ueber die Fortpflanzung ebener Luftwellen von endlicher Schwingungsweite, *Gött. Abh. Math. Cl.*, **8**, 43-65.

62. Risebro, N. H. (1993), A front-tracking alternative to the random choice method, *Proc. Amer. Math. Soc.*, **117**, 1125-1129.

63. Schwendeman, D. W. (2002), On converging shock waves of spherical and polyhedral form, *J. Fluid Mech.*, **454**, 365-386.

64. Schwendeman, D. W. and Whitham, G. B. (1987), On converging shock waves, *Proc. R. Soc. Lond. A*, **413**, 297-311.

65. Shrira, V. I. (1980), Nonlinear refraction of solitons, *Sov. Phys. JETP*, **51**, No.1, 44-49.

66. Smoller, J. (1983), *Shock Waves and Reaction-diffusion Equations*, Springer-Verlag, New York (2/e, 1994).

67. Stokes, G. G. (1848), On a difficulty in the theory of sound, *Phil. Mag.* **23**, No. 3, 349-356 (Papers **2**, 51-58).

68. Strang, G. (1968), On the construction and comparison of difference schemes, *SIAM J. Numer. Anal.*, **5**(3), 506-517.

69. Sturtevant, B. (1989), The physics of shock focusing in the context of extracorporeal shock wave lithotripsy, *Proceedings of the International Workshop on Shock Wave Focusing*, ed. Takayama, K., Shock Wave Research Center, Institute of Fluid Science, Tohoku University, Tohoku.

70. Sturtevant, B. and Kulkarni, V. A. (1976), The focusing of weak shock waves, *J. Fluid Mech.*, **73,** 651-671.

71. Temple, B. (1985), No L^1-contractive metric for systems of conservation laws, *Trans. AMS*, **288**, 471-480.

72. Thomas, C. L. (1972), Extrapolation of sonic boom pressure signatures by the waveform parameter method, *NASA TN* **D-6832**.

73. Toro, E. F. (1997), *Riemann Solvers and Numerical Methods for Fluid Dynamics*, Springer-Verlag, Heidelberg.

74. Wanner, J. C. L., Vallee, J., Vivier, C. and Thery, C. (1972), Theoretical and experimental studies of the focus of sonic booms, *J. Acoust. Soc. Am.*, **52**, 13.

75. Whitcomb, R. T. and Fishcetti, T. L. (1953), Development of a supersonic area rule and an application to the design of a wing-body combination having high lift-to-drag ratios, *NASA RM*, **L53H31a**.

76. Whitham, G. B. (1952), The flow pattern of a supersonic projectile, *Comm. Pure Appl. Math.*, **5**, 301-348.

77. Whitham, G. B. (1956), On the propagation of weak shock waves, *J. Fluid Mech.*, **1**, 290-318.

78. Whitham, G. B. (1957), A new approach to problems of shock dynamics, Part I, Two dimensional problems, *J. Fluid Mech.*, **2**, 145-171.

79. Whitham, G. B. (1959), A new approach to shock dynamics, Part II, Three-dimensional problems, *J. Fluid Mech.*, **5**, 369-386.

80. Whitham, G. (1974), *Linear and nonlinear waves*, John Wiley & Sons, New York.

81. Zakharov, V. E. (1986), Shock waves propagated on solitons on the surface of a fluid, *Radiophys and Quantum Electronics*, **29**, 1073 - 1079.